STRESS ANALYSIS OF PRESSURE VESSELS WITH ATTACHMENTS

by

KEMAL GUPGUPOGLU

A thesis
presented to the School of Graduate Studies
of the University of Ottawa
in partial fulfillment of the
requirements for the degree of
Master of Applied Science
in
Department of Mechanical Engineering
University of Ottawa
Ottawa, Ontario, Canada

OTTAWA, Ontario, 1982

ABSTRACT

Stress analysis of attachments to pressure vessels is the main concern of this study. The stresses caused in pressure vessels are the combination of longitudinal forces and moments.

Equations expressing the deformations caused by longitudinal stresses are the solution of an eighth order differential equation which is the reduced form of the three partial differential equations of thin shell theory. The load is applied on a band along the circumference and expressed in terms of Fourier series. Results for an axially symmetric loading are generated for several shell and loading parameters.

The stresses developed by the presence of the integral lug attachments are analysed by finite element method where a 17 noded doubly curved shell element and Front Solver technique are utilized. Numerical calculations have been generated for several lug sizes and radius to thickness ratios of the shell. Comparisons of the present method with the available methods has also been presented.

ACKNOWLEDGEMENT

The author would like to express his gratitude to Dr. S. Mirza under whose supervision this work was carried out, for his critical discussions, valuable suggestions and constant encouragement.

The author also wishes to express his sincere thanks to Dr. R. Natarajan.

The financial support provided by NSERC is gratefully appreciated.

NOMENCLATURE

a	radius of a shell
C_L	stress index for longitudinal moment due to axial maximum stress
C_L^*	stress index for longitudinal moment due to circumferential maximum stress
c_1	half-length of the loaded area in the circumferential direction
c_2	half-length of the loaded area in the axial direction
D	flexural rigidity of a shell
D^*	$= Et/(1-\nu^2)$
$[D]$	elasticity matrix
E	modulus of elasticity
G	shear modulus of elasticity
k	an integer
$[J]$	Jacobian matrix
ℓ	length of a shell
ℓ_1/ℓ	starting position of external load
$\ell_2-\ell_1/\ell$	band width
M_L	longitudinal external moment
M_x, M_y, M_{xy}, M_{yx}	bending and twisting moments per unit length
$M_x, M_\phi, M_{x\phi}, M_{\phi x}$	bending and twisting moments per unit length of a cylindrical shell

N_i	shape functions
N_x, N_y	membrane forces per unit length
N_{xy}, N_{yx}	membrane shear forces per unit length
N_x, N_ϕ	membrane forces per unit length of a cylindrical shell
$N_{x\phi}, N_{\phi x}$	membrane shear forces per unit length of a cylindrical shell
P_x, P_y, P_z	external loads applied to a shell
P_t	total external load applied to a shell along the axial direction
p	intensity of external force per unit surface
P_k	coefficient of Fourier series for external loading
Q_x, Q_y	shearing forces
Q_x, Q_ϕ	shearing forces of a cylindrical shell
r_x, r_y	radii of curvature of the middle surface of a shell
$[S]$	stiffness matrix
S_ℓ	$= 3M_L/4c_1c_2$
t	thickness of a shell
u_k	Fourier coefficient of axial deformation
u, v, w	components of displacements
V_1, V_2, V_3	direction cosine vectors
w_k	Fourier coefficient of radial displacement
X, Y, Z	global coordinates
x, y, z	rectangular coordinates
x', y', z'	coordinate axes defined in the element

α_i, β_i	degrees of freedom of an element, rotations around V_{2i} and V_{1i}
β	$= 12(1-\nu^2)/ a^2 t^2$
β_1	$= c_1/a$
β_2	$= c_2/a$
$\varepsilon_x, \varepsilon_y, \varepsilon_z$	unit elongations in x, y and z directions
ε_0	initial strain
$\sigma_x, \sigma_y, \sigma_z$	normal components of stress parallel to x,y and z directions
σ_0	initial stress
$\tau_{xy}, \tau_{xz}, \tau_{yz}$	shearing stress components
γ	shearing strain in the middle surface of a shell
$\gamma_{xy}, \gamma_{xz}, \gamma_{yz}$	shearing strain components
ν	Poisson's ratio
χ_x, χ_y	changes of curvature of a shell
χ_{xy}	the twist of the middle surface
$\varepsilon_1, \varepsilon_2$	unit elongations of the middle surface in the x and y directions
ξ, η, ζ	curvilinear coordinates
ϕ	cylindrical coordinate in circumferential direction of a shell
ψ	$= 12\nu\,(1-\nu^2)/ Eat^3$

CONTENTS

ABSTRACT ii

ACKNOWLEDGEMENT iii

NOMENCLATURE iv

Chapter page

I. INTRODUCTION 1

II. REVIEW OF SHELL THEORY 6

GENERAL 6
BENDING STRESSES IN SHELLS 8
CIRCULAR CYLINDRICAL SHELLS UNDER GENERAL LOADS 11
CIRCULAR CYLINDRICAL SHELLS UNDER LOCALIZED LOADS 16

III. RING ATTACHMENTS TO PRESSURE VESSELS 20

INTRODUCTION 20
DERIVATION OF THE SINGLE EIGHTH ORDER DIFFERENTIAL EQUATION 21
EQUILIBRIUM EQUATIONS 25
EXTERNAL LOADING 25
RADIAL AND AXIAL DEFORMATIONS 26
STRESSES IN THE CIRCULAR CYLINDRICAL SHELLS . . 28

IV. INTEGRAL LUG ATTACHMENTS TO PRESSURE VESSELS . . . 29

INTRODUCTION 29
THE FINITE ELEMENT METHOD 31
ELEMENT PROPERTIES 33
FINITE ELEMENT MODELLING 38

V. DISCUSSION OF RESULTS 40

RING ATTACHMENTS 40
GENERAL 40
INTERPRETATION OF RESULTS 41
INTEGRAL LUG ATTACHMENTS 61
GENERAL 61
COMPUTATIONS ON DEFORMATIONS 62
COMPUTATIONS ON STRESSES 67
SQUARE LOADED AREAS 69

RECTANGULAR LOADED AREAS 72
COMPARATIVE STUDY 76
SQUARE LOADED AREAS 76
RECTANGULAR LOADED AREAS 81
CHANGING THE POSITION OF THE LUGS ALONG THE LENGTH 86

VI. CONCLUSIONS 88

Appendix		page
A.	FRONT SOLVER	90
B.	SHAPE FUNCTIONS	94
C.	FLOW CHART OF THE COMPUTER PROGRAM	95
D.	. . . .	[illegible]
E.	. . . .	10[illegible]

BIBLIOGRAPHY 162

LIST OF FIGURES

Figure		page
1.	. . . .	9
2.	. . . .	12
3.	Cylindrical shell subjected to band load along the generatrix	20
4.	Typical lug arrangement	30
5.	Curved shell element with degrees of freedom	33
6.	Typical finite element model considered	38
7.	Typical bending moment, M_x/Et, and membrane force, N_ϕ /Et, variation due to axial load	44
8-23	Radial and axial deformations, and membrane force, N_x /Et, variation due to axial load	45 – 60
24	Radial deformation variation (Lug-vessel interface)	63
25.	Axial deformation variation along the lug centerline due to longitudinal moment, for square lugs . . .	64
26.	Radial deformation variation along the lug centerline due to longitudinal moment, for rectangular lugs	65
27.	Axial deformation variation along the lug centerline due to longitudinal moment, for rectangular lugs	66
28.	Typical stress distribution along lug centerline . .	68
29.	Stress distribution along lug centerline due to the change in the position of the lug	87
A-1.	Flow chart for Front Solver technique	93

LIST OF TABLES

Table — page

1. Stress indices for longitudinal moment loading on square lug attachments (β =0.05) 70
2. Stress indices for longitudinal moment loading on square lug attachments (β =0.10) 70
3. Stress indices for longitudinal moment loading on square lug attachments (β =0.20) 71
4. Stress indices for longitudinal moment loading on rectangular attachments (β =0.05, β =0.10) . 74
5. Stress indices for longitudinal moment loading on rectangular attachments (β =0.20, β =0.10) . 74
6. Stress indices for longitudinal moment loading on rectangular attachments (β =0.40, β =0.10) . . 75
7. Stress indices for longitudinal moment loading on rectangular attachments (β =0.05, β =0.20) . 75
8. Comparisons on square loaded areas for β =0.05 . . 78
9. Comparisons on square loaded areas for β =0.10 . . 79
10. Comparisons on square loaded areas for β =0.20 . . 80
11. Comparisons on rectangular loaded areas for β =0.40, β =0.10 82
12. Comparisons on rectangular loaded areas for β =0.20, β =0.10 83
13. Comparisons on rectangular loaded areas for β =0.05, β =0.10 84
14. Comparisons on rectangular loaded areas for β =0.05, β =0.20 85

Chapter I

INTRODUCTION

Pressure vessels have long been used in industry for storage, industrial processing and power generation.

The original design philosophy of pressure vessels was first added to the ASME Boiler Construction Code in 1925 under the title, (Section VIII) Unfired Pressure Vessels . In 1968 the title was changed and Section VIII published in two parts, Division 1, Rules for Construction of Pressure Vessels, and Division 2, Alternative Rules [1].

In the design of pressure vessels, the minimum required loadings to be considered are stated in Division 1, Par. UG-22. According to Division 2, calculated stresses caused by these loadings are divided into various categories. These categories are:

a) Primary Stress

  i) General Primary Membrane Stress

  ii) Local Primary Membrane Stress

  iii) Primary Bending Stress

b) Secondary Stress

c) Peak Stress

One of the requirements for the acceptability of a design is that the calculated stresses will not exceed the limits described in the Code[1]. The basic limits for the various categories defined in Division 2 (See Code Table AD-150.1 and Fig. 4-130.1) are lower than those permitted in Division 1. However, in order to maintain the required safety, design and quality control, a detailed stress analysis is assigned in Division 2.

One of the loadings that has to be considered, in the design, is the loading resulting in localized stresses due to the attachments such as lugs, rings, skirts etc.(See Code UG-22). Stresses caused by these type of loadings fall into local primary membrane stress category.

The main characteristic of primary stresses is that, they are not self limited, i.e. their magnitude remains the same no matter how large deformations they produce. Therefore, a lower allowable stress limit is given for this type of stress than to Secondary stress.

In Division 1 of the Code, some general design guidance is given for attachments to pressure vessels (See Par. UG-55 and UG-82, and Appendix G). However, for most of the attachments design procedures are not provided and left up to the designer.

Although Division 1 recommends [8,16 and 19] as an additional guidance on the design of integral attachments, comparative study presented in [16] shows large discrepancies in the results.

---

[1] Code as used in this text refers to ASME Boiler and Pressure Vessel Code, Section VIII.

When attachments are welded, brazed or bolted to the outside or inside of the shell, they cause localized loadings. One of the approaches, in analysing the effect of local loadings on shells, is to distribute the load over a rectangular area. The major investigation in this field is the one conducted by Bijlaard [4]. Bijlaard represented thrust, longitudinal and circumferential moment loading by double Fourier series, which enabled him to express the deformations and stresses also in this form.

The second approach, which has been presented by Hoff, Kemper and Pohle [10], is to distribute localized loadings along the circumferential and axial directions by line loading.

Wichman, Hopper and Mershon [19] presented Bijlaard's analytical work in a much simpler and convenient way in order to make the results readily available for design engineers. Based on available experimental work some adjustments to Bijlaard's results are recommended.

W.G. Dodge [8] simplified the solution procedure introducing stress index concept used in ASME Boiler and Pressure Vessel Code, Section III, Nuclear Power Plant Components. Dodge defined the stress index for a moment loading as " The ratio of the maximum stress intensity in the pipe component to the nominal bending stress in straight pipe subjected to the same moment". Whereas, the stress index, for a radial loading, is normalized by the average shearing stress in the pipe. Based on the numerical study done on Bijlaard's results, Dodge gave a single approximate formula to calculate stress indices for integral lug attachments.

Rodabaugh, Dodge and Moore's work [16] uses the same approach presented in [8]. However, the definition of stress index is changed and re-defined as "The ratio of the maximum stress intensity in the pipe component to the nominal bending stress in the lug", which, in fact, predicts conservative results in comparasion with [8,19].

For comparative study, this definition of stress index has also been utilized in this study.

It is the purpose of this investigation to give detailed stress analysis for two types of attachments to pressure vessels, (i) Ring attachments, (ii) Integral lug attachments.

An analytical procedure adopted here in analysing the ring attachments has similarities to those used in [4,21]. It is the advantage of this procedure to deal with a single differential equation. An eighth order differential equation in terms of radial deformation alone is derived in case of longitudinal loading. Expressing this type of loading as trigonometric series allows the solution for deflections to be written in terms of Fourier series. Numerical computations have been done for an axially symmetric loading.

The second design consideration is given to integral lug attachments. The pressure vessel is assumed to be supported by four lugs separated 90 degrees apart along the circumferential direction. This type of structural attachment causes longitudinal bending moment and axial shear loading on the shell. In this study, the stress distribution resulting from the bending moment is analysed by finite element method which uses a 17 noded doubly curved shell element and the simplified 'Front Solver' technique. Results are generated for different lug sizes and radius to thickness ratios of the shell. The effect of each variable is analysed, and, in addition, comparative study is provided between the results obtained here and in [8,16 and 19].

Chapter II

REVIEW OF SHELL THEORY

2.1 GENERAL

A shell may be defined as an object bounded by two curved surfaces, the distance between the surfaces, thickness, being small in comparison with the other dimensions. Some describe a shell as a structure which can be derived from a thin plate by initially forming the middle plane to a single (doubly) curved surface. It is geometrically defined if the shape of the middle surface and its thickness are known for every point.

There are two different types of shells - thick shells and thin shells. A shell is considered to be thin if the ratio of thickness to radius is less than 1/10. From this point on shell theory can be divided into a theory of shells of arbitrary thickness and into a theory of thin shells. From the definition of 'thin-ness' some of the terms may be neglected, in basic formulation, in order to keep equations linear. In addition to this fact the following three assumptions can be made for the simplicity of solution :

1. Shell deflections are assumed to be small,
2. The stress, σ_z, in the direction normal to the thin dimension is negligible,

3. A line originally normal to the shell middle surface will remain normal to the deformed shell middle surface.

The analysis of shell structures include two versions of shell theory -membrane theory and bending theory. Membrane stresses are simple to calculate, however, there are some limitations.

In membrane stress analysis all external loads must be applied in such a way that the internal stresses are generated in the plane of the shell only. If the shell is carrying a concentrated load or an edge loading condition the bending stresses are significant. For this theory there are no conditions on w or its derivatives, which implies that clamp boundary conditions can not be fully satisfied.

Bending shell theory includes bending stresses and transverse shear forces in addition to membrane stresses. But here number of unknown stress resultants exceed the number of static equilibrium equations and so additional differential equations have to be derived from the deformation relations. Bending theory is also capable of discontinuities in the stress distribution in the vicinity of a load.

2.2 BENDING STRESSES IN SHELLS

Thin shell theory employed in this section and the following one has been adopted from Timoshenko [17].

Considering the infinitesimal element shown in Fig. (1(a)),we take the coordinate axes x and y tangent at O to the lines of principal curvature and the axis z normal to the middle surface. The stresses acting on the plane faces of the element are shown in Fig. (1(b))(M^* denotes $M + \partial M/\partial X dx$, etc.). r_x and r_y being the principal radii of curvature, the resultant forces and moments per unit length of the normal sections are given by

$$\begin{Bmatrix} N_x \\ N_y \\ N_{xy} \\ N_{yx} \\ Q_x \\ Q_y \end{Bmatrix} = \int_{-t/2}^{t/2} \begin{Bmatrix} \sigma_x(1-z/r_y) \\ \sigma_y(1-z/r_x) \\ \tau_{xy}(1-z/r_y) \\ \tau_{yx}(1-z/r_x) \\ \tau_{xz}(1-z/r_y) \\ \tau_{yz}(1-z/r_x) \end{Bmatrix} dz$$

$$\begin{Bmatrix} M_x \\ M_y \\ M_{xy} \\ M_{yx} \end{Bmatrix} = \int_{-t/2}^{t/2} \begin{Bmatrix} \sigma_x(1-z/r_y) \\ \sigma_y(1-z/r_x) \\ -\tau_{xy}(1-z/r_y) \\ \tau_{yx}(1-z/r_x) \end{Bmatrix} z\, dz \tag{1}$$

Shearing forces N_{xy} and N_{yx} are not generally equal due to the fact that in general $r_x \neq r_y$. However for thin shells, thickness is small relative to r_x and r_y , and so, z/r_x and z/r_y may be neglected in comparison with unity, then $N_{xy} = N_{yx}$, and also $M_{xy} = M_{yx}$.

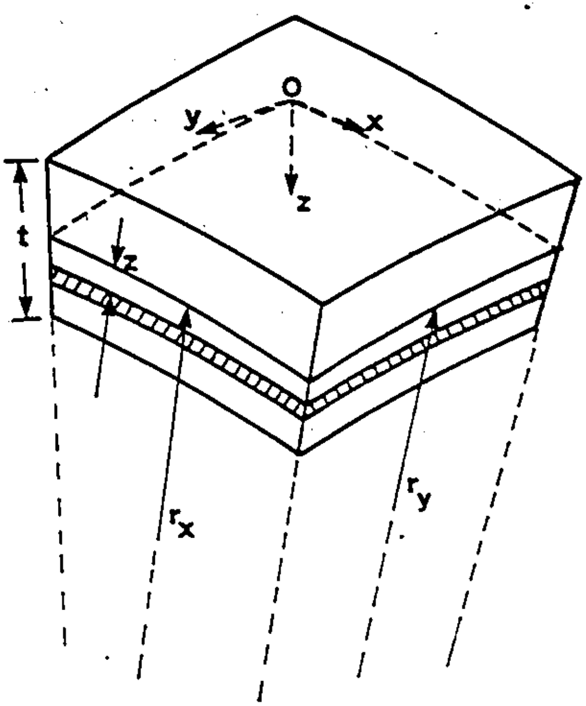

(a)

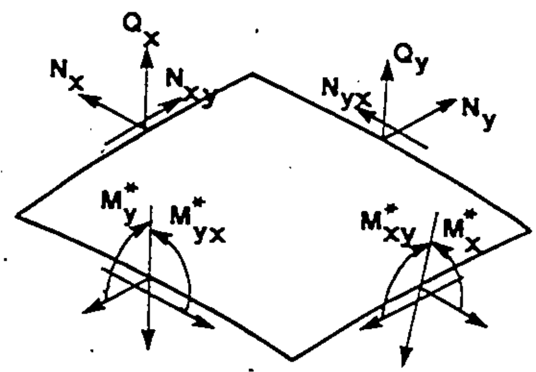

(b)

Figure 1:

According to assumption (2), the stress in z direction is neglected ($\sigma_z=0$). The following expressions for the components of stress are obtained from Hooke's law :

$$\sigma_x = \frac{E}{1-\nu^2} (\varepsilon_x + \nu\varepsilon_y)$$

$$\sigma_y = \frac{E}{1-\nu^2} (\varepsilon_y + \nu\varepsilon_x) \qquad (2)$$

$$\tau_{xy} = \gamma_{xy} G$$

where E= Modulus of elasticity

G= Shear modulus of elasticity.

The strains, ϵ_x, ϵ_y and γ_{xy}, are given as follows :

$$\varepsilon_x = \varepsilon_1 - \chi_x z$$

$$\varepsilon_y = \varepsilon_2 - \chi_y z \qquad (3)$$

$$\gamma_{xy} = \gamma - 2z\, \chi_{xy}$$

where ϵ_1 and ϵ_2 are the unit elongations of the middle surface along x and y, respectively.

γ shear stress in the middle surface of the shell.

χ_x, χ_y and χ_{xy} represent the change of curvature of the midsurface.

Upon substitution of Eq. (3) into (2), and later to Eq. (1), we obtain the stress resultants as

$$N_x = \frac{Et}{1-\nu^2}(\varepsilon_1 + \nu\varepsilon_2) \qquad M_x = -D(\chi_x + \nu\chi_y)$$

$$N_y = \frac{Et}{1-\nu^2}(\varepsilon_2 + \nu\varepsilon_1) \qquad M_y = -D(\chi_y + \nu\chi_x) \qquad (4)$$

$$N_{xy} = N_{yx} = \frac{\gamma Et}{2(1+\nu)} \qquad M_{xy} = -M_{yx} = D(1-\nu)\chi_{xy}$$

where

$$D = Et^3 / 12(1-\nu^2)$$

2.3 CIRCULAR CYLINDRICAL SHELLS UNDER GENERAL LOADS

Now we proceed to establish the differential equations for the displacements u, v and w which define the deformation of a cylindrical shell along the coordinates x, y and z, respectively.

The shell element separated from a cylinder is shown in Fig. (2(a)), and Fig. (2(b)) shows resultant forces and moments . Projecting resultant forces and moments on three coordinate axes, the following equations can be obtained:

$$a\frac{\partial N_x}{\partial x} + \frac{\partial N_{\phi x}}{\partial \phi} - a\,Q_x\frac{\partial^2 w}{\partial x^2} - a\,N_{x\phi}\frac{\partial^2 v}{\partial x^2} -$$

$$Q_\phi\left(\frac{\partial v}{\partial x} + \frac{\partial^2 w}{\partial x\,\partial \phi}\right) - N_\phi\left(\frac{\partial^2 v}{\partial x\,\partial \phi} - \frac{\partial w}{\partial x}\right) + P_x\,a = 0 \qquad (5a)$$

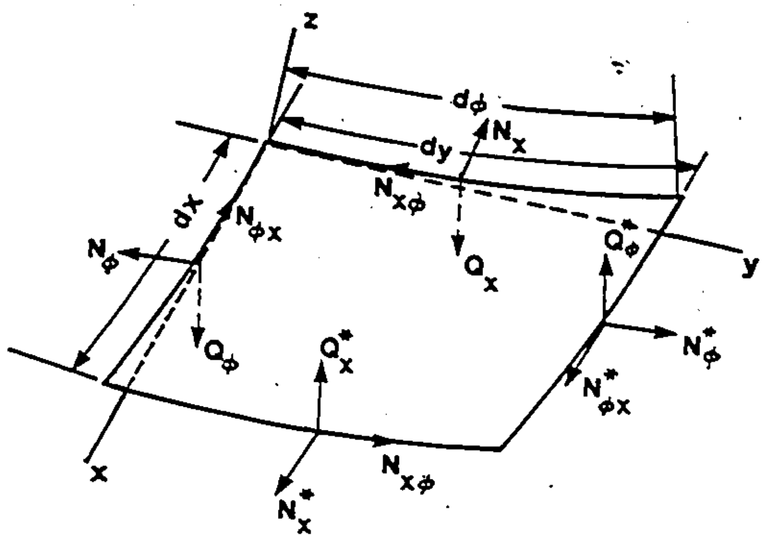
z
dϕ
dy
N_x
dx
$N_{x\phi}$
$N_{\phi x}$
N_ϕ
Q_x
Q_ϕ^*
y
Q_ϕ
Q_x^*
N_ϕ^*
$N_{\phi x}^*$
x
$N_{x\phi}$
N_x^*

(a)

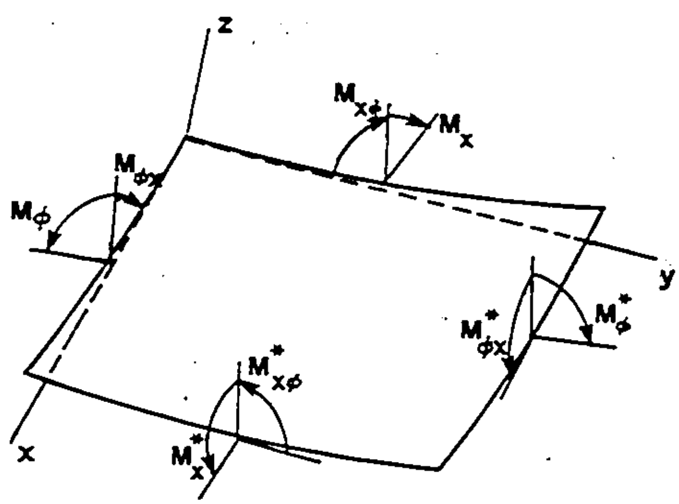
z
$M_{x\phi}$
M_x
$M_{\phi x}$
M_ϕ
y
$M_{\phi x}^*$
M_ϕ^*
$M_{x\phi}^*$
x
M_x^*

(b)

Figure 2:

$$\frac{\partial N_\phi}{\partial \phi} + a\,\frac{\partial N_{x\phi}}{\partial x} + a\,N_x\,\frac{\partial^2 v}{\partial x^2} - Q_x\left(\frac{\partial v}{\partial x} + \frac{\partial^2 w}{\partial x\,\partial \phi}\right) +$$

$$N_{\phi x}\left(\frac{\partial^2 v}{\partial x\,\partial \phi} - \frac{\partial w}{\partial x}\right) - Q_\phi\left(1 + \frac{\partial v}{a\,\partial \phi} + \frac{\partial^2 w}{a\,\partial \phi^2}\right) + P_y\,a = 0 \qquad (5b)$$

$$a\,\frac{\partial Q_x}{\partial x} + \frac{\partial Q_\phi}{\partial \phi} + N_{x\phi}\left(\frac{\partial v}{\partial x} + \frac{\partial^2 w}{\partial x\,\partial \phi}\right) + a\,N_x\,\frac{\partial^2 w}{\partial x^2}$$

$$+ N_\phi\left(1 + \frac{\partial v}{a\,\partial \phi} + \frac{\partial^2 w}{a\,\partial \phi^2}\right) + N_{\phi x}\left(\frac{\partial v}{\partial x} + \frac{\partial^2 w}{\partial x\,\partial \phi}\right) + P_z\,a = 0 \qquad (5c)$$

$$a\,\frac{\partial M_{x\phi}}{\partial x} - \frac{\partial M_\phi}{\partial \phi} - a\,M_x\,\frac{\partial^2 v}{\partial x^2} - M_{\phi x}\left(\frac{\partial^2 v}{\partial x\,\partial \phi} - \frac{\partial w}{\partial x}\right) + a\,Q_\phi = 0 \qquad (5d)$$

$$\frac{\partial M_{\phi x}}{\partial \phi} + a\,\frac{\partial M_x}{\partial x} + a\,M_{x\phi}\,\frac{\partial^2 v}{\partial x^2} - M_\phi\left(\frac{\partial^2 v}{\partial x\,\partial \phi} - \frac{\partial w}{\partial x}\right) - a\,Q_x = 0 \qquad (5e)$$

$$M_x\left(\frac{\partial v}{\partial x} + \frac{\partial^2 w}{\partial x\,\partial \phi}\right) + a\,M_{x\phi}\,\frac{\partial^2 w}{\partial x^2} + M_{\phi x}\left(1 + \frac{\partial v}{a\,\partial \phi} + \frac{\partial^2 w}{a\,\partial \phi^2}\right) -$$

$$M_\phi\left(\frac{\partial v}{\partial x} + \frac{\partial^2 w}{\partial x\,\partial \phi}\right) + a\left(N_{x\phi} - N_{\phi x}\right) = 0 \qquad (5f)$$

If buckling of shell is not considered, some of the terms can be neglected in Eq. (5). Equation (5.f) becomes identity, as a result of the relation $\tau_{xy}=\tau_{yx}$. Therefore, Eq. (5) becomes

$$a\frac{\partial N_x}{\partial x}+\frac{\partial N_{\phi x}}{\partial \phi}+P_x\,a=0$$

$$\frac{\partial N_\phi}{\partial \phi}+a\frac{\partial N_{x\phi}}{\partial x}-Q_\phi+P_y\,a=0$$

$$\frac{\partial Q_\phi}{\partial \phi}+a\frac{\partial Q_x}{\partial x}+N_\phi+P_z\,a=0$$

$$a\frac{\partial M_{x\phi}}{\partial x}-\frac{\partial M_\phi}{\partial \phi}+aQ_\phi=0$$

$$a\frac{\partial M_x}{\partial x}+\frac{\partial M_{\phi x}}{\partial \phi}-a\,Q_x=0$$

The transverse shears Q_x and Q_ϕ may be eliminated from the above expressions. We finally obtain the following three equilibrium equations :

$$\begin{aligned}
&a\frac{\partial N_x}{\partial x}+\frac{\partial N_{\phi x}}{\partial \phi}+P_x\,a=0\\
&\frac{\partial N_\phi}{\partial \phi}+a\frac{\partial N_{x\phi}}{\partial x}-\frac{1}{a}\frac{\partial M_\phi}{\partial \phi}+\frac{\partial M_{x\phi}}{\partial x}+P_y\,a=0\\
&\frac{1}{a}\frac{\partial^2 M_\phi}{\partial \phi^2}+a\frac{\partial^2 M_x}{\partial x^2}+\frac{\partial^2 M_{\phi x}}{\partial x\,\partial \phi}-\frac{\partial^2 M_{x\phi}}{\partial x\,\partial \phi}+N_\phi+P_z\,a=0
\end{aligned}\qquad(6)$$

Kinematic expressions and changes in curvatures are expressed by :

$$\varepsilon_x = \frac{\partial u}{\partial x} \qquad \varepsilon_\phi = \frac{1}{a}\left(\frac{\partial v}{\partial \phi} - w\right) \qquad \gamma_{x\phi} = \frac{\partial v}{\partial x} + \frac{\partial u}{a\,\partial \phi}$$

$$\chi_x = \frac{\partial^2 w}{\partial x^2} \qquad \chi_\phi = \frac{1}{a^2}\left(\frac{\partial v}{\partial \phi} + \frac{\partial^2 w}{\partial \phi^2}\right) \qquad \chi_{x\phi} = \frac{1}{a}\left(\frac{\partial v}{\partial x} + \frac{\partial^2 w}{\partial \phi\,\partial x}\right) \tag{7}$$

Introducing Eq. (7) to (4) results in the following stress-displacement relations

$$N_x = \frac{Et}{1-\nu^2}\left[\frac{\partial u}{\partial x} + \nu\left(\frac{1}{a}\frac{\partial v}{\partial \phi} - \frac{w}{a}\right)\right]$$

$$N_\phi = \frac{Et}{1-\nu^2}\left[\frac{1}{a}\frac{\partial v}{\partial \phi} - \frac{w}{a} + \nu\frac{\partial u}{\partial x}\right]$$

$$N_{x\phi} = \frac{Et}{2(1+\nu)}\left[\frac{\partial v}{\partial x} + \frac{1}{a}\frac{\partial u}{\partial \phi}\right] \tag{8}$$

$$M_x = -D\left[\frac{\partial^2 w}{\partial x^2} + \frac{\nu}{a^2}\left(\frac{\partial v}{\partial \phi} + \frac{\partial^2 w}{\partial \phi^2}\right)\right]$$

$$M_\phi = -D\left[\frac{1}{a^2}\left(\frac{\partial v}{\partial \phi} + \frac{\partial^2 w}{\partial \phi^2}\right) + \nu\frac{\partial^2 w}{\partial x^2}\right]$$

$$M_{x\phi} = -D(1-\nu)\frac{1}{a}\left(\frac{\partial v}{\partial x} + \frac{\partial^2 w}{\partial x\,\partial \phi}\right)$$

Substituting the expressions for N_x, N_ϕ, $N_{x\phi}$, M_x, M_ϕ and $M_{x\phi}$ into Eq. (6), we obtain the following differential equations of bending of a circular cylindrical shell :

$$\frac{\partial^2 u}{\partial x^2} + \frac{1-\nu}{2a^2}\frac{\partial^2 u}{\partial \phi^2} + \frac{1+\nu}{2a}\frac{\partial^2 v}{\partial x \partial \phi} - \frac{\nu}{a}\frac{\partial w}{\partial x} = -\frac{p_x}{Et}(1-\nu^2) \tag{9a}$$

$$\frac{1+\nu}{2}\frac{\partial^2 u}{\partial x \partial \phi} + a\,\frac{1-\nu}{2}\frac{\partial^2 v}{\partial x^2} + \frac{1}{a}\frac{\partial^2 v}{\partial \phi^2} - \frac{1}{a}\frac{\partial w}{\partial \phi} + \frac{t^2}{12a}\left(\frac{\partial^3 w}{\partial x^2 \partial \phi} + \frac{\partial^3 w}{a^2 \partial \phi^3}\right) + \frac{t^2}{12a}\left[(1-\nu)\frac{\partial^2 v}{\partial x^2} + \frac{\partial^2 v}{a^2 \partial \phi^2}\right] = -\frac{p_y(1-\nu^2)}{Et} \tag{9b}$$

$$\nu\frac{\partial u}{\partial x} + \frac{\partial v}{a\,\partial \phi} - \frac{w}{a} - \frac{t^2}{12}\left(a\frac{\partial^4 w}{\partial x^4} + \frac{2}{a}\frac{\partial^4 w}{\partial x^2 \partial \phi^2} + \frac{\partial^4 w}{a^3 \partial \phi^4}\right) - \frac{t^2}{12}\left(\frac{2-\nu}{a}\frac{\partial^3 v}{\partial x^2 \partial \phi} + \frac{\partial^3 v}{a^3 \partial \phi^3}\right) = -\frac{p_z(1-\nu^2)}{Et} \tag{9c}$$

There are many shell theories that have been developed such as Sanders, Flügge [9], etc., and these show small discrepancy when compared term by term. This is due to the difference in expressing the relationship between the strain and stress resultants.

The well known 'Donnell equation' has been generated by neglecting the terms containing $t^2/12a^2$ in Eq. (9), making it simpler and more applicable to numerical solutions. However, many investigations have demostrated certain shortcomings of the equation.

2.4 CIRCULAR CYLINDRICAL SHELLS UNDER LOCALIZED LOADS

Attachments, which can be divided into two categories- integral and non-integral ones, are the structural elements which connect a vessel to its support. When attachments, such as nozzles, lugs, skirts, saddles, etc. exist, a vessel will have concentrated loads which are assumed to be directly transmitted to the vessel across the area of contact. Therefore, in complete design of many pressure vessels and shell structures the effect of attachments has to be considered.

Early studies of shell structures under localized loading were conducted in the late thirties. A.Aas Jakobsen expressed equilibrium equations in terms of the radial displacement alone in order to reduce the large amount of work necessary to obtain numerical results. In 1941, he demonstrated how concentrated load problems could be solved using his technique. S.W. Yuan [21] in 1946, solved Donnell's single eighth order differential equation in terms of w for an infinitely long cylinder. The two concentrated loads, equal and opposite, were represented by Fourier method. The definite integrals for radial deflection are utilized by Cauchy's theorem of residue. In 1956, Yuan and Ting [22] reinvestigated the problem, this time by using Flugge's equations.

From 1952 to 1954 a series of papers were published by Hoff, Kempner and Pohle [10]. Close form solutions were given for the displacement, moment and membrane stress quantities for the thin circular cylindrical shell subjected to radial forces or circumferential moments using Donnell's differential equation.

Using the iteration technique developed by Jakobsen, Bijlaard [4] solved the problem of a simply supported cylindrical shell subjected to radial loading, or moment loading in longitudinal and circumferencial directions, assuming Fourier series expansion for the displacements.

In discussion of the first paper published by Bijlaard, authors Weil, Laupa and Murphy proposed retaining the last term on the left hand side of Eq. (9,b), which has been neglected in [4], to be able to get an exact and finite value for w for a finite load. Later the same author [2,3,5 and 6] gave a variety of numerical results for the most practical problems as well as a comparison with the experimental results obtained with Cranch [6] and by Schoessow and Kooistra.

The solution procedure presented in Nash and Bridgland's work in 1960 [14] shows similarities to that of Yuan's, but in many ways the type of loading and differential equations are not the same. Flugge's differential equations have been used instead of simpler Donnell equation.

In 1965, Wichman, Hopper and Marshon [19] presented their results in WRC-107, following Bijlaard's work and considering a more idealized and simplified solution of the problem. Bijlaard's data has been modified based on the available experimental work. It was found that in some cases discrepancies can be quite significant.

The former study, which has been done in 1974 by W.G.Dodge [8] follows the simplified analysis procedure given in ASME Boiler and Pressure Vessel Code, Section III, and defines three stress indices for thrust, longitudinal and circumferential moment loadings. For bending moments, stress indices are defined as "The ratio of maximum stress intensity in the component due to a moment loading to the nominal stress in the straight pipe subjected to the same moment loading". Whereas, stress index defined for a radial load uses the average shearing stress in the pipe as the normalizing factor. Although these stress indices are based on a numerical parameter study, using analytical results obtained in [4] as a guide, numerical computations have been redone with the following modifications to Bijlaard's equations: (i) The last term on the left hand side of equation (9,b) has been retained, as recommended by Weil et. al. (ii) The angular effect on distribution of loadings along the circumferential direction is found significant and considered by adding new terms in calculations of resultant loads, (iii) Since the stress-index method covers the beam bending effect on the pipe separately, it has been subtracted out from Bijlaard's results.

The later work [16] follows the same solution procedure outlined in [8]. However, the normalizing base of Dodge's stress index is changed to the nominal bending stress in the lug. The analysis of the results presented in [16] shows conservative results in comparison with [8,19]. Addition of a new paragraph to ASME Boiler and Pressure Vessel Code, Section III, is recommended for integral attachments.

Chapter III

RING ATTACHMENTS TO PRESSURE VESSELS

3.1 INTRODUCTION

A literature survey shows that quite satisfactory results have been obtained on stress analysis of shells subjected to concentrated loading, line loading, radial loading and circumferential and longitudinal moments but not much work is available on the subject of cylindrical shells with axial loading applied along circumferential bands generated by the attachments.

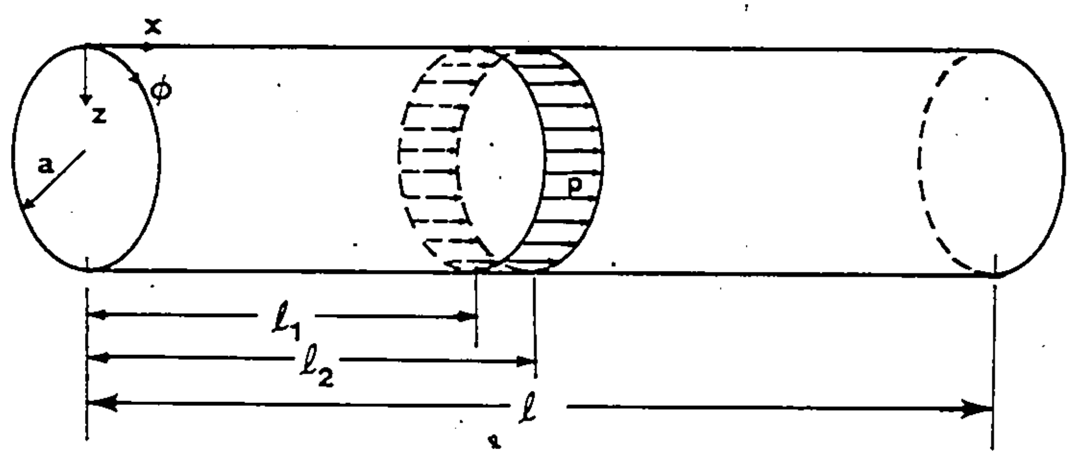

Figure 3: Cylindrical shell subjected to band load along the generatrix

The shell, shown in Fig. (3), is defined by three axes x, ϕ and z. a is the mean radius, t is the thickness and ℓ is the total length of the shell.

Dimensionless quantities ℓ_1/ℓ and ℓ_2/ℓ are introduced to define the position of loading along the generatrix. The cylindrical shell considered here is fixed along the axial direction at one end, i.e. at x=0 axial deformation is zero, and it is free at the other end. At the fixed end, a force boundary condition is imposed to satisfy the support condition, i.e. $N_x = P_t$, where P_t is the total load applied to the shell.

3.2 DERIVATION OF THE SINGLE EIGHTH ORDER DIFFERENTIAL EQUATION

For the solution of the current problem, the similar iteration technique used in [21] and [4] can be applied to Eq. (9) without neglecting any of the terms containing $t^2/12a^2$, at the beginning. But, since the loading considered in this study is along the axial direction only, P_y and P_z are set to zero.

The following steps have been taken to develop a single eighth order differential equation from the three differential equations of the thin-shell theory [17]:

a)

i) Apply $\partial^2/\partial x^2$ to Eq.(9,a), solve for $\partial^4 v/a\,\partial x^3 \partial\phi$

ii) Apply $\partial^2/a^2\partial\phi^2$ to Eq.(9,a), solve for $\partial^4 v/a^3 \partial x \partial\phi^3$

iii) Apply $\partial^2/ a\partial x \partial \phi$ to Eq.(9,b), substitute the results obtained in step (i) and (ii) into the latter, and multiply by $a\,(1+\nu)/\,(\nu-1)$, to obtain

$$a\,\nabla^4 u = \nu \frac{\partial^3 w}{\partial x^3} - \frac{\partial^3 w}{a^2 \partial x \partial \phi^2} + \frac{1+\nu}{1-\nu}\,\frac{t^2}{12\,a^2}\left(\frac{\partial^5 w}{\partial x^3 \partial \phi^2} + \frac{\partial^5 w}{a^2 \partial x \partial \phi^4}\right)$$

$$- \frac{a}{D^*}\frac{\partial^2 p_x}{\partial x^2} - \frac{2}{aD(1-\nu)}\frac{\partial^2 p_x}{\partial \phi^2} + \qquad (10)$$

$$\frac{1+\nu}{1-\nu}\,\frac{t^2}{12a^2}\left[(1-\nu)\frac{\partial^4 v}{\partial x^3 \partial \phi} + \frac{\partial^4 v}{a^2 \partial x \partial \phi^3}\right]$$

where

$$D^* = Et\,/\,(1-\nu^2)$$

b)

i) Apply $\partial^2/\partial x^2$ to Eq.(9,b), solve for $\partial^4 u/ a\partial x^3 \partial \phi$

ii) Apply $\partial^2/ a^2 \partial \phi^2$ to Eq.(9,b), solve for $\partial^4 u/\partial x \partial \phi^3$

iii) Apply $\partial^2/ a\partial x \partial \phi$ to Eq.(9,a), insert the results obtained in (i) and (ii), into the latter and multiply by $a\,(1+\nu)/\,(1-\nu)$ to obtain

$$a\,\nabla^4 v = (2+\nu)\frac{\partial^3 w}{a\,\partial x^2 \partial \phi} + \frac{\partial^3 w}{a^3 \partial \phi^3} - \frac{t^2}{12a^2}\left(\frac{2a}{1-\nu}\frac{\partial^5 w}{\partial x^4 \partial \phi} + \right.$$

$$\left.\frac{3-\nu}{1-\nu}\,\frac{\partial^5 w}{a\;\partial x \partial \phi^3} + \frac{\partial^5 w}{a^3 \partial \phi^5}\right) + \frac{1}{D^*}\frac{1+\nu}{1-\nu}\frac{\partial^2 p_x}{\partial x \partial \phi} - \qquad (11)$$

$$\frac{2t^2}{12a(1-\nu)}\left[(1-\nu)\frac{\partial^4 v}{\partial x^4} + \frac{\partial^4 v}{a^2 \partial x^2 \partial \phi^2}\right] -$$

$$\frac{t^2}{12a^3}\,\frac{1+\nu}{1-\nu}\left[\,(1-\nu)\frac{\partial^4 v}{\partial x^2 \partial \phi^2} + \frac{1}{a^2}\frac{\partial^4 v}{\partial \phi^4}\right]$$

where

$$D^* = Et\,/\,(1-\nu^2)$$

c)

i) Apply $\partial/\partial x$ to Eq.(10),

ii) Apply $\partial/a\partial\phi$ to Eq.(11),

iii) Apply the operation $a\nabla^4$ to Eq.(9,c) and insert the results obtained in (i) and (ii) into the latter, where ∇^4 denotes

$$\left(\frac{\partial^2}{\partial x^2}+\frac{\partial^2}{a^2\partial\phi^2}\right)^2$$

Finally, the following single eighth order differential equation is obtained

$$\begin{aligned}
&\nabla^8 w+\frac{12(1-\nu^2)}{a^2t^2}\frac{\partial^4 w}{\partial x^4}+\frac{6+\nu-\nu^2}{a^4}\frac{\partial^6 w}{\partial x^4\partial\phi^2}+\frac{7+\nu}{a^6}\frac{\partial^6 w}{\partial x^2\partial\phi^4}+\\
&\frac{2}{a^8}\frac{\partial^6 w}{\partial\phi^6}+\frac{12\nu}{at^2D^*}\frac{\partial^3 p_x}{\partial x^3}-\frac{12}{a^3t^2D^*}\frac{\partial^3 p_x}{\partial x\partial\phi^2}+\\
&\frac{1}{a^3D^*}\frac{1+\nu}{1-\nu}\frac{\partial^3}{\partial x\partial\phi^2}\left[(2-\nu)\frac{\partial^2 p_x}{\partial x^2}+\frac{1}{a^2}\frac{\partial^2 p_x}{\partial\phi^2}\right]-\frac{2-\nu}{a^3}\frac{\partial^3\psi_1}{\partial x^2\partial\phi}-\\
&-\frac{1}{a^5}\frac{\partial^3\psi_1}{\partial\phi^3}+\frac{t^2}{12a^5}\left[\frac{2a(2-\nu)}{1-\nu}\frac{\partial^8 w}{\partial x^6\partial\phi^2}+\frac{(2-\nu)(3-\nu)}{a(1-\nu)}\frac{\partial^8 w}{\partial x^4\partial\phi^4}+\right.\\
&\left.\frac{2-\nu}{a^3}\frac{\partial^8 w}{\partial x^2\partial\phi^6}+\frac{2}{a(1-\nu)}\frac{\partial^8 w}{\partial x^4\partial\phi^4}+\frac{3-\nu}{a^3(1-\nu)}\frac{\partial^8 w}{\partial x^2\partial\phi^6}+\frac{1}{a^5}\frac{\partial^8 w}{\partial\phi^8}\right]-\\
&\frac{12}{at^2}\left[\frac{\nu t^2}{12a^3}\frac{1+\nu}{1-\nu}\psi_2-\frac{2t^2}{12a^3(1-\nu)}\psi_2-\frac{t^2}{12a^5}\frac{1+\nu}{1-\nu}\left[(1-\nu)\frac{\partial^5 v}{\partial x^2\partial\phi^3}+\right.\right.\\
&\left.\left.\frac{1}{a^2}\frac{\partial^5 w}{\partial\phi^5}\right]\right]=0
\end{aligned}\tag{12}$$

where

$$\Psi_1 = \frac{2t^2}{12a(1-\nu)} \left[(1-\nu) \frac{\partial^4 v}{\partial x^4} + \frac{\partial^4 v}{a^2 \partial x^2 \partial \phi^2} \right] +$$

$$\frac{t^2}{12a^3} \frac{1+\nu}{1-\nu} \left[(1-\nu) \frac{\partial^4 v}{\partial x^2 \partial \phi^2} + \frac{1}{a^2} \frac{\partial^4 v}{\partial \phi^4} \right]$$

$$\Psi_2 = (1-\nu) \frac{\partial^5 v}{\partial x^4 \partial \phi} + \frac{\partial^5 v}{a^2 \partial x^2 \partial \phi^3} .$$

$$D^* = Et / (1-\nu^2)$$

Recall that for thin shells $t/a < 1/10$, so that $t^2/12a^2 = 1/1200$, therefore the contribution of the terms containing $t^2/12a^2$ in the above equation can be neglected.

Furthermore the derivatives of displacements with respect to ϕ can also be eliminated in case of axisymmetric loading. Then, Eq. (12) becomes

$$\frac{d^8 w}{dx^8} + \beta \frac{d^4 w}{dx^4} + \psi \frac{d^3 p_x}{dx^3} = 0 \tag{13}$$

where,

$$\beta = \frac{12(1-\nu^2)}{a^2 t^2}$$

$$\psi = \frac{12\, \nu}{a t^2 D^*} \quad ., \quad D^* = Et/(1-\nu^2)$$

The equations derived in [4,21], using the same iteration technique explained above, are somewhat different than Eq. (13) in the text. It is due to the fact that the shell is subjected to radial loading in References [4,21].

3.3 EQUILIBRIUM EQUATIONS

Due to the symmetry of the problem circumferential displacement, v, and its derivatives, as well as the derivatives of u and w with respect to ϕ are zero. Therefore Eq. (9,b) is identically satisfied, and Eq. (9,a) and (9,c) become

$$\frac{d^2u}{dx^2} - \frac{\nu}{a}\frac{dw}{dx} + \frac{p_x(1-\nu^2)}{Et} = 0 \qquad (14)$$

$$\nu\frac{du}{dx} - \frac{w}{a} - \frac{at^2}{12}\frac{d^4w}{dx^4} = 0 \qquad (15)$$

3.4 EXTERNAL LOADING

The external loading, P_x, in Eq. (13), applied on a band along the circumferential, can be expressed as

$$p_x = \Sigma\, P_k \sin\frac{k\pi x}{\ell} \qquad (16)$$

p = intensity of force per unit surface

ℓ_1/ℓ = denotes starting position of external load

$\frac{\ell_2 - \ell_1}{\ell}$ = band width

$$p_k = \frac{4p}{k\pi}\sin\frac{k\pi}{2\ell}(\ell_1 + \ell_2)\sin\frac{k\pi}{2\ell}(\ell_2 - \ell_1)$$

This allows the solution for deflections to be written in terms of Fourier series.

3.5 RADIAL AND AXIAL DEFORMATIONS

The single eighth order differential equation developed in Section (3,2), Eq. (13), can be solved developing w in cosine series as

$$w = A_0 + \Sigma\, w_k \cos \frac{k\pi x}{\ell} \tag{17}$$

Insertion of Eq. (16) and (17) into (13) yields

$$\Sigma \left[w_k \left(\frac{k\pi}{\ell}\right)^8 + \beta\, w_k \left(\frac{k\pi}{\ell}\right)^4 - \psi\, P_k \left(\frac{k\pi}{\ell}\right)^3 \right] \cos \frac{k\pi x}{\ell} = 0 \tag{18}$$

Equation (18) has to be satisfied for all values of x which implies that the expression prior to the cosine term has to be zero, and can be solved for the unknown Fourier coefficient w_k ,

$$w_k = \frac{\psi\, P_k}{\left(\frac{k\pi}{\ell}\right)^5 + \beta\left(\frac{k\pi}{\ell}\right)} \tag{19}$$

Going back to the equilibrium equations, it is observed that Eq. (14) contains an even derivative of u and an odd derivative of w. On the contrary, Eq. (15) contains an odd derivative of u and an even derivative of w. Therefore, for the simplicity of the solution, axial deflection can be assumed to be in sine series with an additional constant C_0 as

$$u = C_0 x + \Sigma\, u_k \sin \frac{k\pi x}{\ell} \tag{20}$$

By expressing u as such, the boundary condition, u=0 at x=0, has also been satisfied.

Introducing Eq. (17) and (20) into Eq. (15) yields

$$\left(\nu C_0 - \frac{1}{a} A_0\right) + \Sigma \left[u_k \left(\frac{k\pi}{\ell}\right) - \frac{w_k}{a} - \frac{at^2}{12} w_k \left(\frac{k\pi}{\ell}\right)^4 \right] \cos \frac{k\pi x}{\ell} = 0 \tag{21}$$

There seems only one way to satisfy Eq. (21) for all values of x, that is by setting the first term and the term prior to cosine equal to zero. This yields the following two equations

$$\nu C_0 - \frac{1}{a} A_0 = 0 \tag{22}$$

$$\Sigma \left[u_k \left(\frac{k\pi}{\ell}\right) - \frac{w_k}{a} - \frac{at^2}{12} w_k \left(\frac{k\pi}{\ell}\right)^4 \right] \cos \frac{k\pi x}{\ell} = 0 \tag{23}$$

Equation (23) can be solved for u_k, yielding

$$u_k = w_k \left[\frac{\ell}{k\pi a} + \frac{at^2}{12} \left(\frac{k\pi}{\ell}\right)^3 \right] \tag{24}$$

Applying the force boundary condition to Eq. (8,a) at x=0, the following expression for the two constants C_0 and A_0 can be obtained,

$$C_0 - \nu \frac{A_0}{a} = P_t \frac{1-\nu^2}{Et} + \Sigma \left(\frac{\nu w_k}{a} - u_k \frac{k\pi}{\ell} \right) \tag{25}$$

Substitution of Eq. (22) to Eq. (25) determines C_0 as

$$C_0 = \frac{P_t}{Et} + \frac{1}{1-\nu^2} \Sigma \left(\frac{w_k \nu}{a} - u_k \frac{k\pi}{\ell} \right) \tag{26}$$

Having obtained the expressions for the unknowns C_0, A_0, w_k and u_k, u and w can be expressed, in nondimensional form, as follows

$$\frac{w}{a} = \nu C_0 + \frac{48\nu(1-\nu^2)P/E}{\pi^2} \Sigma \frac{\sin \frac{k\pi}{2\ell}(\ell_1+\ell_2) \quad \sin \frac{k\pi}{2\ell}(\ell_2-\ell_1)}{k^2 \left[(k\pi)^4 \left(\frac{a}{\ell}\right)^2 \left(\frac{t}{\ell}\right)^3 + 12\,(1-\nu^2)\,\frac{t}{\ell} \right]} \cos \frac{k\pi x}{\ell} \tag{27}$$

$$\frac{u}{a} = C_0 \left(\frac{\ell}{a}\right) \left(\frac{x}{\ell}\right) + \Sigma \left(\frac{u_k}{a} \right) \sin \frac{k\pi x}{\ell} \tag{28}$$

where u_k and C_0 are defined in Eq. (24) and (26), respectively.

3.6 STRESSES IN THE CIRCULAR CYLINDRICAL SHELLS

Finally, substitution of equations (27) and (28) to equation (8) in case of axisymmetric loads gives the following expressions for the stresses

$$\frac{M_x}{Et^2} = \frac{(\frac{t}{a})\ \pi^2\ (\frac{a}{\ell})^2}{12(1-\nu^2)}\ \Sigma\ (\frac{w_k}{a})\ k^2 \sin\frac{k\pi x}{\ell} \tag{29}$$

$$\frac{M_\phi}{Et^2} = \nu\ \frac{M_x}{Et^2} \tag{30}$$

$$\frac{N_x}{Et} = \frac{1}{1-\nu^2}\ [\ C_0\ (1-\nu^2) + \Sigma\ [\ u_k\ (\frac{k\pi}{\ell}) - w_k\ ]\ \cos\frac{k\pi x}{\ell}\ ] \tag{31}$$

$$\frac{N_\phi}{Et} = \frac{1}{1-\nu^2}\ \Sigma\ [\ \nu\ u_k\ (\frac{k\pi}{\ell}) - \frac{w_k}{a}\ ]\ \cos\frac{k\pi x}{\ell} \tag{32}$$

Chapter IV

INTEGRAL LUG ATTACHMENTS TO PRESSURE VESSELS

4.1 INTRODUCTION

Various integral and non-integral attachments usually generate localized loadings in a vessel. In the third chapter, the special case of an axially symmetric shell with axial loading applied along circumferential bands, has been considered and a close form solution is discussed.

Vertical vessels supported by integral lug attachments, which is integral by means of a full penetration weld, generate local shear forces and moments. It is the subject of this chapter to analyse the stresses caused by axial moment alone because of the presence of four integral lugs separated 90 degrees apart along the circumferential direction, as shown in Fig. (4).

Although the Code has published the work presented in [8,16 and 19] as recommended practice, due to large discrepancies in the results, it is found essential to reinvestigate the problem.

The stress analysis technique employed here is a widely used numerical method in the literature. Because of its diversity and flexibility finite element method is well suited to the present problem. The existing finite element program

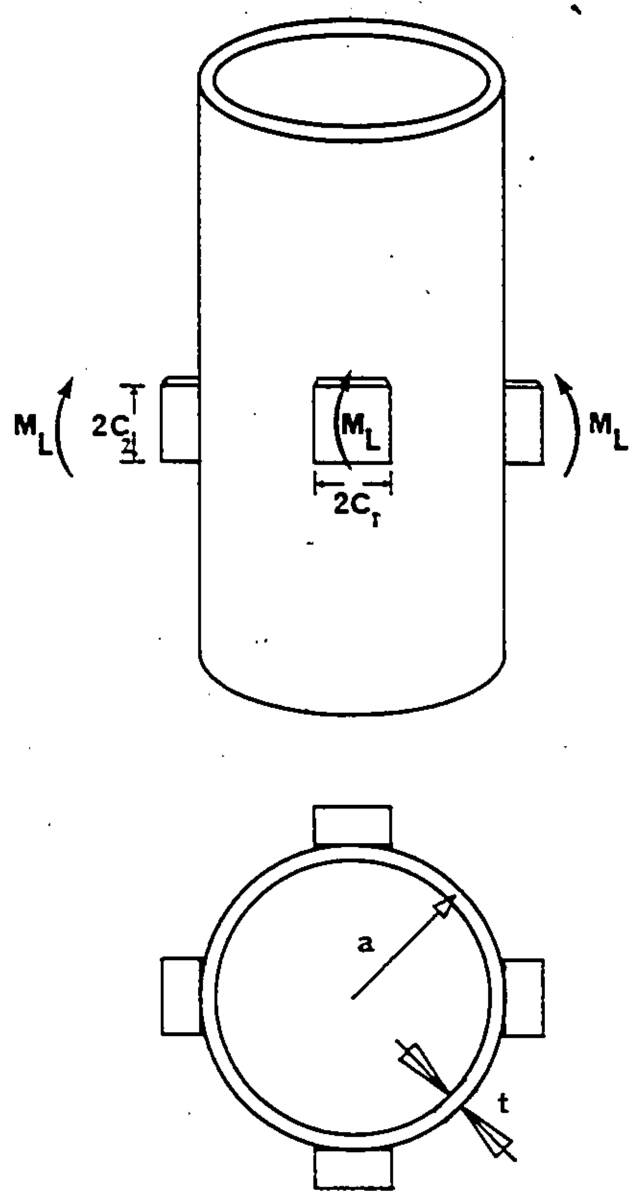

Figure 4: Typical lug arrangement

[15] is modified to fit for the geometry of the shell and the type of loading.

In setting up the model, a curved shell element and a simpler version of 'Front Solver' solution technique is used. A brief discussion on this techinique is available in Appendix (A) for the interested reader.

4.2 THE FINITE ELEMENT METHOD

For many engineering problems, it becomes extremely difficult to obtain exact-close form solutions. The difficulty arises from the fact that either the geometry or some other feature of the problem is irregular or arbitrary.

Now that the digital computers are readily available, numerical methods have become the preferred methods for solution. Finite Element method, which was developed in early 60's, is the most widely used numerical method in the literature.

In this method the continuum is divided into small, interconnected elements. With the combination of these small elements complex shapes can be analysed within the accuracy of the method. For each element an approximate function is assumed to express the unknown field, usually the displacement field. These approximate functions, known as interpolation functions, are defined at specified points called nodal points. Number of nodal points and their positions within the element change from one type of element to the other.

There are four basic approaches in defining the element properties -direct, variational, weighted residual and energy balance.

In direct stiffness or displacement method, displacements of each nodal points are represented by a stiffness matrix which can be generated using either the principle of virtual work or principle of minimum potential energy. Since at each node equilibrium and compatibility conditions have to be satisfied, a set of algebraic equations are obtained which then can be solved by several techniques.

In the recent years the last three approaches- variational, weighted residual and energy balance- have achieved a fair amount of consideration in extending the range of applicability of the method. Detailed information on these three approaches can be found in [11,23] and the references therein.

In short, the following steps have to be considered in the present method:

a) Discretizing the domain and choosing the element shape,

b) Selecting appropriate interpolation functions,

c) Finding the element properties- derivation of the element characteristic equations,

d) Assembly and boundary conditions,

e) Solution technique.

4.2.1 ELEMENT PROPERTIES

A curved shell element used in this analysis has five degrees of freedom at each node, three displacements u, v and w along x, y and z and two rotations α and β. In the derivation of a curved shell element, direct displacement method has been used by minimizing total potential energy. Considering the shell element in Fig. (5), ξ, η and ζ are defined as the curvilinear coordinates in the middle plane, using the same nomenclature and the sign convention as in Ref. [23].

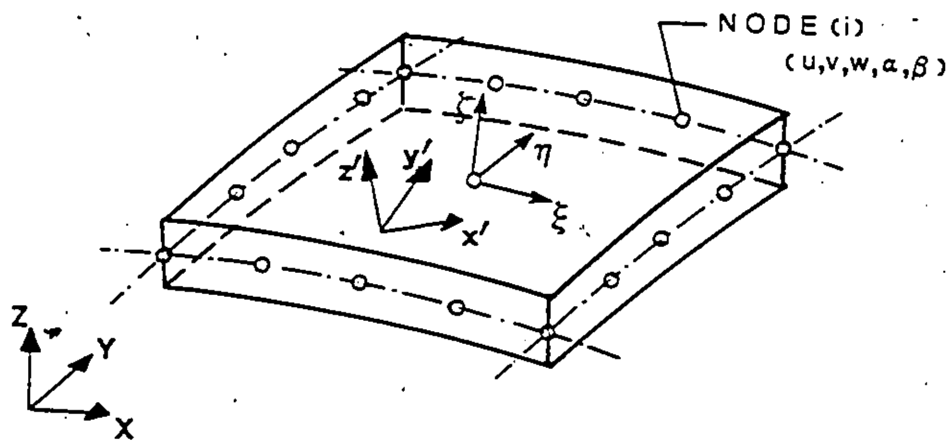

Figure 5: Curved shell element with degrees of freedom

The relation between the Cartesian coordinates and curvilinear coordinates, and the displacement u, v, w at any point in the element in terms of nodal displacements can be written as follows:

$$\begin{Bmatrix} x \\ y \\ z \end{Bmatrix} = \Sigma \; N_i \begin{Bmatrix} x_i \\ y_i \\ z_i \end{Bmatrix} + \Sigma \; N_i \; \zeta/2 \; V_{3i} \tag{33}$$

$$\begin{Bmatrix} u \\ v \\ w \end{Bmatrix} = \Sigma \; N_i \begin{Bmatrix} u_i \\ v_i \\ w_i \end{Bmatrix} + \Sigma \; N_i \; \zeta \; t_i/2 \left[V_{1i}, \; - V_{2i} \right] \begin{Bmatrix} \alpha_i \\ \beta_i \end{Bmatrix} \tag{34}$$

where N_i is a shape function in terms of curvilinear coordinates (see Appendix B) and the two rotations α_i and β_i are the rotations of the vector V_{3i} which connects upper and lower surfaces along the thickness t. V_{1i} and V_{2i} with V_{3i} form orthogonal axes and define the direction cosines of the local axes. Since curvilinear coordinate system need not be mutually perpendicular, another coordinate system - (') notation coordinates- has been used to describe the state of stress and strain in the element itself.

Keeping in mind the usual assumption of thin shell analysis - the strain along the thickness being negligible- strain-displacement and stress-strain relationships, in 3-D stress-strain analysis, [18], are given as follows

$$\epsilon' = \begin{bmatrix} \epsilon_{x'} \\ \epsilon_{y'} \\ \gamma_{x'y'} \\ \gamma_{x'z'} \\ \gamma_{y'z'} \end{bmatrix} = \begin{bmatrix} \dfrac{\partial u'}{\partial x'} \\ \dfrac{\partial v'}{\partial y'} \\ \dfrac{\partial u'}{\partial y'} + \dfrac{\partial v'}{\partial x'} \\ \dfrac{\partial w'}{\partial x'} + \dfrac{\partial u'}{\partial z'} \\ \dfrac{\partial w'}{\partial y'} + \dfrac{\partial v'}{\partial z'} \end{bmatrix} \tag{35}$$

where $\epsilon_{x'}$ and $\epsilon_{y'}$ are unit elongations in the x', y' directions respectively and $\gamma_{x'y'}\gamma_{x'z'}$ and $\gamma_{y'z'}$ are the three unit shear strains along x', y' and z'.

$$\sigma' = \begin{Bmatrix} \sigma_{x'} \\ \sigma_{y'} \\ \tau_{x'y'} \\ \tau_{x'z'} \\ \tau_{y'z'} \end{Bmatrix} = D' (\epsilon' - \epsilon'_0) + \sigma'_0 \tag{36}$$

$$D' = \frac{E}{1-\nu^2} \begin{bmatrix} 1 & \nu & 0 & 0 & 0 \\ & 1 & 0 & 0 & 0 \\ & & \frac{1-\nu}{2} & 0 & 0 \\ \text{SYM.} & & & \frac{1-\nu}{2.4} & 0 \\ & & & & \frac{1-\nu}{2.4} \end{bmatrix}$$

Elasticity matrix, D', is derived from 3-D analysis by simply substituting $\sigma_{z'}=0$ into the general form of D'.

Stiffness matrix, S, in usual notation can be defined as

$$S = \int_V B'^T D' B' \, dx' dy' dz' \qquad (37)$$

where

$$\varepsilon' = B' a^e$$

a^e being the displacements of an element.

One of the important parts of any finite element analysis is the evaluation of integrals involved in Eq. (37). The accuracy of the results are directly proportional to the accuracy of the integrations. It is sometimes possible to obtain close-form exact expressions. But, when it is extremely difficult and lengthy, numerical procedures are available. Compared to other procedures, Gaussian formulation leads to better accuracy within the limits of -1 and +1.

In order to make use of the above formulation, B' matrix, which is presently in global coordinates in Eq. (37), has to be expressed in terms of curvilinear coordinates.

In order to do so, two sets of transformations are necessary to relate the derivatives of local displacements with respect to local coordinates to the derivatives of global displacements with respect to curvilinear coordinates.

a) The derivatives of global displacements with respect to curvilinear coordinates have to be established through Jacobian matrix, J.

b) After the directions of the local axes have been defined, the derivatives of local displacements have to be expressed in terms of the global derivatives of displacements.

Hence,

$$\begin{bmatrix} \frac{\partial u'}{\partial x'} & \frac{\partial v'}{\partial x'} & \frac{\partial w'}{\partial x'} \\ \frac{\partial u'}{\partial y'} & \frac{\partial v'}{\partial y'} & \frac{\partial w'}{\partial y'} \\ \frac{\partial u'}{\partial z'} & \frac{\partial v'}{\partial z'} & \frac{\partial w'}{\partial z'} \end{bmatrix} = \theta^T \, J^{-1} \begin{bmatrix} \frac{\partial u}{\partial \xi} & \frac{\partial v}{\partial \xi} & \frac{\partial w}{\partial \xi} \\ \frac{\partial u}{\partial \eta} & \frac{\partial v}{\partial \eta} & \frac{\partial w}{\partial \eta} \\ \frac{\partial u}{\partial \zeta} & \frac{\partial v}{\partial \zeta} & \frac{\partial w}{\partial \zeta} \end{bmatrix} \theta \qquad (38)$$

Where

$$\theta = [\, V_1 \, , V_2 \, , \, V_3 \,]$$

$$[J] = \begin{bmatrix} \frac{\partial x}{\partial \xi} & \frac{\partial y}{\partial \xi} & \frac{\partial z}{\partial \xi} \\ \frac{\partial x}{\partial \eta} & \frac{\partial y}{\partial \eta} & \frac{\partial z}{\partial \eta} \\ \frac{\partial x}{\partial \zeta} & \frac{\partial y}{\partial \zeta} & \frac{\partial z}{\partial \zeta} \end{bmatrix}$$

From the components of the left hand side of Eq. (38), B' matrix can be found.

The last step before the integration procedure is expressing the infinitesimal volume in terms of curvilinear coordinates. This can easily be accomplished by the formula given below

$$dx\, dy\, dz = \det |J| \; d\xi\, d\eta\, d\zeta \qquad (39)$$

In the analysis of shell structures, strains and stresses are generally given in terms of a local coordinate system and therefore, further transformation of stresses to global coordinates is not considered in this study.

Once the element properties have been defined, the consistent load matrix can be obtained as

$$F = \int N^T q \; dV \tag{40}$$

where q is the distributed load

The flow chart of the computer program used in this analysis for calculating the element stiffness and consistent load matrix is shown in Fig. (C-1) of Appendix C.

4.2.2 FINITE ELEMENT MODELLING

Having obtained the element properties, we are now ready to discretize the domain.

Due to the symmetry of the problem only a 90 degree segment of the vessel is meshed, as shown in Fig. (6).

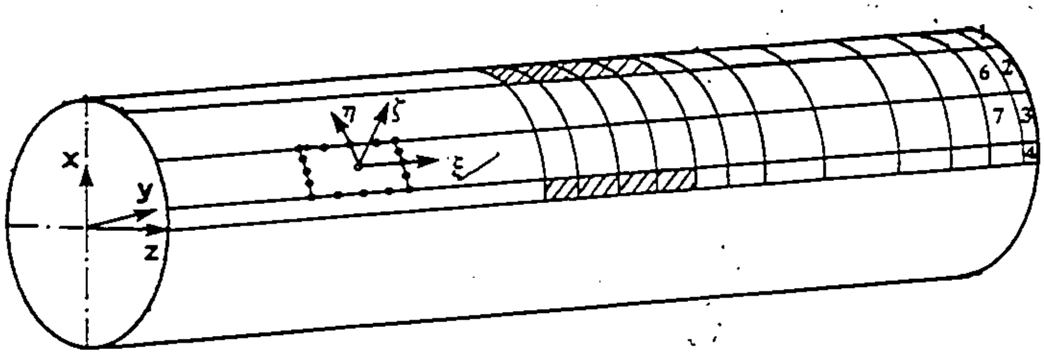

Figure 6: Typical finite element model considered

Typically 22 rings and 4 elements in each ring, a total of 88 elements are taken. Lugs are placed far enough from the ends to avoid end effects in the results. Axial moment loading caused by the lugs considered in this study is generated by a radial load that is distributed symmetrically with respect to the mid point of the loaded area. The total moment loading, M_L, for values of β =0.05,0.1 and 0.2 is distributed on 4,8 and 12 elements respectively. The shaded area in Fig. (6) represents the case β =0.10.

Shorter elements are preferred in the vicinity of the loading area and at the ends. The vessel itself is considered to be free at one end and fixed along y on the other end.

Chapter V

DISCUSSION OF RESULTS

5.1 RING ATTACHMENTS

5.1.1 GENERAL

The analytical procedure discussed in Chapter III has been used to generate the numerical results. The variables considered are:

1. Distance of loading from one end of the shell (ℓ_1/ℓ), varying as 0.3,0.5,0.7 and 0.9.
2. Width of the band over which the load is distributed ($\ell_2-\ell_1/\ell$), varying as 0.02,0.04,0.08 and 0.10.
3. Length to radius ratio of the shell, varying as 4,8,10 and 80.
4. Radius to thickness ratio of the shell, varying as 10,20,40 and 80.

The value of (P/E) and Poisson's ratio, ν, are taken as 150000 and 0.3, respectively.

In most cases an absolute convergence has been achieved with few terms in the series. However, for long shells, ℓ/a= 80, the calculations had to be extended up to 250 terms.

From the above combinations of variables, only 64 cases are presented here. Figures (8) through (23) represent the general trend of the effects of each variable. The results generated for the remaining cases can be found in Appendix (E).

5.1.2 INTERPRETATION OF RESULTS

The typical distribution of bending moment, M_x/Et, and membrane force N_ϕ/Et are plotted in Fig. (7). The value of M_x/Et is plotted along the vertical line on the right hand side. Whereas, for N_ϕ/Et, vertical axis on the left hand side has to be used.

A quick look at Fig. (7) and (20) indicates that M_x/Et and N_ϕ/Et are small compared to N_x/Et. For example, for the case where $\ell_1/\ell = 0.3$ (Fig. (20)), the maximum value of N_x/Et is $0.110*10^{-4}$, whereas from Fig.(7), for the same parameters, the maximum value of M_x/Et and N_ϕ/Et are $0.153*10^{-6}$ and $0.108*10^{-5}$, respectively. This type of behavior was expected for the loading considered here.

Although bending moment M_x/Et is small, the variation seen in Fig. (7) has significant effect on radial deformation in the vicinity of loading. This effect on w can be explained by recalling that M_x/Et is related to the second derivatives of radial deformation. However, the results presented in Figs. (8) through (23) for radial deformation indicate that this effect vanishes when $\ell/a > 10$. It is also observed that increase in a/t results in lower peak values for w in the vicinity of loading.

As expected, in the region $x/\ell < \ell_2/\ell$, it is found that membrane force, N_x/Et, is equal to the total load applied on the shell and outside this region it is zero.

Bending moment, M_ϕ/Et, is not shown in figures. It can be calculated by using the simple expression given in Eq. (30).

In Figs. (8) through (23) axial and radial deformations are plotted against the nondimensional distance parameter x/ℓ. Due to large differences in the magnitudes of deformations, different scales are chosen to represent u/a and w/a. The scale for u/a is given on the left hand side and that for w/a on the hand right side. In addition, the membrane force, N_x/Et, is plotted and has to be read from the vertical axis on the left hand side.

From these figures it is observed that axial deformation is linearly increasing up to the end of the loading area ($x/\ell = \ell_2/\ell$). It reaches its maximum value at $x/\ell = \ell_2/\ell$ and remains constant thereon. However for relatively long shells, axial deformation decreases towards the end.

In the region where $x/\ell < \ell_1/\ell$, radial deformation starts with a constant value. As it gets close to the load, however, it slighly increases, due to increase in bending moment.

Since N_x/Et is the dominant force, it is expected to have large axial deformation. The results presented here indicate this fact and show two orders of magnitude difference between the deformations.

In order to analyse the effect of individual variables on the deformations, magnitudewise comparisons are made. For this comparative test the maximum value of axial deformation and the value of radial deformation at x=0 have been considered.

1. An increase in ℓ/a by a factor α : This causes the radial deformation to increase by the same factor and the axial deformation by α^2 (Figs. (8) through (11)).
2. An increase in a/t by a factor α : Both deformations increase by the factor α (Figs. (12) through (15)), which had been predicted by the elementary theory.
3. An increase in band width (Figs. (16) though (19)): The factor of α increase in band width causes radial deformation to increase by the same multiplier. However, it has been observed that an increase in band width from 0.02 to 0.04 or from 0.04 to 0.08 causes the axial deformation to increase rapidly.
4. An increase in ℓ_1/ℓ (Figs. (20) through (23)): Results indicate that the location of load does not have much effect on the magnitude of radial deformation. The same can not be said about the axial deformation as it does depend on the location of the load.

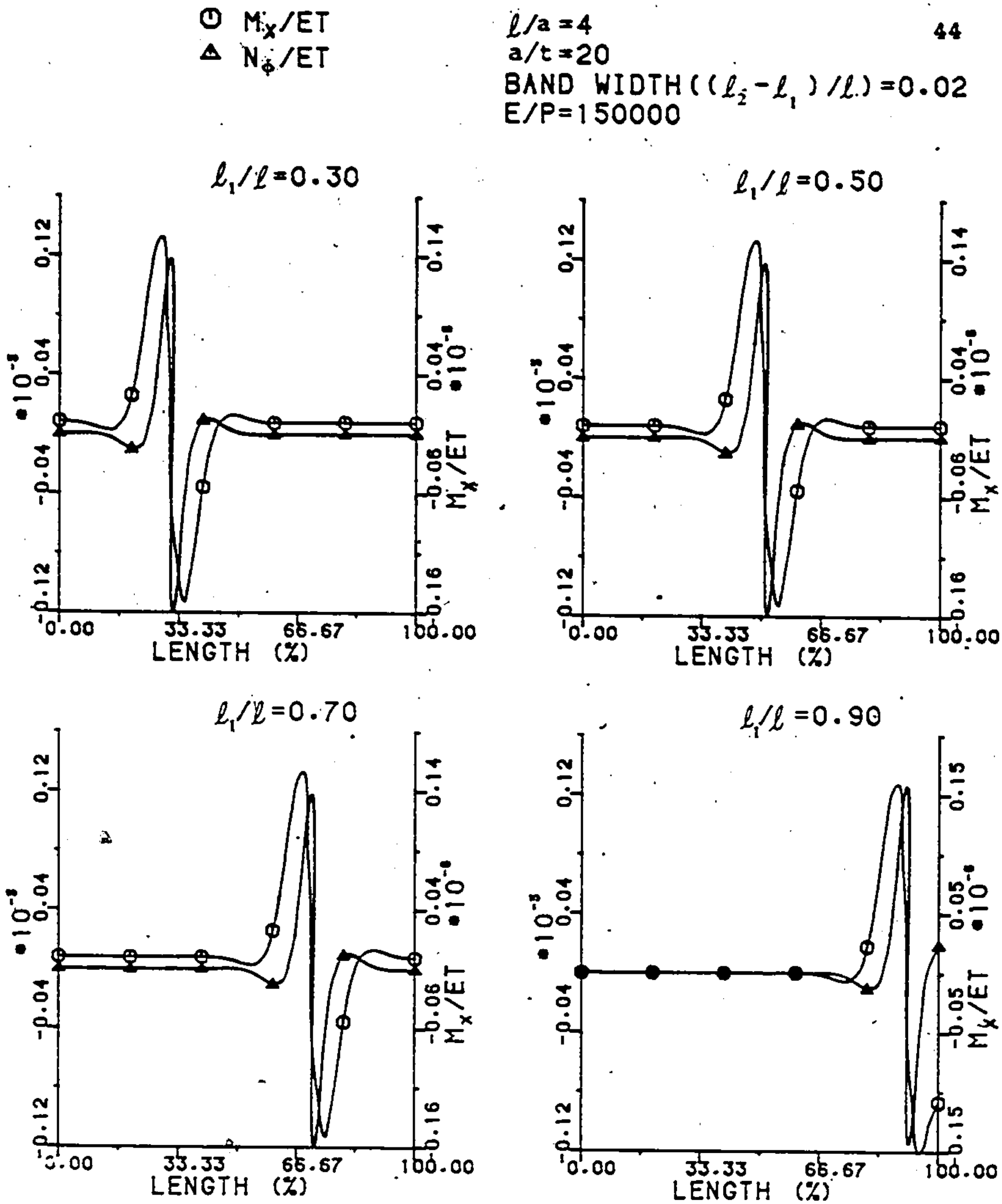

Figure 7: Typical bending moment, M_x/Et, and membrane force, N_ϕ/Et, variation due to axial load

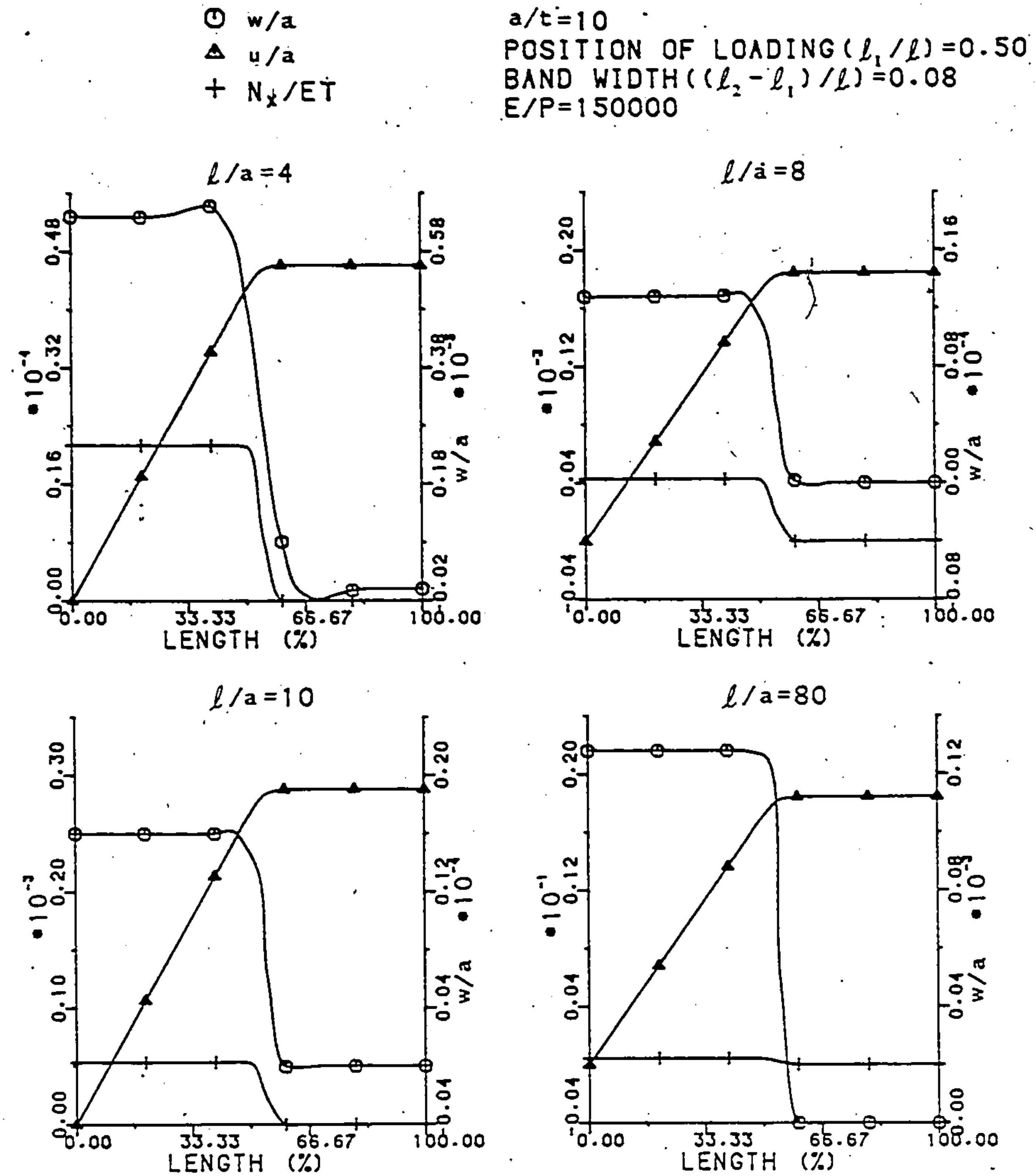

w/a
u/a
N_x/ET
a/t=10
POSITION OF LOADING(ℓ_1/ℓ)=0.50
BAND WIDTH(($\ell_2-\ell_1$)/ℓ)=0.08
E/P=150000
ℓ/a=4
ℓ/a=8
ℓ/a=10
ℓ/a=80
LENGTH (%)
0.00
33.33
66.67
100.00
w/a

Figure : 8

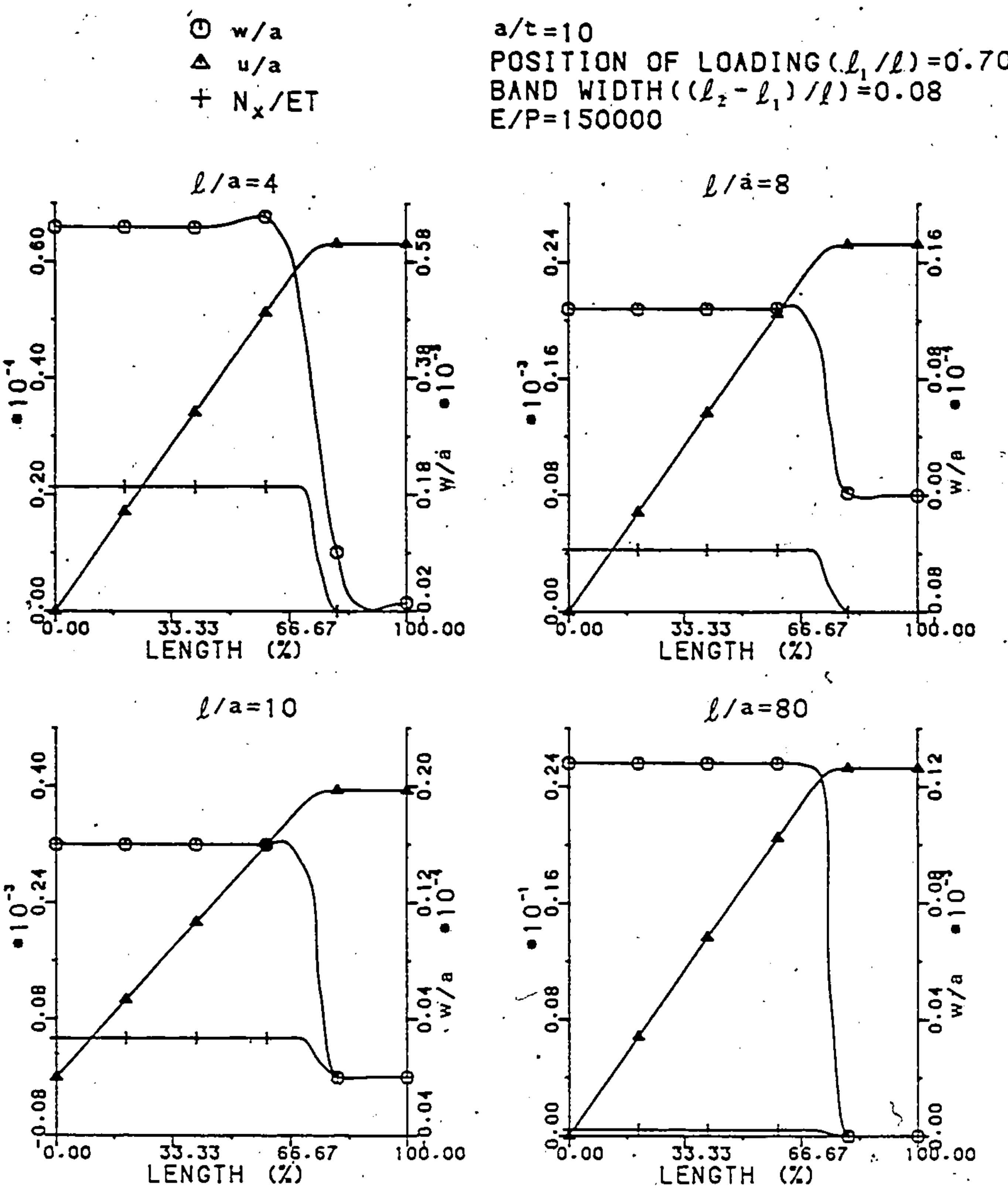

O w/a
Δ u/a
+ N_x/ET
a/t=10
POSITION OF LOADING(ℓ_1/ℓ)=0.70
BAND WIDTH(($\ell_2-\ell_1$)/ℓ)=0.08
E/P=150000
ℓ/a=4
ℓ/a=8
ℓ/a=10
ℓ/a=80
LENGTH (%)
0.00
33.33
66.67
100.00
w/a

Figure : 9

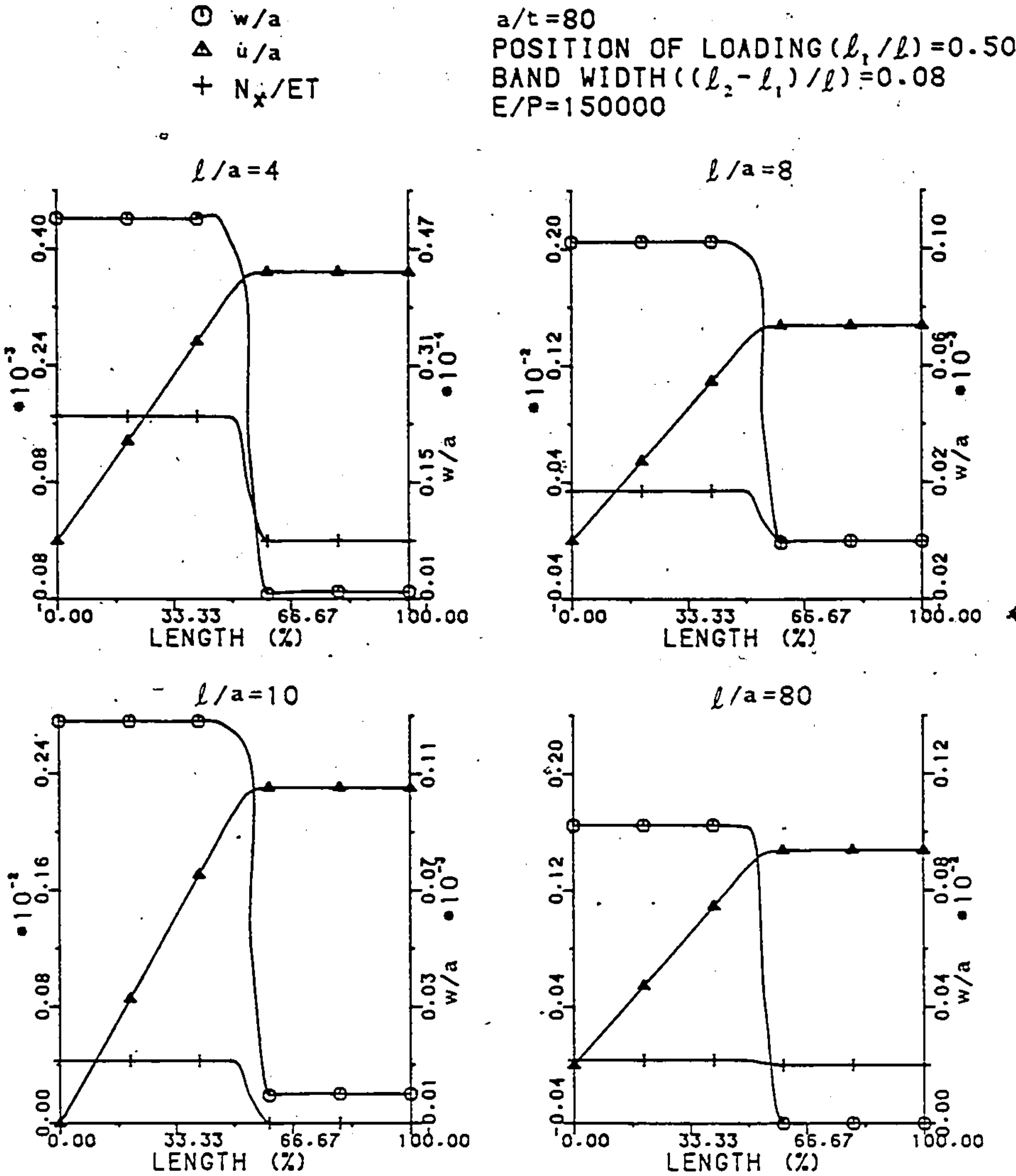
w/a
u/a
N_x/ET
a/t=80
POSITION OF LOADING(ℓ_1/ℓ)=0.50
BAND WIDTH(($\ell_2-\ell_1$)/ℓ)=0.08
E/P=150000
ℓ/a=4
ℓ/a=8
ℓ/a=10
ℓ/a=80
LENGTH (%)
w/a

Figure : 10

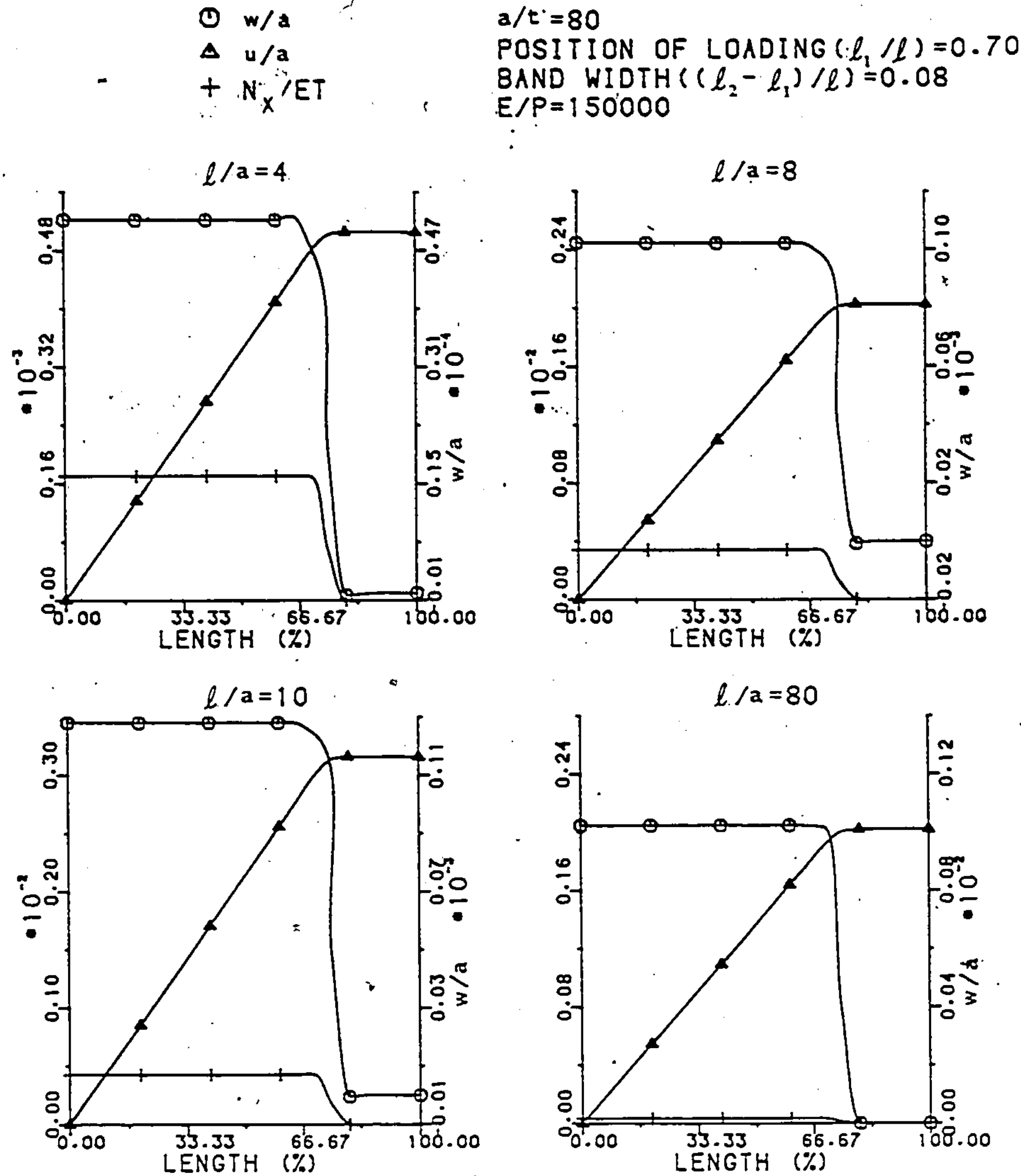

w/a
u/a
N_X/ET
a/t=80
POSITION OF LOADING(ℓ₁/ℓ)=0.70
BAND WIDTH((ℓ₂-ℓ₁)/ℓ)=0.08
E/P=150000
ℓ/a=4
ℓ/a=8
ℓ/a=10
ℓ/a=80
LENGTH (%)
0.00
33.33
66.67
100.00
w/a
*10^-3
*10^-2

Figure : 11

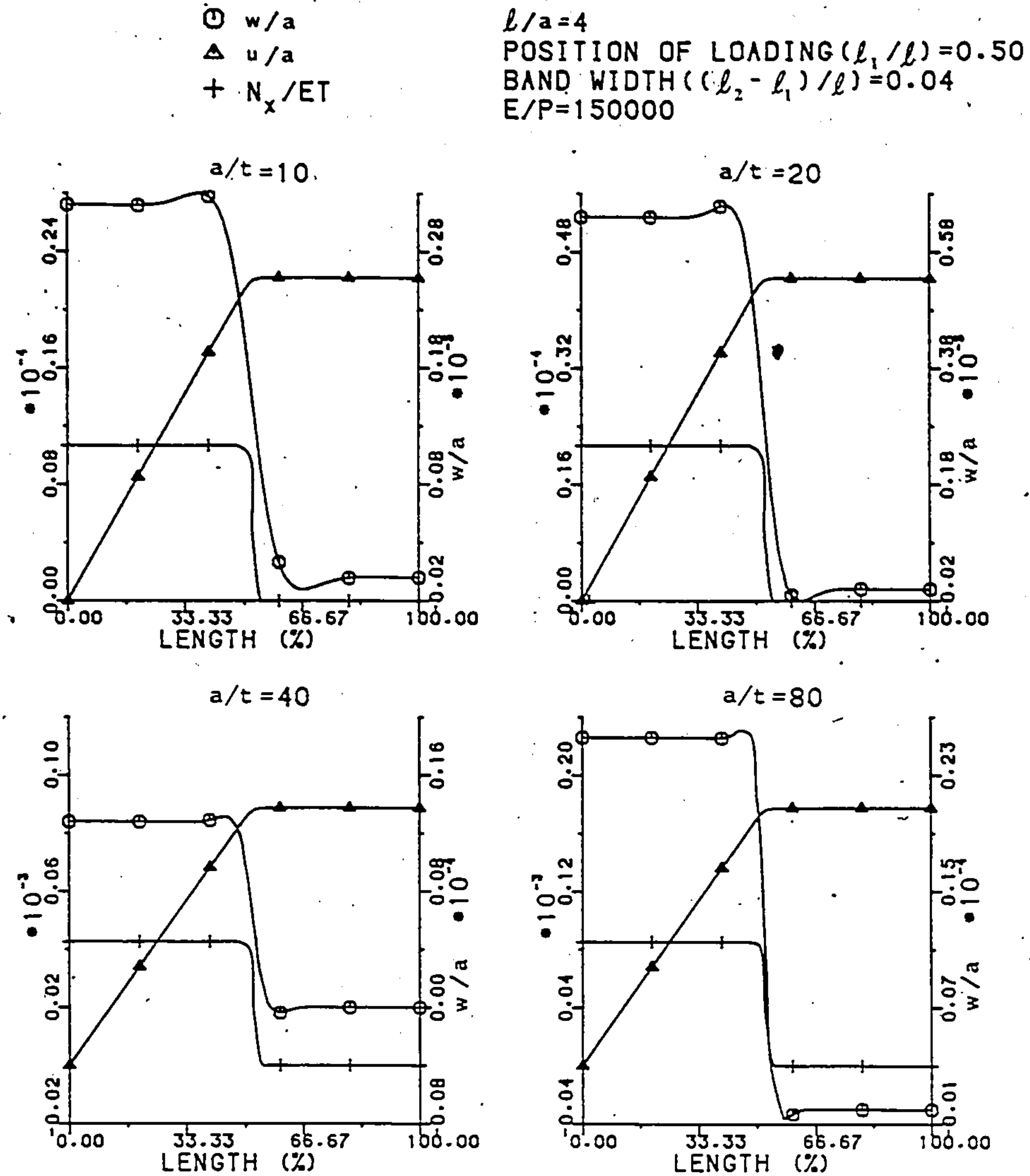

w/a
u/a
N_x/ET
ℓ/a=4
POSITION OF LOADING(ℓ_1/ℓ)=0.50
BAND WIDTH(($\ell_2-\ell_1$)/ℓ)=0.04
E/P=150000
a/t=10
a/t=20
a/t=40
a/t=80
LENGTH (%)
w/a

Figure : 12

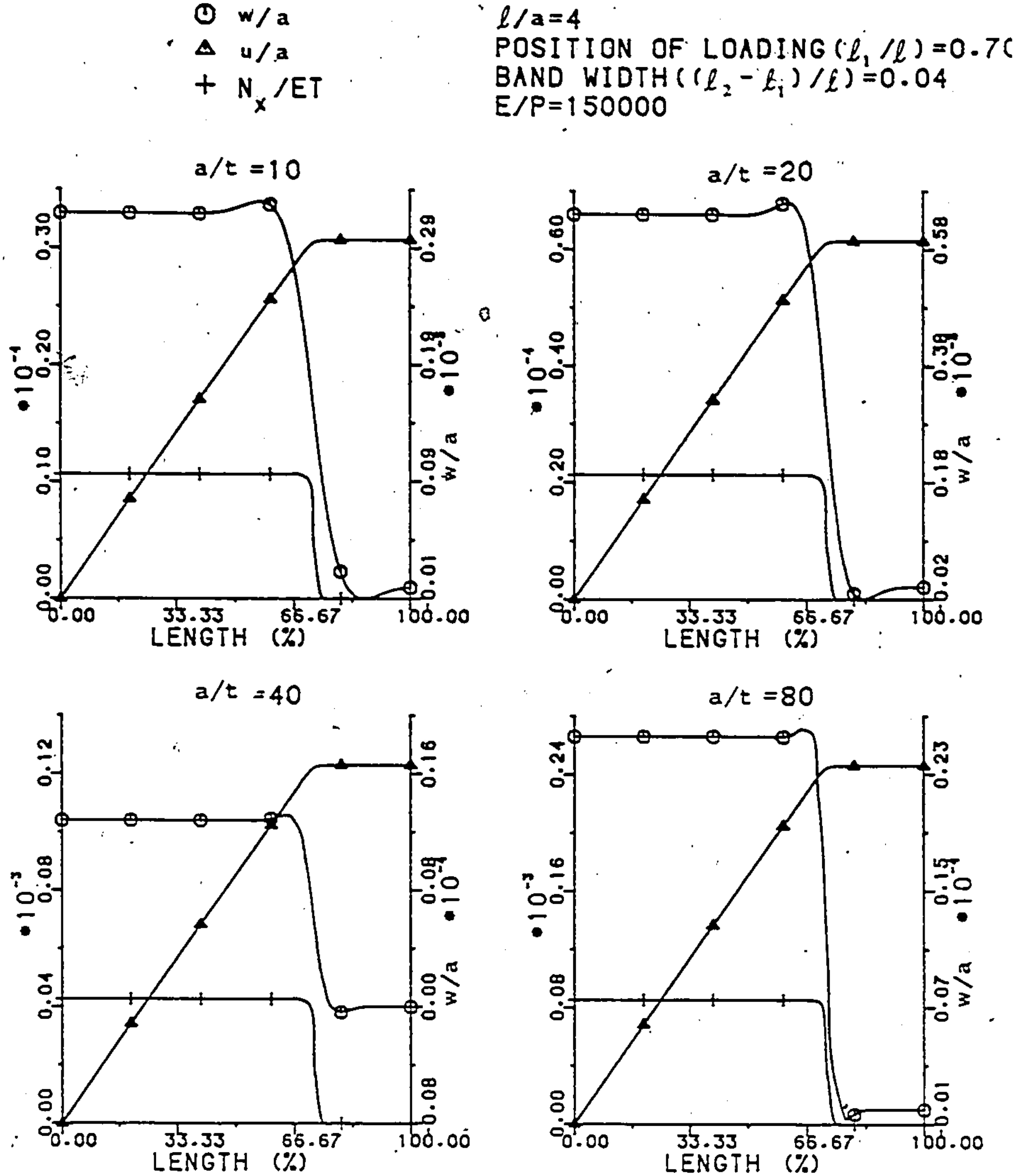

w/a
u/a
N_x/ET
ℓ/a=4
POSITION OF LOADING(ℓ_1/ℓ)=0.70
BAND WIDTH((ℓ_2-ℓ_1)/ℓ)=0.04
E/P=150000
a/t =10
a/t =20
a/t =40
a/t =80
LENGTH (%)
0.00
33.33
66.67
100.00
w/a

Figure : 13

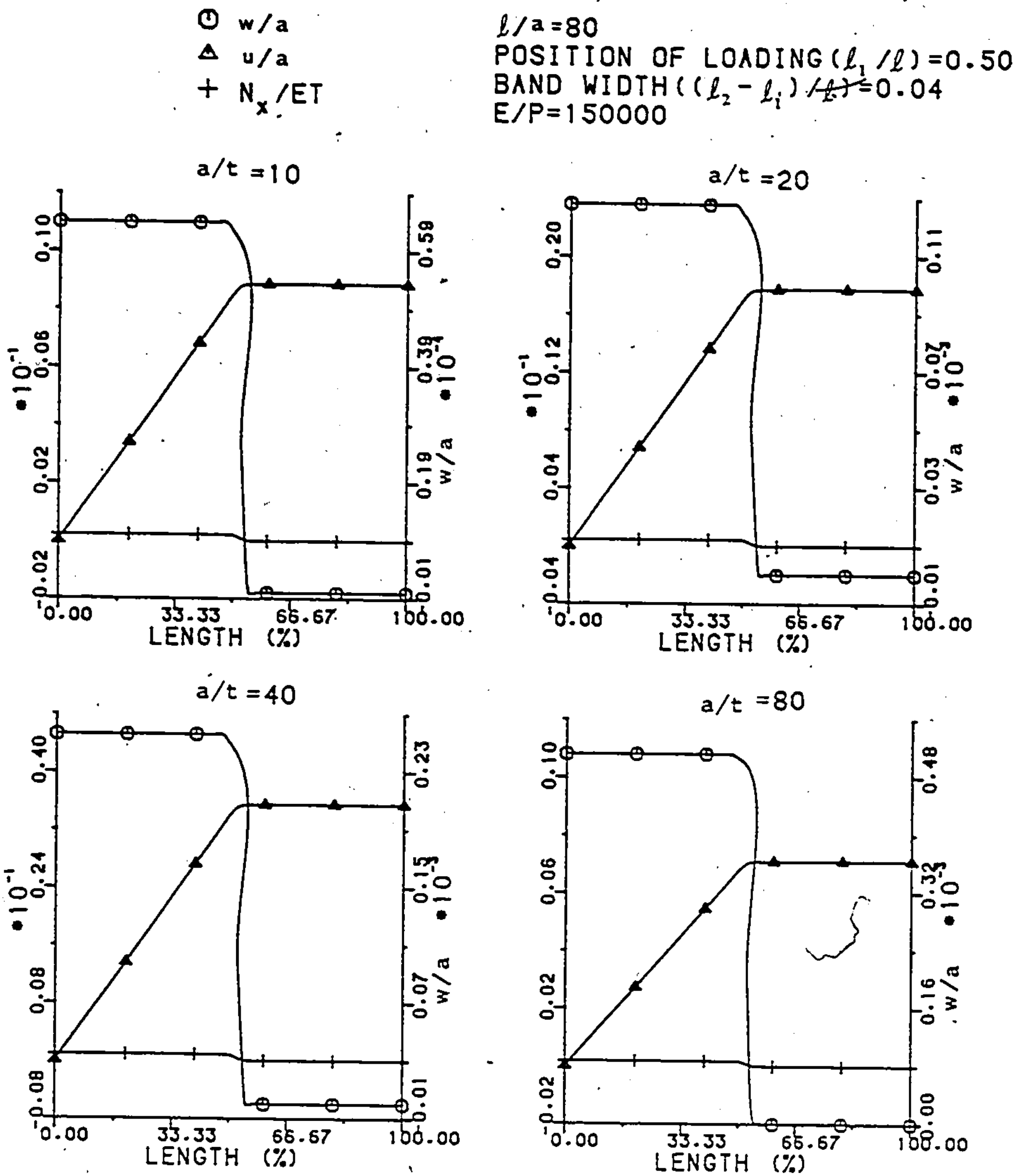

⊕ w/a
△ u/a
+ N_x/ET
ℓ/a=80
POSITION OF LOADING(ℓ_1/ℓ)=0.50
BAND WIDTH((ℓ_2-ℓ_1)/~~ℓ~~)=0.04
E/P=150000
a/t =10
a/t =20
a/t =40
a/t =80
LENGTH (%)
w/a

Figure : 14

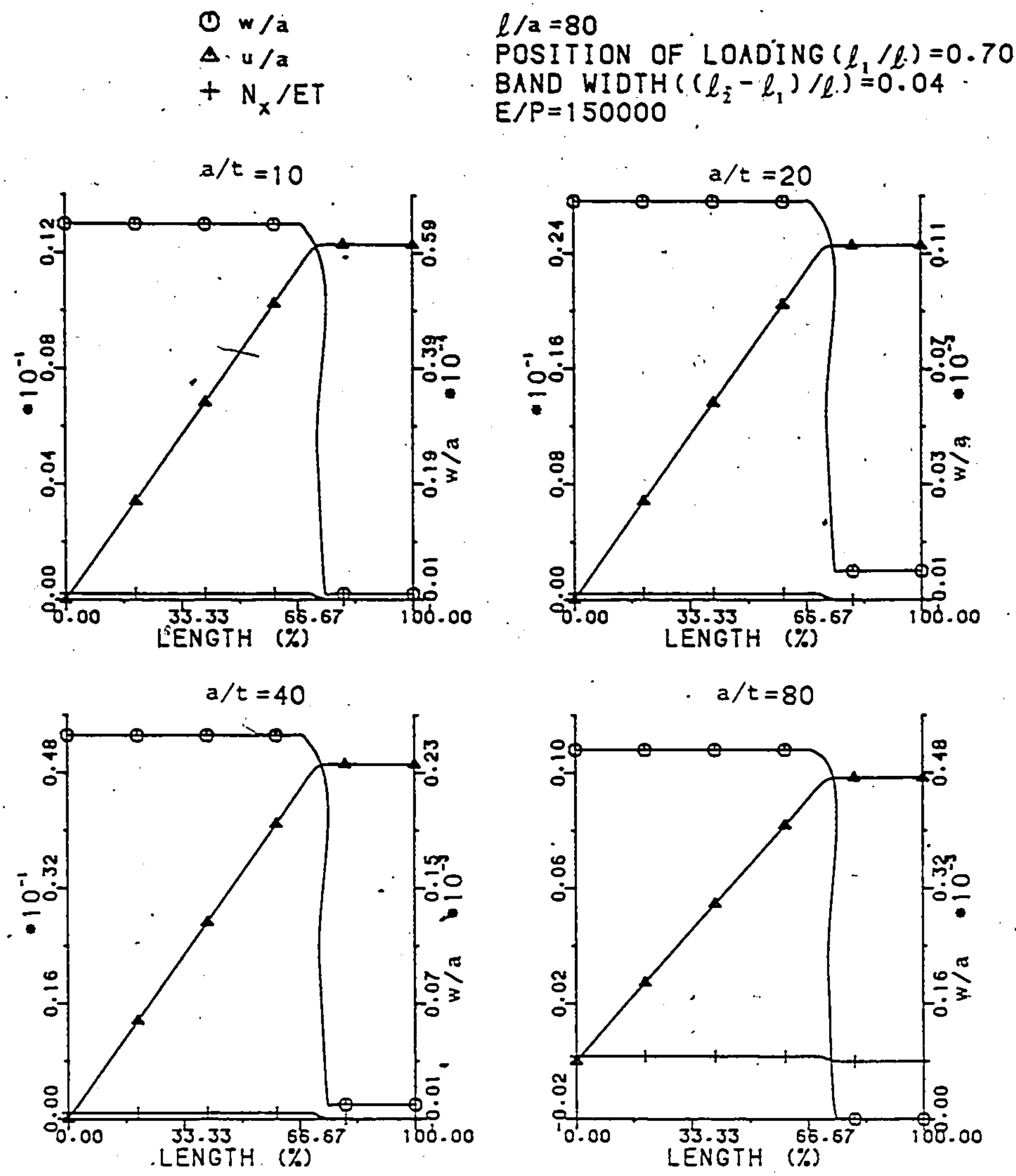

ⓘ w/a
△ u/a
+ N_x/ET
ℓ/a =80
POSITION OF LOADING(ℓ_1/ℓ)=0.70
BAND WIDTH(($\ell_2-\ell_1$)/ℓ)=0.04
E/P=150000
a/t =10
a/t =20
a/t =40
a/t =80
LENGTH (%)
w/a
$\cdot 10^{-1}$
$\cdot 10^{-3}$

Figure : 15

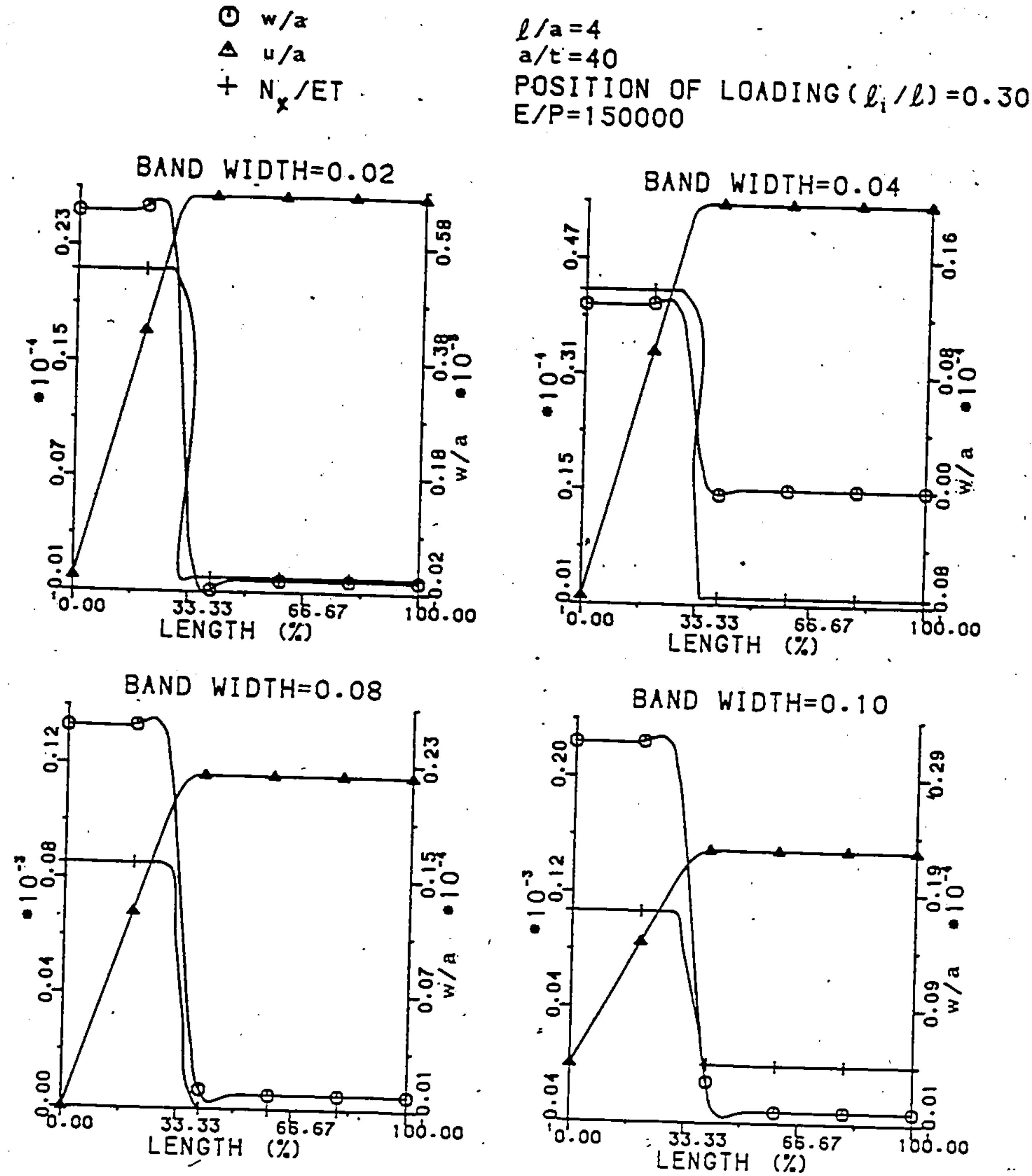

w/a
u/a
N_x/ET
ℓ/a=4
a/t=40
POSITION OF LOADING(ℓ_i/ℓ)=0.30
E/P=150000
BAND WIDTH=0.02
BAND WIDTH=0.04
BAND WIDTH=0.08
BAND WIDTH=0.10
LENGTH (%)
w/a
0.00
33.33
66.67
100.00

Figure. : 16

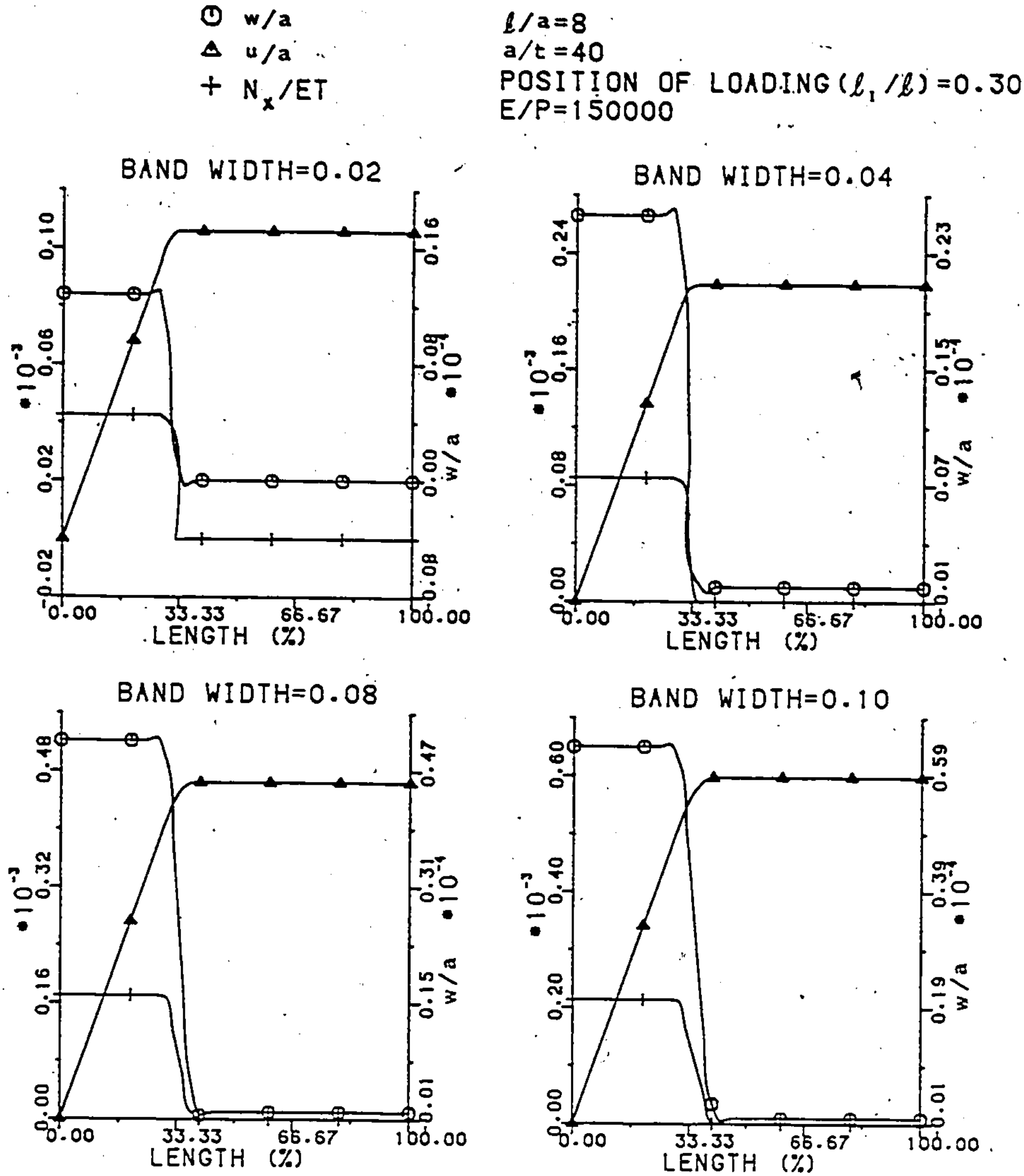

w/a
u/a
N_x/ET
ℓ/a=8
a/t=40
POSITION OF LOADING (ℓ_1/ℓ)=0.30
E/P=150000
BAND WIDTH=0.02
BAND WIDTH=0.04
BAND WIDTH=0.08
BAND WIDTH=0.10
LENGTH (%)
0.00
33.33
66.67
100.00
w/a

Figure : 17

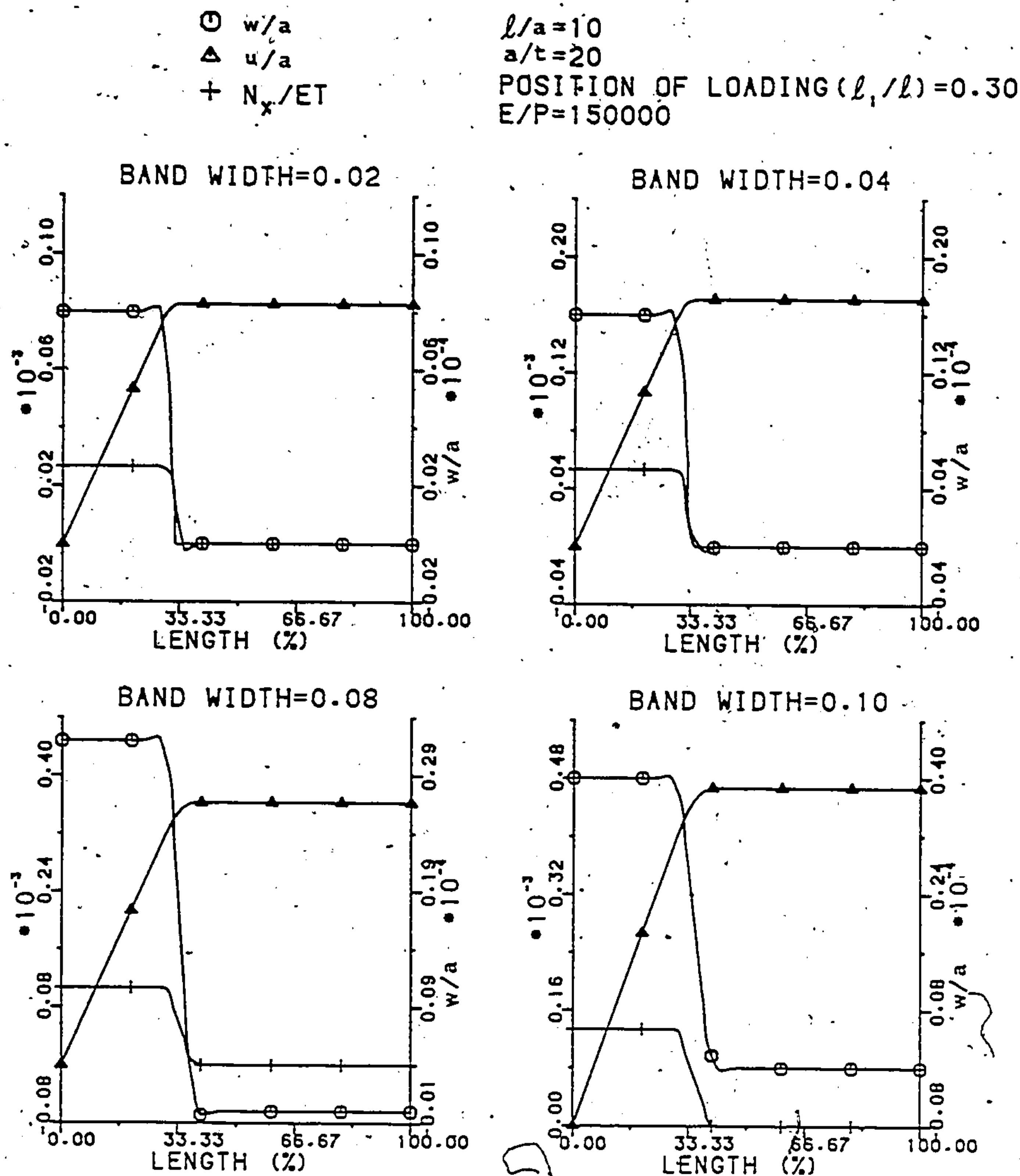

w/a
u/a
N_x/ET
ℓ/a=10
a/t=20
POSITION OF LOADING (ℓ_1/ℓ)=0.30
E/P=150000
BAND WIDTH=0.02
BAND WIDTH=0.04
BAND WIDTH=0.08
BAND WIDTH=0.10
LENGTH (%)
0.00
33.33
66.67
100.00
$\cdot 10^{-3}$
w/a

Figure : 18

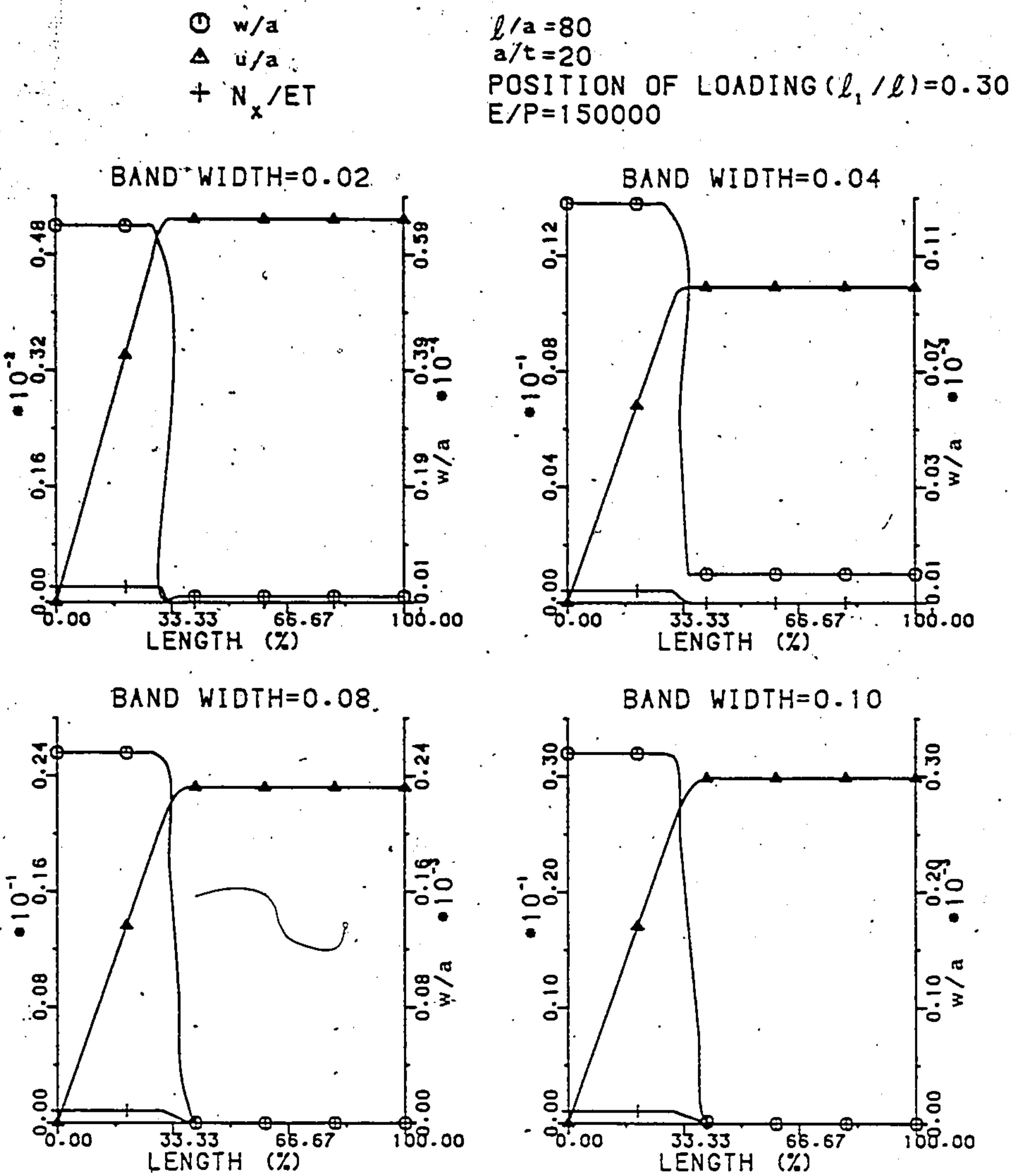
w/a
u/a
N_x/ET
ℓ/a=80
a/t=20
POSITION OF LOADING (ℓ_1/ℓ)=0.30
E/P=150000
BAND WIDTH=0.02
BAND WIDTH=0.04
BAND WIDTH=0.08
BAND WIDTH=0.10
LENGTH (%)
w/a
0.00
33.33
66.67
100.00

Figure : 19

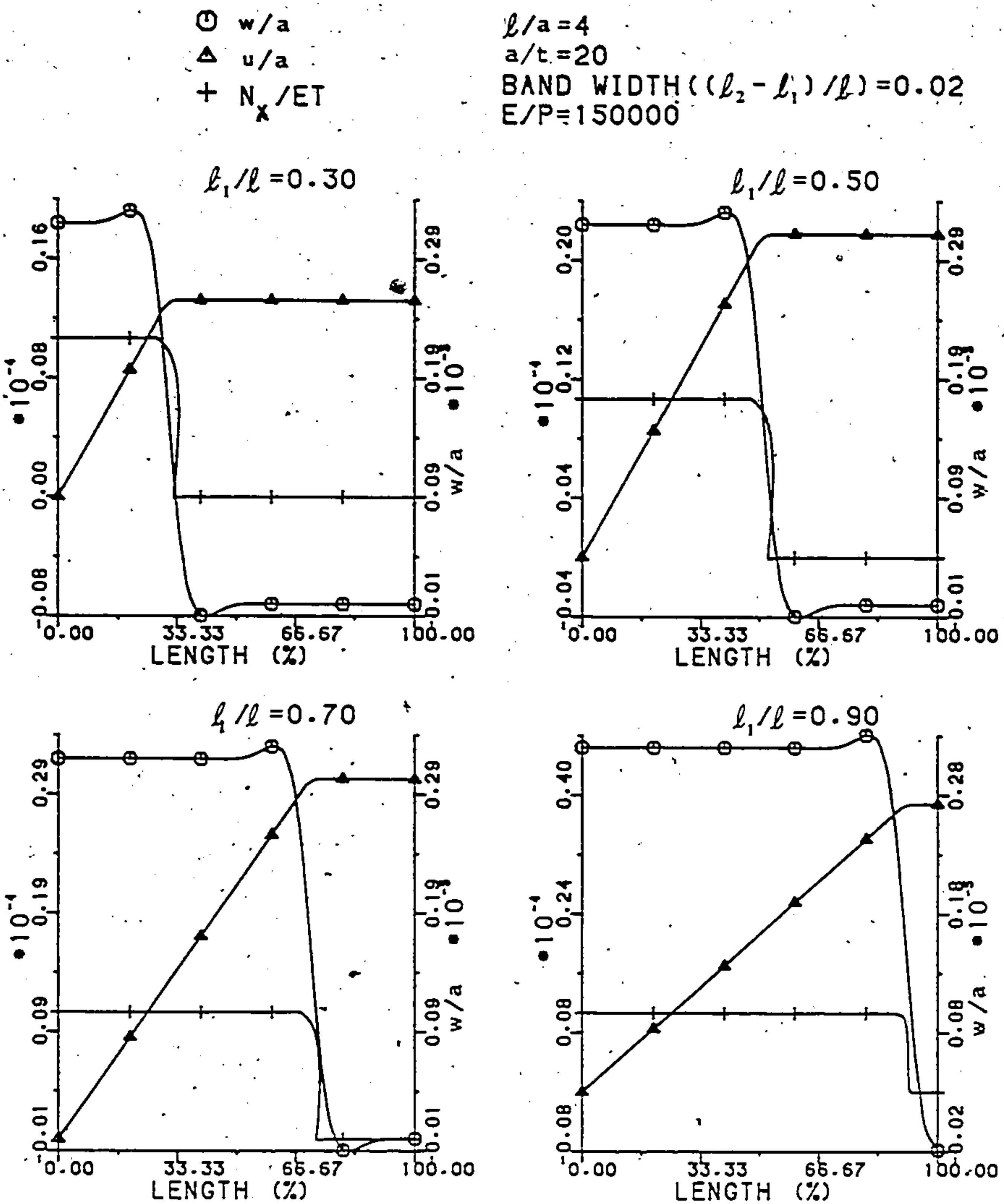

ʘ w/a
△ u/a
+ N_X/ET
ℓ/a=4
a/t=20
BAND WIDTH((ℓ₂-ℓ₁)/ℓ)=0.02
E/P=150000
ℓ₁/ℓ=0.30
ℓ₁/ℓ=0.50
ℓ₁/ℓ=0.70
ℓ₁/ℓ=0.90
•10⁻⁴
•10⁻³
w/a
LENGTH (%)
0.00
33.33
66.67
100.00

Figure : 20

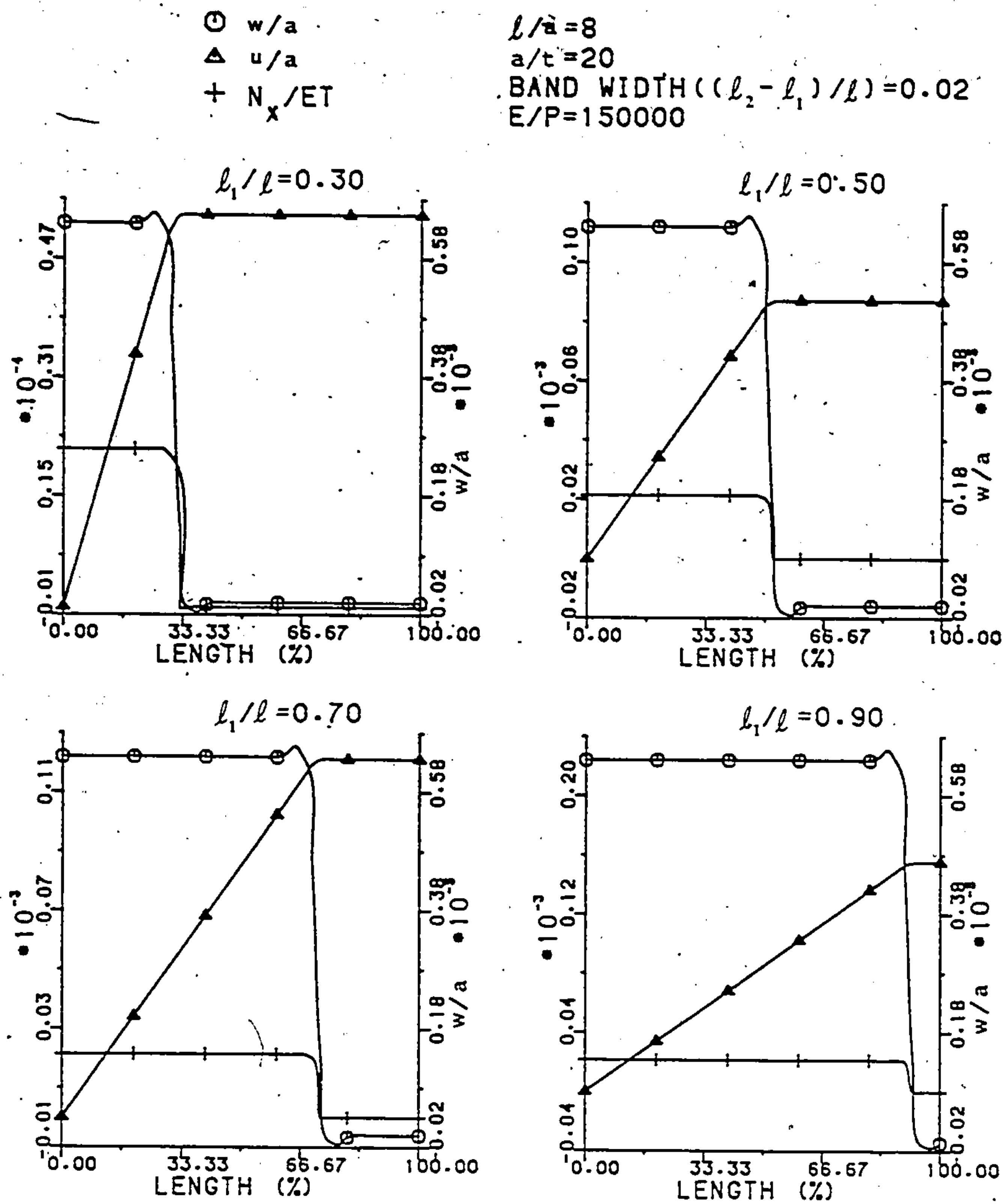

w/a
u/a
N_x/ET
ℓ/a=8
a/t=20
BAND WIDTH((ℓ₂-ℓ₁)/ℓ)=0.02
E/P=150000
ℓ₁/ℓ=0.30
ℓ₁/ℓ=0.50
ℓ₁/ℓ=0.70
ℓ₁/ℓ=0.90
LENGTH (%)
0.00
33.33
66.67
100.00
w/a

Figure : 21

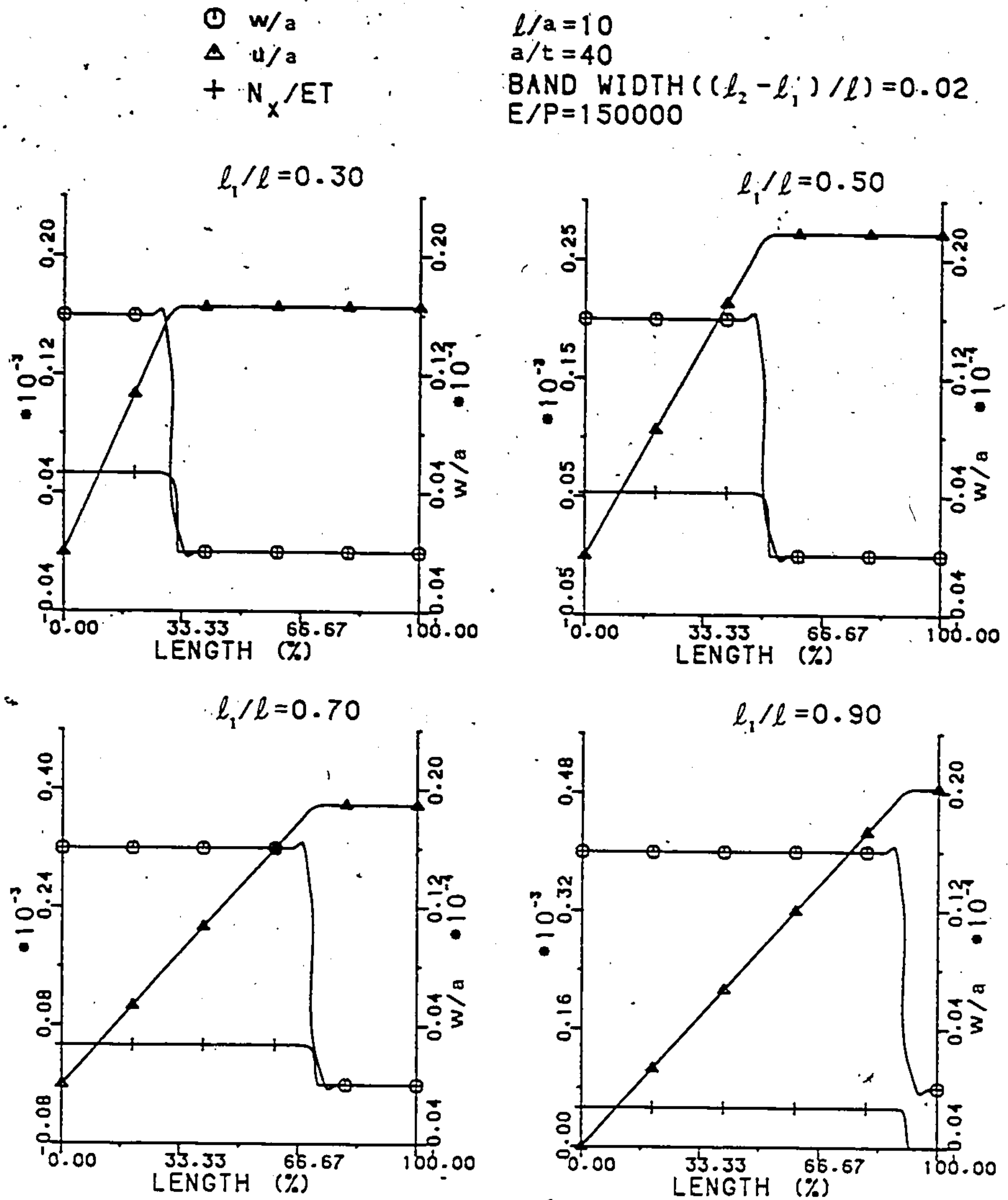

w/a
u/a
N_x/ET
ℓ/a=10
a/t=40
BAND WIDTH((ℓ₂-ℓ₁)/ℓ)=0.02
E/P=150000
ℓ₁/ℓ=0.30
ℓ₁/ℓ=0.50
ℓ₁/ℓ=0.70
ℓ₁/ℓ=0.90
LENGTH (%)
w/a

Figure : 22

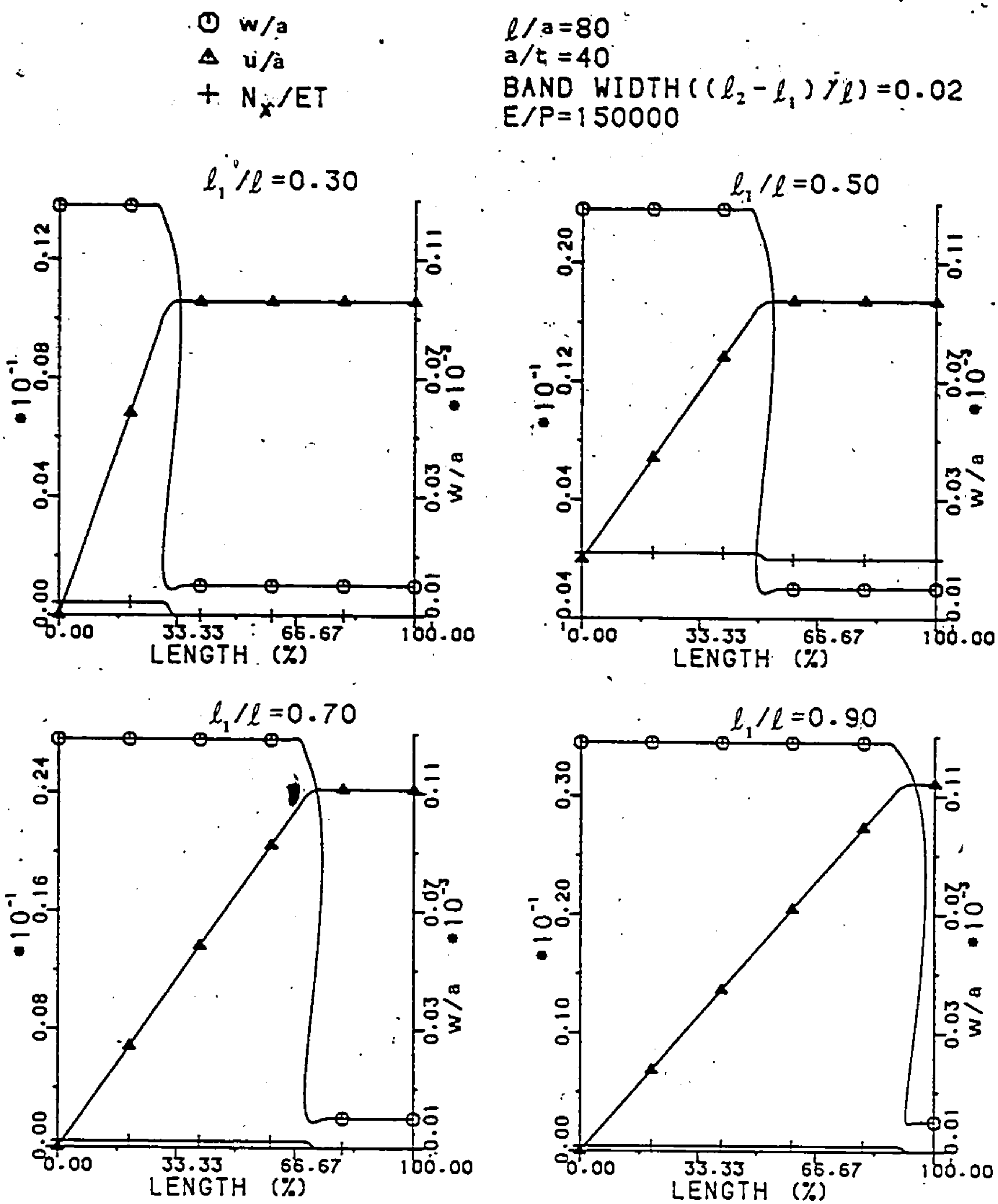

w/a
u/a
N_x/ET
ℓ/a=80
a/t=40
BAND WIDTH(($\ell_2-\ell_1$)/ℓ)=0.02
E/P=150000
ℓ_1/ℓ=0.30
ℓ_1/ℓ=0.50
ℓ_1/ℓ=0.70
ℓ_1/ℓ=0.90
$*10^{-1}$
w/a $*10^{-3}$
LENGTH (%)
0.00
33.33
66.67
100.00

Figure : 23

5.2 INTEGRAL LUG ATTACHMENTS

5.2.1 GENERAL

The numerical method adopted in Chapter IV has been used to analyse the effect of integral lug attachments on pressure vessels.

In any finite element analysis, a check on the convergence of the method has great importance. The element properties as well as the computer program itself were tested for relatively simple problems and the computational accuracy was found to be excellent [15].

In modelling of the present problem, considerable amount of work has been done in discretizing the domain inside the loaded area as well as outside the loaded area. The convergence achieved with the given model has been found to be excellent as the number of elements are increased and displaced along the circumferential and longitudinal directions.

Numerical results are generated for five values of a/t, i.e. 5,10,20,40 and 80. These values show a broad spectrum of radius to thickness ratio covering from thick shells to thin shells. However, the results for thick shells have to be used with caution.

Usually the lugs are placed at least a diameter away from the ends to avoid end effect. This requirement has been satisfied by taking the parameter, ℓ/a, as four.

The two nondimensional variables β_1 and β_2 considered here determine the size of the lug in circumferential and longitudinal directions, respectively. β_1 is one half the width of the lug divided by the radius of the shell. Similarly, β_2 is defined as the ratio of half the length of the lug to radius of the shell. For all practical design consideration, the following β_1 and β_2 combinations are taken as

β_1	β_2
0.05	0.05
0.05	0.10
0.05	0.20
0.10	0.10
0.20	0.10
0.20	0.20
0.40	0.10

Poisson's ratio, ν, and modulus of Elasticity, E, are taken as 0.3 and $30*10^6$, respectively.

5.2.2 COMPUTATIONS ON DEFORMATIONS

The axial and radial deformations of the centerline of the lug, for β =0.20 and a/t= 10,40,80, are plotted in Figs. (25) and (26), respectively.

A symmetry is observed, Fig. (25), with respect to half the length of the lug for all values of a/t. The large variation in axial deformation shown for a/t=10 within the loaded area vanishes as a/t values are increased.

Although a rapid decaying pattern is seen in radial deformation for a/t=10, Fig. (26), it seems to spread over the entire length of the shell for a/t=80. More localized behavior is observed in the region where the lug is positioned.

A relatively wide and short lug design is considered in Fig. (27) (β_1=0.40, β_2=0.10), where dotted lines represent the position of the lug. For a/t=5, axial deformation reaches its maximum value within the loaded area. But, for values of a/t=20 and 80, the maximum is found to be outside the loaded area.

The results presented up to now reveal the fact that as the shell gets thinner, membrane forces become dominant.

Typical variation of w along the circumferential direction is plotted in Fig. (24), where dotted lines represent the undeformed shape of the shell. Radial deformation, plotted with the scale of 500 at lug-vessel interface, shows complete symmetry.

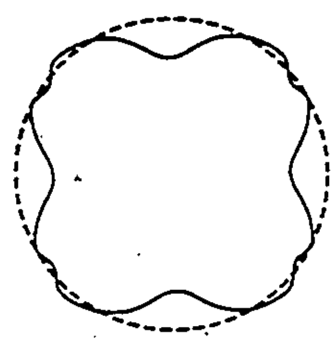

Figure 24 : Radial deformation variation (Lug-vessel interface)

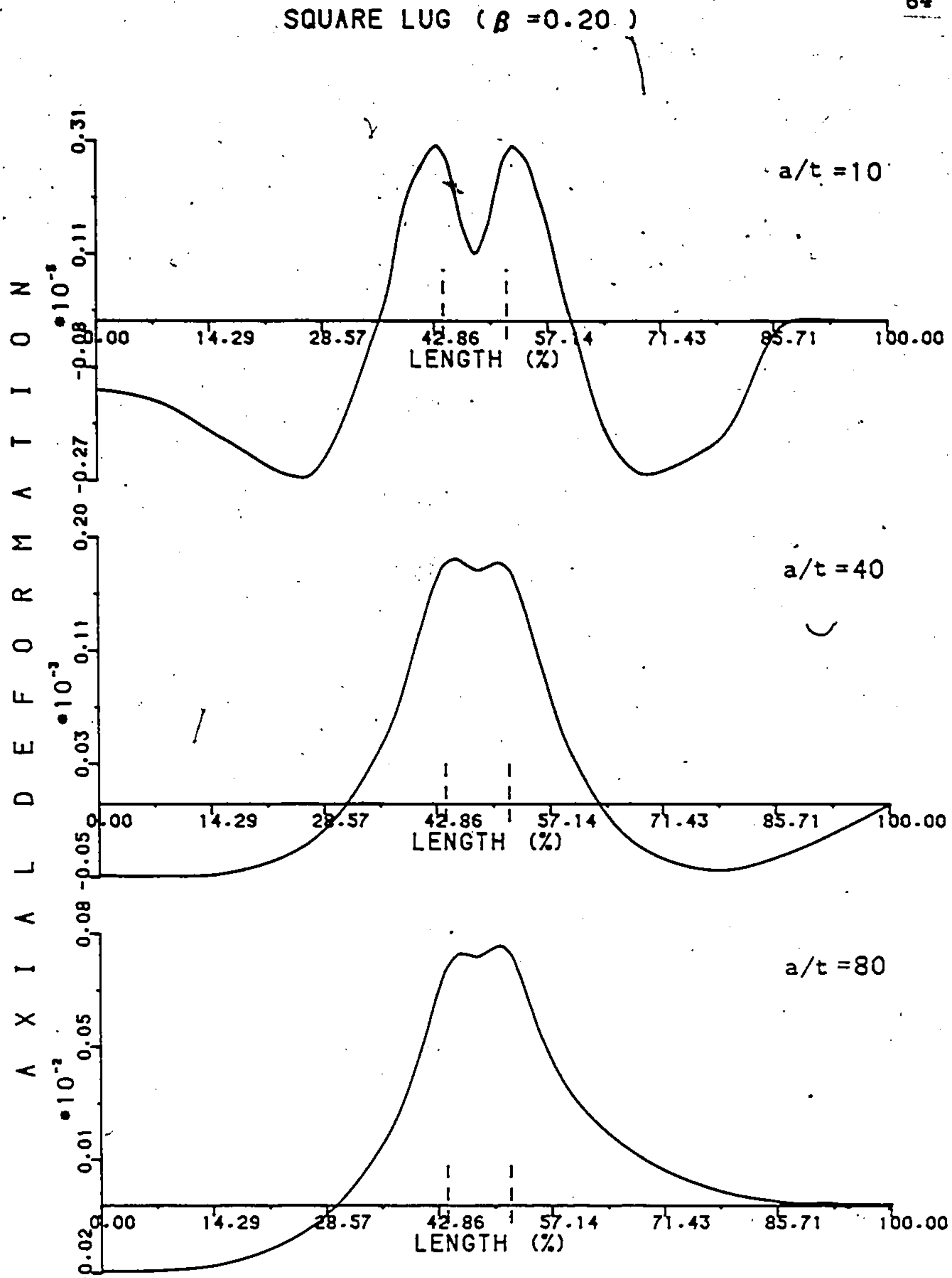

Figure 25.: Axial deformation variation along the lug centerline due to longitudinal moment, for square lugs

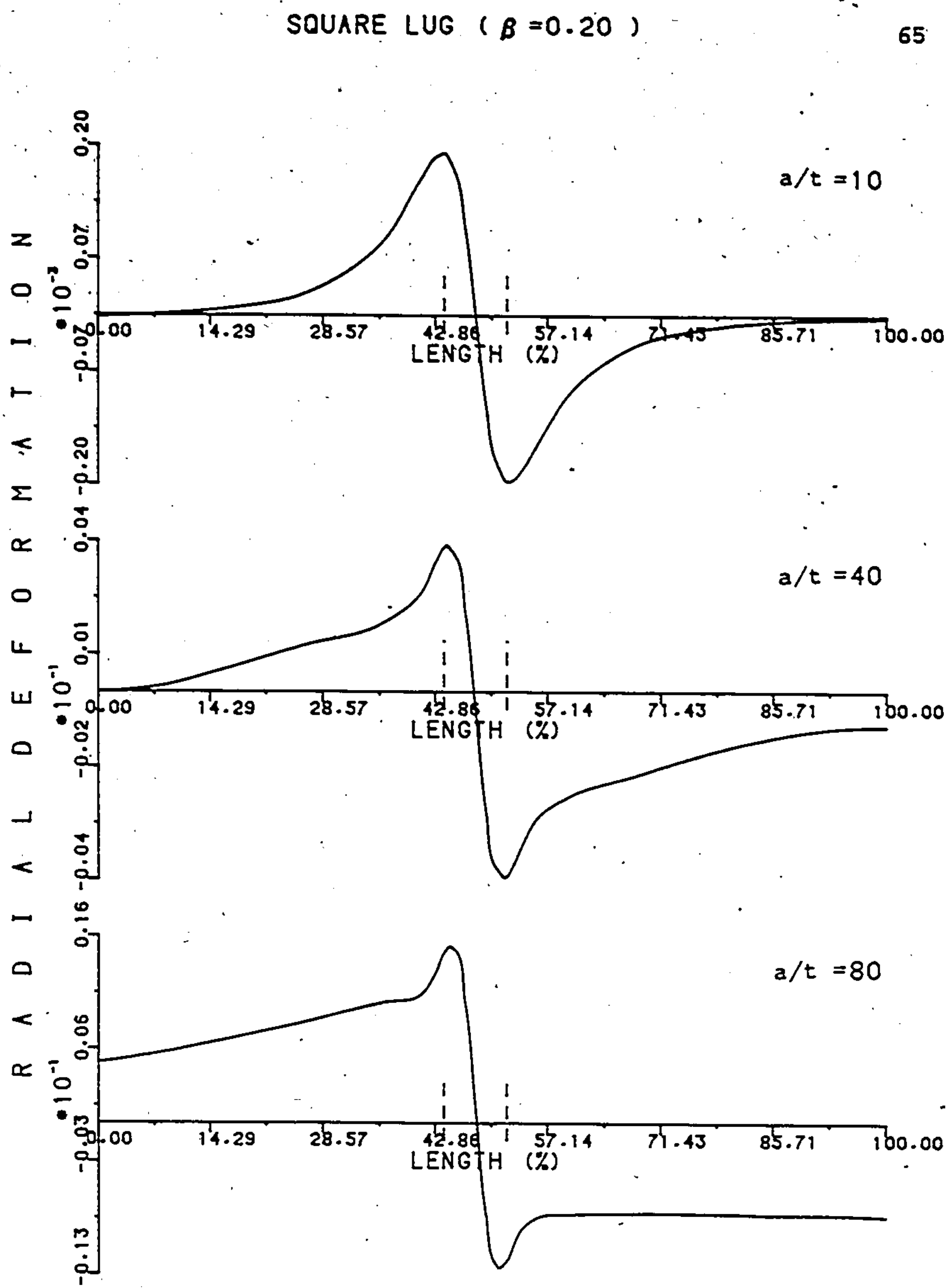

Figure 26: Radial deformation variation along the lug centerline due to longitudinal moment, for rectangular lugs

RECTANGULAR LUG (β_1=0.40 , β_2=0.10)

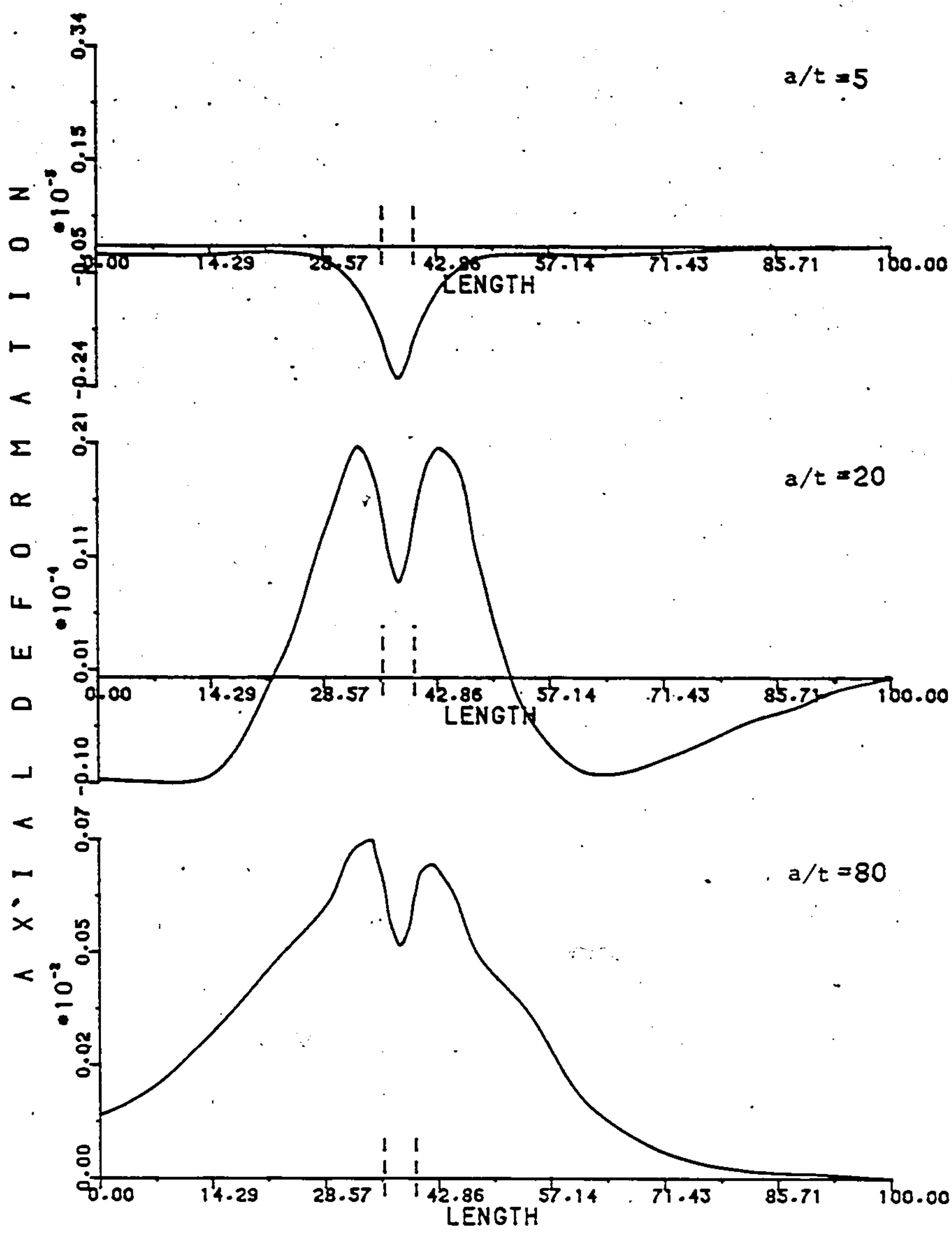

Figure 27: Axial deformation variation along the lug centerline due to longitudinal moment, for rectangular lugs

5.2.3 COMPUTATIONS ON STRESSES

A typical stress distribution at the lug-vessel centerline has been plotted in Fig. (28) for the values of $\beta_1 = \beta_2 = \beta = 0.20$ and $a/t=10$.

Recalling that the stress index is defined as the ratio of the maximum stress intensity in the component to the nominal stress in the lug [16], we write,

$$C_L = \sigma_x / S_\ell \qquad \text{and} \qquad C_L^* = \sigma_\phi / S_\ell$$

where

$$S_\ell = 3M_L / 4c_1 c_2^2$$

An examination of Fig. (28) shows that maximum stress intensity in axial and circumferential directions is within the loaded area and occurs in the element located to the upper end of the lug-vessel interface. The stress distribution is antisymmetric with respect to the half-length of the lug. From Fig. (28), it is observed that both stresses vanish at the ends. This result reveals the fact that there is no end effect on the results and taking ℓ/a as 4 is satisfactory. Further discussions on this can be found in Section (5.2.5) where the effect of changing the position of the lug is examined.

The maximum outside and inside stresses, in both directions, are presented in Tables (1) through (7) and discussed in the following two subsections for square and rectangular loaded areas.

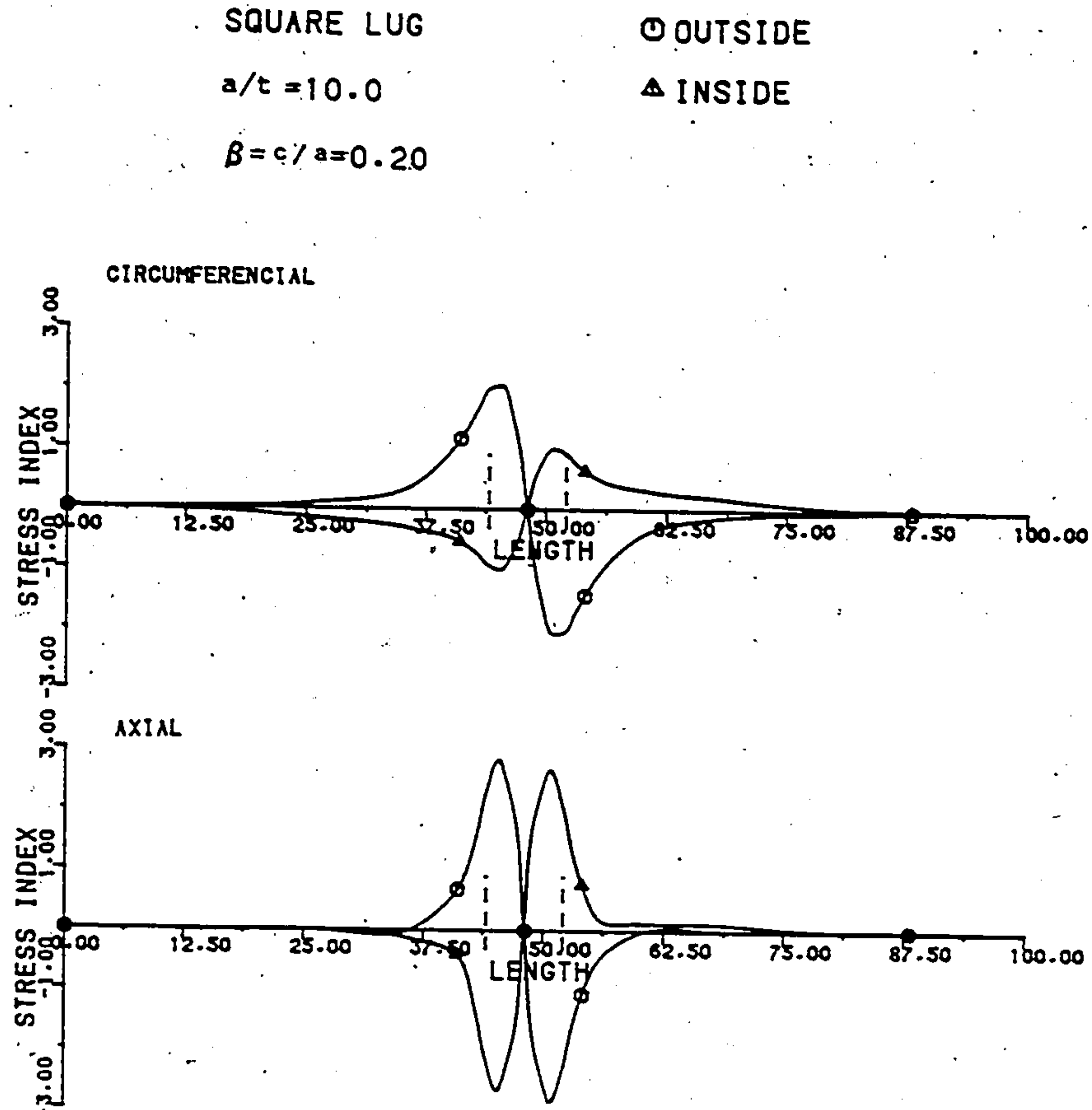

Figure 28: Typical stress distribution along lug centerline

5.2.3.1 SQUARE LOADED AREAS

In general it can be seen from Tables (1),(2) and (3) that maximum stress occurs on the outside surface of the shell and it is in axial direction. For the case where $\beta_1 = \beta_2 = \beta$ $=0.20$ and $a/t=80$ (Table (3)), the present method predicts the maximum stress on the outside surface of the shell but in circumferential direction.

The results show that for a specific β value, the maximum axial and circumferential stress index increases as a/t is increased. Similarly, for a given value of a/t, an increase in β value results in higher stresses in the shell.

Calculations presented in Table (D-1) (Appendix D) are found to be helpful in understanding the effects of β and a/t on the maximum stress index. It is observed that when a/t is constant, increase in β causes percent difference of maximum stress index to decrease. This decrease in maximum stress index is more drastic for a/t=40 and 80. As a/t increases, percent difference of maximum stress index values corresponding to increase in β decrease.

TABLE 1

Stress indices for longitudinal moment loading on square lug attachments

β	a/t	C_L^* outside	C_L^* inside	C_L outside	C_L inside
0.05	5	−0.0379	0.0267	−0.0559	0.0565
	10	−0.1446	0.1124	−0.2229	0.2221
	20	−0.5700	0.4444	−0.8589	0.8471
	40	−2.3000	1.6665	−3.2300	3.2300
	80	−9.1833	5.7673	−11.4371	10.8141

TABLE 2

Stress indices for longitudinal moment loading on square lug attachments

β	a/t	C_L^* outside	C_L^* inside	C_L outside	C_L inside
0.10	5	−0.1440	0.1056	−0.2235	0.2256
	10	−0.5723	0.4021	−0.8747	0.8576
	20	−2.2341	1.3963	−3.2533	3.0949
	40	−8.4981	4.2112	−11.4453	10.4645
	80	−30.9147	10.6229	−36.8139	32.1621

TABLE 3

Stress indices for longitudinal moment loading on square lug attachments

β	a/t	C_L^*		C_L	
		outside	inside	outside	inside
0.20	5	−0.5547	0.3029	−0.7808	0.7723
	10	−2.1504	1.0112	−2.8587	2.6795
	20	−7.9104	2.7136	−9.6427	8.4992
	40	−25.3141	3.8997	−28.2112	22.3787
	80	−65.3099	7.4112	−64.3115	44.9237

5.2.3.2 RECTANGULAR LOADED AREAS

The results in Tables (4),(5) and (6) show that maximum stress occurs in axial direction for all values of a/t. However, in Table (7), for values of $a/t \geqslant 20$ maximum stress calculated by the present method is found in circumferential direction.

Tables (4) through (7) show that increase in a/t value results in higher stresses regardless of the size of the lug.

Comparisons of Tables (4),(5),(6) and (7) for a given value of a/t indicate that an increase in lug size in any of the directions yields relatively higher maximum stress on the shell. In order to study this effect in detail, Tables (D-2) and (D-3) have been prepared and included in Appendix D. In view of the percent study presented in Tables (D-2) and (D-3), the following results are observed.

1. Increase in lug size along the circumferential direction Table (D-2): For values of $a/t \leqslant 20$, increasing the lug size β_1 from 0.05 to 0.20 causes a rapid increase in maximum stress. Whereas for the cases where a/t=40 and 80, the rate of increase is slower (26 %). Beyond $\beta_1 = 0.20$, the rate of increase of maximum stress is found to be slow. A 15% increase is observed for the case where a/t=5, and the percent increase for the cases of a/t=40,80 is found to be insignificant.

2. Increase in lug size along the longitudinal direction: As a/t is increased, the rate of increase of maximum stress is slower (Table (D-3)). For $a/t \leq 20$, an increase in β_2 results in a rapid increase (106%). For a/t=40 and 80, on the other hand, it is found to be slow (55%).

TABLE 4

Stress indices for longitudinal moment loading on rectangular attachments

β_1	β_2	a/t	C_L^* outside	C_L^* inside	C_L outside	C_L inside
0.05	0.10	5	−0.1069	0.0896	−0.1419	0.1381
		10	−0.4251	0.3445	−0.5536	0.5341
		20	−1.6584	1.2400	−2.0307	1.9208
		40	−8.5040	4.1643	−11.5790	10.5487
		80	30.8297	10.1826	37.0800	32.3400

TABLE 5

Stress indices for longitudinal moment loading on rectangular attachments

β_1	β_2	a/t	C_L^* outside	C_L^* inside	C_L outside	C_L inside
0.2	0.1	5	−0.1740	0.0942	−0.3022	0.3088
		10	−0.6779	0.3553	−1.1716	1.1532
		20	−2.6433	1.1022	−4.3308	4.1070
		40	−9.6384	−2.3307	−14.56	13.32
		80	−30.12	5.58	−41.60	37.0581

TABLE 6

Stress indices for longitudinal moment loading on rectangular attachments

β_1	β_2	a/t	$\overset{*}{C}_L$ outside	$\overset{*}{C}_L$ inside	C_L outside	C_L inside
0.40	0.10	5	−0.1956	0.061	−0.3488	0.3651
		10	−0.7225	0.2183	−1.3006	1.2993
		20	−2.6901	0.5128	−4.5803	4.4437
		40	−10.0032	−2.1589	−14.6987	13.9584
		80	−32.4843	12.9536	−41.8832	37.8389

TABLE 7

Stress indices for longitudinal moment loading on rectangular attachments

β_1	β_2	a/t	$\overset{*}{C}_L$ outside	$\overset{*}{C}_L$ inside	C_L outside	C_L inside
0.05	0.20	5	−0.2645	0.2219	−0.2937	0.2869
		10	−1.0571	0.8037	−1.1061	1.0366
		20	−3.9154	2.6413	−3.8094	3.4307
		40	−15.3643	8.8672	−13.2971	10.9300
		80	57.6896	−30.9088	44.9536	−28.5771

5.2.4 COMPARATIVE STUDY

Stress analysis of pressure vessels with integral lug attachments has been investigated in [8,16 and 19] as well. Large discrepancies exist between the results presented by these authors. Tables (8),(9) and (10) for square loaded areas and Tables (11) through (14) for rectangular loaded areas have been prepared to demonstrate this clearly.

5.2.4.1 SQUARE LOADED AREAS

Within the range of parameters presented in Tables (8),(9) and (10), a good agreement is observed between WRC-107 and Dodge's results [8,19]. However, comparisons of the present method with these two indicate that this can only be extended for the parameters included in Table (8).

In spite of a good agreement seen for the cases where $a/t \leq 20$ and $\beta = 0.20$ in [8,16 and 19], comparisons of WRC-198 with WRC-107 and Dodge's calculations show large variations. For example, for values of $\beta \leq 0.10$ and $a/t \leq 20$, WRC-198 predictions on the maximum stress index are at least 20% more than the other two. For the case where circumferential stress dominates the design ($\beta = 0.20$, $a/t=80$, Table (8)), discrepancy in the results may reach as high as 70%.

For the cases where $\beta = 0.10$ and $a/t=20,40,80$ (Table (9)), WRC-198 and the present method calculate the same maximum stress index and tend to be conservative in comparison with the other two.

The present method for the given parameters in Table (10), in general agrees, once again, with the results predicted in WRC-198. The present results also indicate about 20% discrepancy in comparison to the other two studies.

In spite of the large variations in predicting the magnitude of the maximum stress index for the parameters considered for square loaded areas, the methods, in general, agree on the direction of the maximum stress.

SQUARE LOADED AREAS

β	a/t	METHOD	C_L^* outside	C_L^* inside	C_L outside	C_L inside
0.05	5	WRC-107	-0.04	0.03	-0.06	0.05
		DODGE	-0.03	0.03	-0.05	0.05
		WRC-198			0.09	
		PRESENT METHOD	-0.0379	0.0267	-0.0559	0.0565
	10	WRC-107	-0.14	0.12	-0.21	0.21
		DODGE	-0.13	0.12	-0.21	0.21
		WRC-198			0.29	
		PRESENT METHOD	-0.1446	0.1124	-0.2229	0.2221
	20	WRC-107	-0.54	0.45	-0.81	0.79
		DODGE	-0.52	0.42	-0.80	0.78
		WRC-198			0.95	
		PRESENT METHOD	-0.5700	0.4444	-0.8589	0.8471
	40	WRC-107	-2.16	1.62	-3.21	3.07
		DODGE	-2.11	1.51	-3.05	2.91
		WRC-198			3.19	
		PRESENT METHOD	-2.3000	1.6665	-3.2300	3.23
	80	WRC-107	-8.51	5.31	-11.95	11.09
		DODGE	-8.29	4.93	-11.08	10.21
		WRC-198			10.70	
		PRESENT METHOD	9.1833	5.7673	-11.4371	10.8141

TABLE 8

SQUARE LOADED AREAS

β	a/t	METHOD	C_L^* outside	C_L^* inside	C_L outside	C_L inside
0.10	5	WRC-107	-0.14	0.12	-0.21	0.21
		DODGE	-0.14	0.12	-0.21	0.21
		WRC-198			0.29	
		PRESENT METHOD	-0.1440	0.1056	-0.2235	0.2256
	10	WRC-107	-0.55	0.40	-0.80	0.76
		DODGE	-0.57	0.42	-0.81	0.78
		WRC-198			0.97	
		PRESENT METHOD	-0.5723	0.4021	-0.8747	0.8576
	20	WRC-107	-2.16	1.30	-2.93	2.71
		DODGE	-2.26	1.40	-2.98	2.76
		WRC-198			3.24	
		PRESENT METHOD	-2.2341	1.3963	-3.2533	3.0949
	40	WRC-107	-7.92	3.86	-10.06	8.89
		DODGE	-8.59	4.21	-10.22	8.98
		WRC-198			10.80	
		PRESENT METHOD	-8.4981	4.2112	-11.4453	10.4645
	80	WRC-107	-27.18	9.69	-29.72	23.53
		DODGE	-30.13	10.58	-31.58	25.25
		WRC-198			36.20	
		PRESENT METHOD	-30.9147	10.6229	-36.8139	32.1621

TABLE 9

SQUARE LOADED AREAS

β	a/t	METHOD	C_L^*		C_L	
			outside	inside	outside	inside
0.20	5	WRC-107	-0.56	0.34	-0.75	0.69
		DODGE	-0.55	0.33	-0.74	0.69
		WRC-198			0.81	
		PRESENT METHOD	-0.5547	0.3029	-0.7808	0.7723
	10	WRC-107	-2.06	0.88	-2.53	2.20
		DODGE	-2.03	0.92	-2.50	2.21
		WRC-198			2.71	
		PRESENT METHOD	-2.1504	1.0112	-2.8587	2.6795
	20	WRC-107	-7.19	2.28	-8.45	6.91
		DODGE	-7.25	2.38	-7.52	5.96
		WRC-198			9.05	
		PRESENT METHOD	-7.9104	2.7136	-9.6427	8.4992
	40	WRC-107	-21.63	4.99	-22.87	16.04
		DODGE	-22.15	4.29	-19.76	12.77
		WRC-198	30.20			
		PRESENT METHOD	-25.3141	3.8997	-28.2112	22.3787
	80	WRC-107	-58.88	2.56	-52.56	25.26
		DODGE	-50.65	4.25	-48.48	21.75
		WRC-198	101.0			
		PRESENT METHOD	-65.3099	7.4112	-64.3115	44.9237

TABLE 10

5.2.4.2 RECTANGULAR LOADED AREAS

Tables (11) through (14) show that Dodge's calculations generally agree with the approximate results obtained in WRC-107. However, for the cases considered in Table (14), both methods have failed to give the actual stress state on the shell. For example, when a/t=80, it is observed that the maximum stress index calculated using the present method is almost 120% more than the result given in WRC-107. Meanwhile, the result is only 20% more than what WRC-198 predicts. On the contrary, it is believed that the results in WRC-198 for a/t=5 and 10 are highly conservative. In addition, for the cases where β_1 =0.05, β_2 =0.20 and a/t=10, the present method calculates the maximum stress in axial direction whereas in WRC-198 it is predicted in circumferential direction.

In Table (11), for a/t $\leq$ 40 an excellent agreement is observed among the methods. But, for a/t=80, the predicted direction of the maximum stress in WRC-107 is found to be misleading.

In carrying out the same argument for the range of parameters in Table (12), WRC-107, once again, fails to predict the direction of maximum stress for a/t=80. For values of a/t=10,20 and 40 the present method and WRC-198 show a good agreement in calculating the maximum stress index.

Table (13) indicates that present method tends to be on the conservative side.

RECTANGULAR LOADED AREAS

β_1	β_2	a/t	METHOD	C_L^* outside	C_L^* inside	C_L outside	C_L inside
0.40	0.10	5	WRC-107	-0.380	0.304	-0.379	0.345
			DODGE	-0.168	0.090	-0.365	0.360
			WRC-198			0.383	
			PRESENT METHOD	-0.1956	0.061	-0.3488	0.3651
		10	WRC-107	-1.42	0.98	-1.29	1.63
			DODGE	-0.679	2.38	-1.32	1.27
			WRC-198			1.28	
			PRESENT METHOD	-0.7225	0.2183	-1.3006	1.2993
		20	WRC-107	-5.23	3.25	-4.44	3.40
			DODGE	-2.57	3.07	-4.38	4.12
			WRC-198			4.28	
			PRESENT METHOD	-2.6901	0.5128	-4.5803	4.4437
		40	WRC-107	-17.65	10.54	-13.90	9.15
			DODGE	-8.65	-1.405	-12.45	11.50
			WRC-198			14.3	
			PRESENT METHOD	-10.0032	-2.1589	-14.6987	13.9584
		80	WRC-107	-53.72	30.06	-34.22	15.03
			DODGE	-25.91	-11.11	-28.52	26.40
			WRC-198			47.7	
			PRESENT METHOD	-32.4843	12.9536	-41.8832	37.8389

TABLE 11

RECTANGULAR LOADED AREAS

β_1	β_2	a/t	METHOD	$C_{L\phi}^{*}$ outside	$C_{L\phi}^{*}$ inside	C_L outside	C_L inside
0.2	0.1	5	WRC-107	-0.238	0.192	-0.285	0.268
			DODGE	-0.155	0.108	-0.293	0.287
			WRC-198			0.368	
			PRESENT METHOD	-0.1740	0.0942	-0.3022	0.3088
		10	WRC-107	-0.897	0.621	-1.05	0.94
			DODGE	-0.632	0.357	-1.12	1.07
			WRC-198			1.23	
			PRESENT METHOD	-0.6779	0.3553	-1.1716	1.1532
		20	WRC-107	-3.46	2.07	-3.69	3.12
			DODGE	-2.48	0.96	-3.97	3.66
			WRC-198			4.11	
			PRESENT METHOD	-2.6433	1.1022	-4.3308	4.1070
		40	WRC-107	-12.28	6.09	-12.12	9.24
			DODGE	-9.00	1.54	-12.67	11.11
			WRC-198			13.7	
			PRESENT METHOD	-9.6384	-2.3307	-14.5600	13.3200
		80	WRC-107	-41:57	16.43	-32.80	19.91
			DODGE	-28.55	-25.43	-34.06	27.40
			WRC-198			45.8	
			PRESENT METHOD	-30.1200	5.5800	-41.6000	37.0581

TABLE 12

RECTANGULAR LOADED AREAS

β_1	β_2	a/t	METHOD	C_L^* outside	C_L^* inside	C_L outside	C_L inside
0.05	0.10	5	WRC-107	-0.081	0.073	-0.130	0.128
			DODGE	-0.098	0.085	-0.124	0.122
			WRC-198			0.197	
			PRESENT METHOD	-0.1069	0.0896	-0.1419	0.1381
		10	WRC-107	-0.302	0.256	-0.489	0.475
			DODGE	-0.392	0.314	-0.469	0.450
			WRC-198			0.658	
			PRESENT METHOD	-0.4251	0.3445	-0.5536	0.5341
		20	WRC-107	-1.174	0.910	-1.839	1.751
			DODGE	-1.595	1.152	-1.814	1.692
			WRC-198			2.20	
			PRESENT METHOD	-1.6584	1.2400	-2.0307	1.9208
		40	WRC-107	-4.301	2.992	-6.63	6.17
			DODGE	-6.199	3.894	-6.43	5.70
			WRC-198			7.34	
			PRESENT METHOD	-8.5040	4.1643	-11.5790	10.5487
		80	WRC-107	-15.18	8.91	-21.45	19.0
			DODGE	-22.63	12.11	-20.97	17.08
			WRC-198	24.5			
			PRESENT METHOD	30.8297	10.1826	37.0800	32.3400

TABLE 13

RECTANGULAR LOADED AREAS

β_1	β_2	a/t	METHOD	C_L^* outside	C_L^* inside	C_L outside	C_L inside
0.05	0.20	5	WRC-107	-0.107	0.069	-0.239	0.233
			DODGE	-0.240	0.183	-0.242	0.229
			WRC-198			0.385	
			PRESENT METHOD	-0.2645	0.2219	-0.2937	0,2869
		10	WRC-107	-0.416	0.180	-0.863	0.827
			DODGE	-0.955	0.661	-0.896	0.806
			WRC-198	1.29			
			PRESENT METHOD	-1.0571	0.8037	-1.1061	1.0366
		20	WRC-107	-1.57	0.368	-3.02	2.84
			DODGE	-3.43	2.103	-2.82	2.31
			WRC-198	4.30			
			PRESENT METHOD	-3.9154	2.6413	-3.8094	3.4307
		40	WRC-107	-5.54	0.0107	-9.85	9.05
			DODGE	-11.85	6.77	-8.59	6.06
			WRC-198	14.4			
			PRESENT METHOD	-15.3643	8.8672	-13.2971	10.93
		80	WRC-107	-19.64	-4.44	-25.37	22.56
			DODGE	-39.34	22.27	-26.79	15.33
			WRC-198	47.9			
			PRESENT METHOD	57.6896	-30.9088	44.9536	-28.5771

TABLE 14

5.2.5 <u>CHANGING THE POSITION OF THE LUGS ALONG THE LENGTH</u>

Finally, the effect of changing the position of the lug along the length has been analysed and presented in Fig. (29). The shell is assumed to be under 615000 lb-in of axial moment and 41000 lb of longitudinal force. Dotted lines in Fig.(29) show the position of the lug along the length. Stresses are in stress units and along the lug centerline.

First the lugs are placed 6 inches away from the free end. The maximum stress is found to be 15033 psi and occurs in the element close to the lower end of the lug-vessel interface along the circumferential direction.

As it is located 25 inches away from the free end, Fig. (29-b), the change in the direction and location of the maximum stress is observed and the magnitude is calculated 12264 psi, representing an 18% decrease in comparison with the maximum stress intensity found in Fig. (29-a).

In Fig. (29-c) where the lug is considered 47 inches away from the free end the magnitude and the direction as well as the location of the maximum stress are found unchanged.

An examination of Fig. (29-a) and (29-b) points out that for some cases placing the lugs at least a diameter away from the ends may be considered as a conservative condition. This can be interpreted in two ways, (i) The lugs may be placed less than the distance specified above, or (ii) The results may be used for ℓ/a values less than four. Further investigation is recommended to establish this clearly.

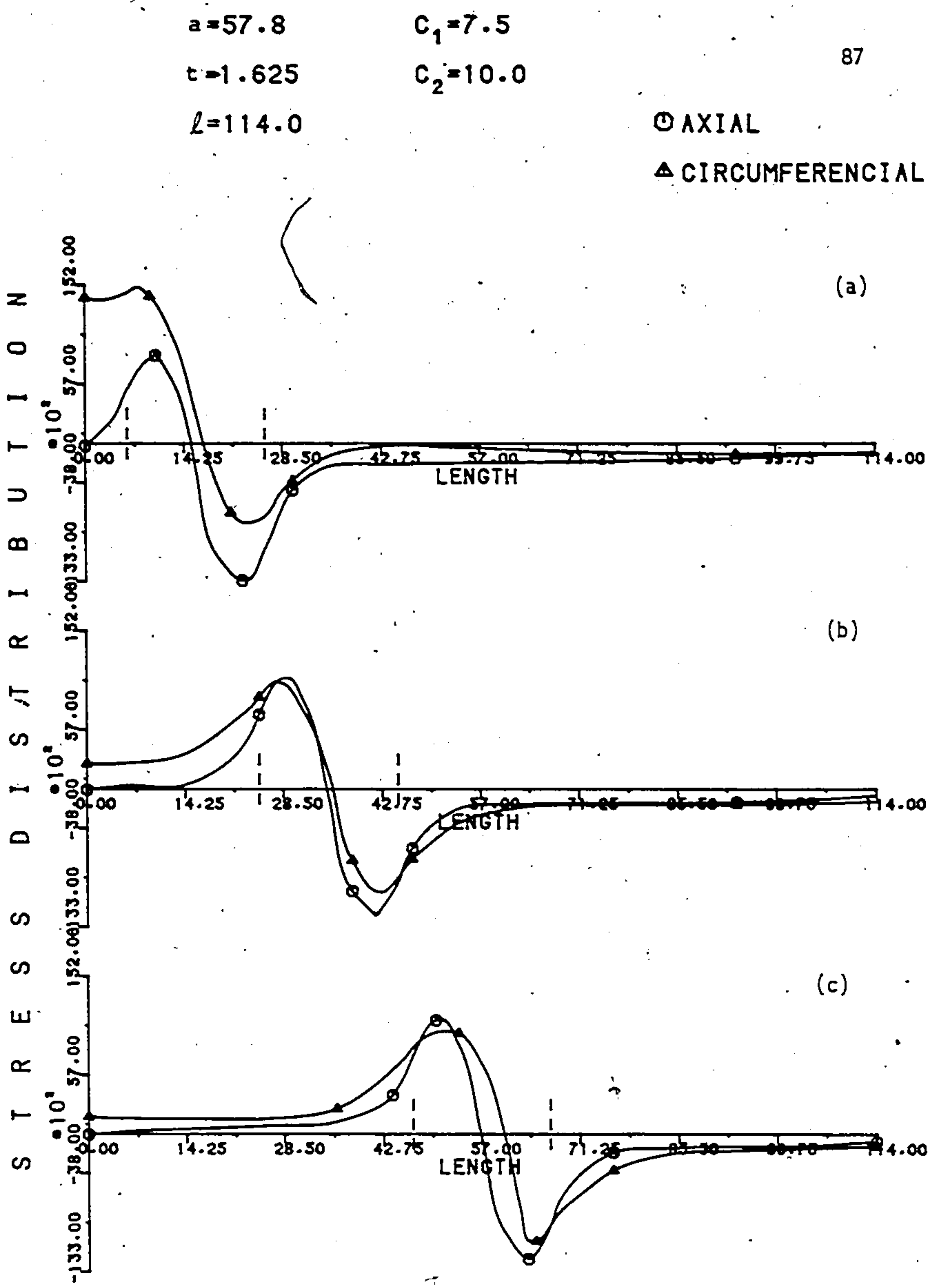

Figure 29: Stress distribution along lug centerline due to the change in the position of the lug

Chapter VI

CONCLUSIONS

The following conclusions can be drawn from this study:

a) Ring attachments:

1. Axial loading caused by the presence of this type of attachments results in a dominant membrane force on the shell. It has no self-limiting characteristics.
2. Large axial deformation is calculated, compared to radial deformation. It is seen that the axial deformation increases until it reaches its maximum value at the upper end of the loaded area and then it remains constant.
3. Among the variables considered, an increase in length to radius ratio, ℓ/a, is the one having the dominant effect on axial deformation.
4. Although bending moments are small compared to N_x/Et, locally they have a significant effect.

b) Integral lug attachments:

1. The maximum stress is located at the upper end of the lug-vessel interface. In addition, it occurs at the outside surface of the shell and for most of the cases considered in this study it is along the axial direction.

2. As a/t increases, membrane forces become dominant.
3. An increase in lug size in any direction causes higher stress state on the shell.
4. The position of the lugs along the length of the shell has significant effect on the magnitude and the location as well as on the direction of the maximum stress.
5. For square loaded areas, in general, the present method agrees with the results predicted in WRC-198. However, the same can not be said for rectangular lug attachments as some discrepancies in the results exist.

Appendix A
FRONT SOLVER

Simplified 'front solver' technique is used for solving the set of simultaneous equations. This method, which is developed by B.M.Irons in 1970 [12], takes care of large core storage problems. It is based on the fact that a large number of zeros in stiffness matrix, including the ones inside the band, do not necessarily have to be stored. Another advantage is the numbering system, node numbering is no more important in the solution but numbering of elements are. In Fig. (A-1) a simple flow chart is given for the front solver technique.

The first operation employed in subroutine PREFRONT is the determination of the maximum front width, in other words maximum number of unknowns at one time. Another subroutine attached to PREFRONT gives numbering sequence for the nodal points.

Starting from the last element, if the nodal number is appearing for the first time, a minus sign is introduced in front of each node number, so that these nodal displacements can be eliminated anywhere within the front width area at the time of forward elimination. As a result of second operation all the nodal numbers appearing for the last element will have a minus sign, indicating that MAIN and STFTR steps can be taken for usual finite element procedure. Meanwhile the location of displacements and forces have to be stored for the assembly of the whole structure.

Next operation which is FORWARD elimination, starts with the calculation of the first element stiffness matrix. If the minus sign appears in front of any nodal numbers for the first element, corresponding sets of equations for that particular node can be eliminated in front width area, using the Gaussian elimination procedure, and stiffness coefficients and the force term can be transfered to a temporary disc storage area.

After the calculation of the stiffness matrix for the next element, usual assembly can be carried out, adding stiffness coefficients which correspond to the same node number and introducing new stiffness coefficients into the front width area which are not yet there.

The same procedure which consists of eliminating corresponding equations for the nodes appearing for the last time and transferring the coefficients to the disc storage area, will be repeated until all the elements in the structure are completed.

When all the elements have been considered, the equations in the front width area can be reduced to one single equation using Gaussian elimination procedure and the unknown, either the displacement or the reaction force can be solved.

Then the next negative node is entered to the working area, for which the stiffness and force coefficients are already known and stored in temporary disc storage area. This procedure, called BACKWARD substitution, is repeated until all the unknowns in the structure have been determined.

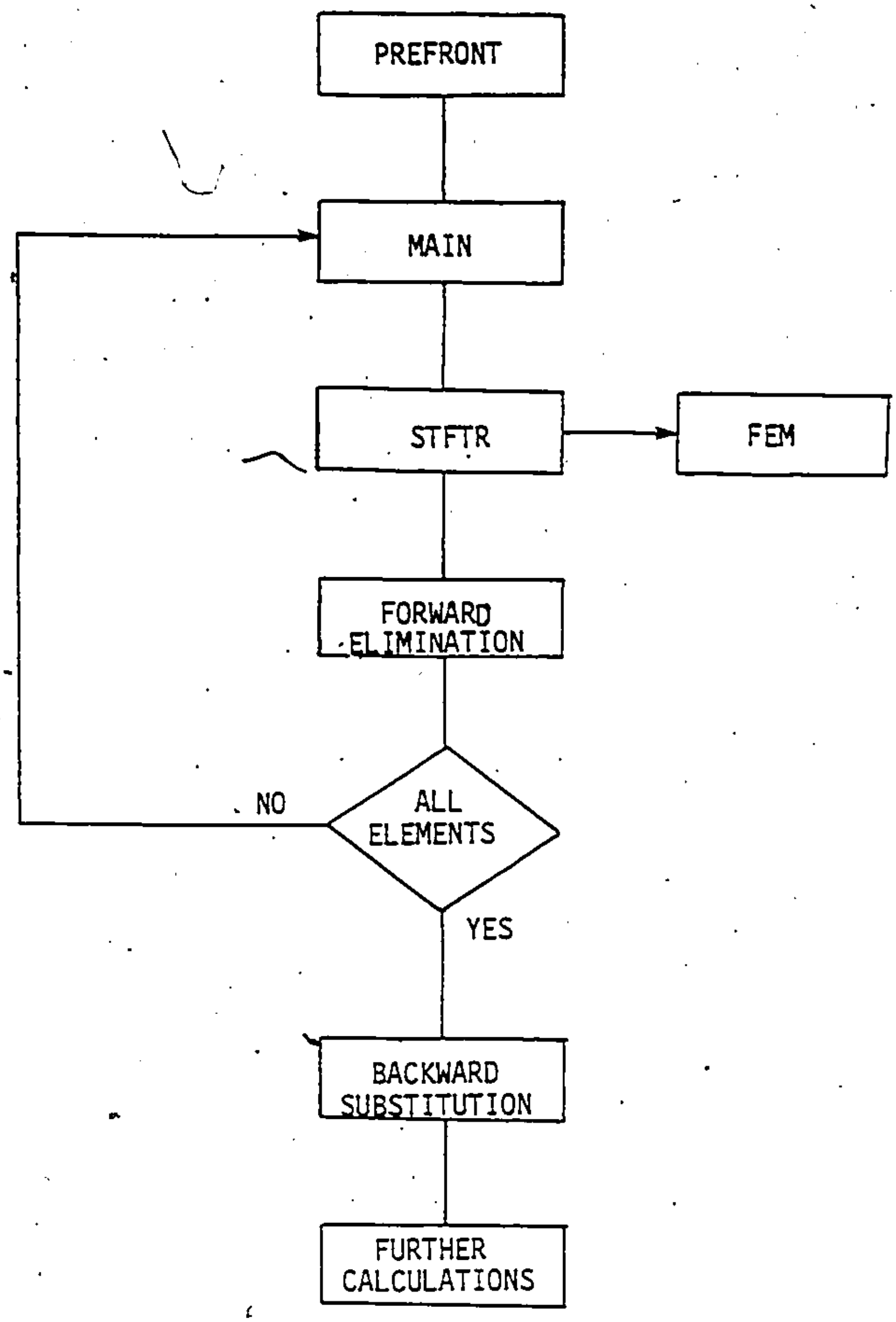

Figure A-1 Flow chart for Front Solver technique

Appendix B

SHAPE FUNCTIONS

$$N_1 = \frac{1}{12}(1-\xi)(1-\eta)\{4[\xi(1-\xi)(1+\xi)+\eta(1-\eta)(1+\eta)]+3\xi\eta\}$$

$$N_2 = -\frac{4}{3}\eta(1-\eta)(1+\eta)(0.5-\eta)(1-\xi)$$

$$N_3 = 2(1+\eta)(1-\eta)(1-\xi)[(0.5-\eta)(0.5+\eta)-\frac{1}{4}(1+\xi)]$$

$$N_4 = \frac{4}{3}\eta(1-\eta)(1+\eta)(0.5+\eta)(1-\xi)$$

$$N_5 = \frac{1}{12}(1-\eta)(1+\eta)\{4[\xi(1-\xi)(1+\xi)-\eta(1-\eta)(1+\eta)]-3\xi\eta\}$$

$$N_6 = -\frac{4}{3}\xi(1+\xi)(1-\xi)(0.5-\xi)(1+\eta)$$

$$N_7 = 2(1+\eta)(1+\xi)(1-\xi)[(0.5-\xi)(0.5+\xi)-\frac{1}{4}(1-\eta)]$$

$$N_8 = \frac{4}{3}\xi(1+\xi)(1-\xi)(0.5+\xi)(1+\eta)$$

$$N_9 = \frac{1}{12}(1+\xi)(1+\eta)\{-4[\xi(1-\xi)(1+\xi)+\eta(1-\eta)(1+\eta)]+3\xi\eta\}$$

$$N_{10} = \frac{4}{3}\eta(1-\eta)(1+\eta)(0.5+\eta)(1+\xi)$$

$$N_{11} = 2(1+\eta)(1-\eta)(1+\xi)[(0.5-\eta)(0.5+\eta)-\frac{1}{4}(1-\xi)]$$

$$N_{12} = -\frac{4}{3}\eta(1-\eta)(1+\eta)(0.5-\eta)(1+\xi)$$

$$N_{13} = \frac{1}{12}(1+\xi)(1-\eta)\{-4[\xi(1-\xi)(1+\xi)-\eta(1-\eta)(1+\eta)]-3\xi\eta\}$$

$$N_{14} = \frac{4}{3}\xi(1+\xi)(1-\xi)(0.5+\xi)(1-\eta)$$

$$N_{15} = 2(1+\xi)(1-\xi)(1-\eta)[(0.5+\xi)(0.5-\xi)-\frac{1}{4}(1+\eta)]$$

$$N_{16} = -\frac{4}{3}\xi(1+\xi)(1-\xi)(0.5-\xi)(1-\eta)$$

$$N_{17} = (1+\xi)(1-\xi)(1+\eta)(1-\eta)$$

Appendix C

FLOW CHART OF THE COMPUTER PROGRAM

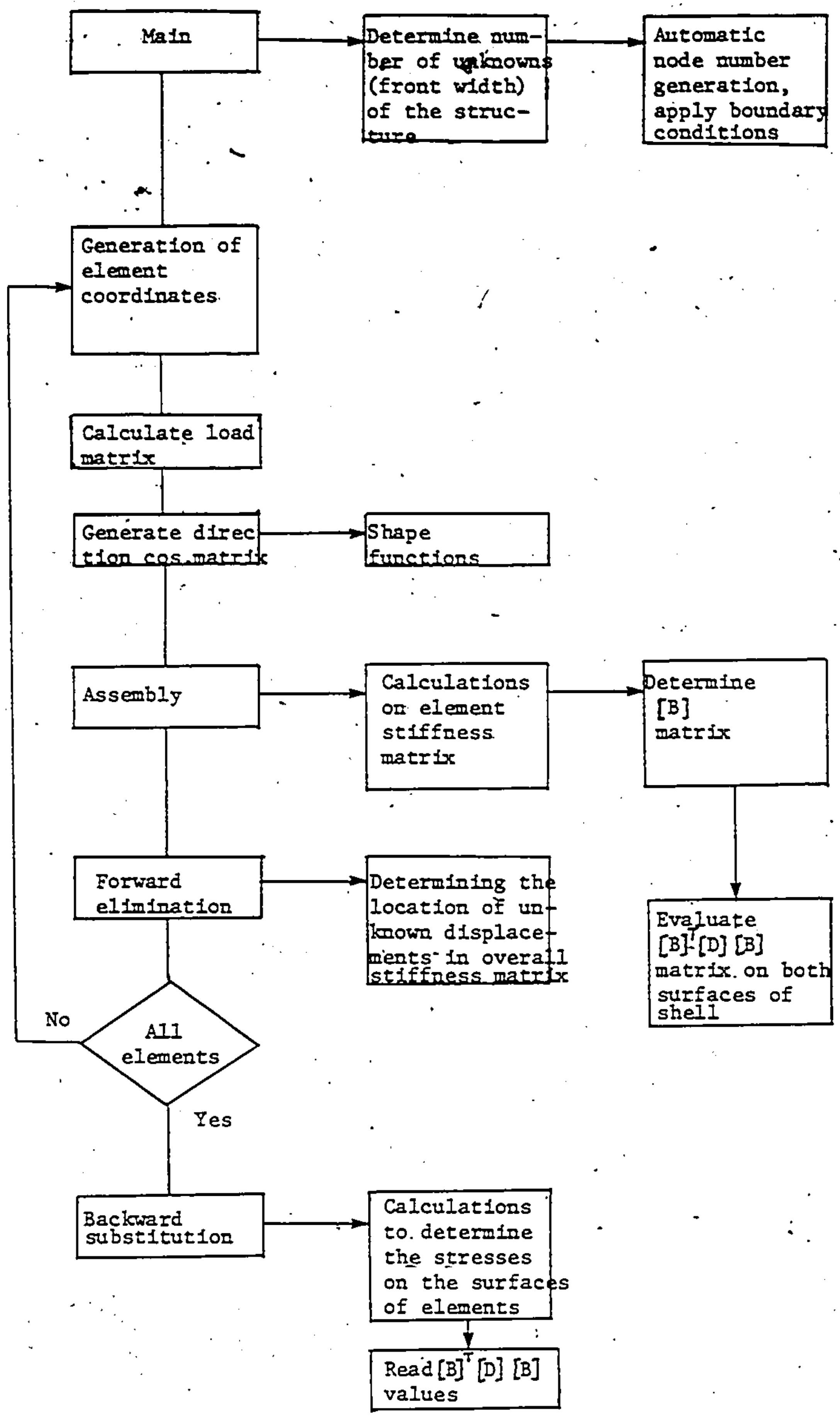
Main
Determine number of unknowns (front width) of the structure
Automatic node number generation, apply boundary conditions
Generation of element coordinates
Calculate load matrix
Generate direction cos.matrix
Shape functions
Assembly
Calculations on element stiffness matrix
Determine [B] matrix
Forward elimination
Determining the location of unknown displacements in overall stiffness matrix
Evaluate $[B]^T[D][B]$ matrix on both surfaces of shell
No
All elements
Yes
Backward substitution
Calculations to determine the stresses on the surfaces of elements
Read $[B]^T[D][B]$ values

Appendix D

β	a/t	Maximum stress index	Percent difference
0.05	5	0.0559	75
0.10	5	0.2235	71
0.20	5	0.7808	
0.05	10	0.2229	74
0.10	10	0.8747	69
0.20	10	2.8587	
0.05	20	0.8589	74
0.10	20	3.2533	66
0.20	20	9.6427	
0.05	40	3.2300	71
0.10	40	11.4453	59
0.20	40	28.2112	
0.05	80	11.4371	69
0.10	80	36.8139	43
0.20	80	65.3099	

TABLE D-1

β_1	β_2	a/t	Maximum stress index	Percent difference
0.05	0.10	5	0.1419	113
0.20	0.10	5	0.3022	15
0.40	0.10	5	0.3488	
0.05	0.10	10	0.5536	112
0.20	0.10	10	1.1716	11
0.40	0.10	10	1.3006	
0.05	0.10	20	2.0307	113
0.20	0.10	20	4.3308	6
0.40	0.10	20	4.5803	
0.05	0.10	40	11.5790	26
0.20	0.10	40	14.5600	1.0
0.40	0.10	40	14.6987	
0.05	0.10	80	37.0800	12
0.20	0.10	80	41.6000	0.7
0.40	0.10	80	41.8832	

TABLE D-2

β_1	β_2	a/t	Maximum stress index	Percent difference
0.05	0.10	5	0.1419	106
0.05	0.20	5	0.2937	
0.05	0.10	10	0.5536	99
0.05	0.20	10	1.1061	
0.05	0.10	20	2.0307	92
0.05	0.20	20	3.9154	
0.05	0.10	40	11.5790	32
0.05	0.20	40	15.3643	
0.05	0.10	80	37.0800	55
0.05	0.20	80	57.6896	

Table D-3

Appendix E

The parameters a, ℓ, ℓ_1, ℓ_2, t, u and w that have been utilized in the text have been referred to as A, L, L1, L2, T, U and W respectively, in the following figures of this appendix.

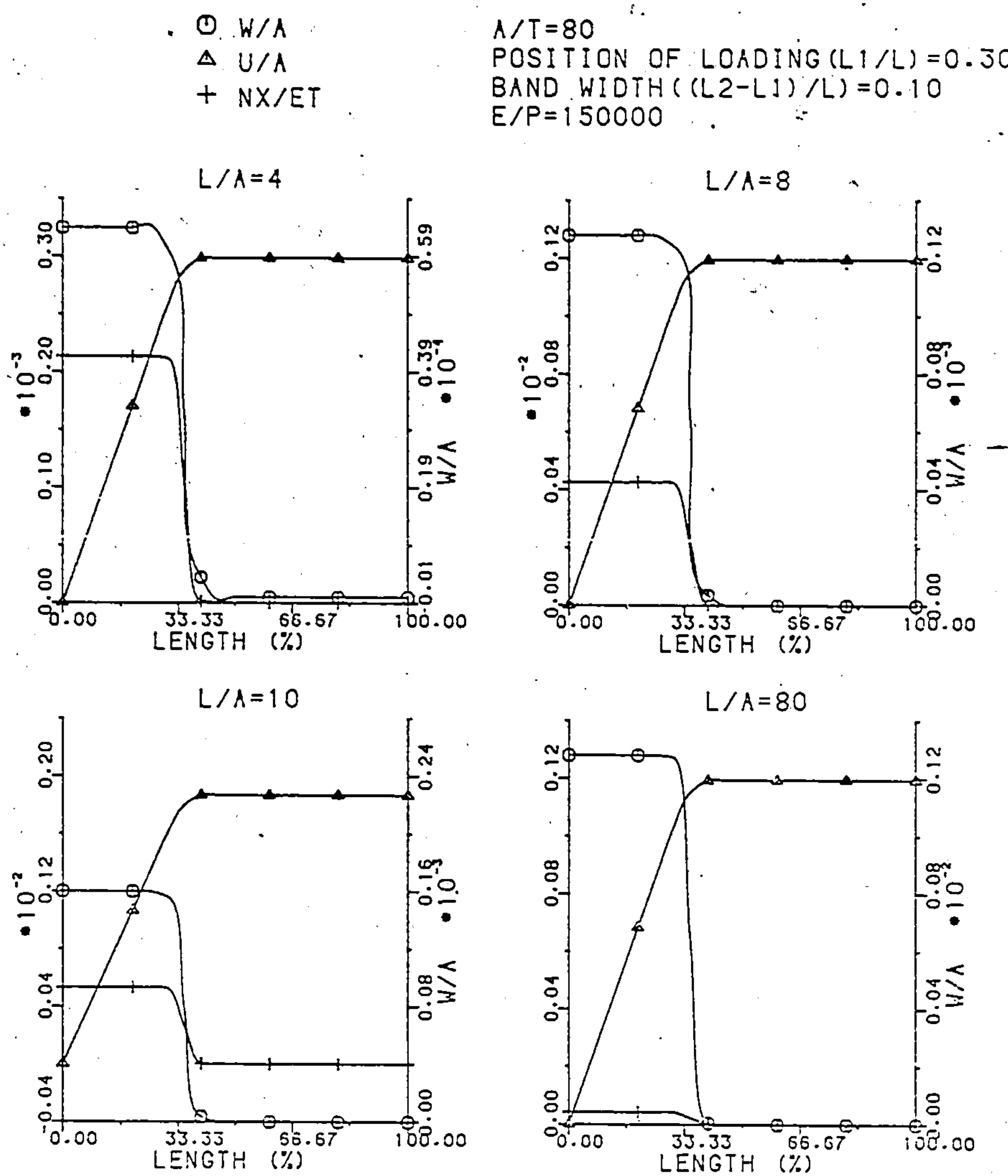

O W/A
Δ U/A
+ NX/ET
A/T=80
POSITION OF LOADING(L1/L)=0.30
BAND WIDTH((L2-L1)/L)=0.10
E/P=150000
L/A=4
L/A=8
L/A=10
L/A=80
LENGTH (%)
W/A
0.00
33.33
66.67
100.00

⊕ W/A
Δ U/A
+ NX/ET

A/T=10
POSITION OF LOADING(L1/L)=0.50
BAND WIDTH((L2-L1)/L)=0.10
E/P=150000

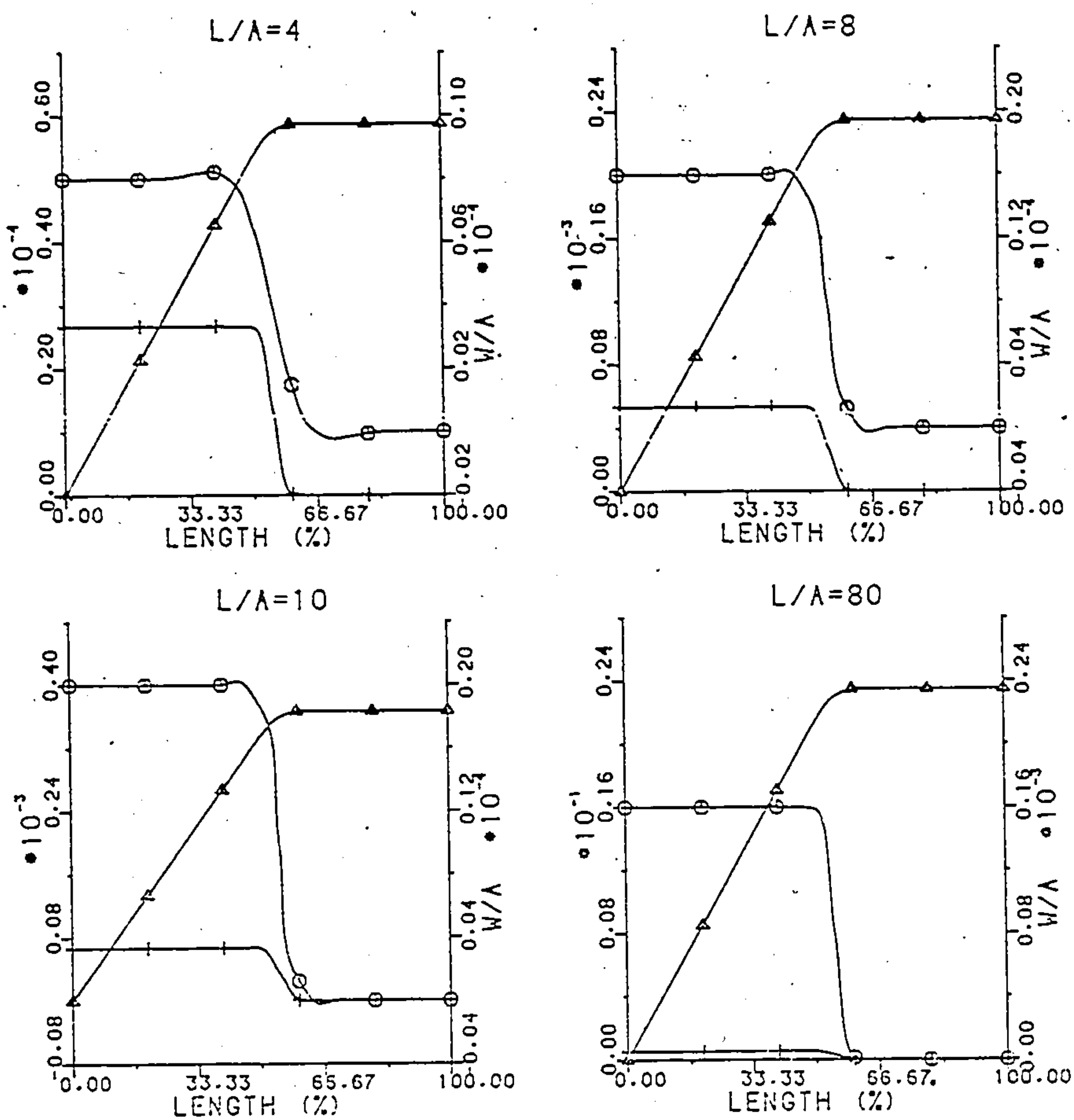

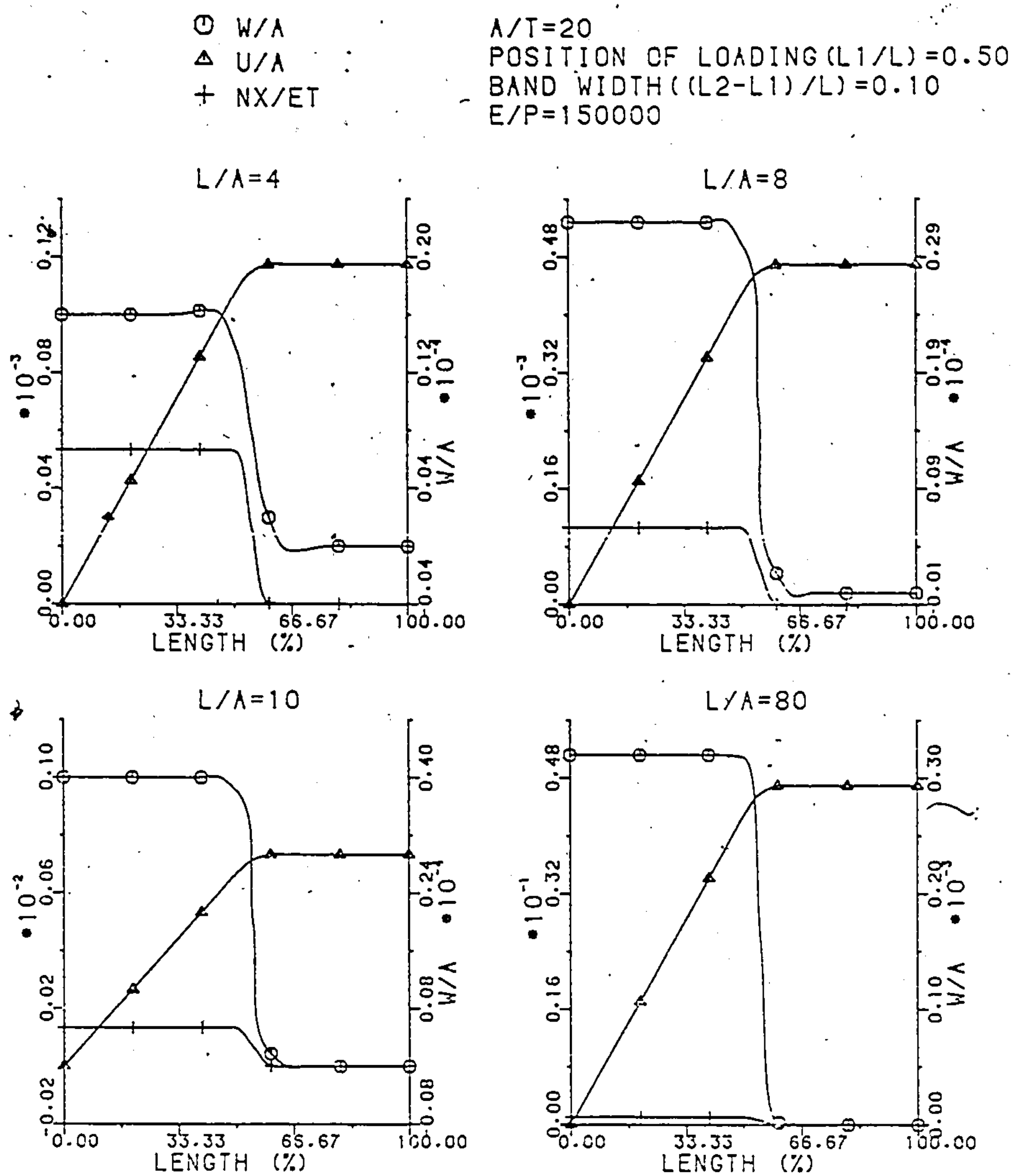

O W/A
△ U/A
+ NX/ET
A/T=20
POSITION OF LOADING(L1/L)=0.50
BAND WIDTH((L2-L1)/L)=0.10
E/P=150000
L/A=4
L/A=8
L/A=10
L/A=80
LENGTH (%)
W/A
0.00
33.33
66.67
100.00

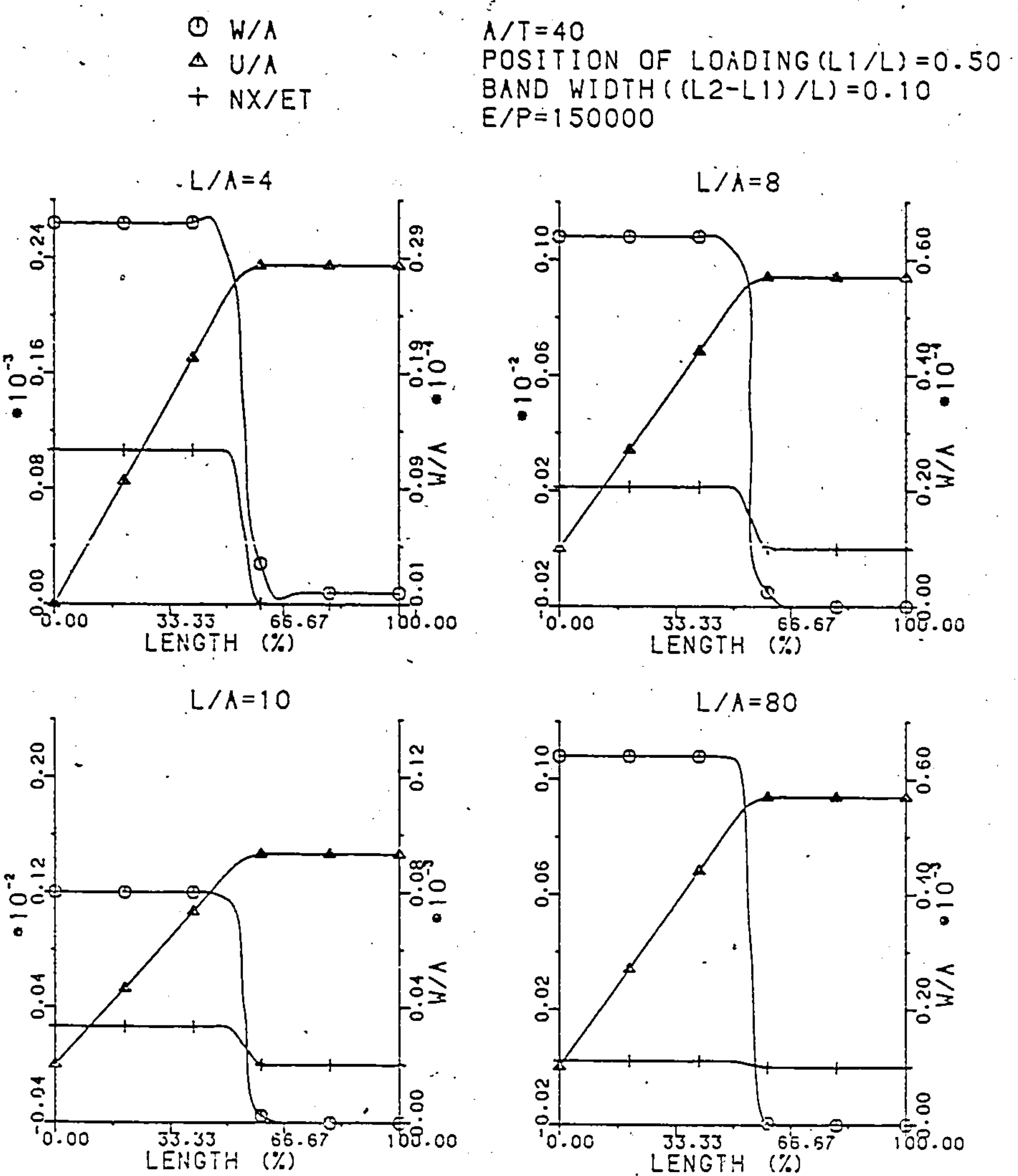

W/A
U/A
NX/ET
A/T=40
POSITION OF LOADING(L1/L)=0.50
BAND WIDTH((L2-L1)/L)=0.10
E/P=150000
L/A=4
L/A=8
L/A=10
L/A=80
LENGTH (%)
W/A
0.00
33.33
66.67
100.00

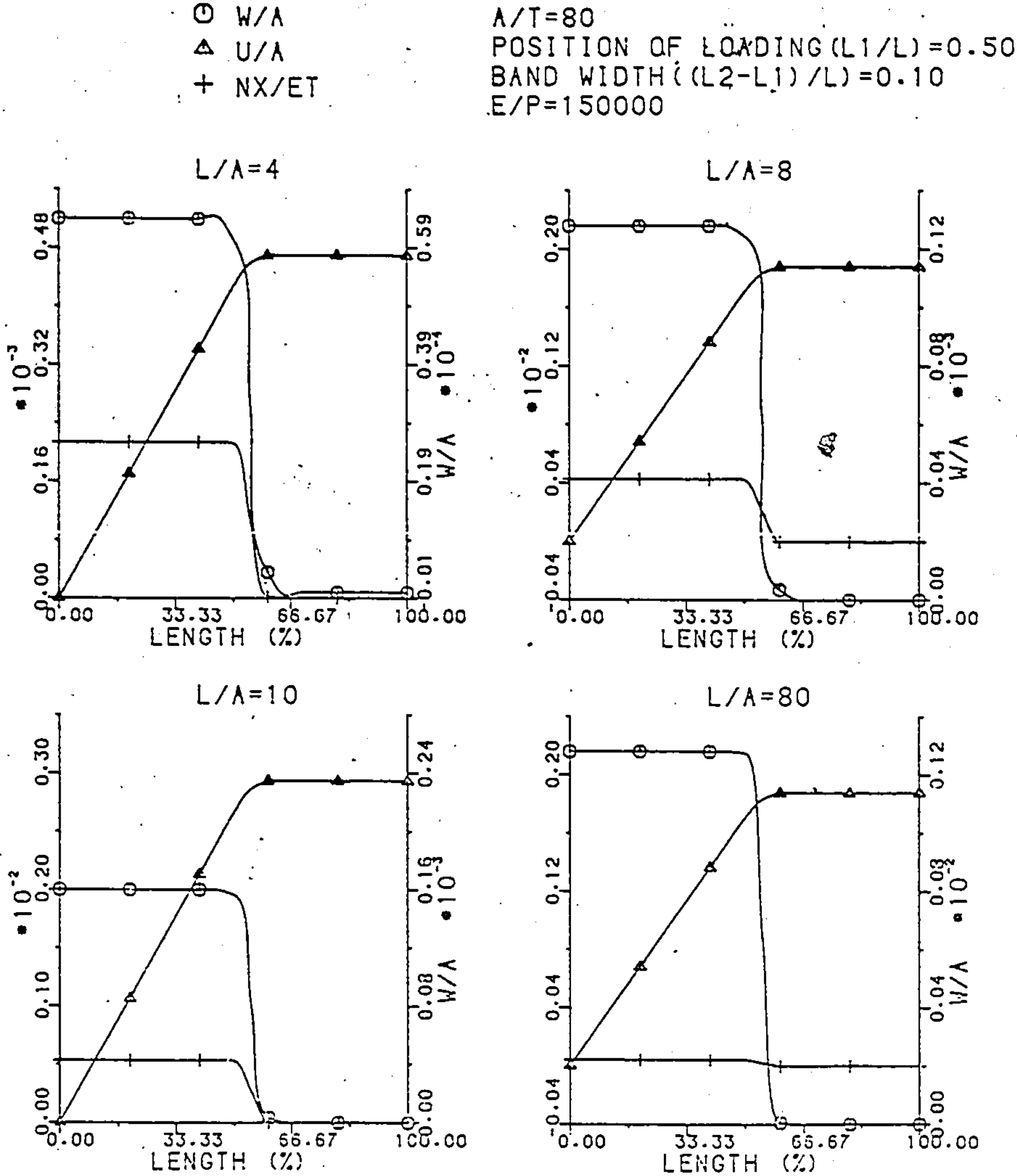

W/Λ
U/Λ
NX/ET
Λ/T=80
POSITION OF LOADING(L1/L)=0.50
BAND WIDTH((L2-L1)/L)=0.10
E/P=150000
L/Λ=4
L/Λ=8
L/Λ=10
L/Λ=80
LENGTH (%)
0.00
33.33
66.67
100.00
W/Λ

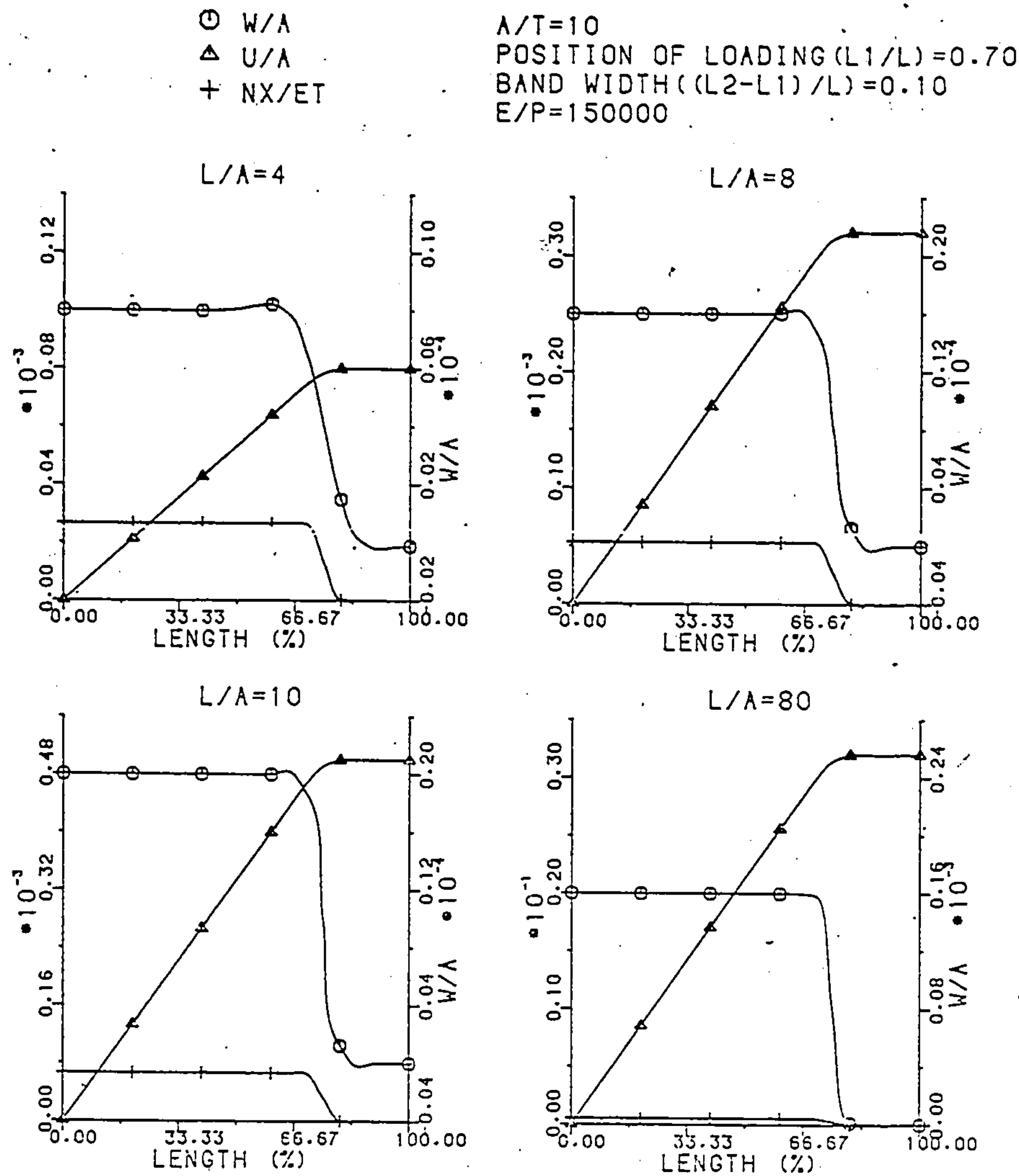

⊖ W/A
△ U/A
+ NX/ET
A/T=10
POSITION OF LOADING(L1/L)=0.70
BAND WIDTH((L2-L1)/L)=0.10
E/P=150000
L/A=4
L/A=8
L/A=10
L/A=80
LENGTH (%)

O W/A
△ U/A
+ NX/ET

A/T=20
POSITION OF LOADING(L1/L)=0.70
BAND WIDTH((L2-L1)/L)=0.10
E/P=150000

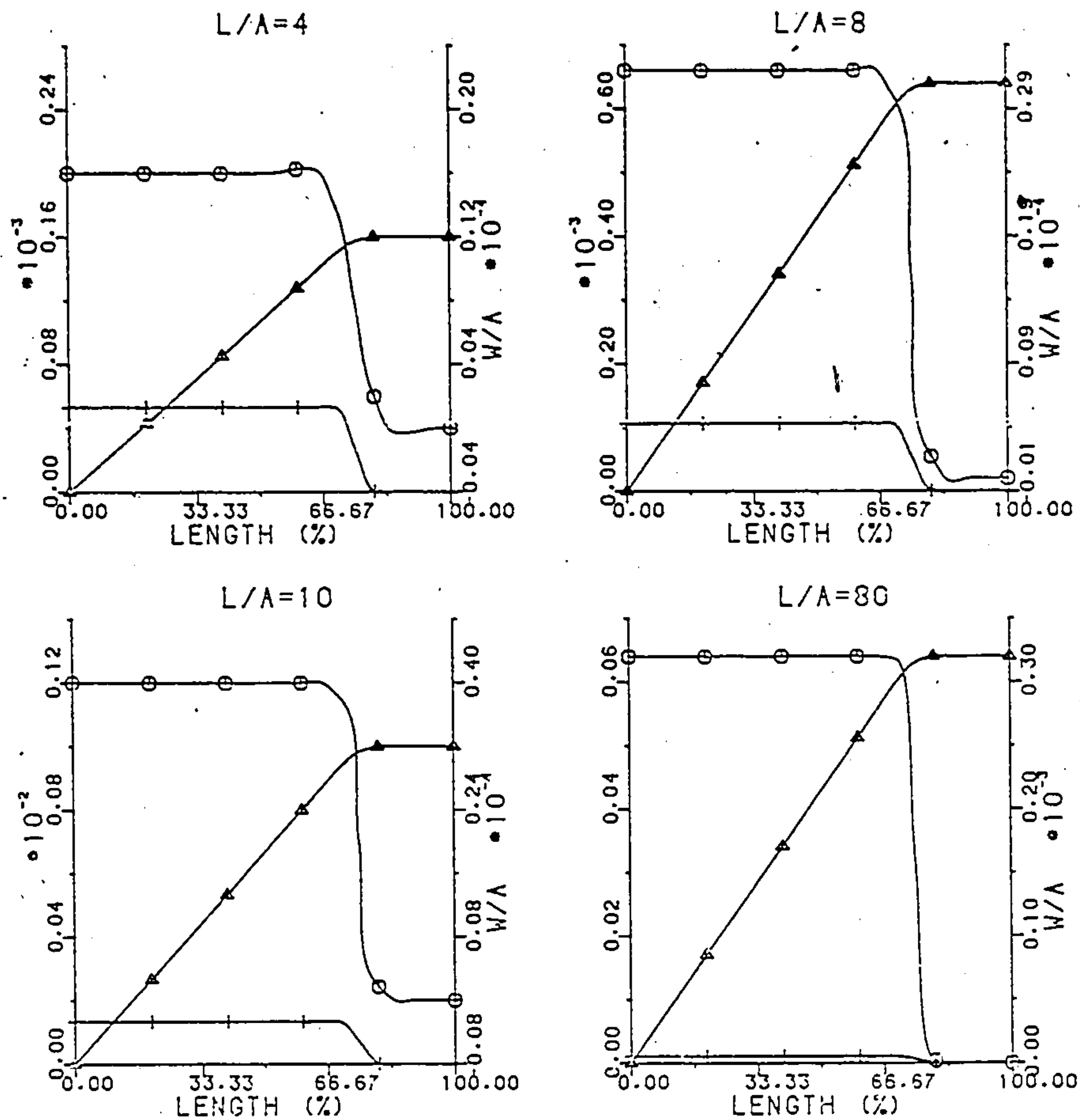

O W/A
Δ U/A
+ NX/ET

A/T=40
POSITION OF LOADING (L1/L)=0.70
BAND WIDTH ((L2-L1)/L)=0.10
E/P=150000

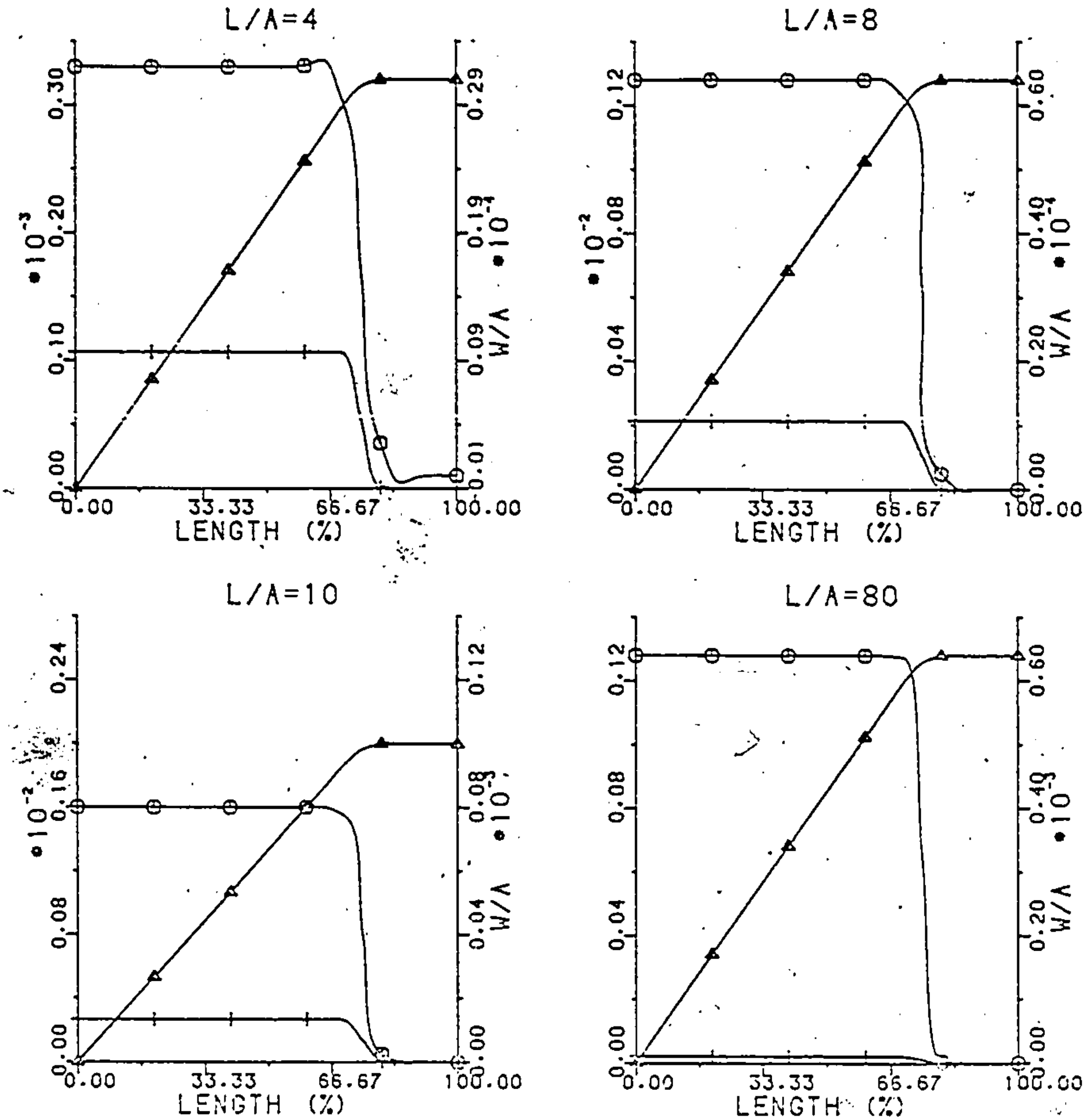

⊕ W/A
△ U/A
+ NX/ET

A/T=80
POSITION OF LOADING(L1/L)=0.70
BAND WIDTH((L2-L1)/L)=0.10
E/P=150000

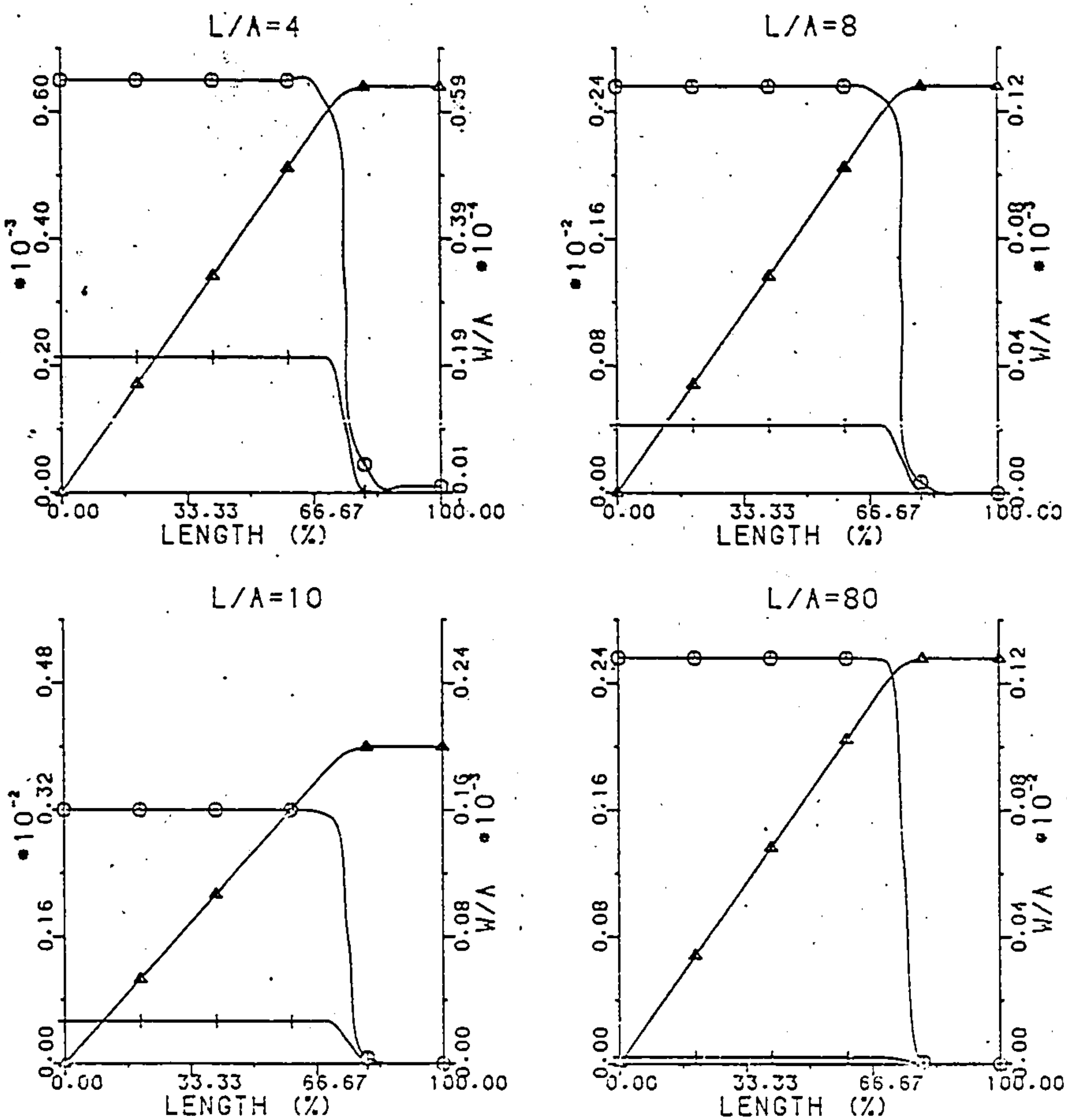

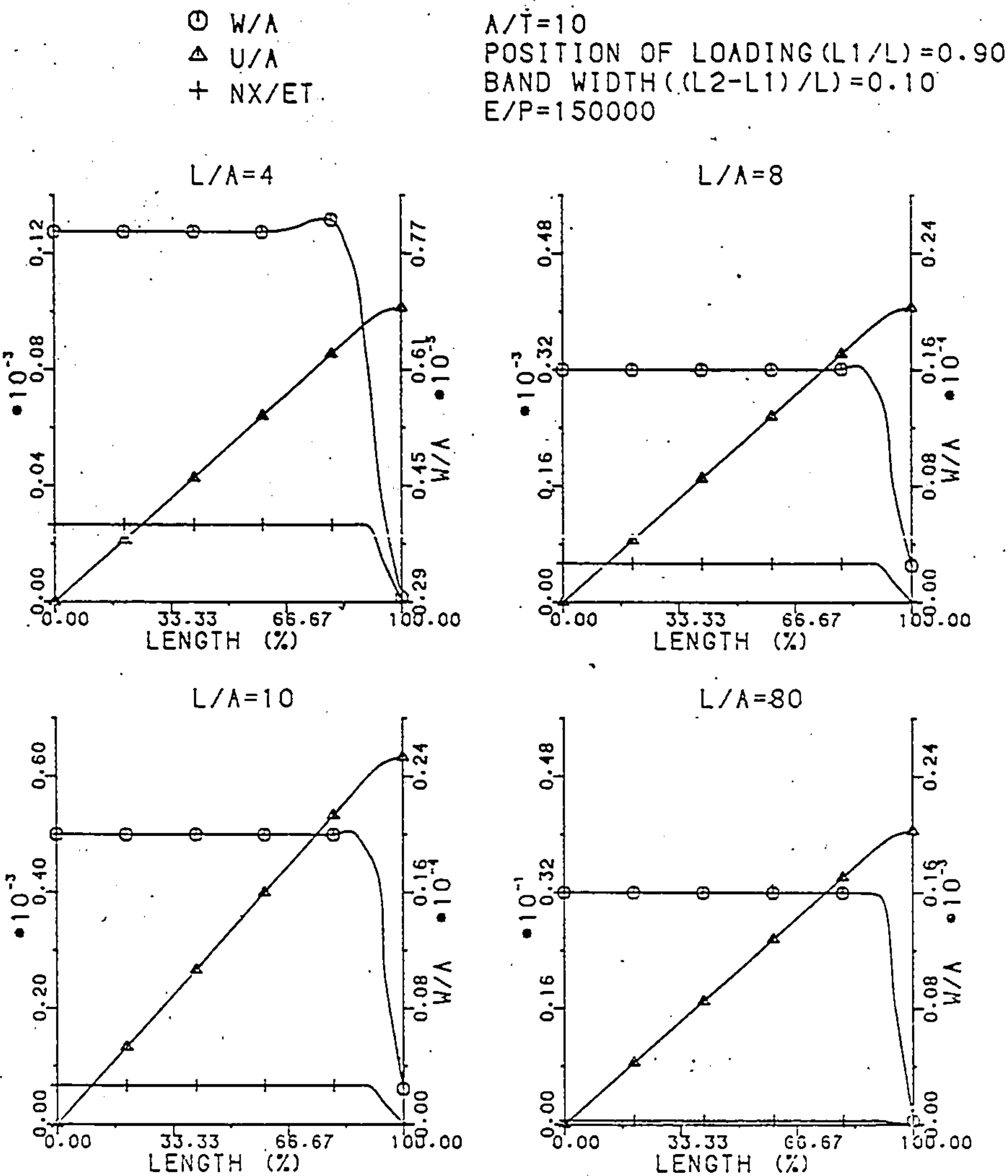

W/A
U/A
NX/ET
A/T=10
POSITION OF LOADING(L1/L)=0.90
BAND WIDTH((L2-L1)/L)=0.10
E/P=150000
L/A=4
L/A=8
L/A=10
L/A=80
LENGTH (%)
W/A
0.00
33.33
66.67
100.00

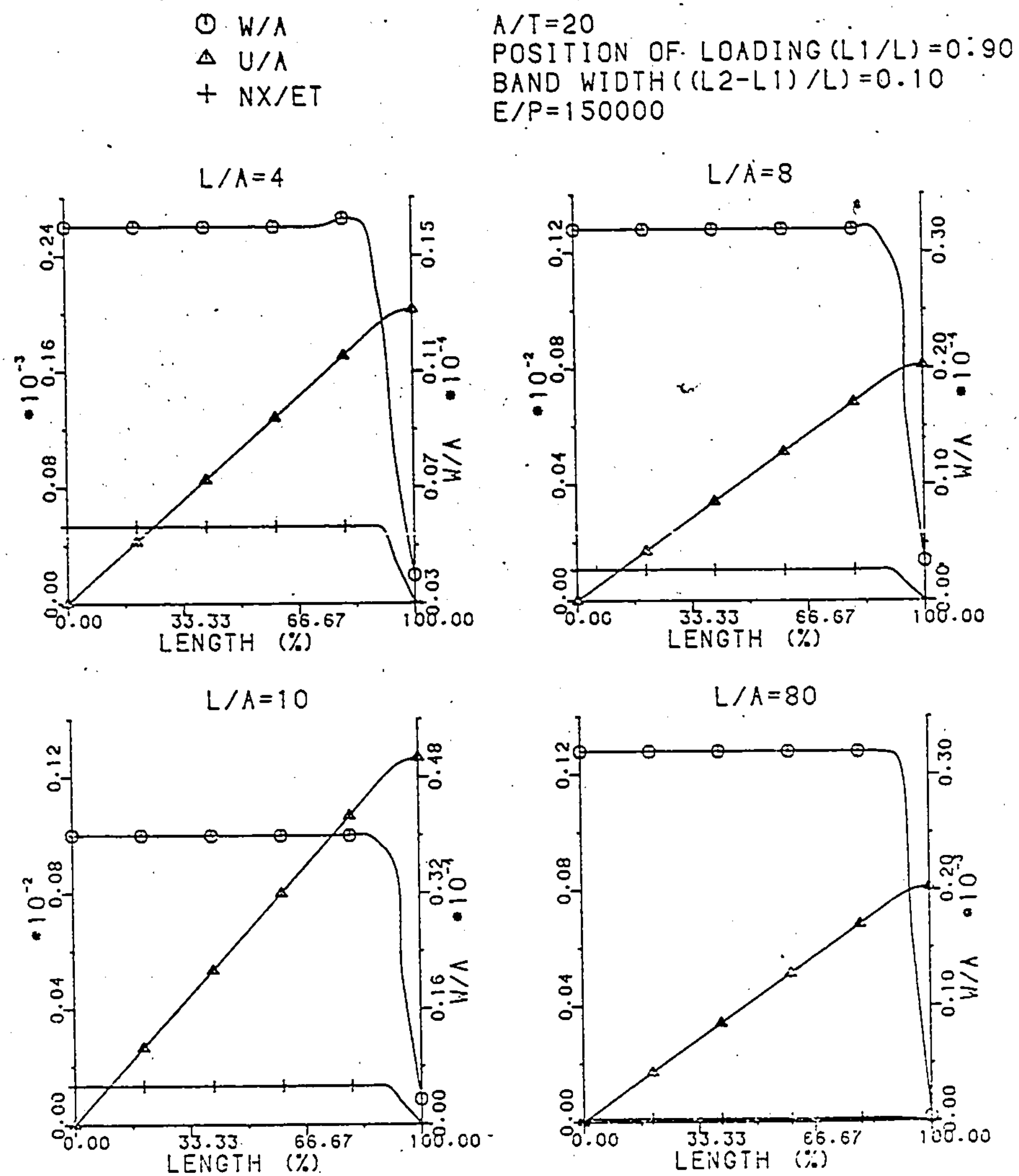

W/A
U/A
NX/ET
A/T=20
POSITION OF LOADING(L1/L)=0.90
BAND WIDTH((L2-L1)/L)=0.10
E/P=150000
L/A=4
L/A=8
L/A=10
L/A=80
LENGTH (%)
0.00
33.33
66.67
100.00

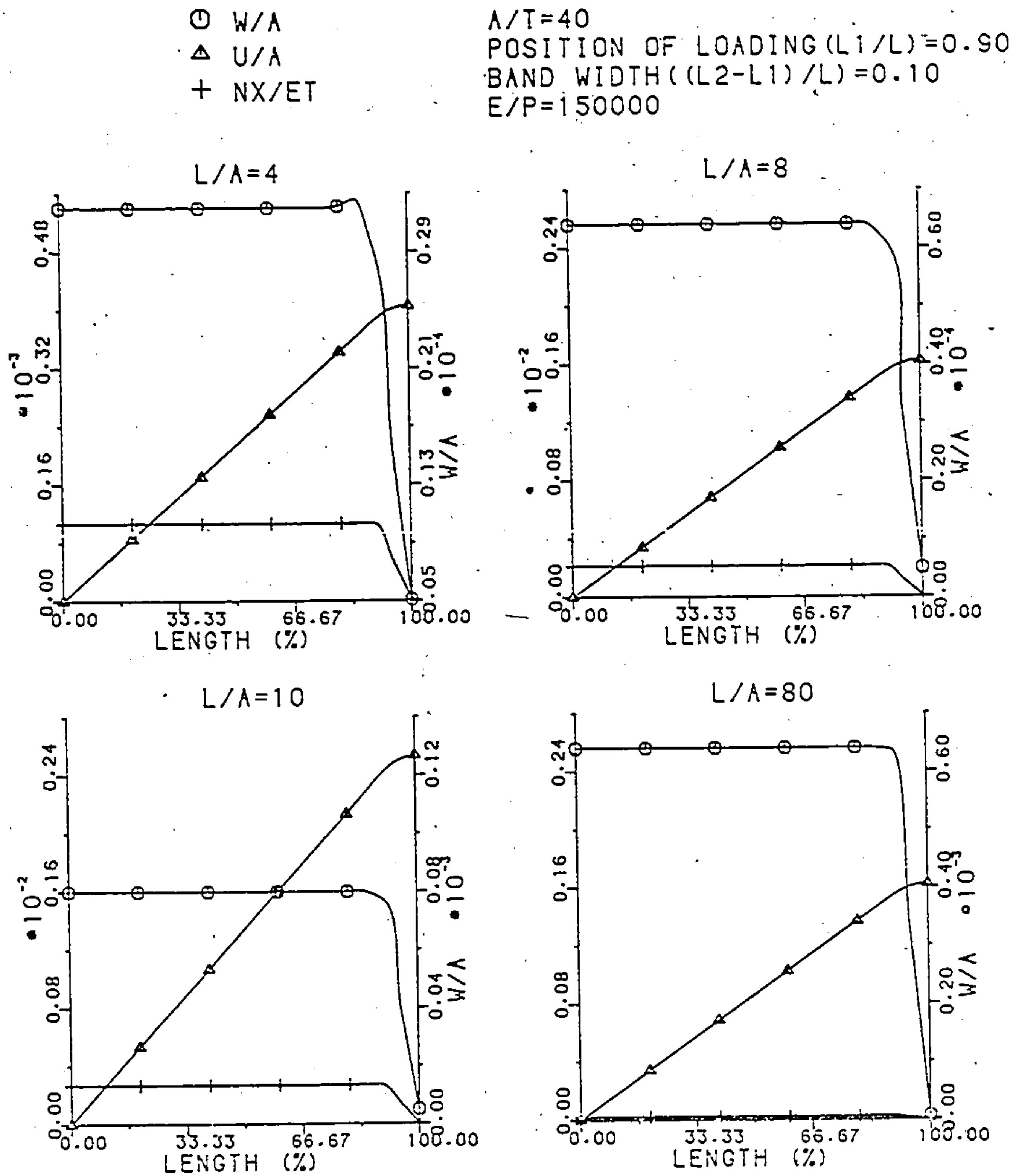

O W/A
Δ U/A
+ NX/ET
A/T=40
POSITION OF LOADING(L1/L)=0.90
BAND WIDTH((L2-L1)/L)=0.10
E/P=150000
L/A=4
L/A=8
L/A=10
L/A=80
0.00
0.16
0.32
0.48
*10^-3
0.05
0.13
0.21
0.29
W/A *10^-1
0.00
0.08
0.16
0.24
*10^-2
0.00
0.20
0.40
0.60
0.04
0.08
0.12
W/A *10^-3
0.00
33.33
66.67
100.00
LENGTH (%)

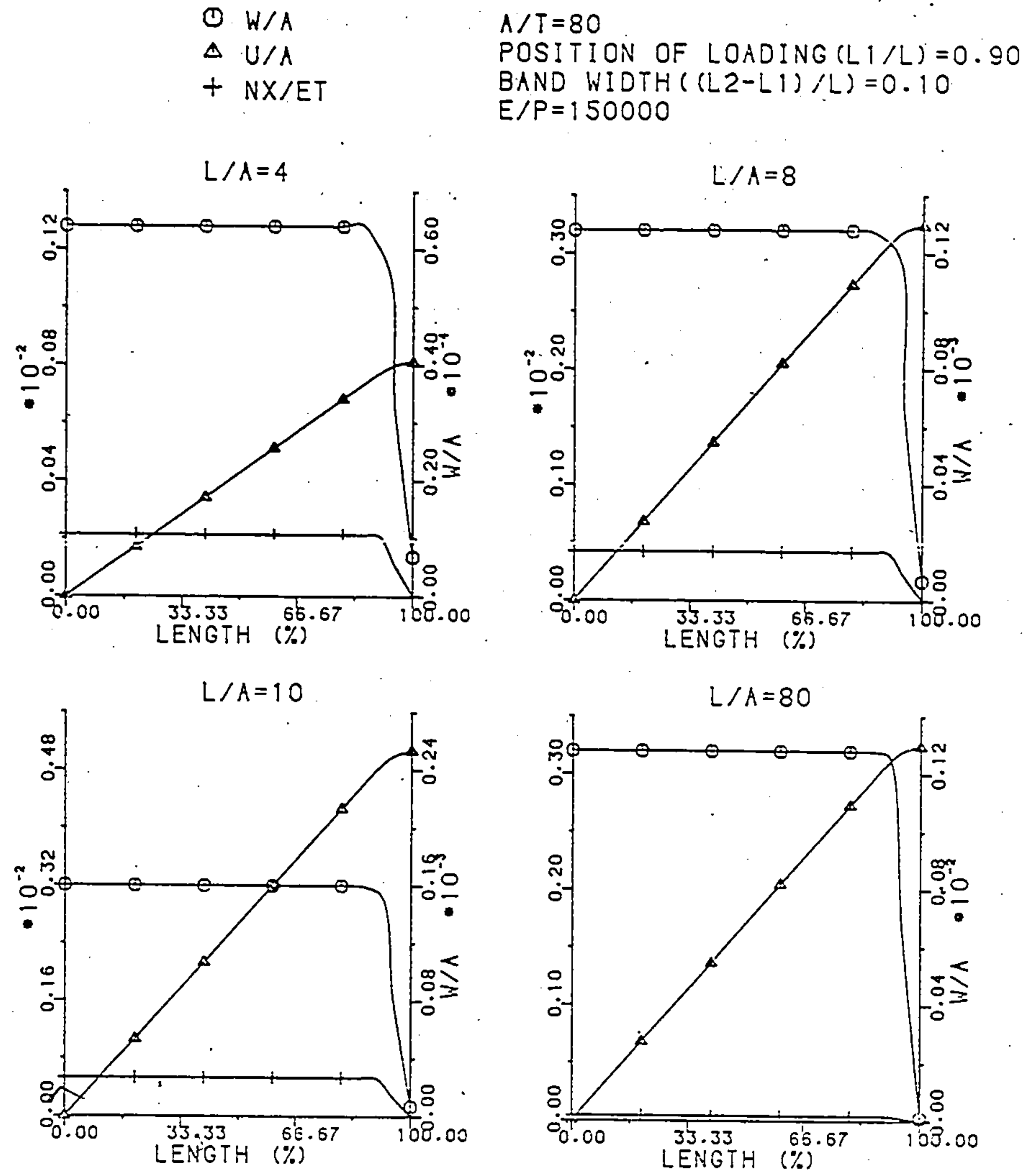

W/A
U/A
NX/ET
A/T=80
POSITION OF LOADING(L1/L)=0.90
BAND WIDTH((L2-L1)/L)=0.10
E/P=150000
L/A=4
L/A=8
L/A=10
L/A=80
LENGTH (%)
0.00
33.33
66.67
100.00
•10^-2
W/A •10^-4
W/A •10^-3

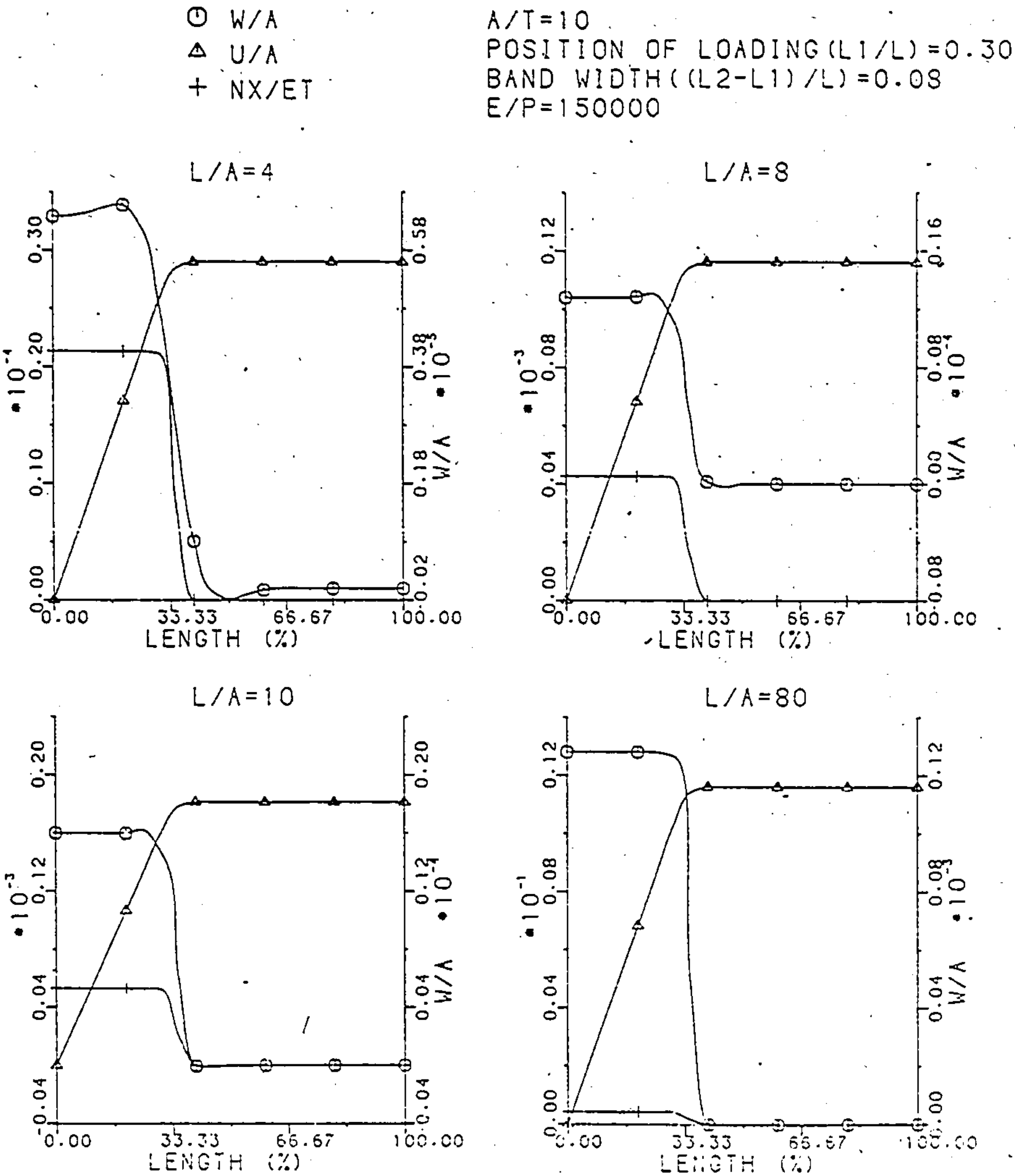

O W/A
Δ U/A
+ NX/ET
A/T=10
POSITION OF LOADING(L1/L)=0.30
BAND WIDTH((L2-L1)/L)=0.08
E/P=150000
L/A=4
L/A=8
L/A=10
L/A=80
LENGTH (%)
W/A
0.00
33.33
66.67
100.00

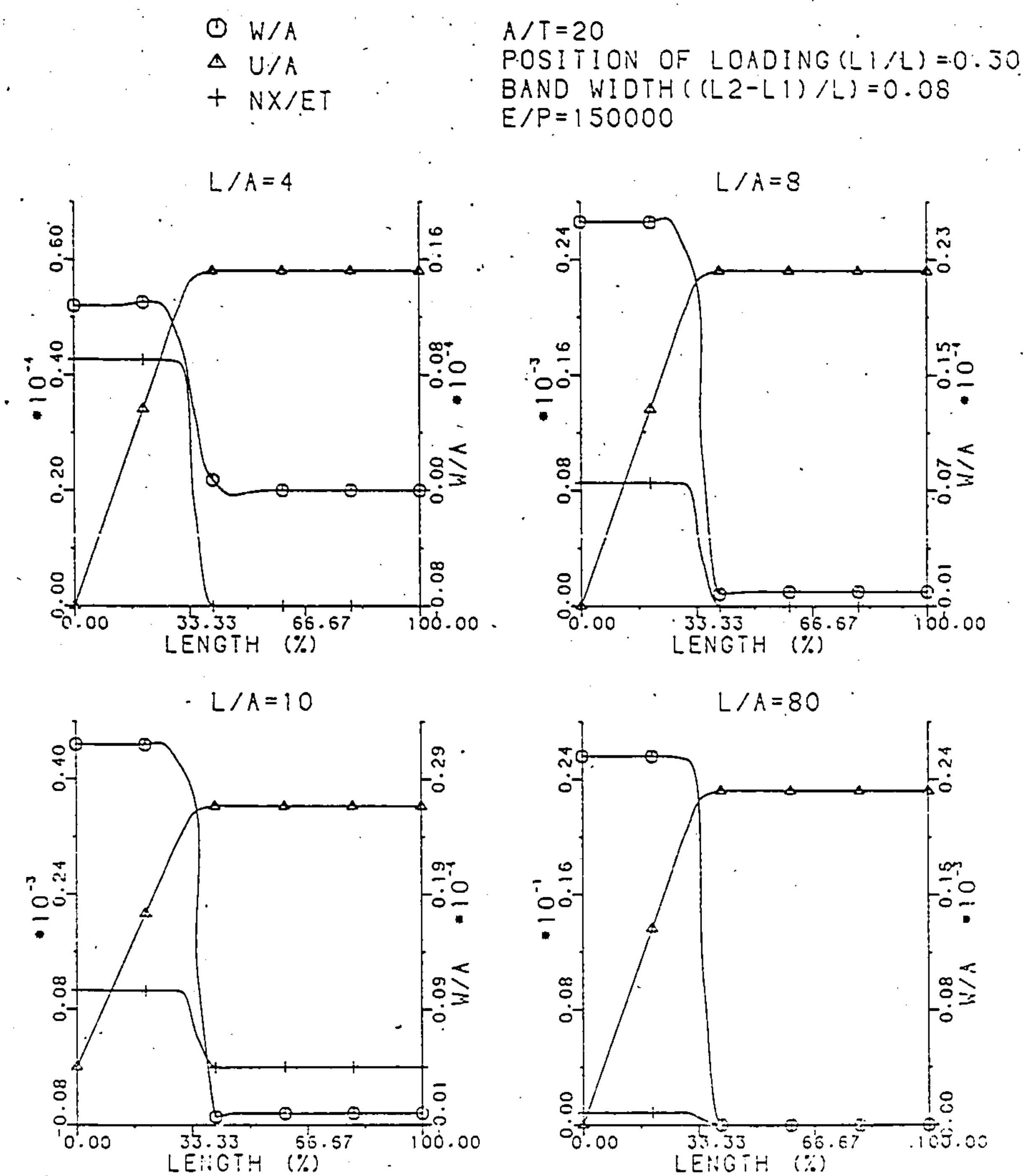
W/A
U/A
NX/ET
A/T=20
POSITION OF LOADING(L1/L)=0.30
BAND WIDTH((L2-L1)/L)=0.08
E/P=150000
L/A=4
L/A=8
L/A=10
L/A=80
LENGTH (%)
W/A

⊖ W/A
Δ U/A
+ NX/ET

A/T=40
POSITION OF LOADING(L1/L)=0.30
BAND WIDTH((L2-L1)/L)=0.08
E/P=150000

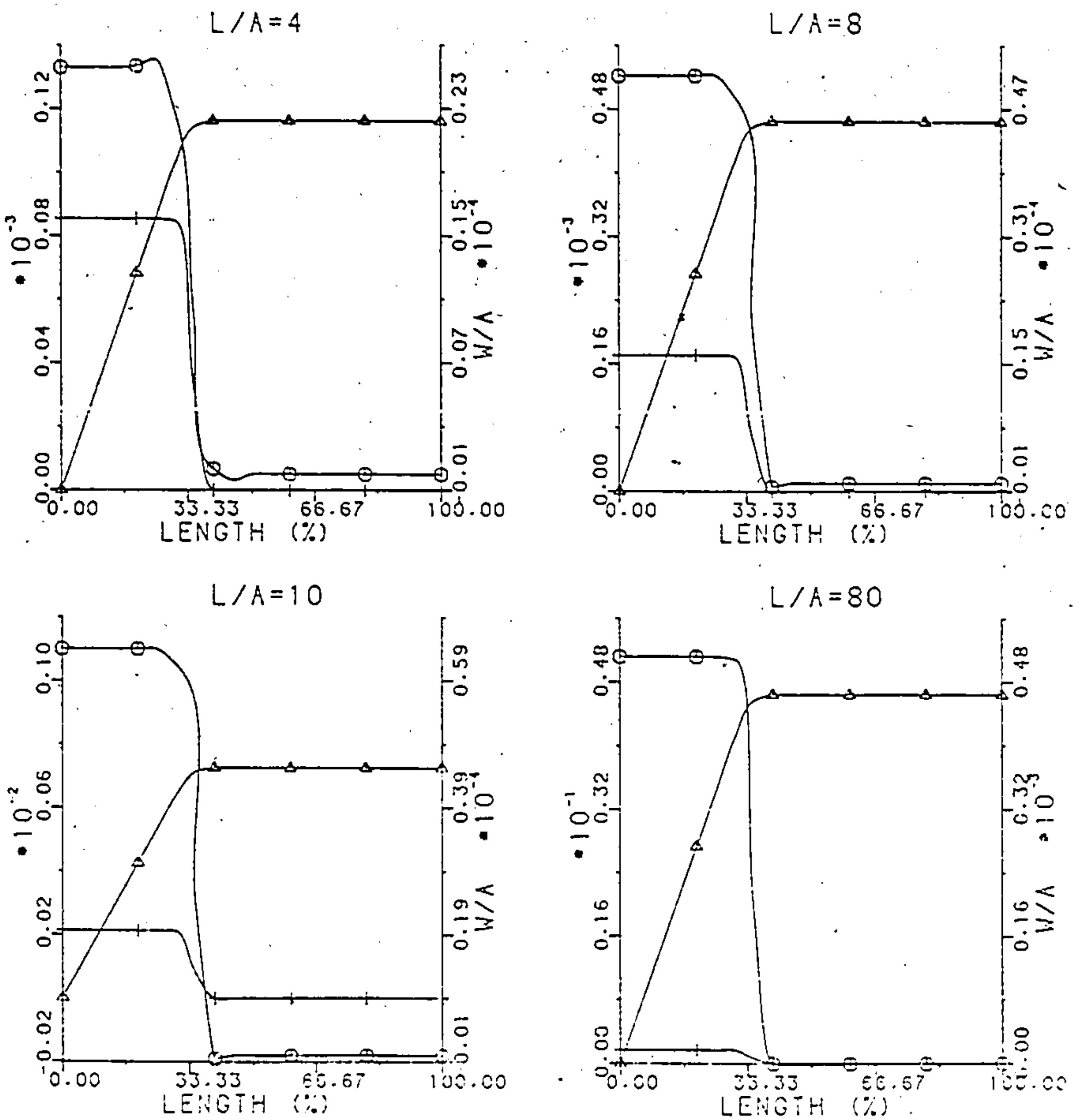

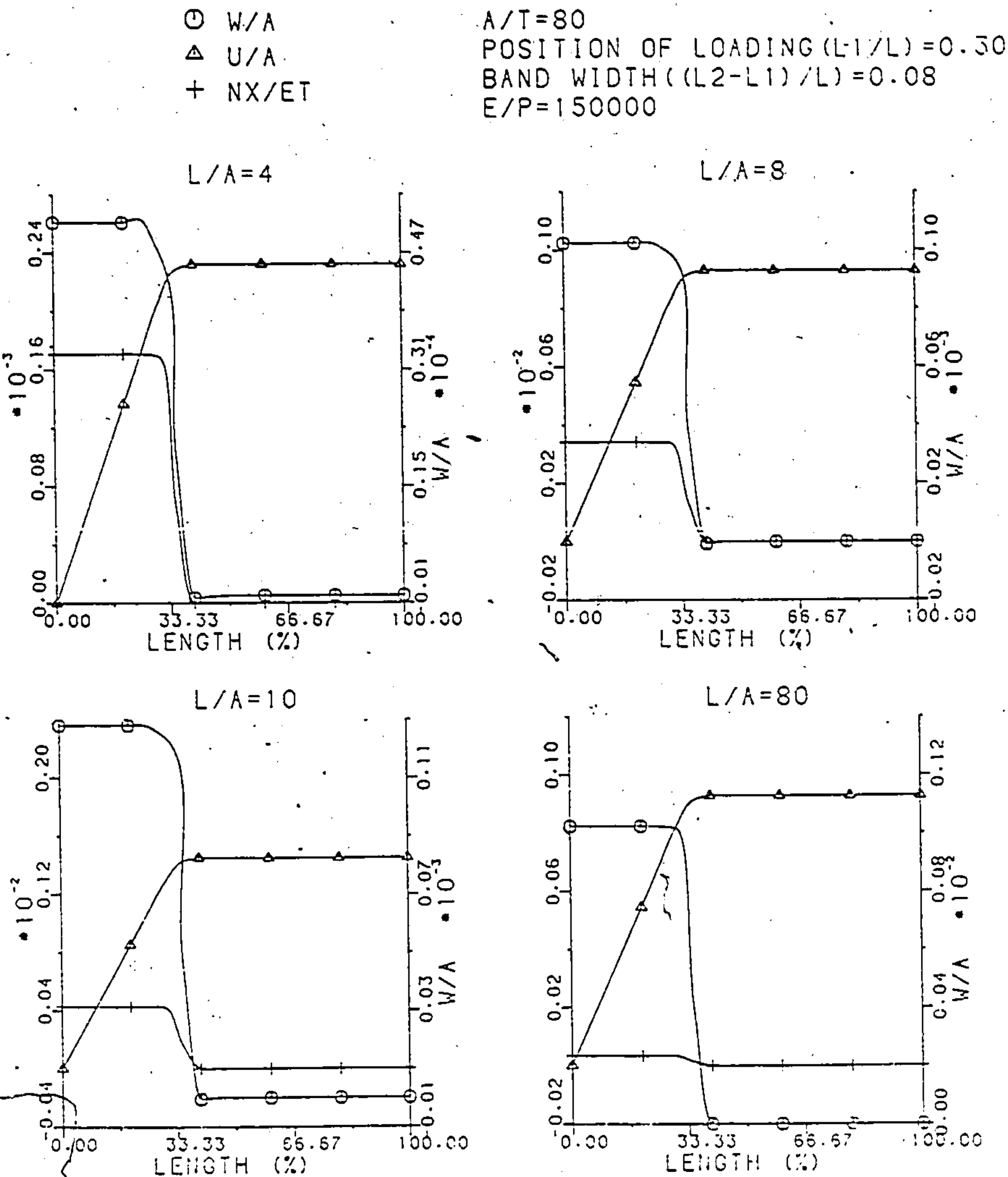

W/A
U/A
NX/ET
A/T=80
POSITION OF LOADING (L1/L)=0.30
BAND WIDTH ((L2-L1)/L)=0.08
E/P=150000
L/A=4
L/A=8
L/A=10
L/A=80
LENGTH (%)
0.00
33.33
66.67
100.00
W/A

O W/A
Δ U/A
+ NX/ET

A/T=10
POSITION OF LOADING (L1/L) = 0.50
BAND WIDTH ((L2-L1)/L) = 0.08
E/P = 150000

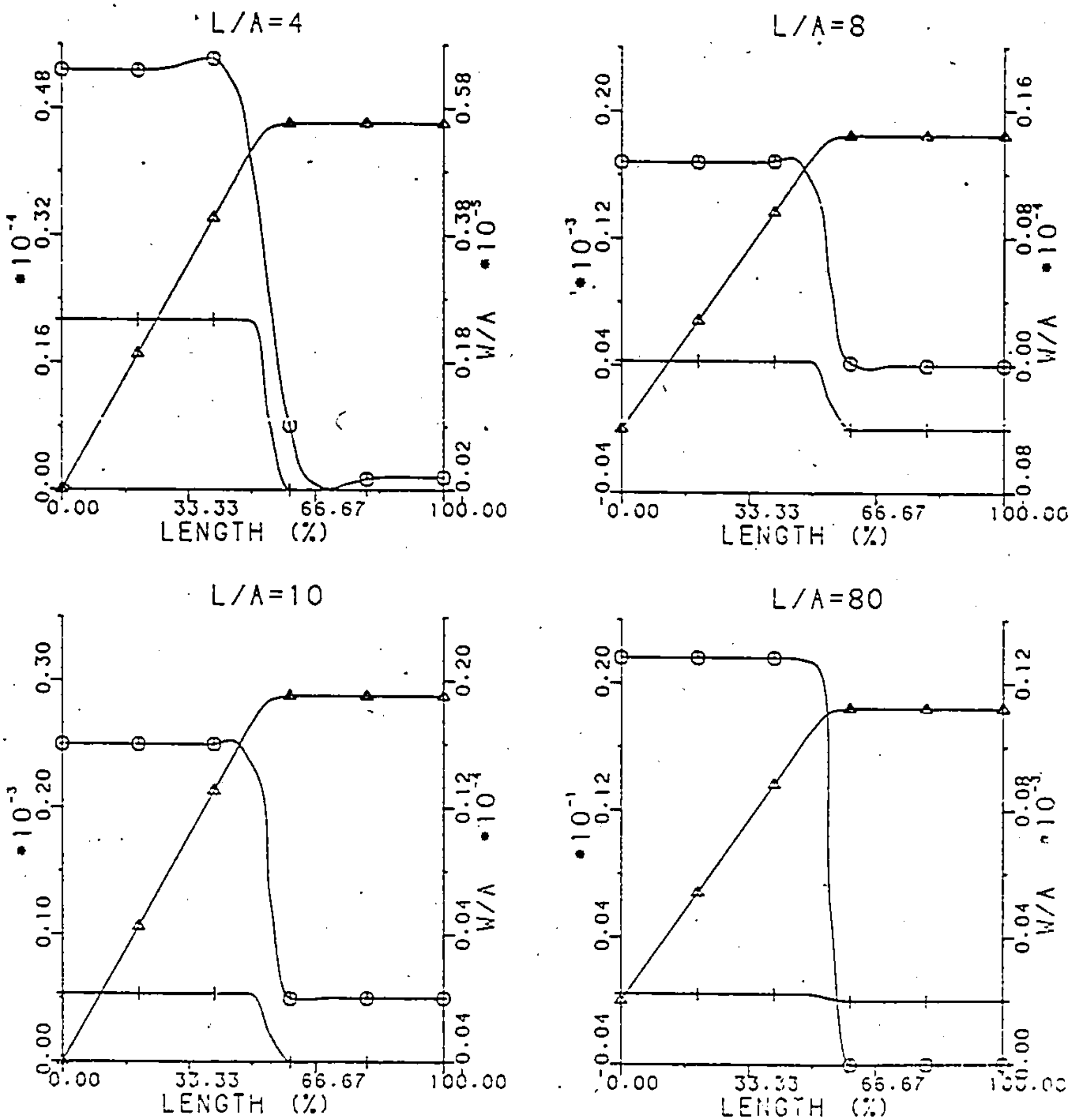

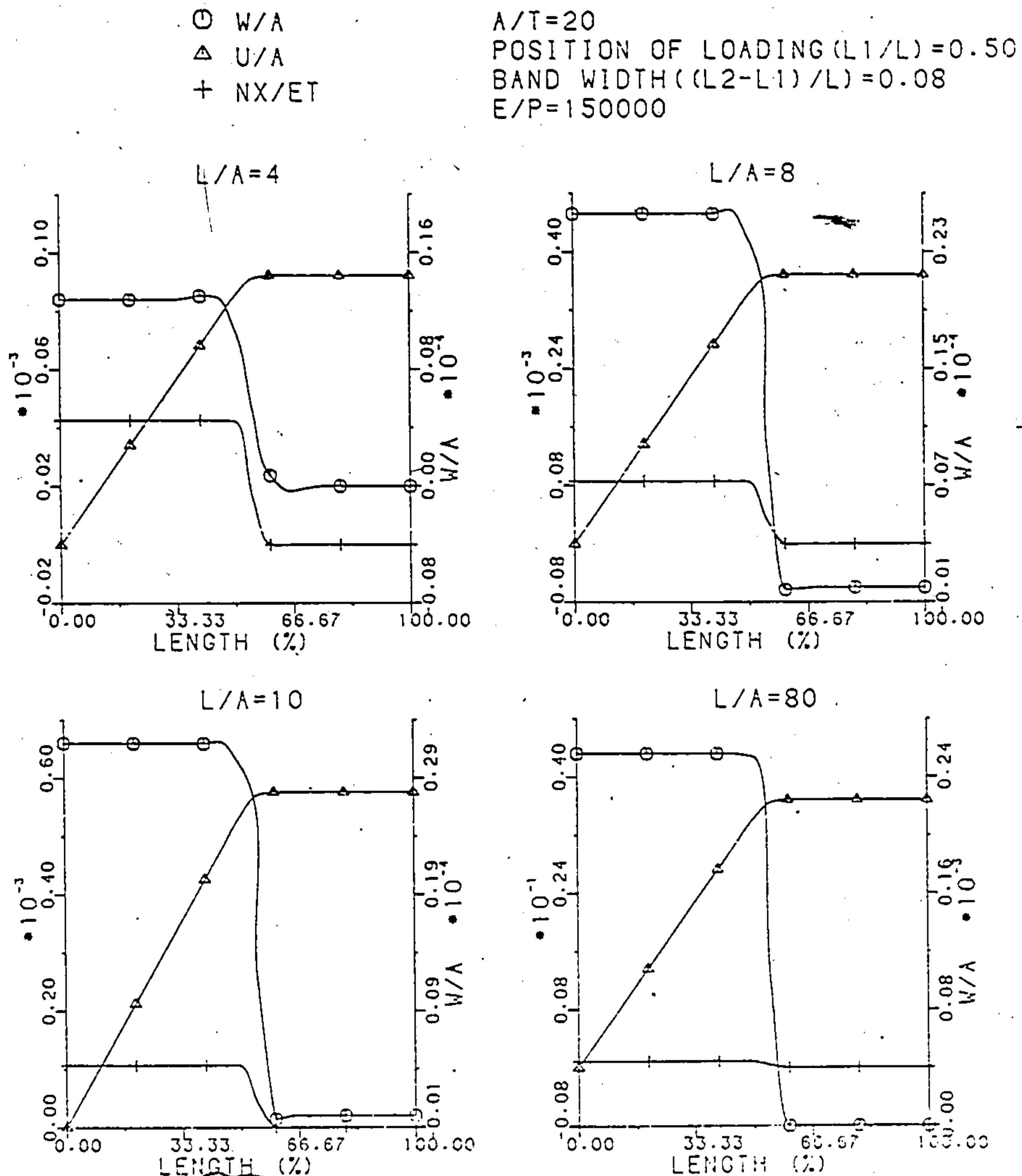

W/A
U/A
NX/ET
A/T=20
POSITION OF LOADING(L1/L)=0.50
BAND WIDTH((L2-L1)/L)=0.08
E/P=150000
L/A=4
L/A=8
L/A=10
L/A=80
LENGTH (%)
W/A

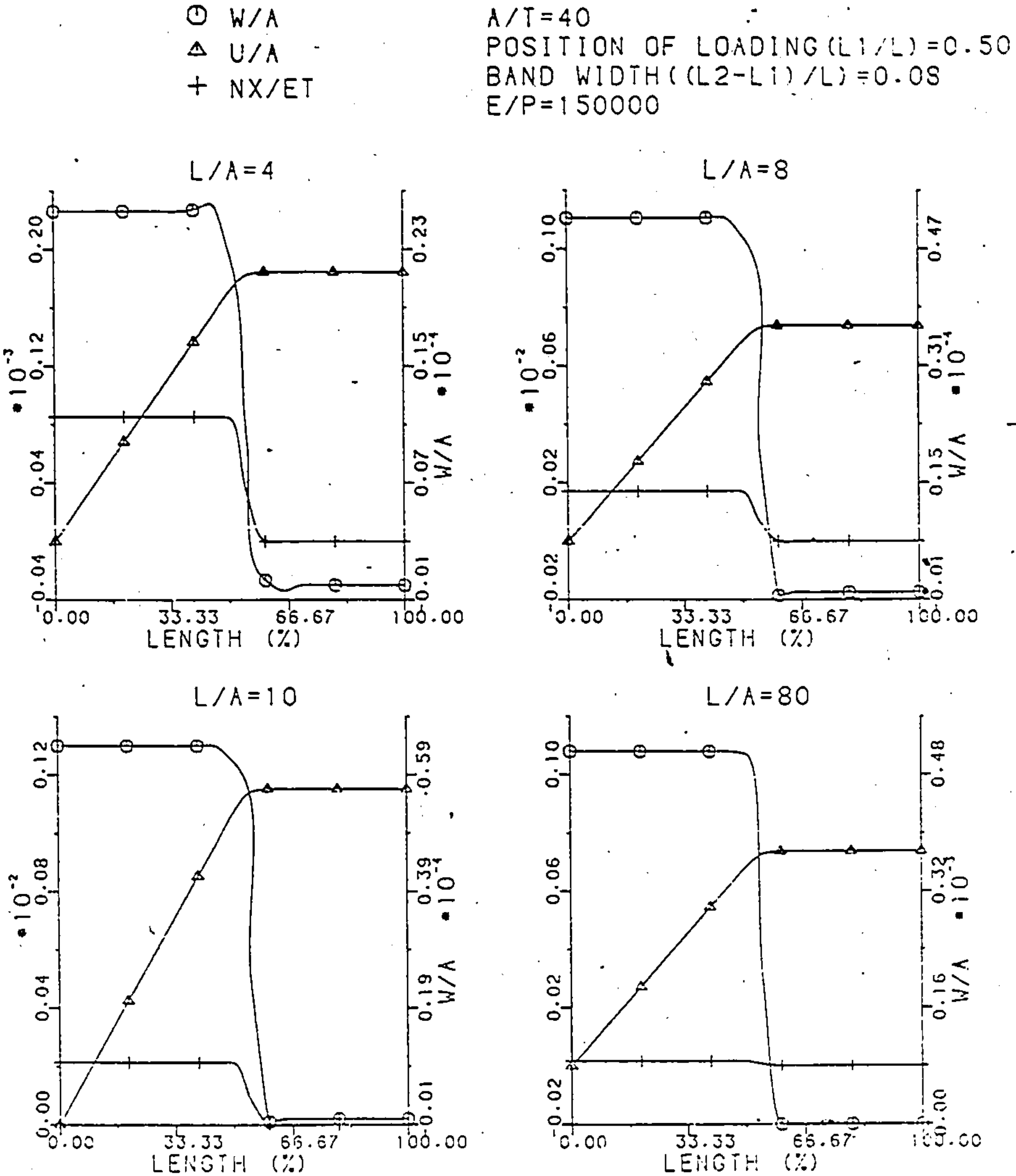

O W/A
Δ U/A
+ NX/ET
A/T=40
POSITION OF LOADING(L1/L)=0.50
BAND WIDTH((L2-L1)/L)=0.0S
E/P=150000
L/A=4
L/A=8
L/A=10
L/A=80
LENGTH (%)
0.00
33.33
66.67
100.00
W/A

⊕ W/A
△ U/A
+ NX/ET

A/T=80
POSITION OF LOADING(L1/L)=0.50
BAND WIDTH((L2-L1)/L)=0.05
E/P=150000

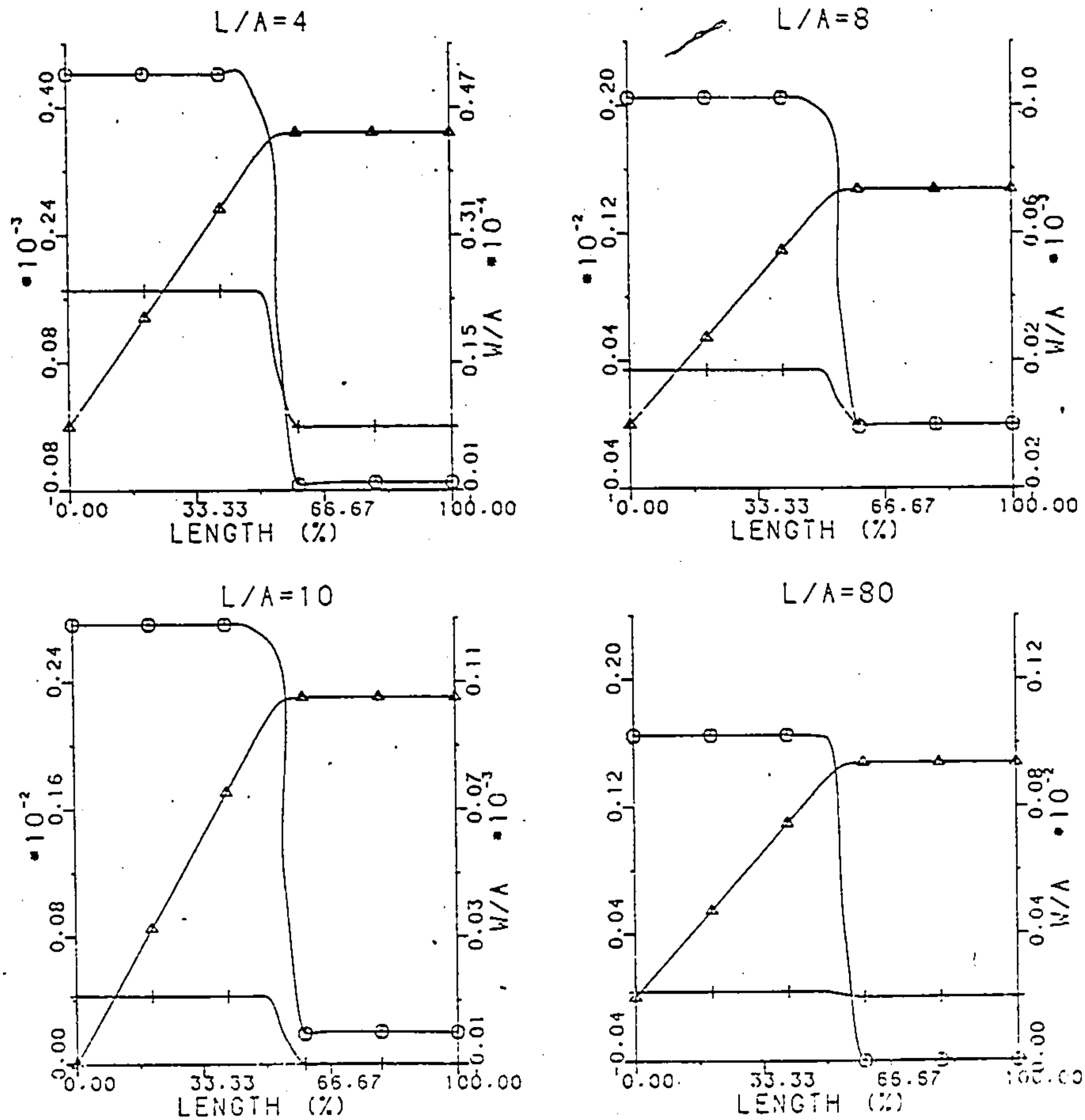

○ W/A
△ U/A
+ NX/ET

A/T=10
POSITION OF LOADING(L1/L)=0.70
BAND WIDTH((L2-L1)/L)=0.08
E/P=150000

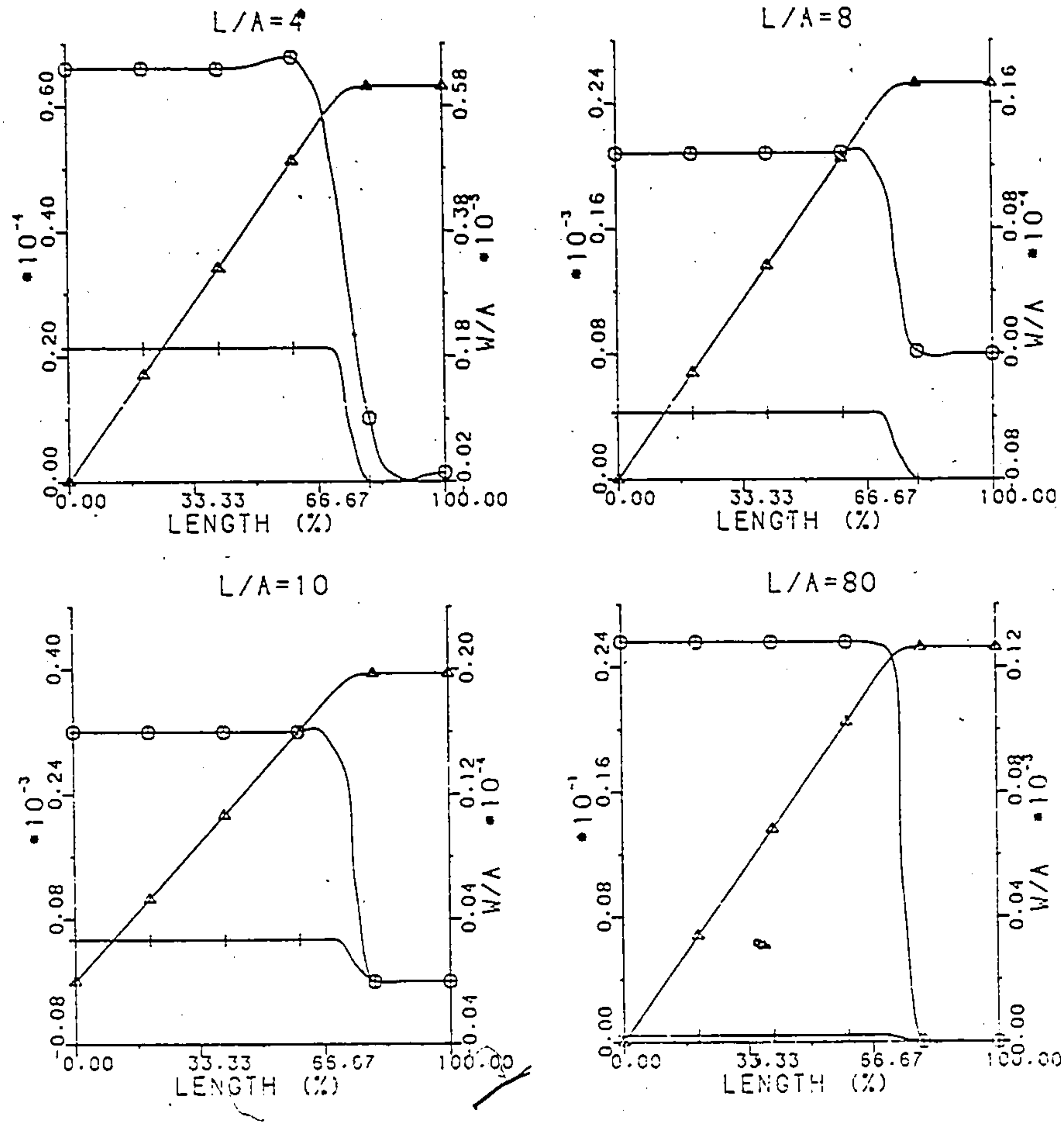

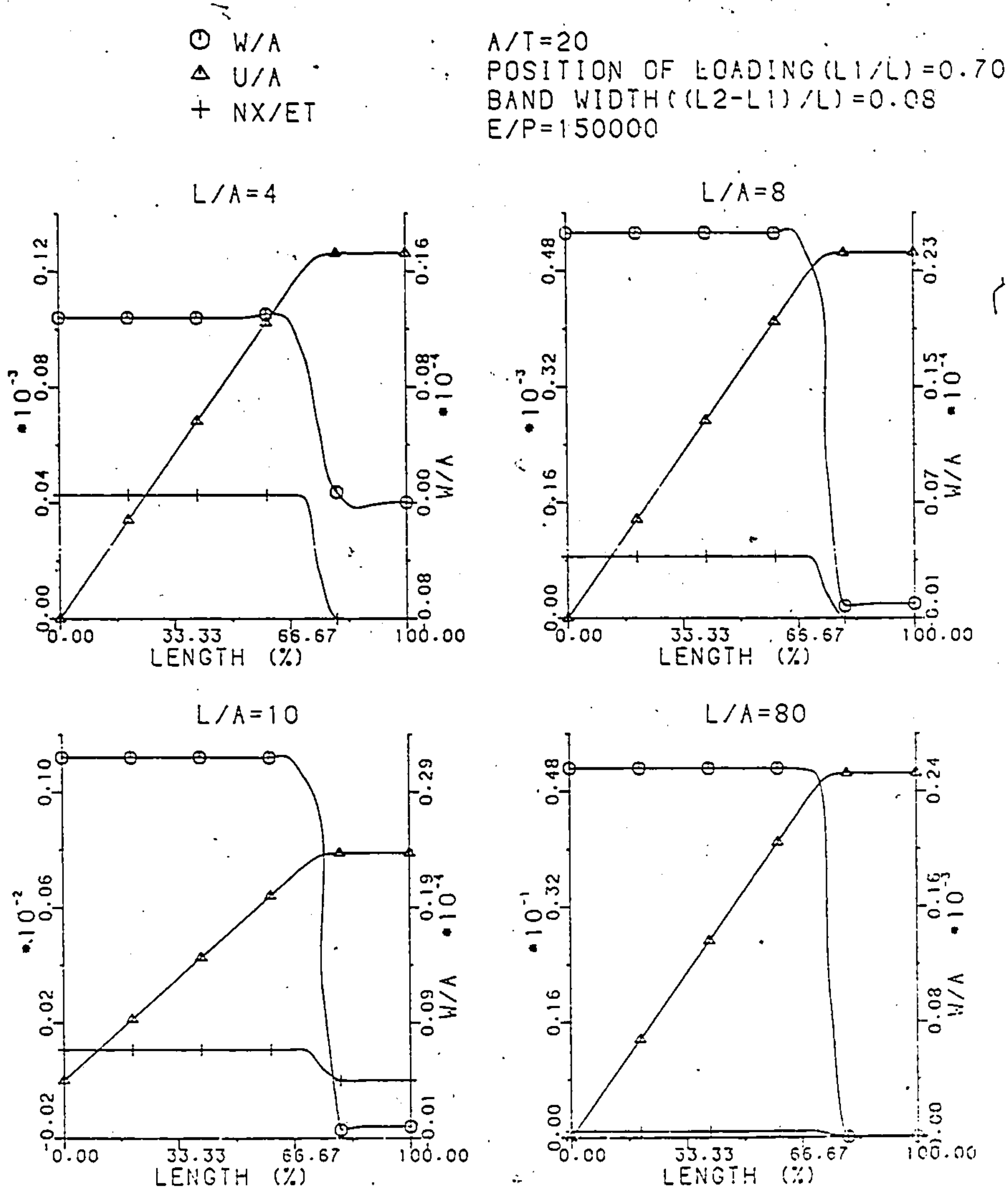

W/A
U/A
NX/ET
A/T=20
POSITION OF LOADING(L1/L)=0.70
BAND WIDTH((L2-L1)/L)=0.08
E/P=150000
L/A=4
L/A=8
L/A=10
L/A=80
LENGTH (%)
W/A
0.00
33.33
66.67
100.00

○ W/A
△ U/A
+ NX/ET

A/T=40
POSITION OF LOADING(L1/L)=0.70
BAND WIDTH((L2-L1)/L)=0.08
E/P=150000

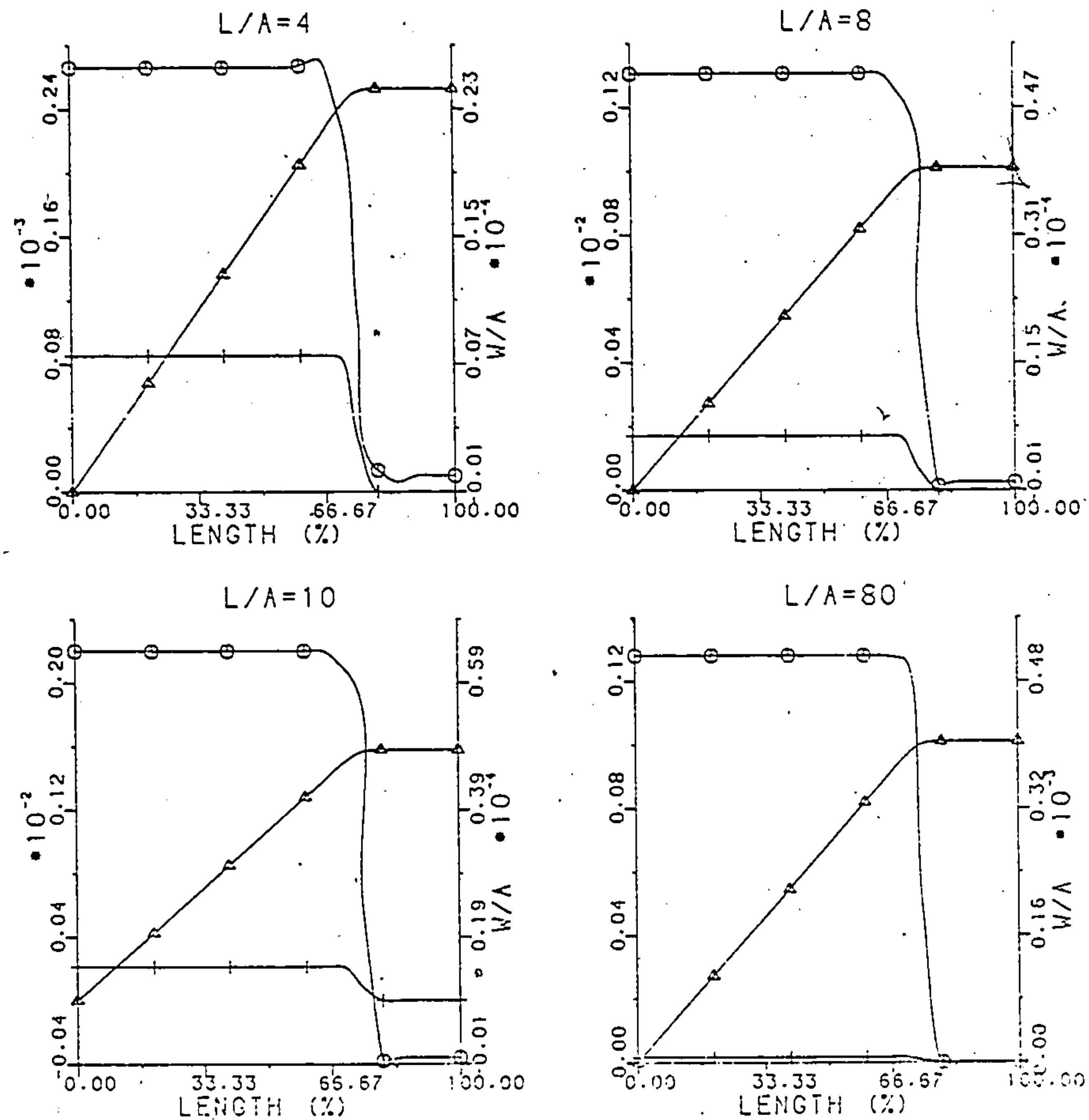

ⵀ W/A
△ U/A
+ NX/ET

A/T=80
POSITION OF LOADING(L1/L)=0.70
BAND WIDTH((L2-L1)/L)=0.08
E/P=150000

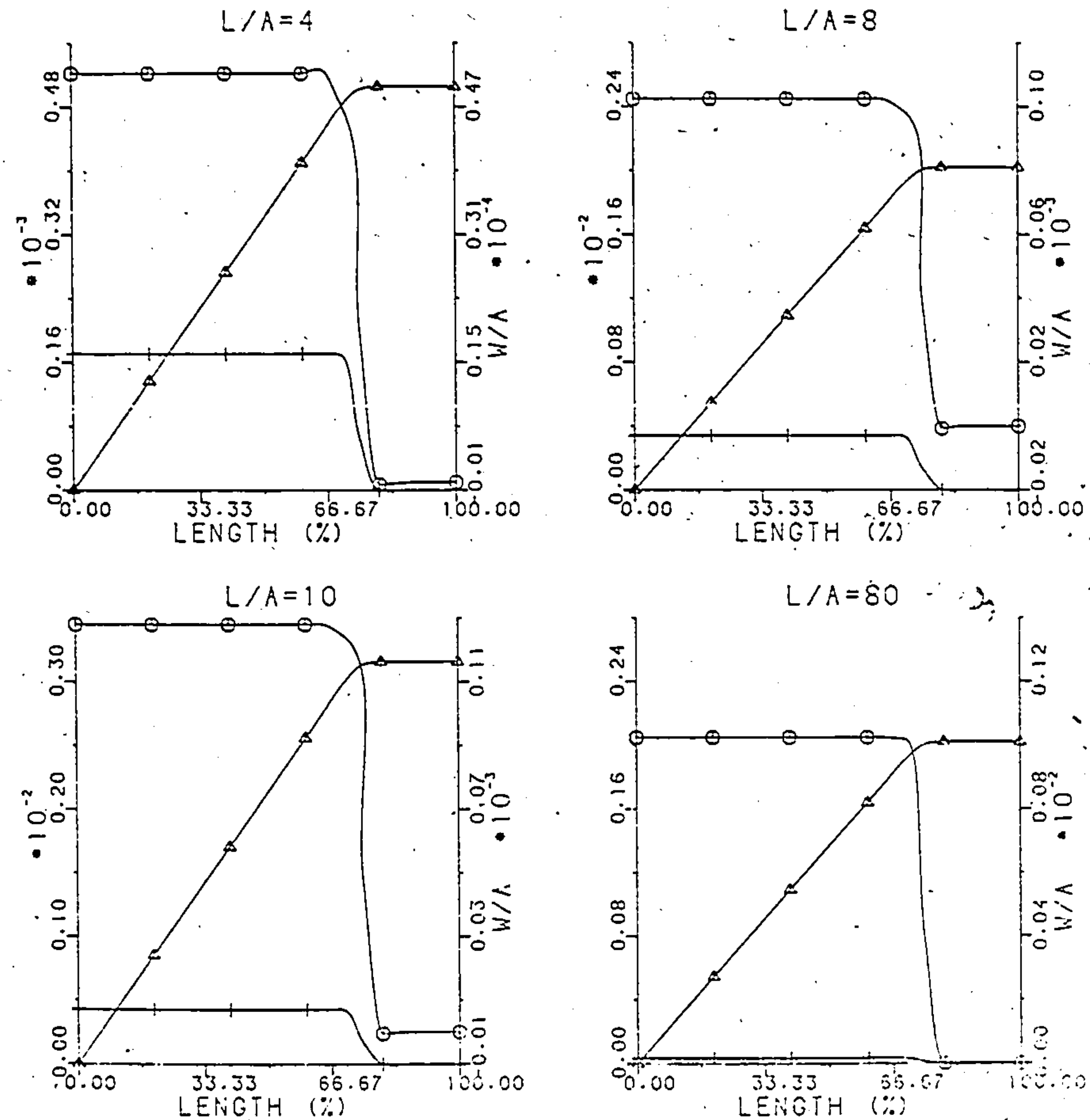

○ W/A
△ U/A
+ NX/ET

A/T=10
POSITION OF LOADING(L1/L)=0.90
BAND WIDTH((L2-L1)/L)=0.08
E/P=150000

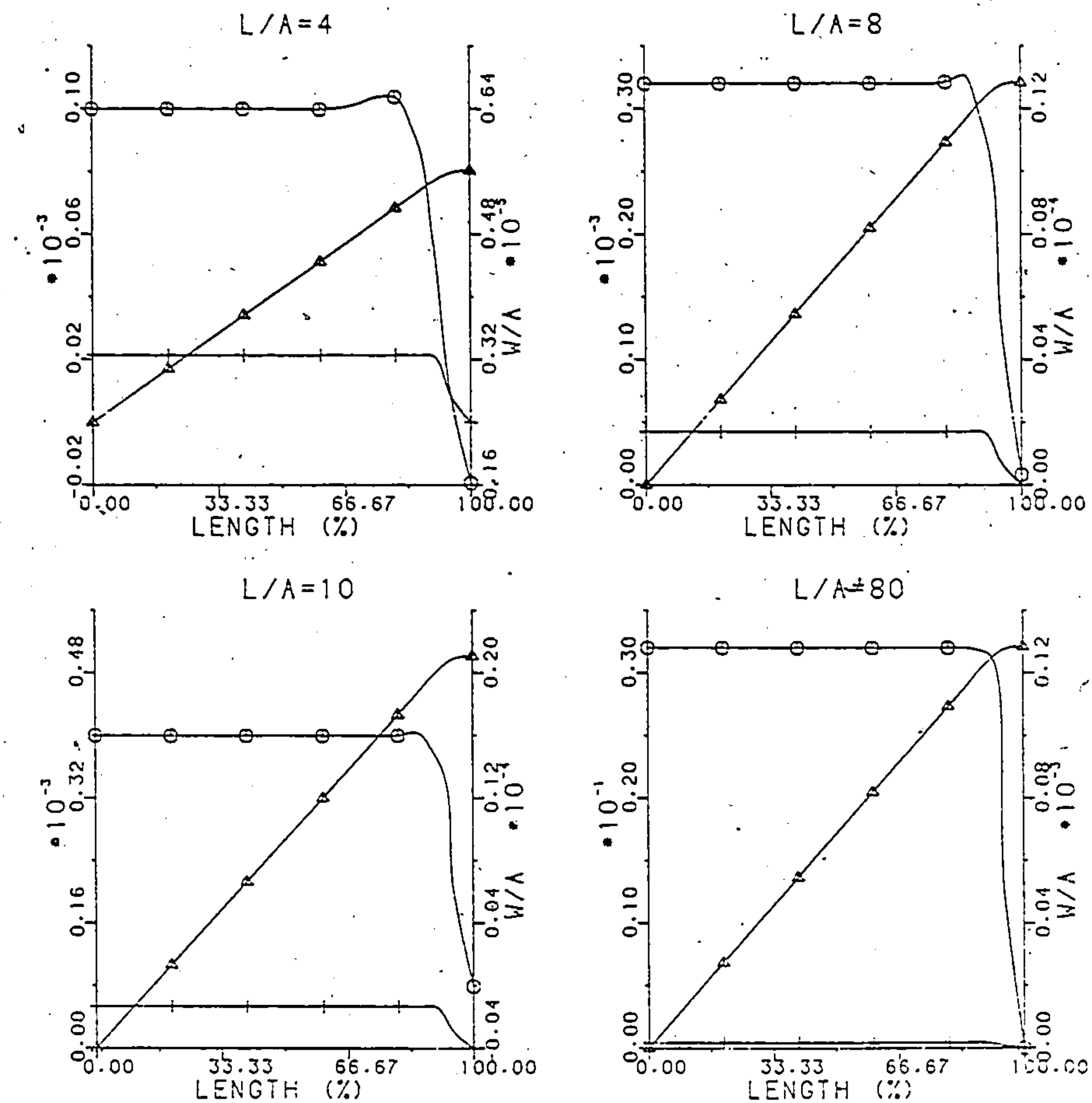

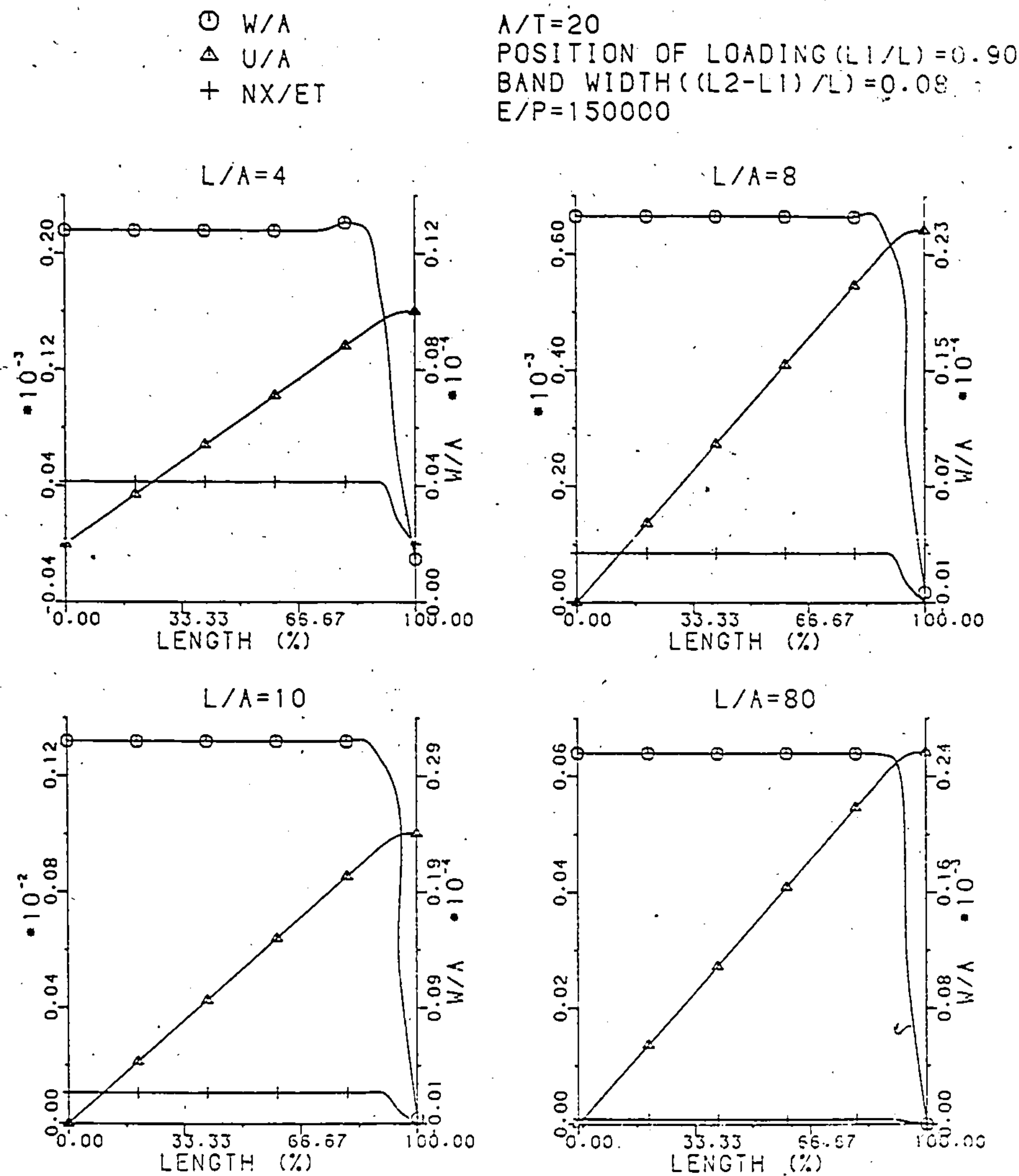

W/A
U/A
NX/ET
A/T=20
POSITION OF LOADING(L1/L)=0.90
BAND WIDTH((L2-L1)/L)=0.08
E/P=150000
L/A=4
L/A=8
L/A=10
L/A=80
LENGTH (%)
0.00
33.33
66.67
100.00
W/A
•10⁻³
•10⁻²
•10⁻⁴

O W/A
Δ U/A
+ NX/ET

A/T=40
POSITION OF LOADING(L1/L)=0.90
BAND WIDTH((L2-L1)/L)=0.08
E/P=150000

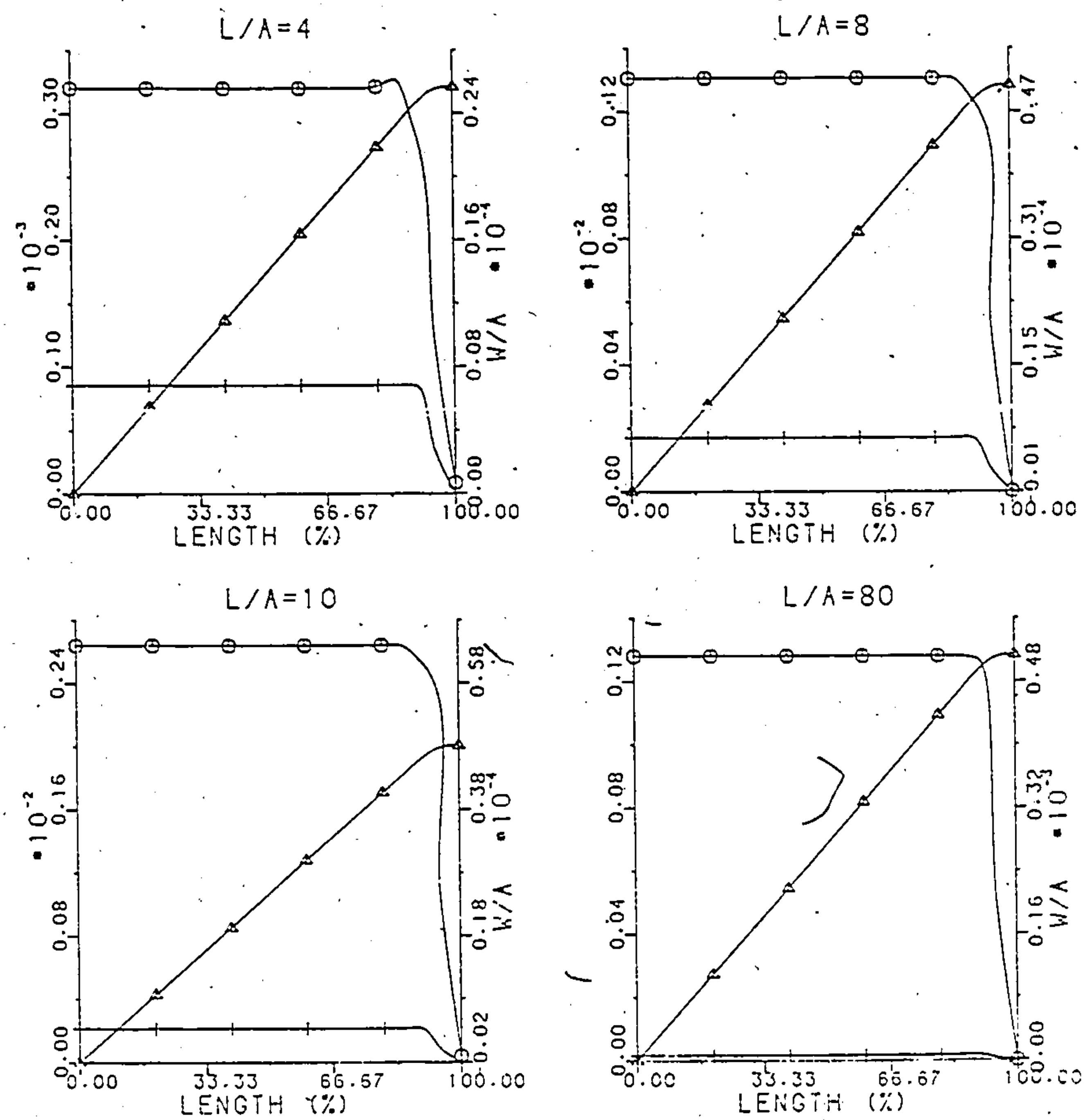

O W/A
Δ U/A
+ NX/ET

A/T=80
POSITION OF LOADING(L1/L)=0.90
BAND WIDTH((L2-L1)/L)=0.08
E/P=150000

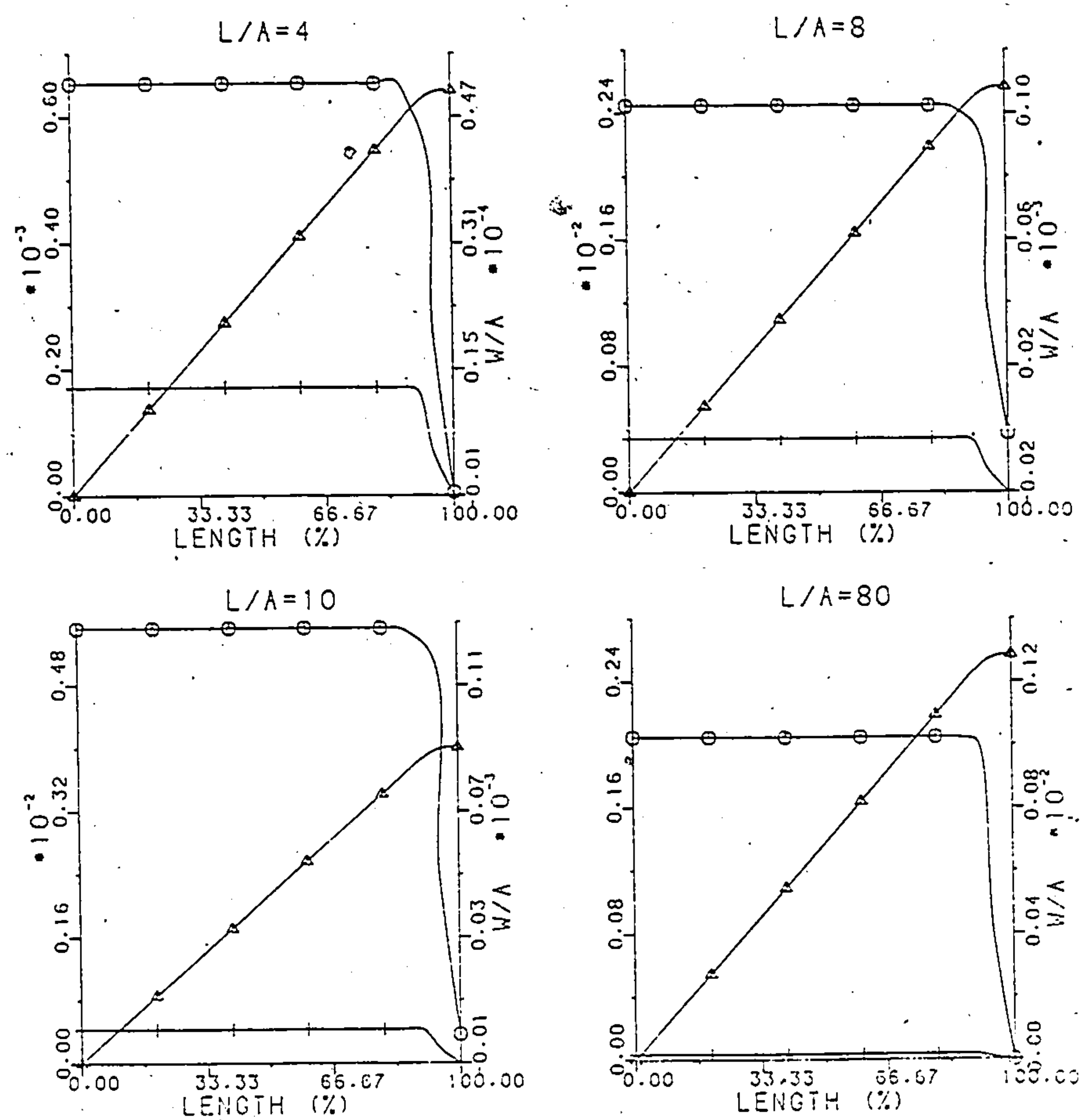

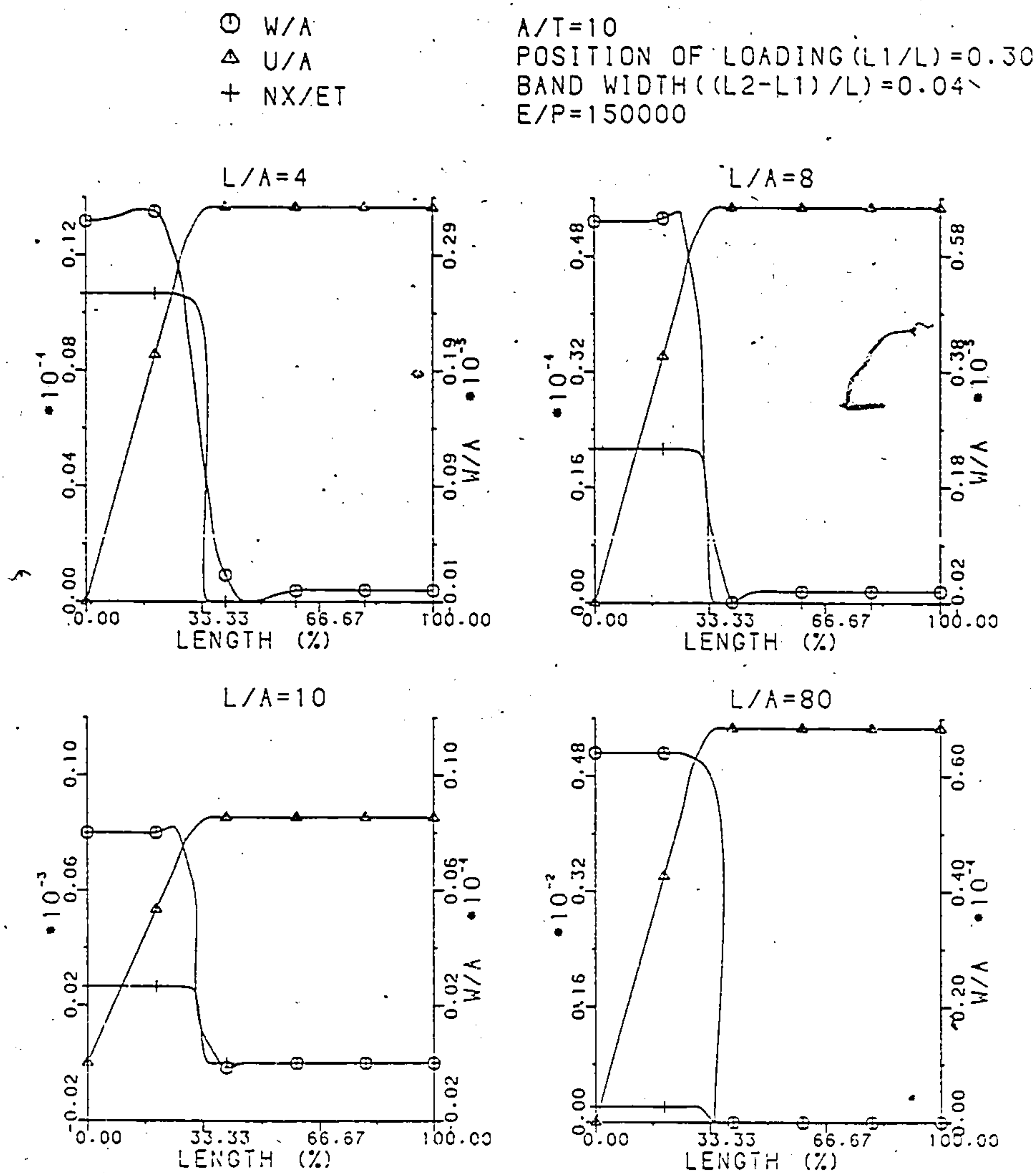

W/A
U/A
NX/ET
A/T=10
POSITION OF LOADING (L1/L)=0.30
BAND WIDTH((L2-L1)/L)=0.04
E/P=150000
L/A=4
L/A=8
L/A=10
L/A=80
LENGTH (%)
W/A

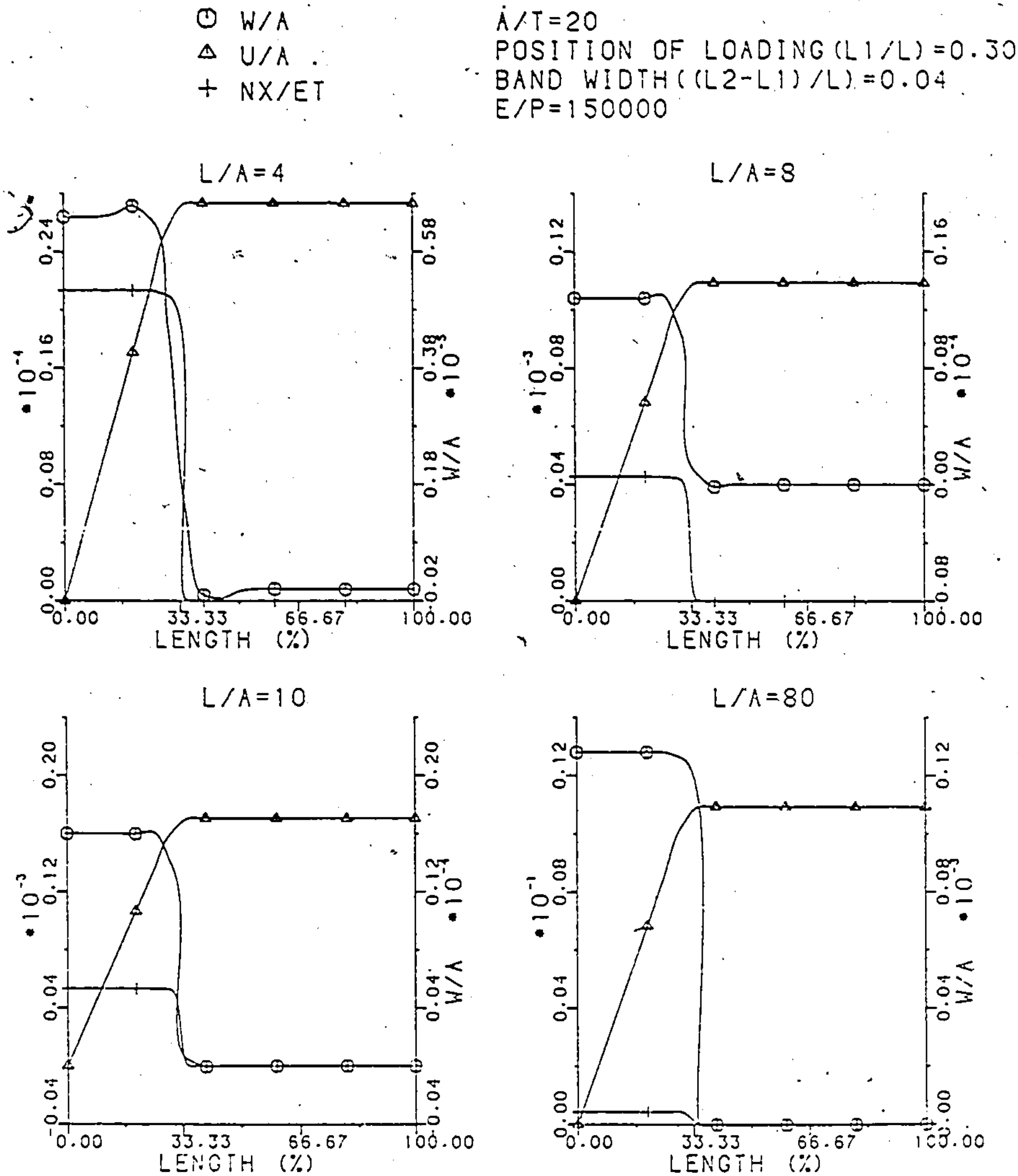

W/A
U/A
NX/ET
A/T=20
POSITION OF LOADING (L1/L)=0.30
BAND WIDTH ((L2-L1)/L)=0.04
E/P=150000
L/A=4
L/A=8
L/A=10
L/A=80
LENGTH (%)
0.00
33.33
66.67
100.00
W/A

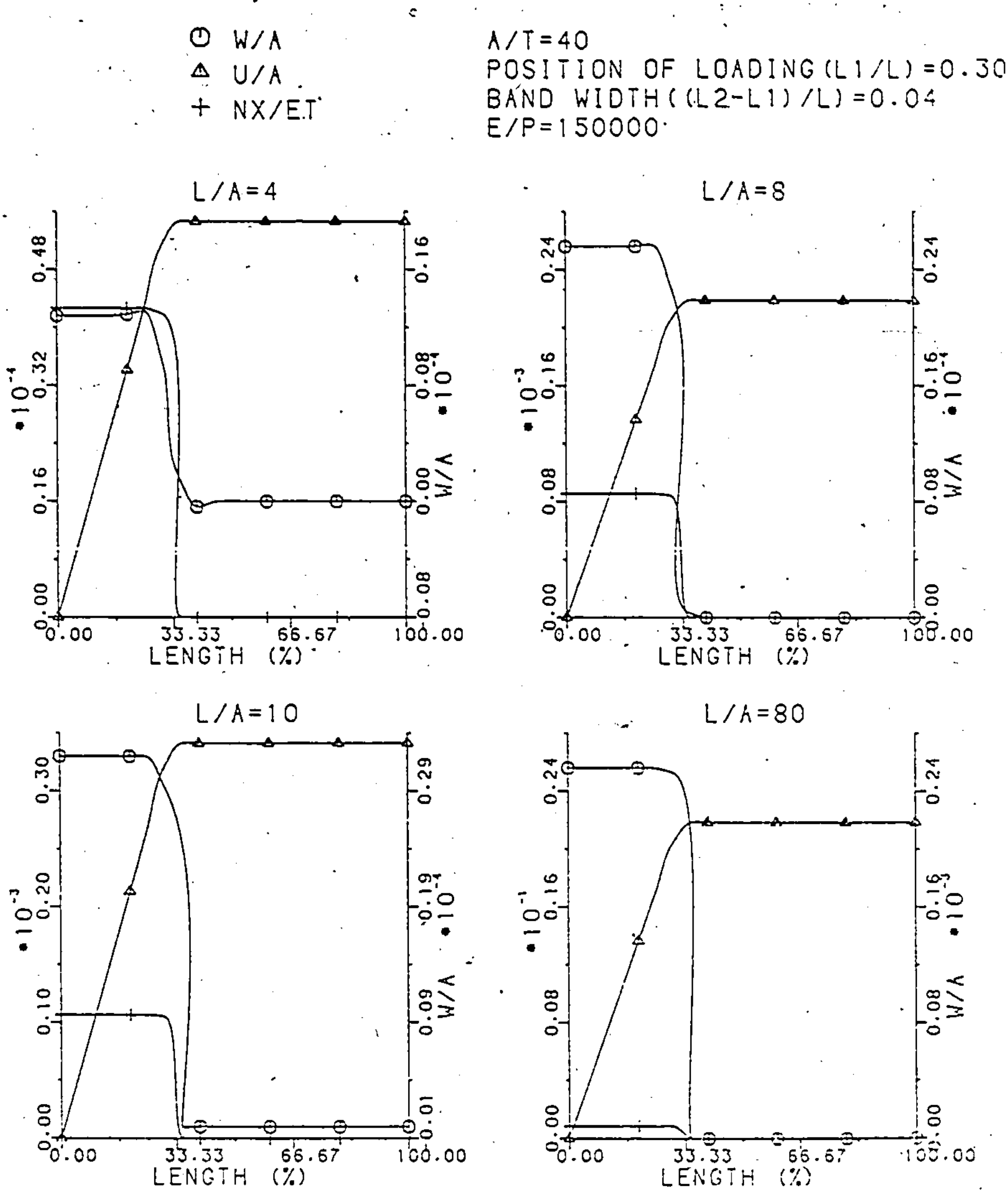
W/A
U/A
NX/ET
A/T=40
POSITION OF LOADING(L1/L)=0.30
BAND WIDTH((L2-L1)/L)=0.04
E/P=150000
L/A=4
L/A=8
L/A=10
L/A=80
LENGTH (%)
W/A
0.00
33.33
66.67
100.00

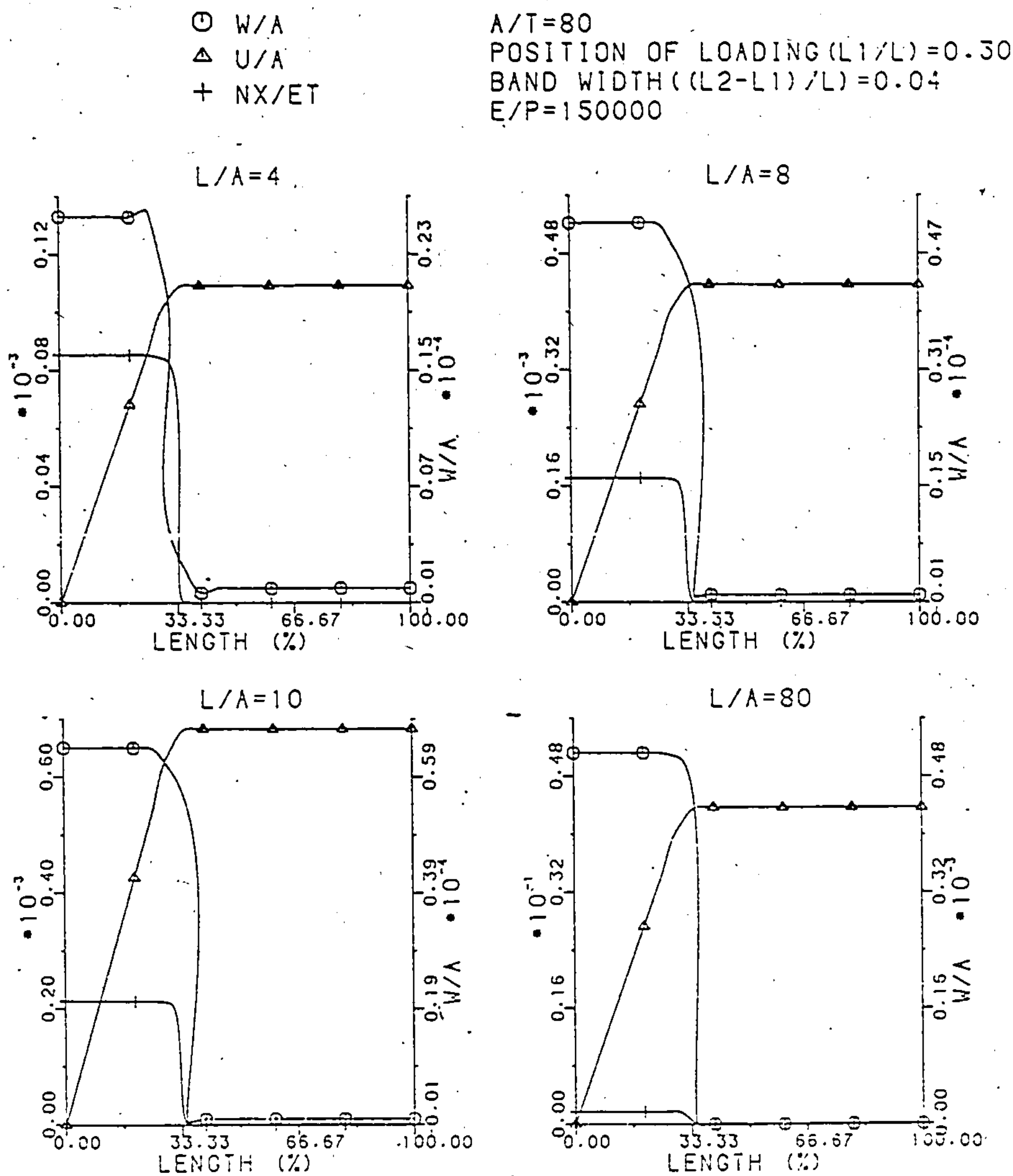

W/A
U/A
NX/ET
A/T=80
POSITION OF LOADING(L1/L)=0.30
BAND WIDTH((L2-L1)/L)=0.04
E/P=150000
L/A=4
L/A=8
L/A=10
L/A=80
LENGTH (%)
W/A

○ W/A
△ U/A
+ NX/ET

A/T=1.0
POSITION OF LOADING(L1/L)=0.50
BAND WIDTH((L2-L1)/L)=0.04
E/P=150000

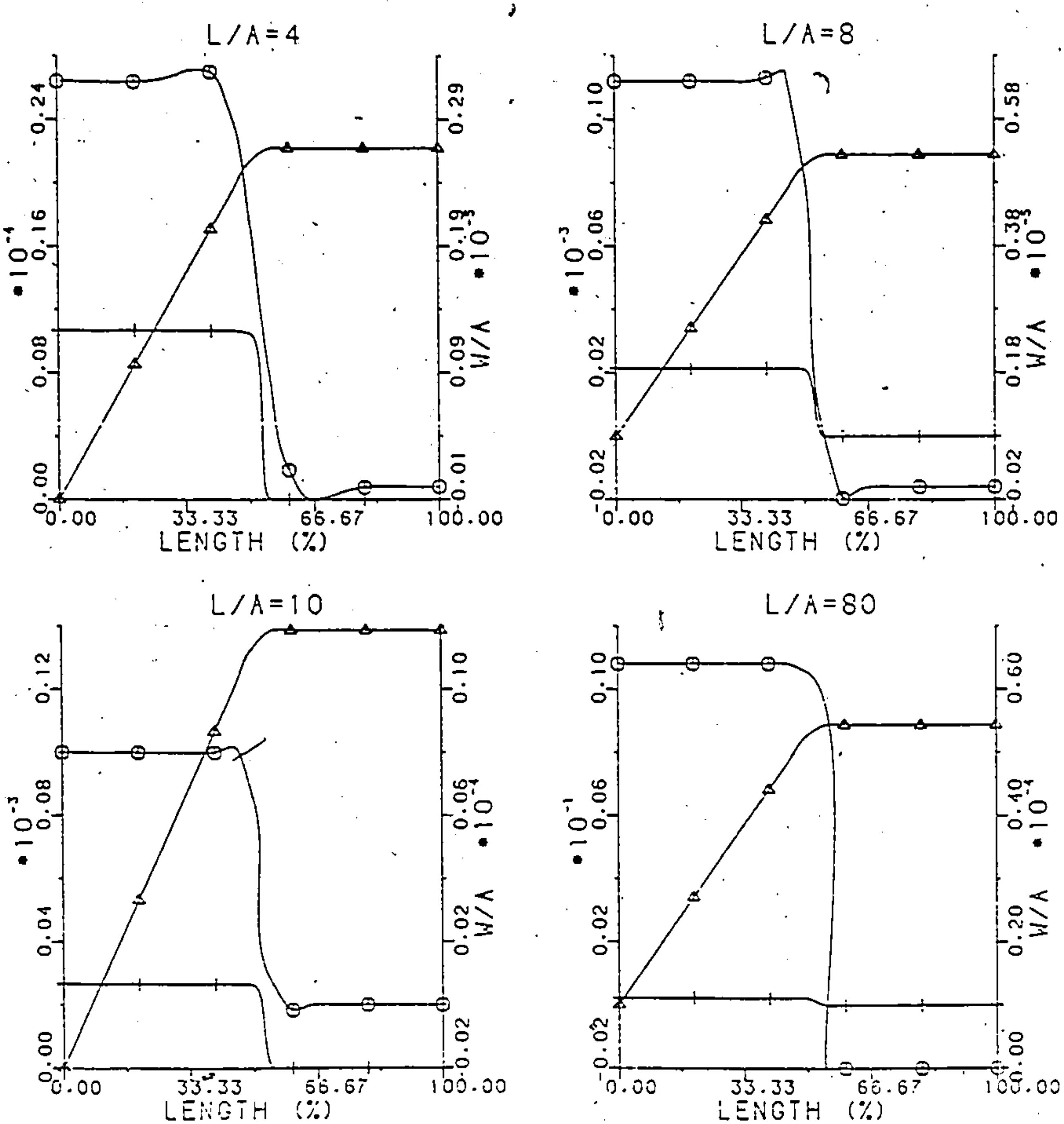

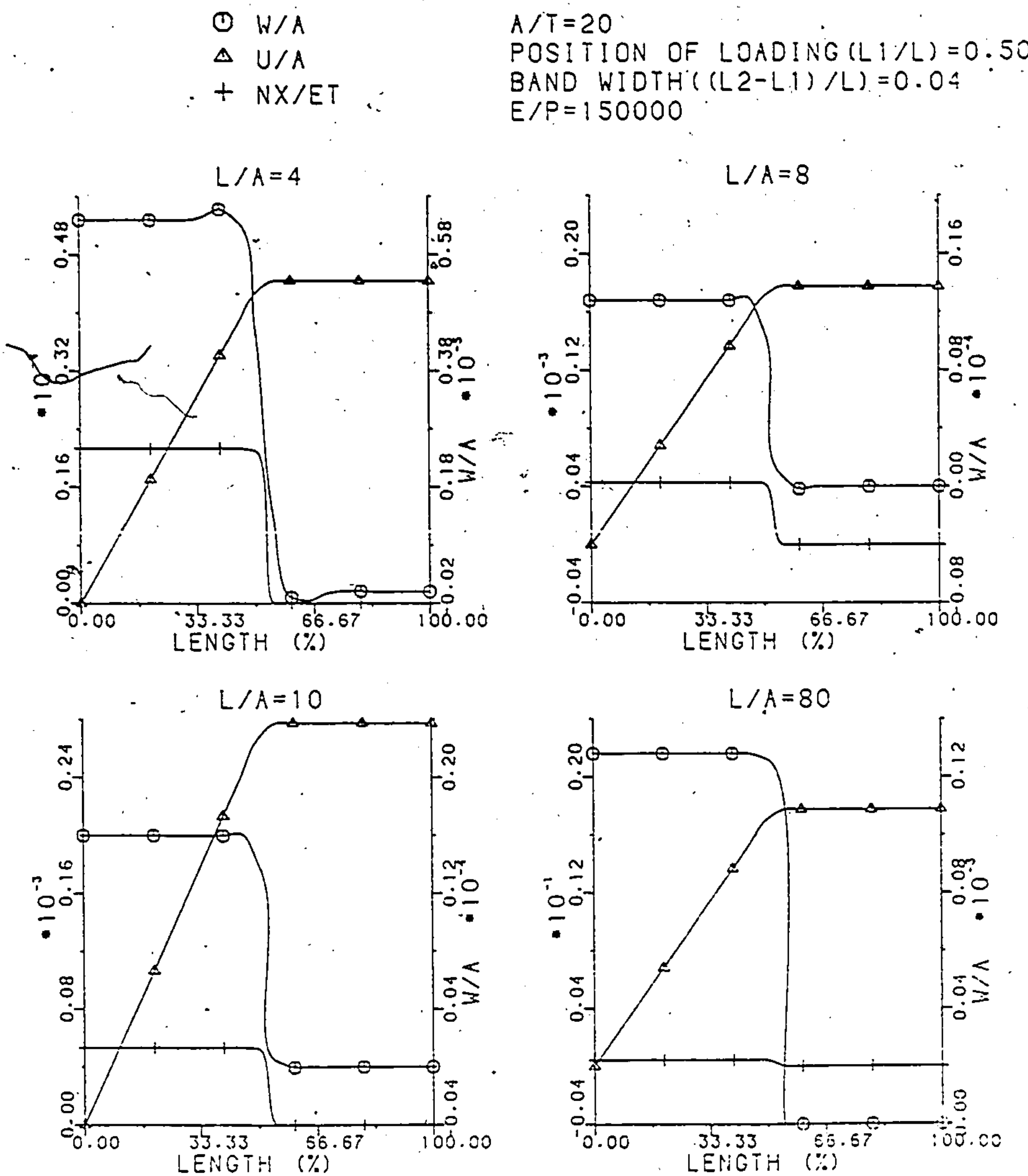

W/A
U/A
NX/ET
A/T=20
POSITION OF LOADING (L1/L)=0.50
BAND WIDTH ((L2-L1)/L)=0.04
E/P=150000
L/A=4
L/A=8
L/A=10
L/A=80
LENGTH (%)
W/A

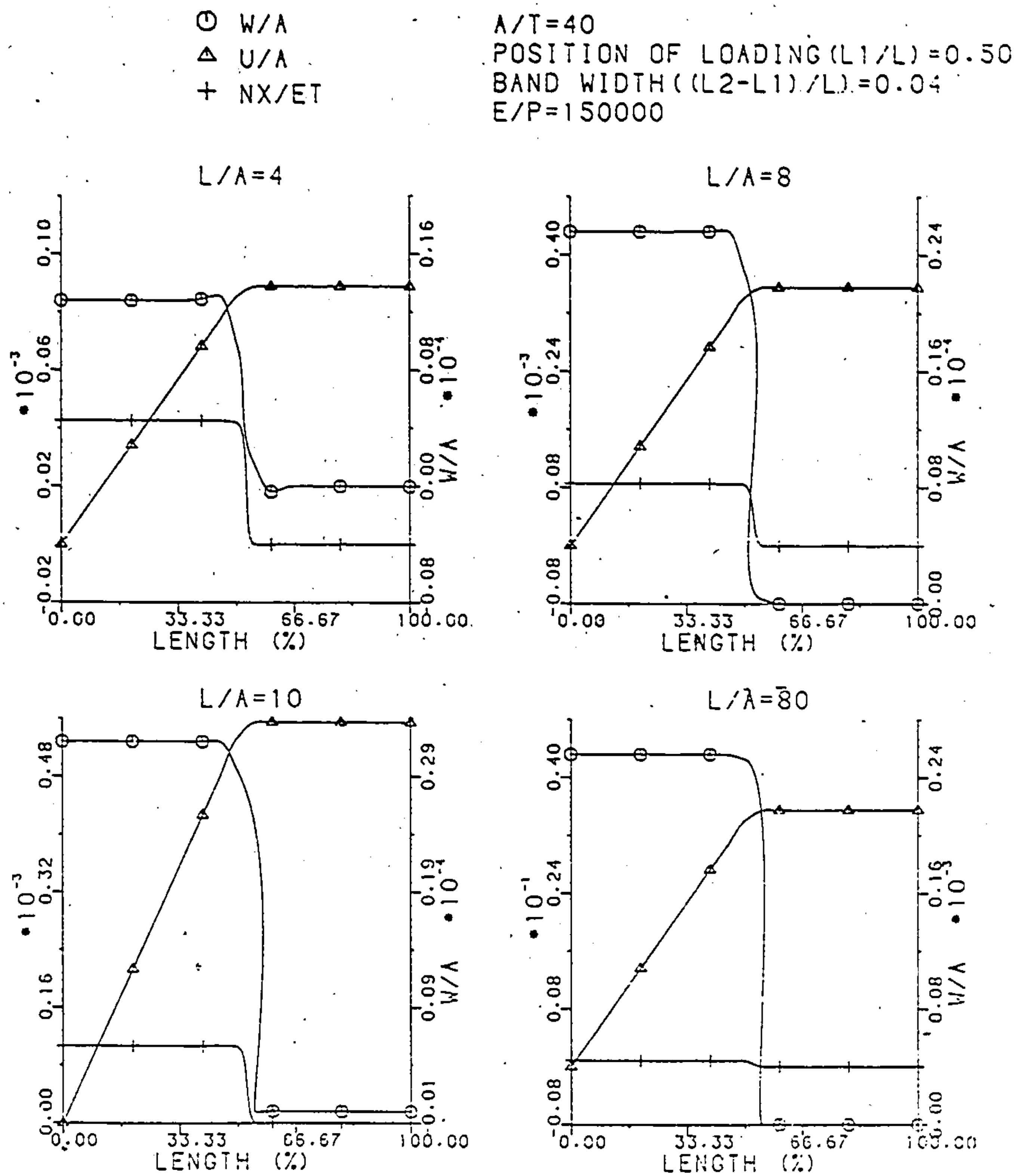
W/A
U/A
NX/ET
A/T=40
POSITION OF LOADING(L1/L)=0.50
BAND WIDTH((L2-L1)/L)=0.04
E/P=150000
L/A=4
L/A=8
L/A=10
L/A=80
LENGTH (%)
W/A
0.00
33.33
66.67
100.00

O W/A
Δ U/A
+ NX/ET

A/T=80
POSITION OF LOADING(L1/L)=0.50
BAND WIDTH((L2-L1)/L)=0.04
E/P=150000

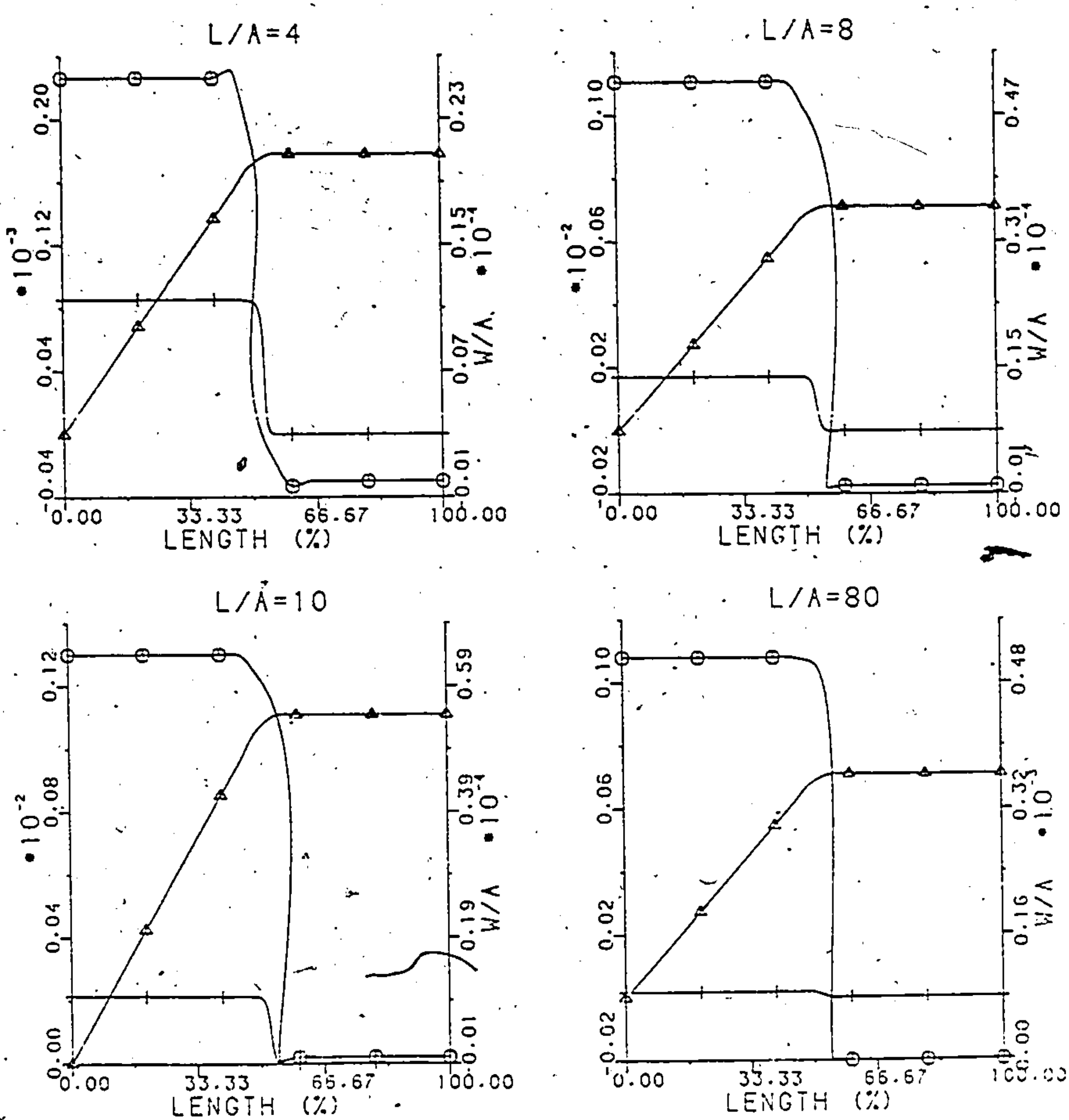

O W/A
△ U/A
+ NX/ET

A/T=10
POSITION OF LOADING(L1/L)=0.70
BAND WIDTH((L2-L1)/L)=0.04
E/P=150000

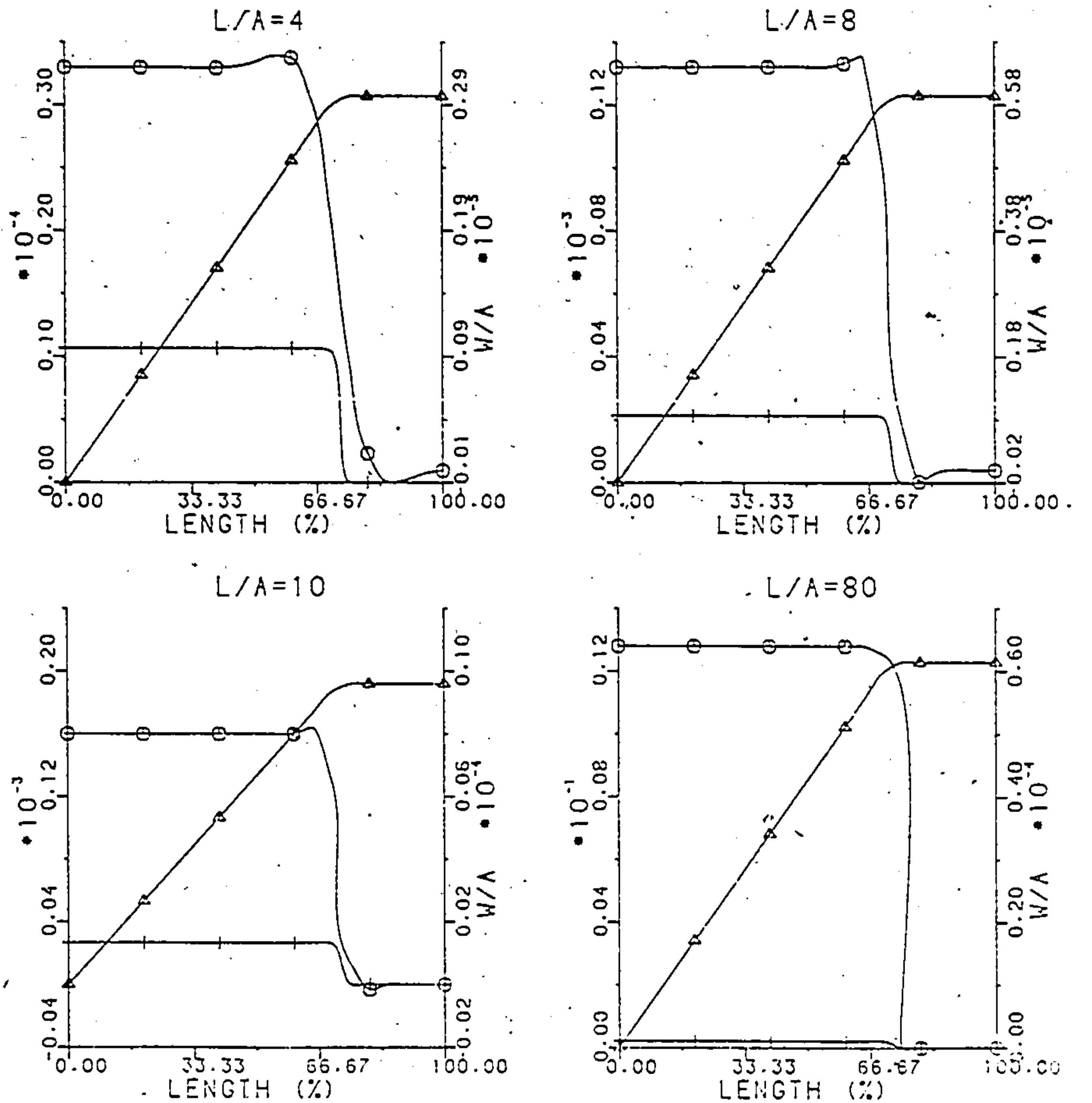

O W/A
Δ U/A
+ NX/ET

A/T=20
POSITION OF LOADING (L1/L)=0.70
BAND WIDTH ((L2-L1)/L)=0.04
E/P=150000

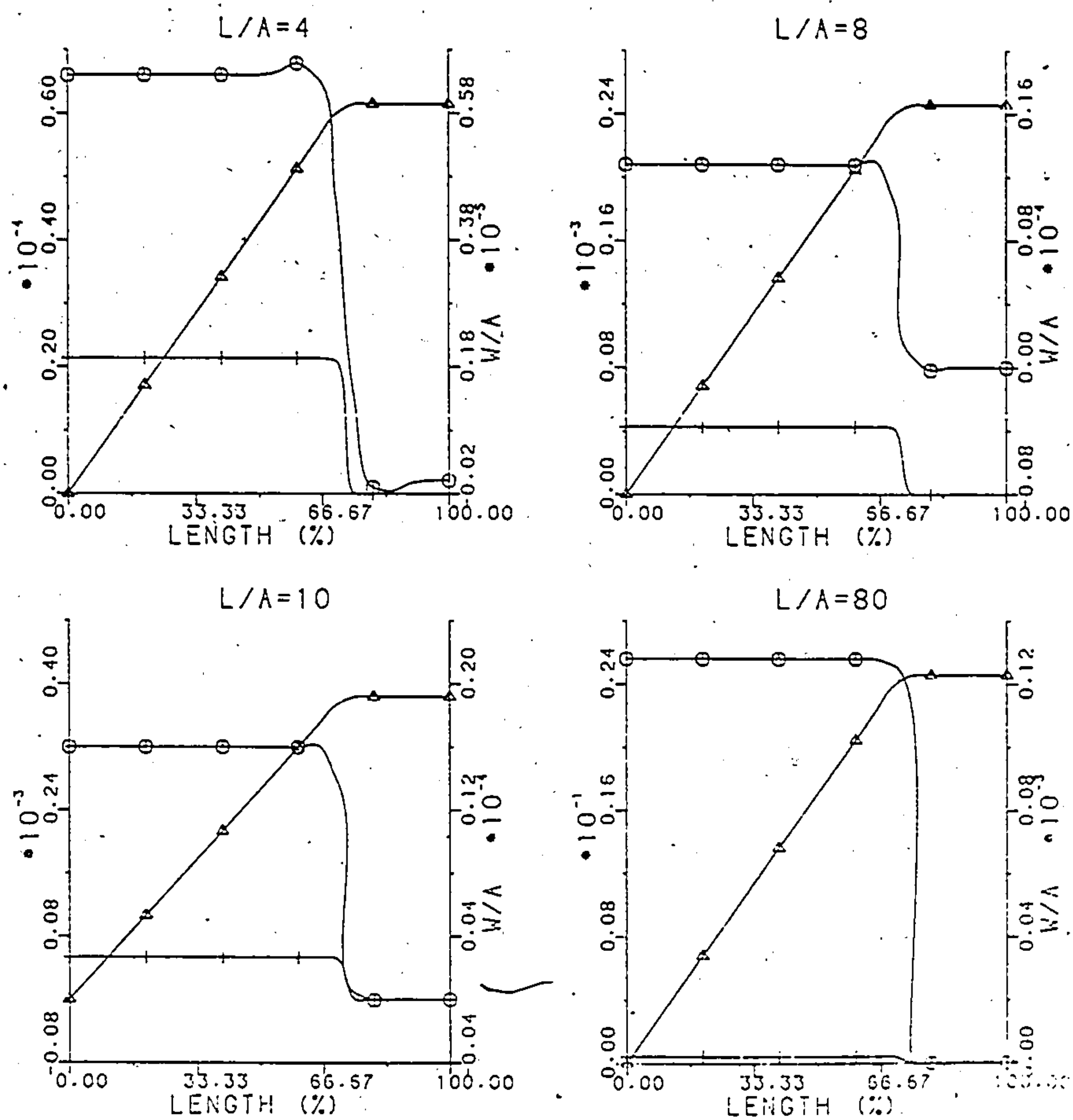

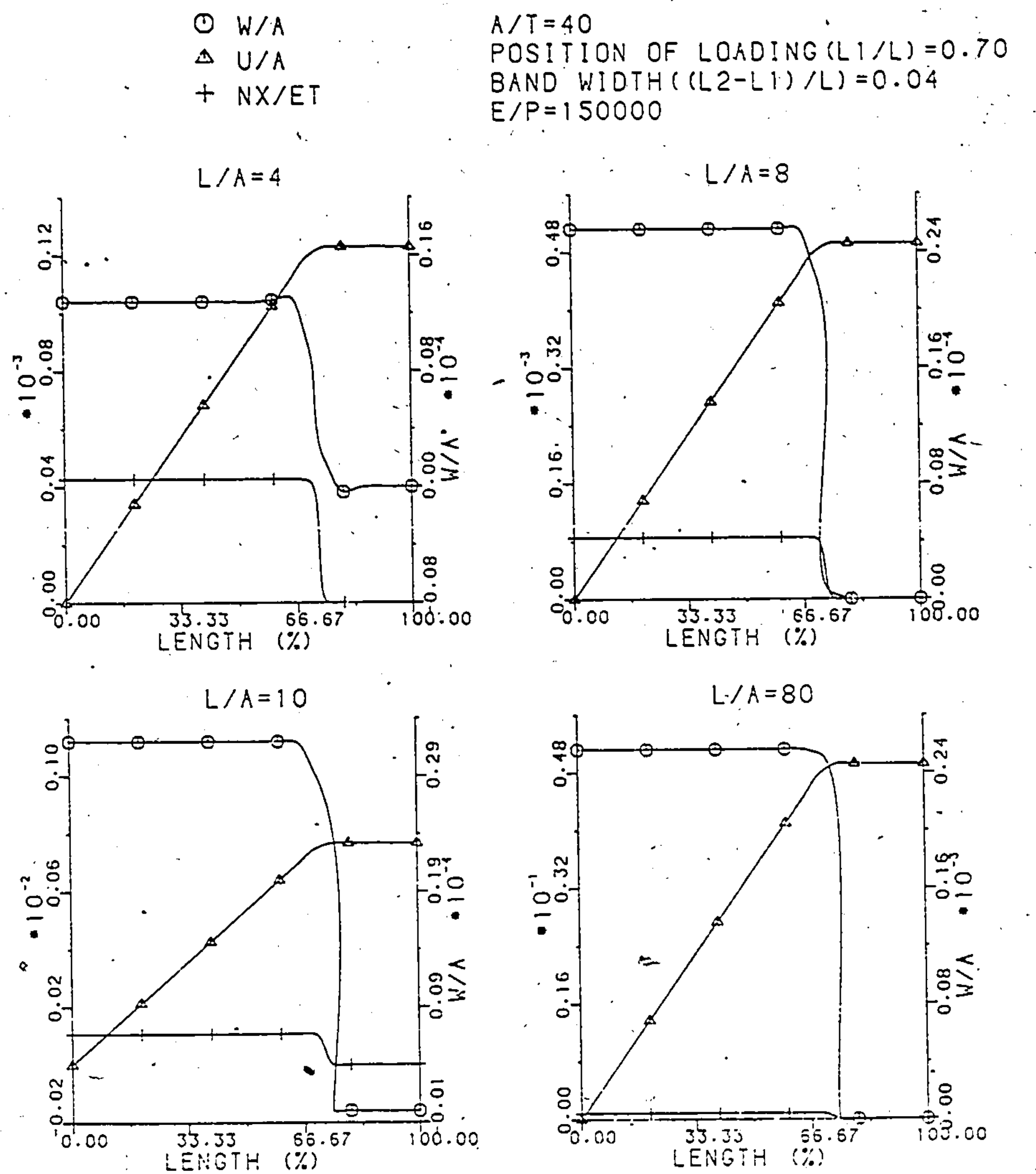

W/A
U/A
NX/ET
A/T=40
POSITION OF LOADING(L1/L)=0.70
BAND WIDTH((L2-L1)/L)=0.04
E/P=150000
L/A=4
L/A=8
L/A=10
L/A=80
LENGTH (%)
0.00
33.33
66.67
100.00
W/A

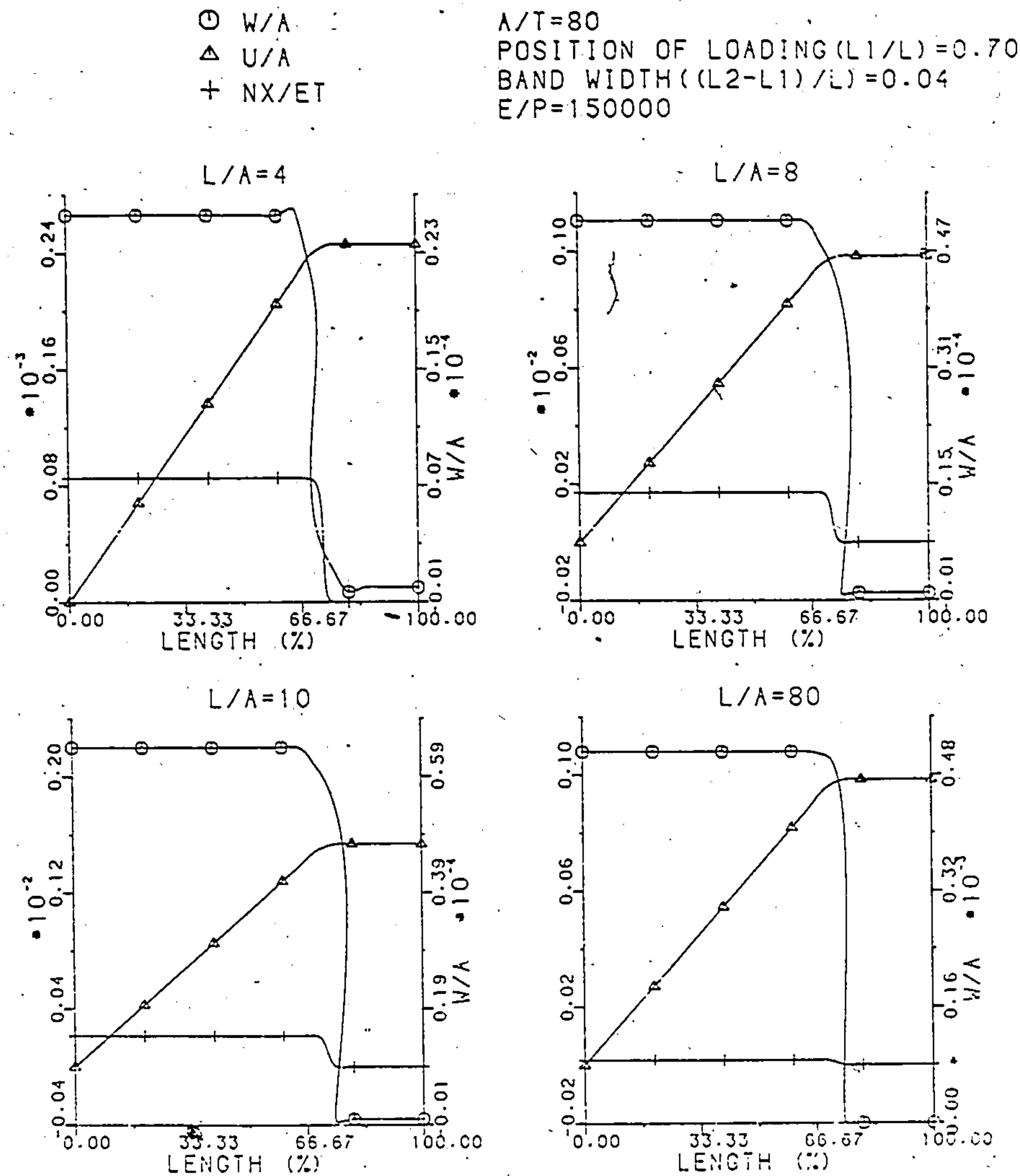

O W/A
Δ U/A
+ NX/ET
A/T=80
POSITION OF LOADING(L1/L)=0.70
BAND WIDTH((L2-L1)/L)=0.04
E/P=150000
L/A=4
L/A=8
L/A=10
L/A=80
LENGTH (%)
W/A

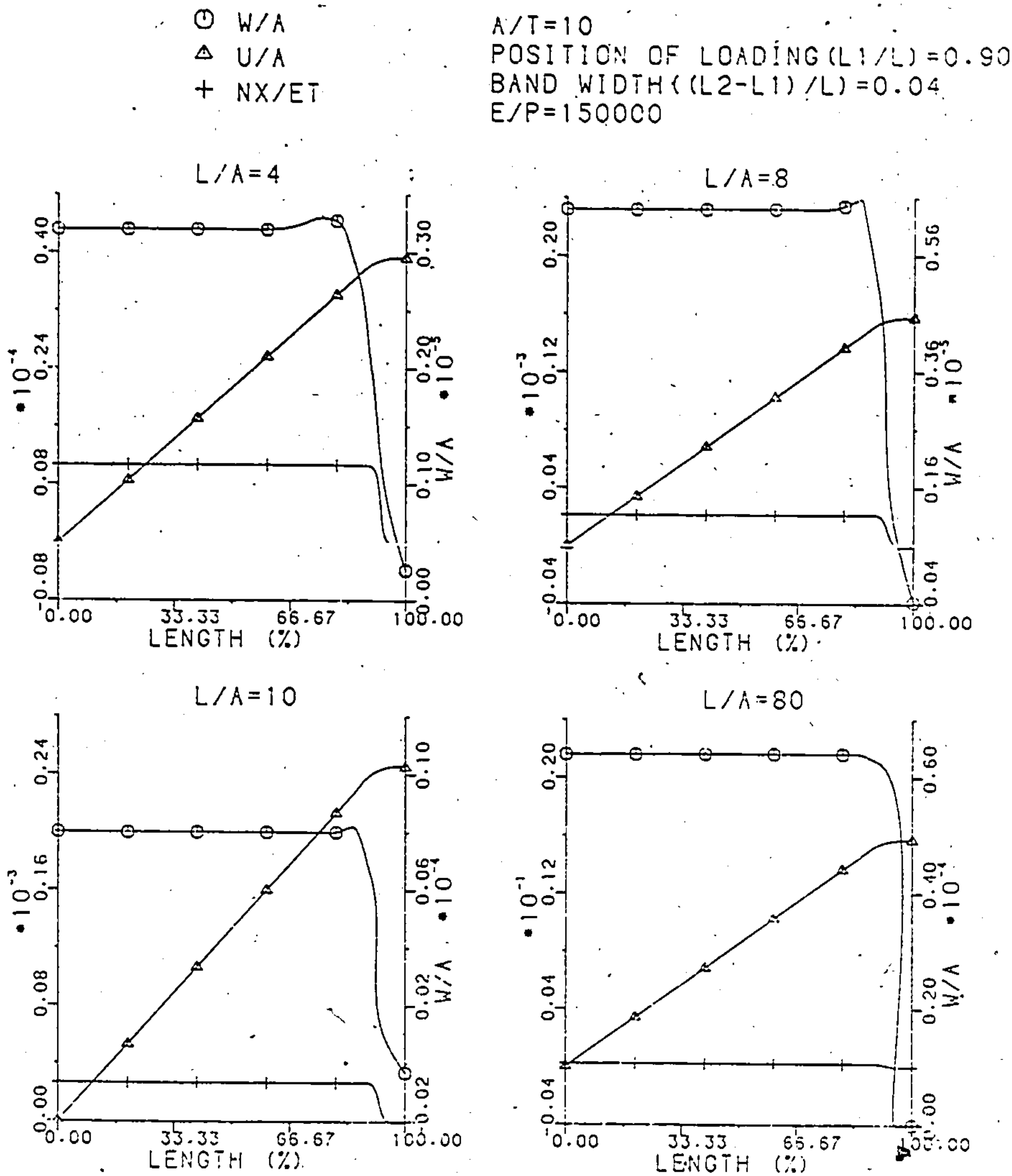

W/A
U/A
NX/ET
A/T=10
POSITION OF LOADING(L1/L)=0.90
BAND WIDTH((L2-L1)/L)=0.04
E/P=150000
L/A=4
L/A=8
L/A=10
L/A=80
LENGTH (%)
W/A

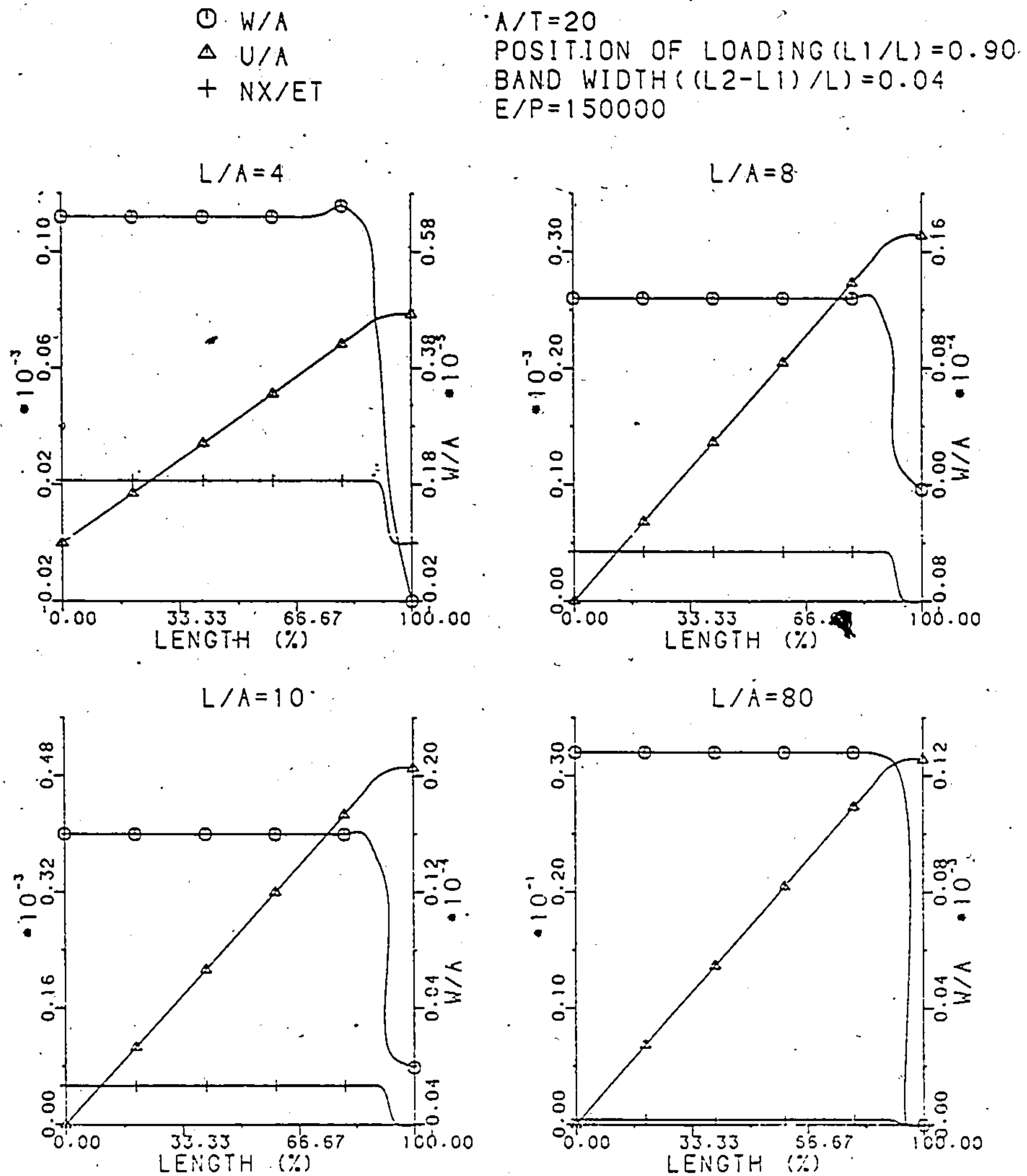

O W/A
Δ U/A
+ NX/ET
A/T=20
POSITION OF LOADING(L1/L)=0.90
BAND WIDTH((L2-L1)/L)=0.04
E/P=150000
L/A=4
L/A=8
L/A=10
L/A=80
LENGTH (%)
W/A

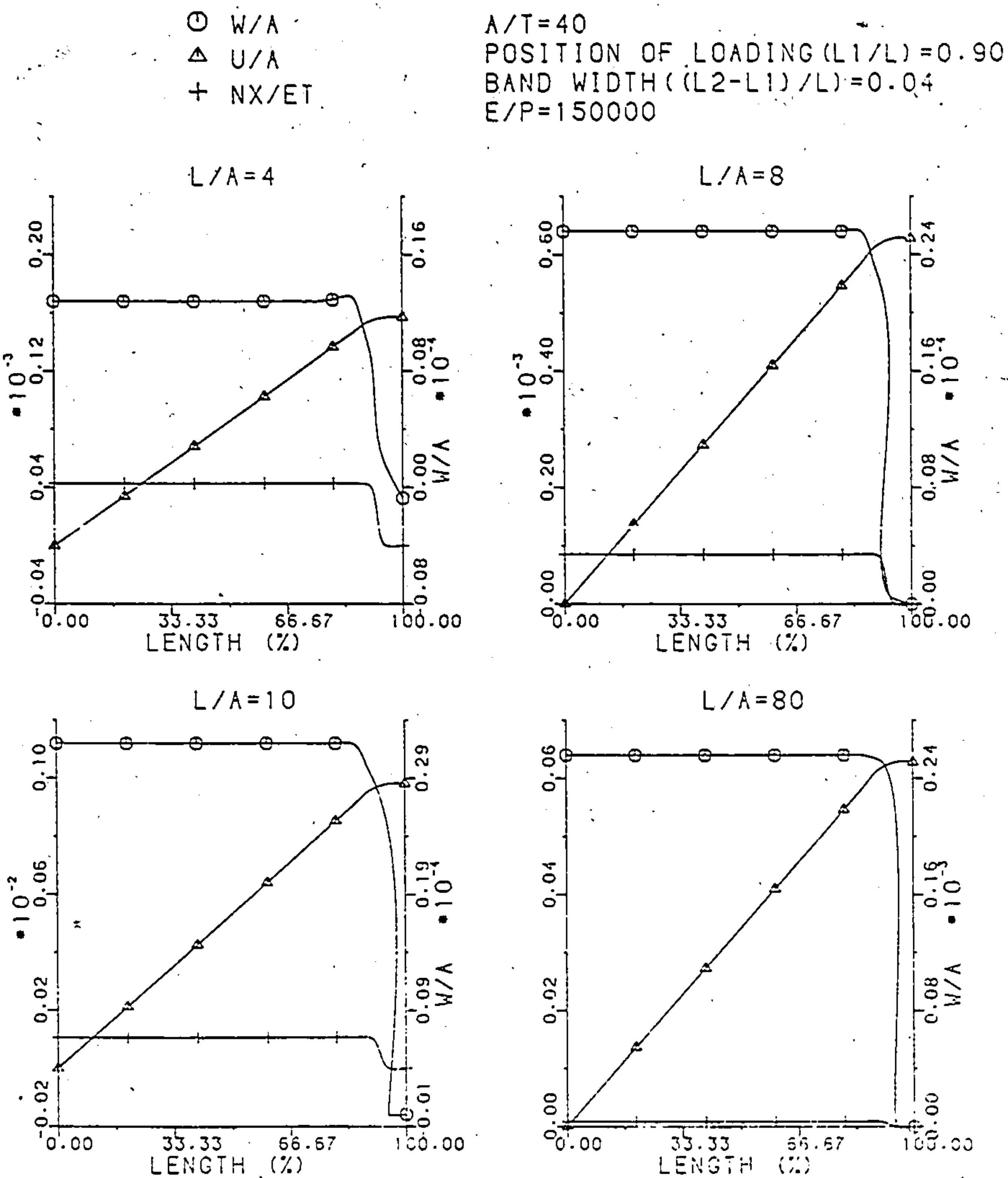

W/A
U/A
NX/ET
A/T=40
POSITION OF LOADING(L1/L)=0.90
BAND WIDTH((L2-L1)/L)=0.04
E/P=150000
L/A=4
L/A=8
L/A=10
L/A=80
LENGTH (%)
W/A

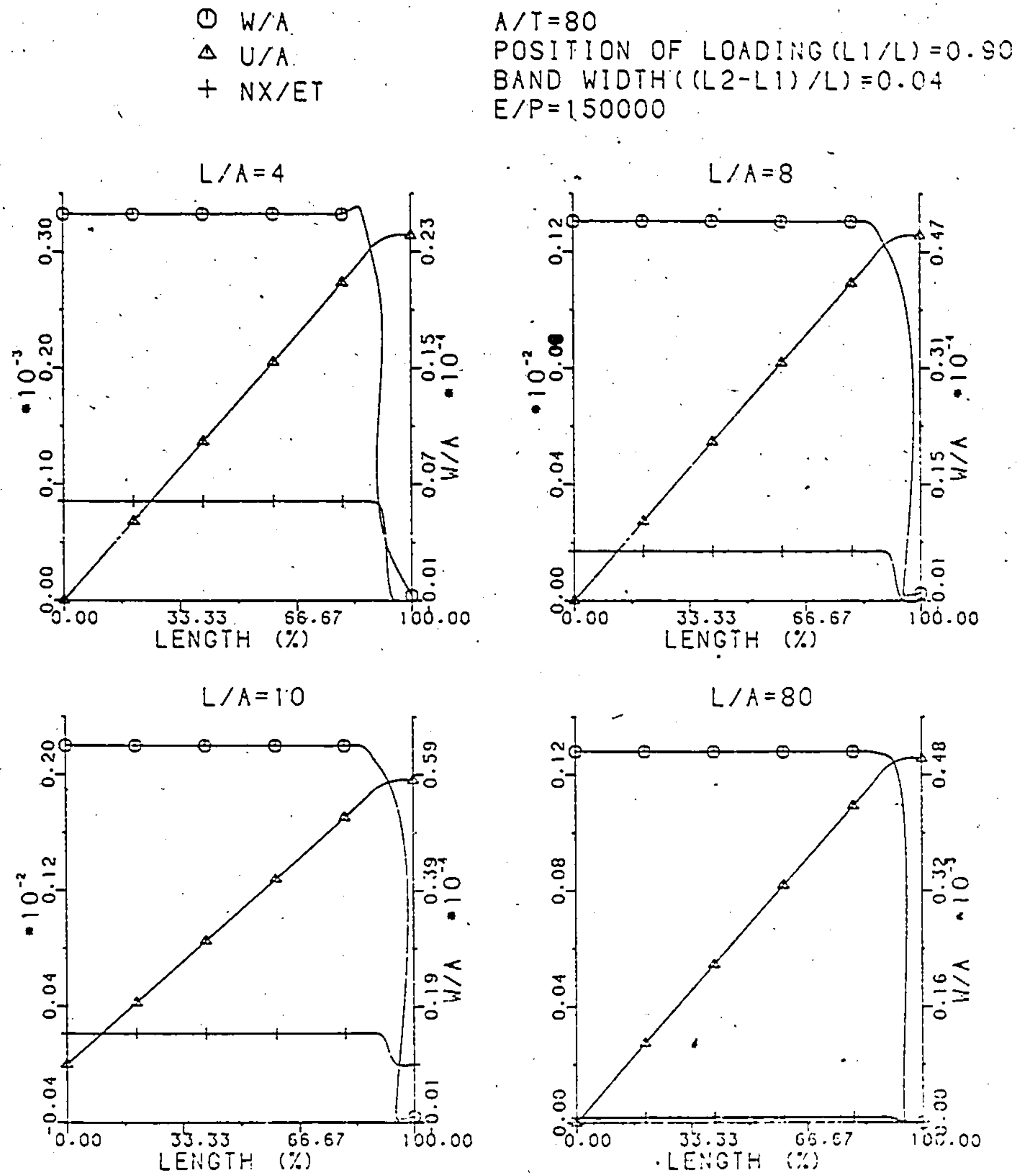

W/A
U/A
NX/ET
A/T=80
POSITION OF LOADING (L1/L)=0.90
BAND WIDTH ((L2-L1)/L)=0.04
E/P=150000
L/A=4
L/A=8
L/A=10
L/A=80
LENGTH (%)
W/A
0.00
33.33
66.67
100.00

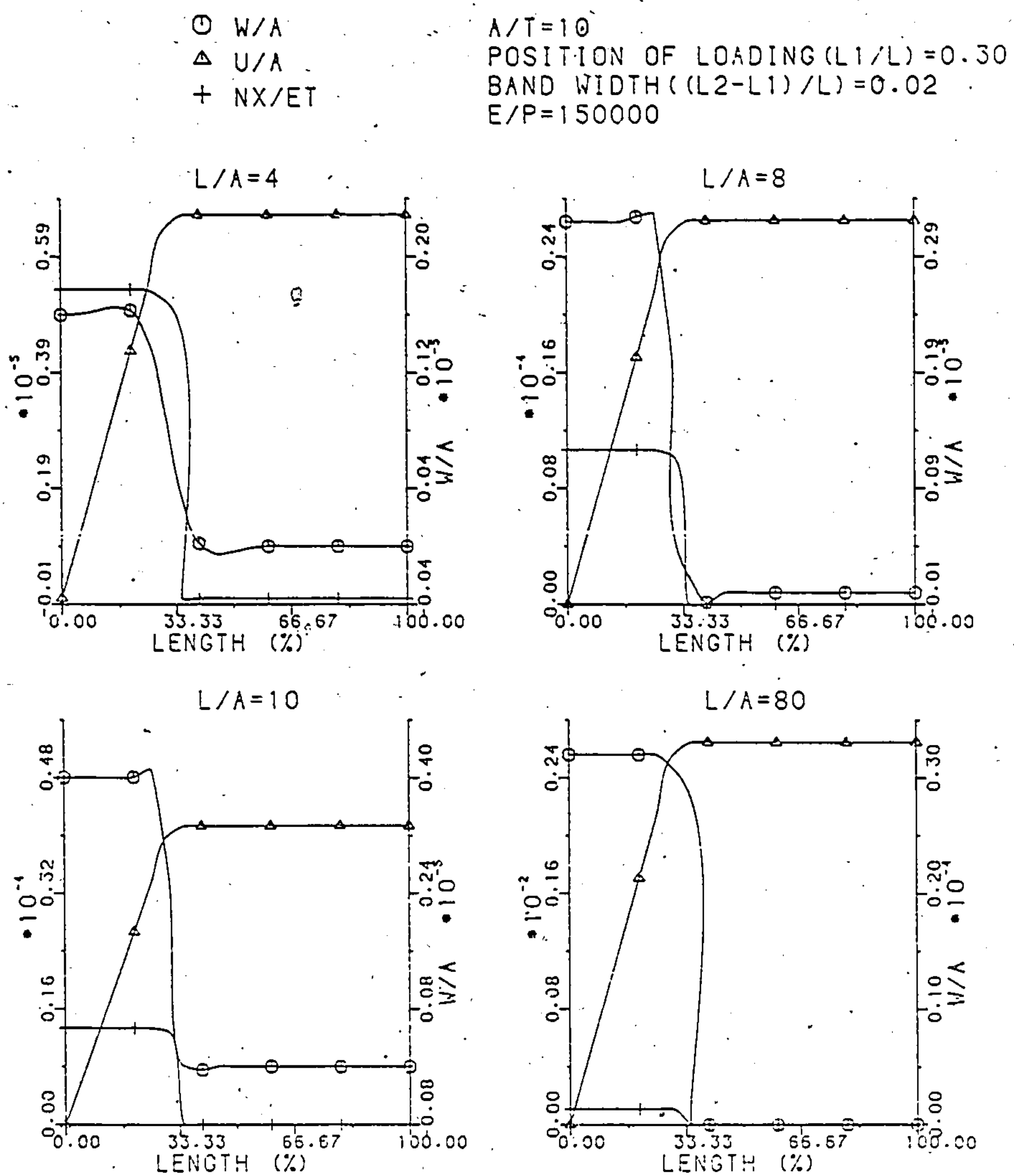

W/A
U/A
NX/ET
A/T=10
POSITION OF LOADING(L1/L)=0.30
BAND WIDTH((L2-L1)/L)=0.02
E/P=150000
L/A=4
L/A=8
L/A=10
L/A=80
LENGTH (%)
W/A

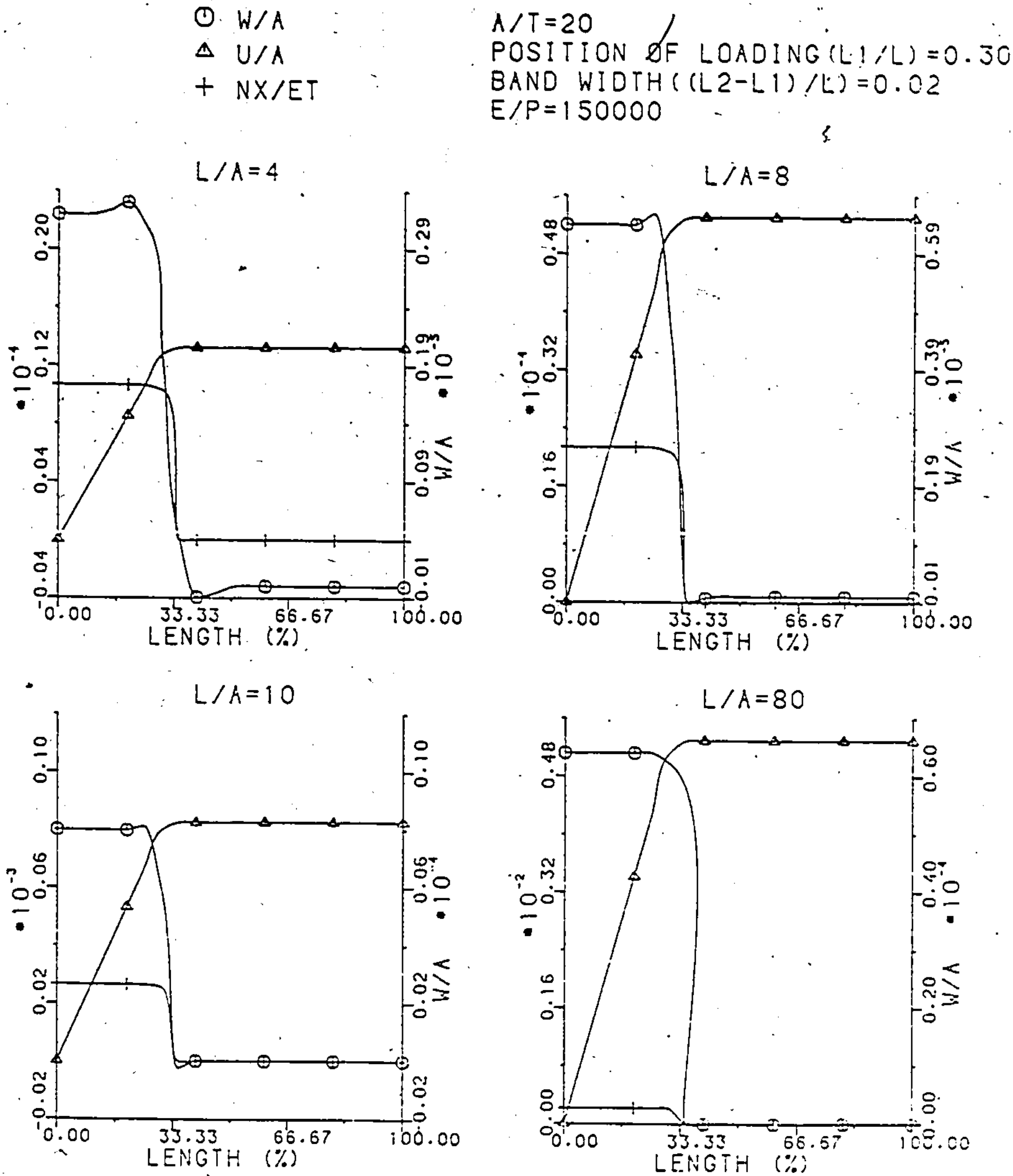

⊙ W/A
△ U/A
+ NX/ET
A/T=20
POSITION OF LOADING (L1/L)=0.30
BAND WIDTH ((L2-L1)/L)=0.02
E/P=150000
L/A=4
L/A=8
L/A=10
L/A=80
LENGTH (%)
0.00
33.33
66.67
100.00
W/A

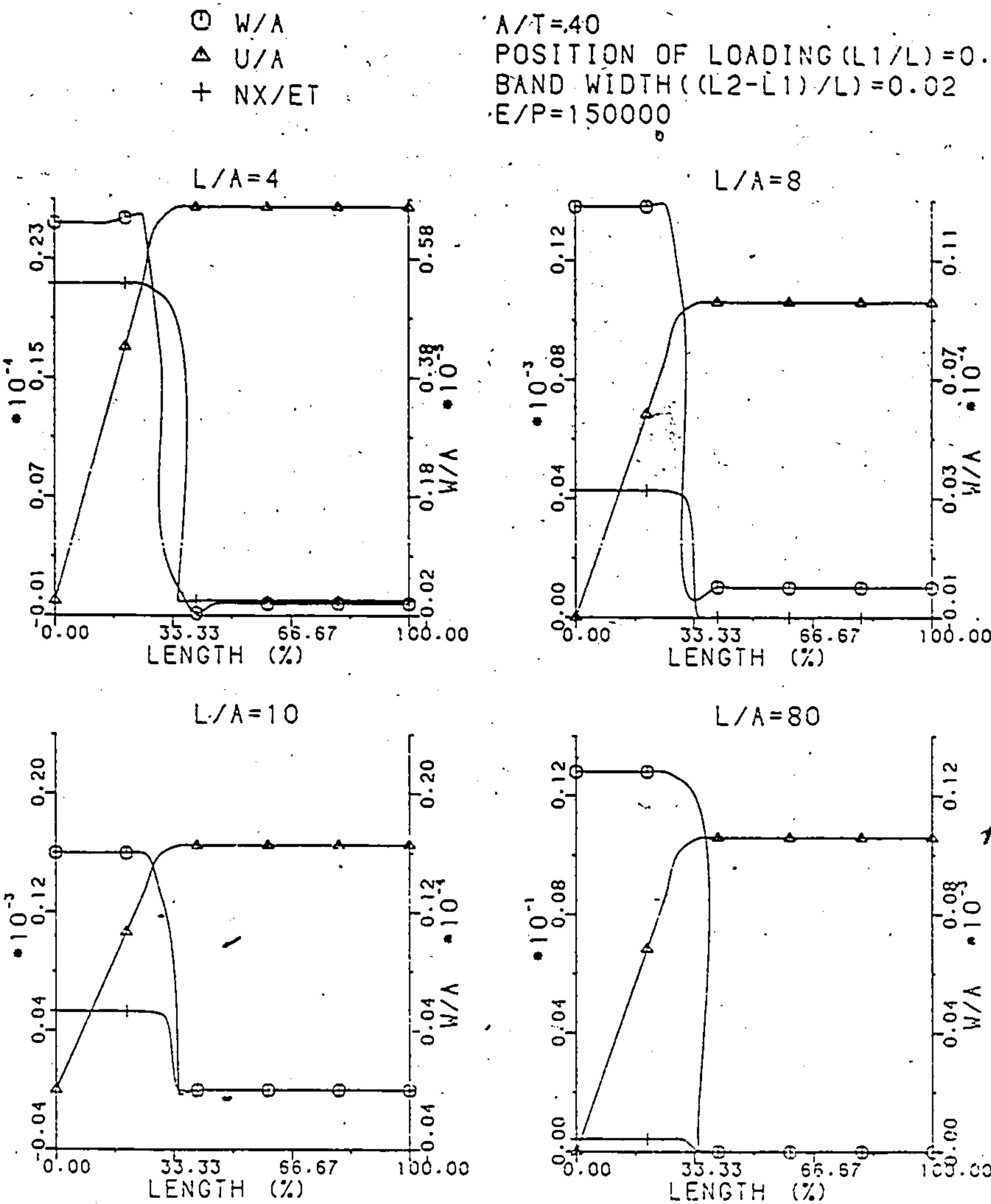

W/A
U/A
NX/ET
A/T=40
POSITION OF LOADING(L1/L)=0.30
BAND WIDTH((L2-L1)/L)=0.02
E/P=150000
L/A=4
L/A=8
L/A=10
L/A=80
LENGTH (%)
W/A
0.00
33.33
66.67
100.00

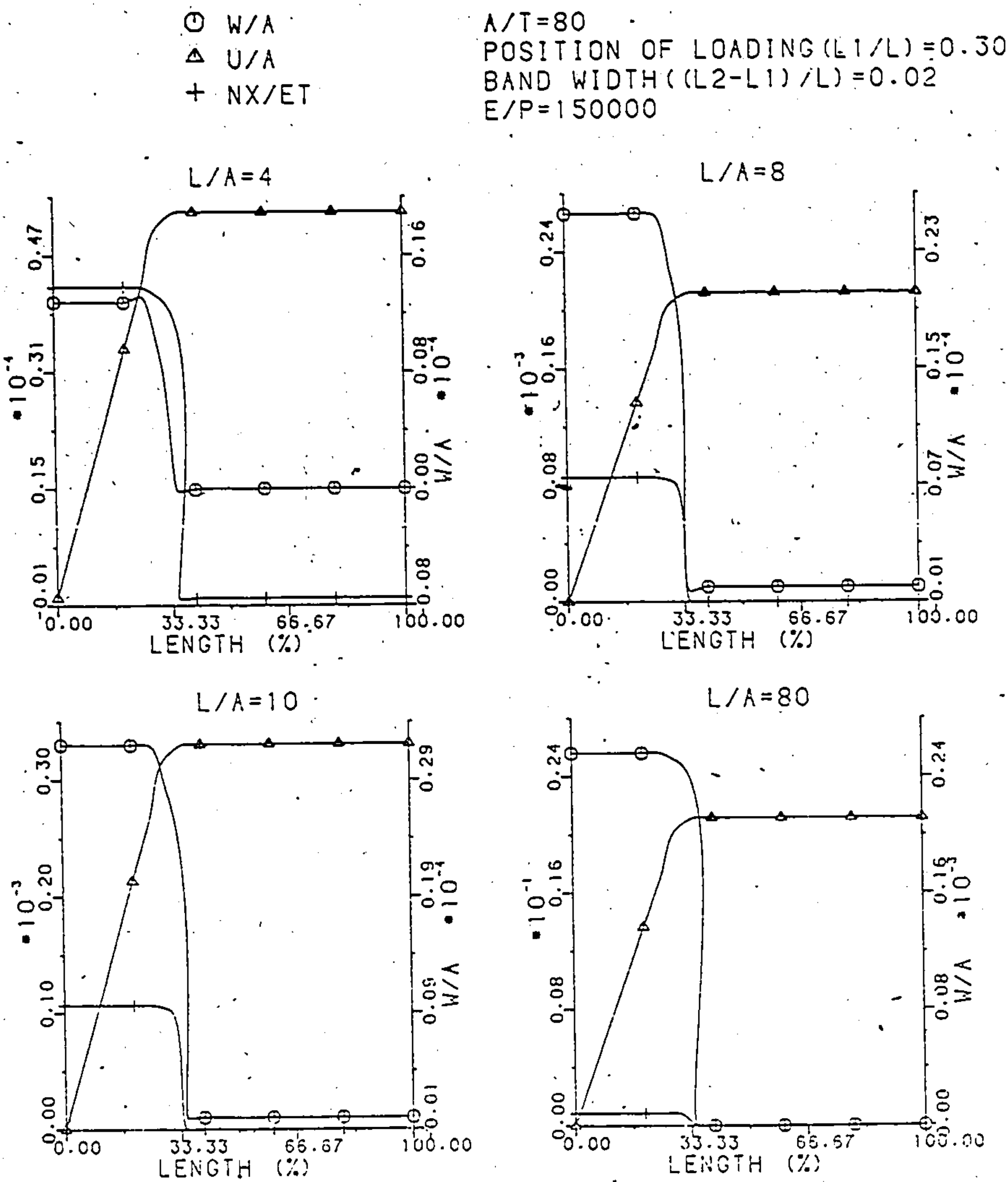

W/A
U/A
NX/ET
A/T=80
POSITION OF LOADING(L1/L)=0.30
BAND WIDTH((L2-L1)/L)=0.02
E/P=150000
L/A=4
L/A=8
L/A=10
L/A=80
LENGTH (%)
LENGTH (%)
LENGTH (%)
LENGTH (%)
W/A
W/A
W/A
W/A

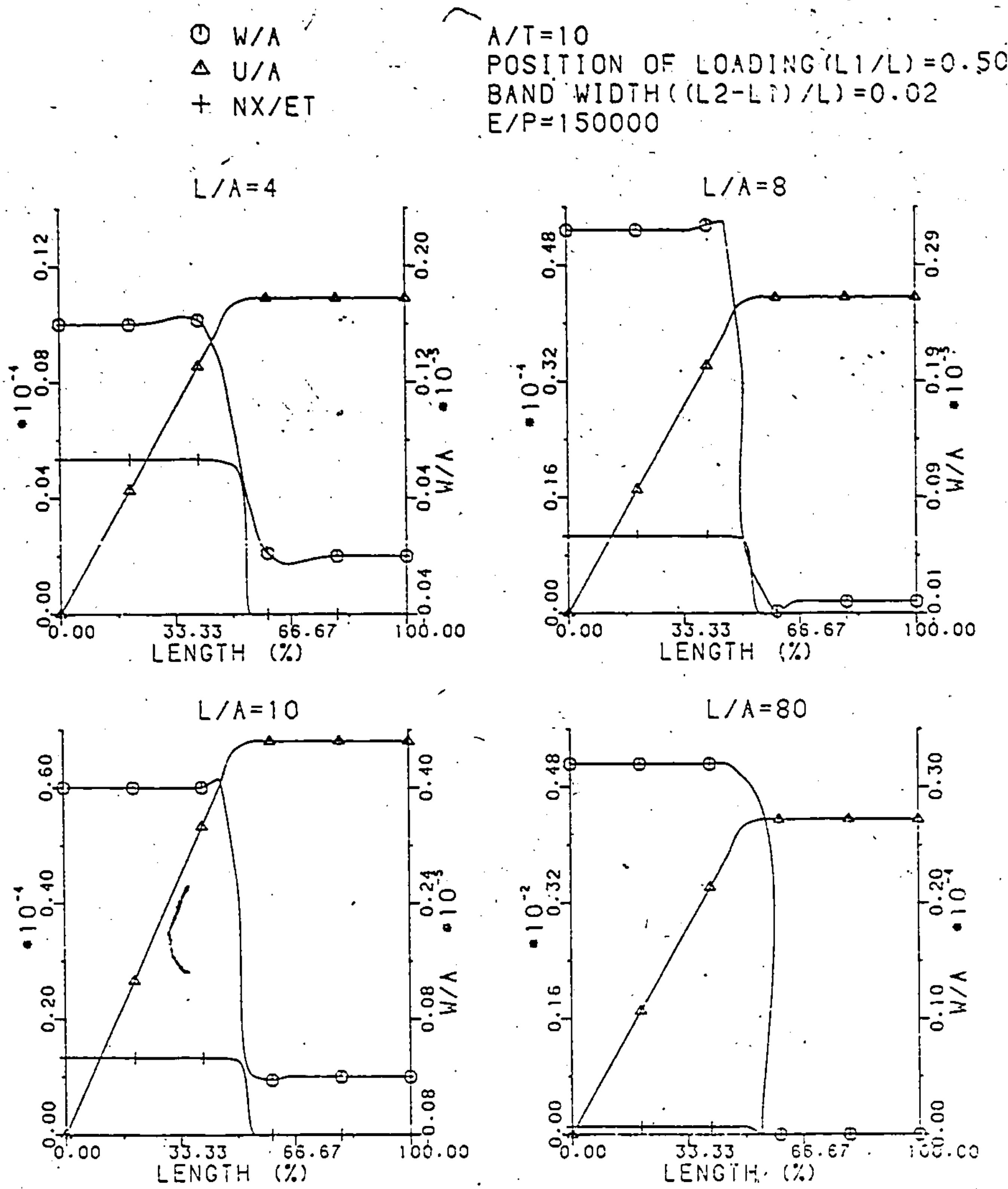

W/A
U/A
NX/ET
A/T=10
POSITION OF LOADING(L1/L)=0.50
BAND WIDTH((L2-L1)/L)=0.02
E/P=150000
L/A=4
L/A=8
L/A=10
L/A=80
LENGTH (%)
W/A

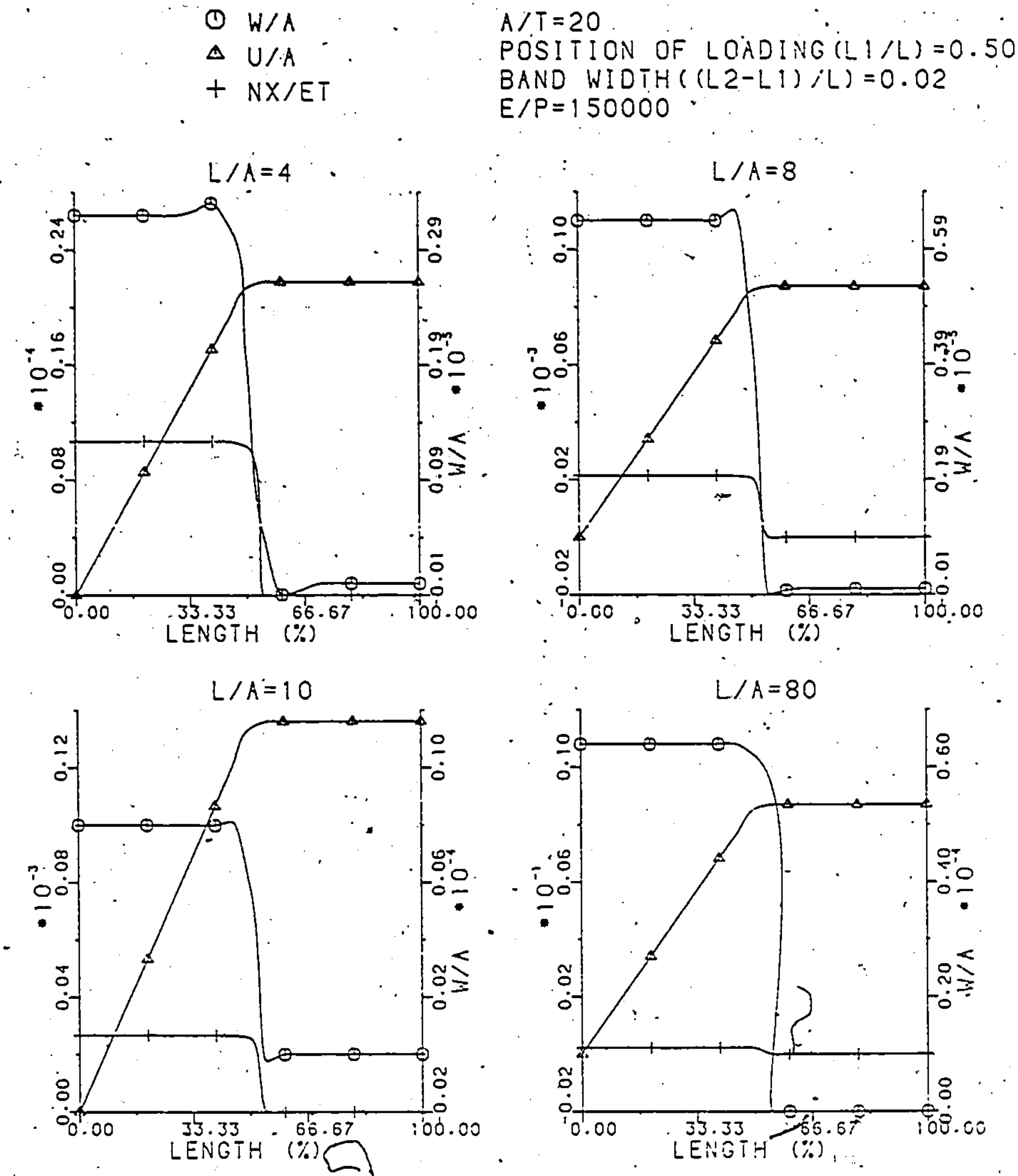
O W/A
△ U/A
+ NX/ET
A/T=20
POSITION OF LOADING(L1/L)=0.50
BAND WIDTH((L2-L1)/L)=0.02
E/P=150000
L/A=4
L/A=8
L/A=10
L/A=80
LENGTH (%)
W/A
0.00
33.33
66.67
100.00

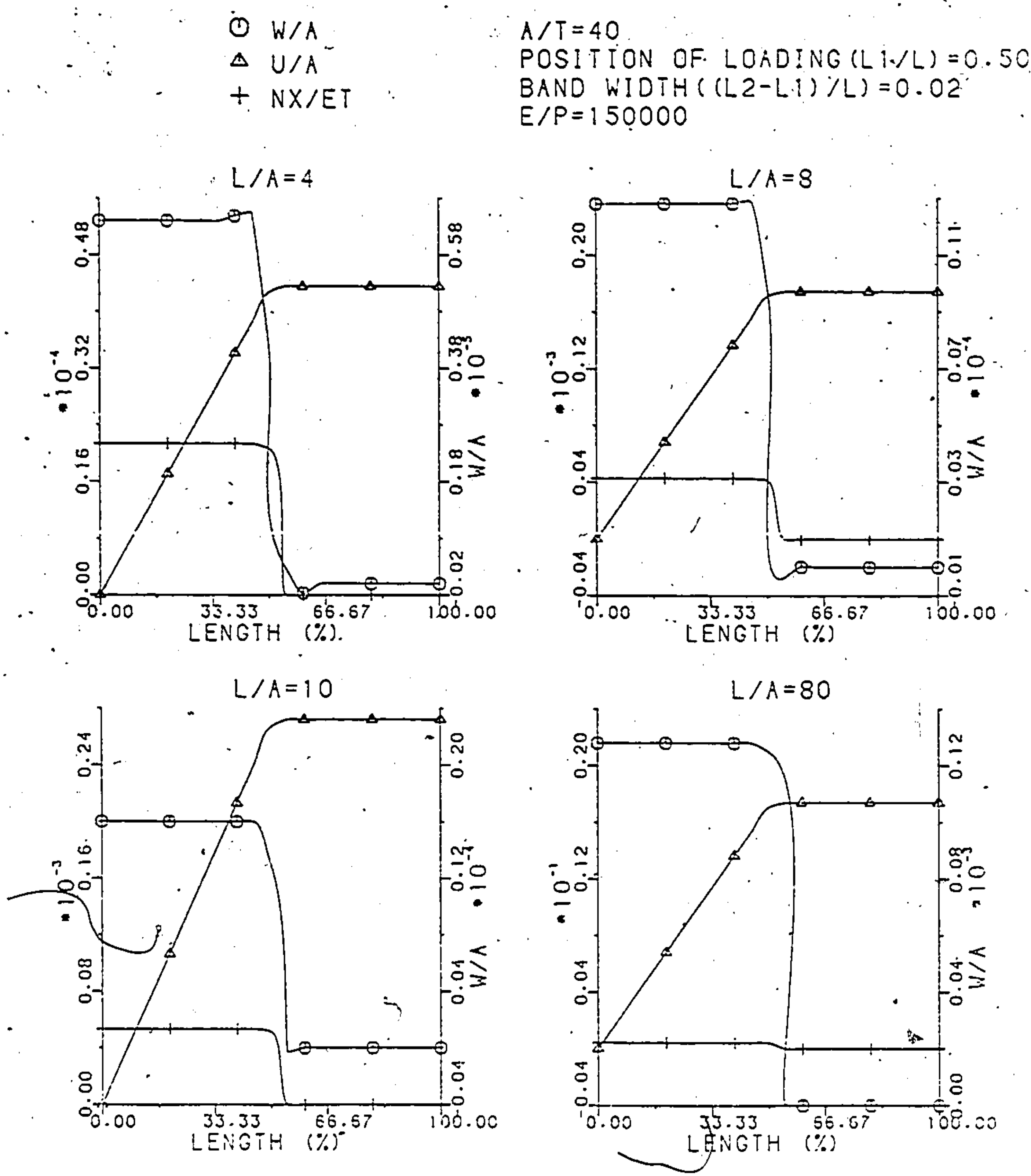

W/A
U/A
NX/ET
A/T=40
POSITION OF LOADING (L1/L)=0.50
BAND WIDTH ((L2-L1)/L)=0.02
E/P=150000
L/A=4
L/A=8
L/A=10
L/A=80
*10^-4
*10^-3
*10^-1
W/A
LENGTH (%)
0.00
33.33
66.67
100.00

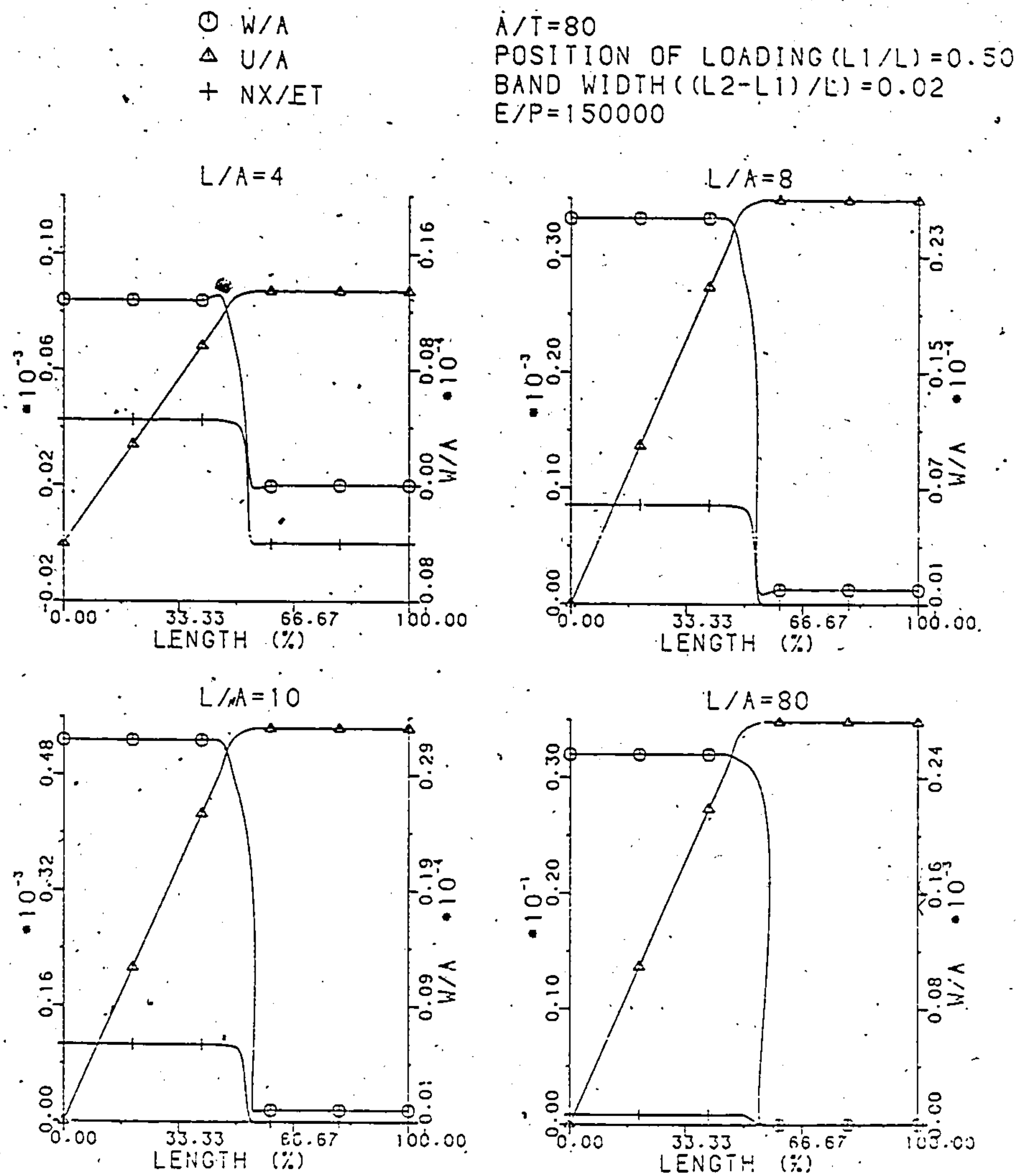
W/A
U/A
NX/ET
A/T=80
POSITION OF LOADING(L1/L)=0.50
BAND WIDTH((L2-L1)/L)=0.02
E/P=150000
L/A=4
L/A=8
L/A=10
L/A=80
LENGTH (%)
0.00
33.33
66.67
100.00

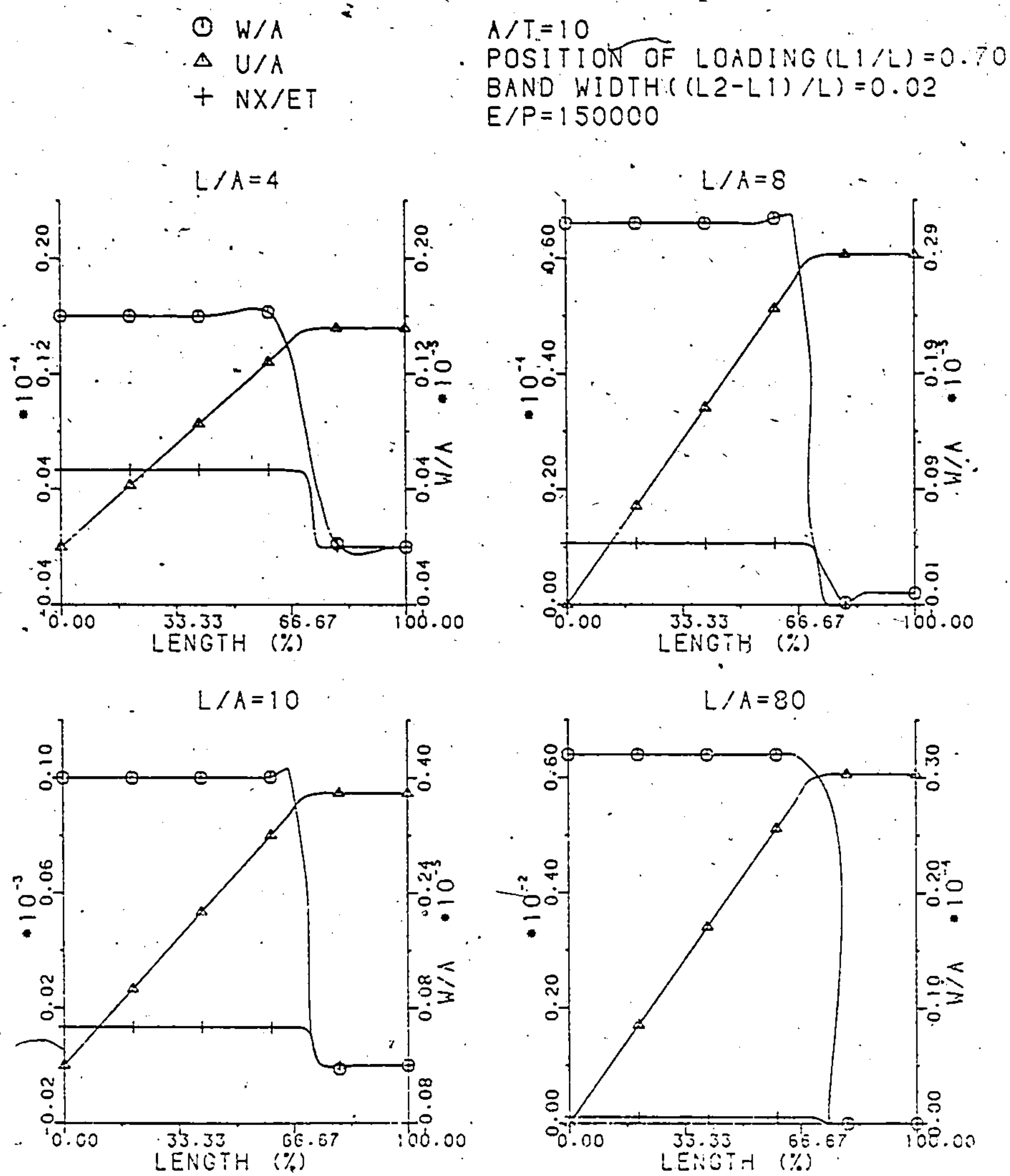
W/A
U/A
NX/ET
A/T=10
POSITION OF LOADING(L1/L)=0.70
BAND WIDTH((L2-L1)/L)=0.02
E/P=150000
L/A=4
L/A=8
L/A=10
L/A=80
LENGTH (%)
W/A
0.00
33.33
66.67
100.00

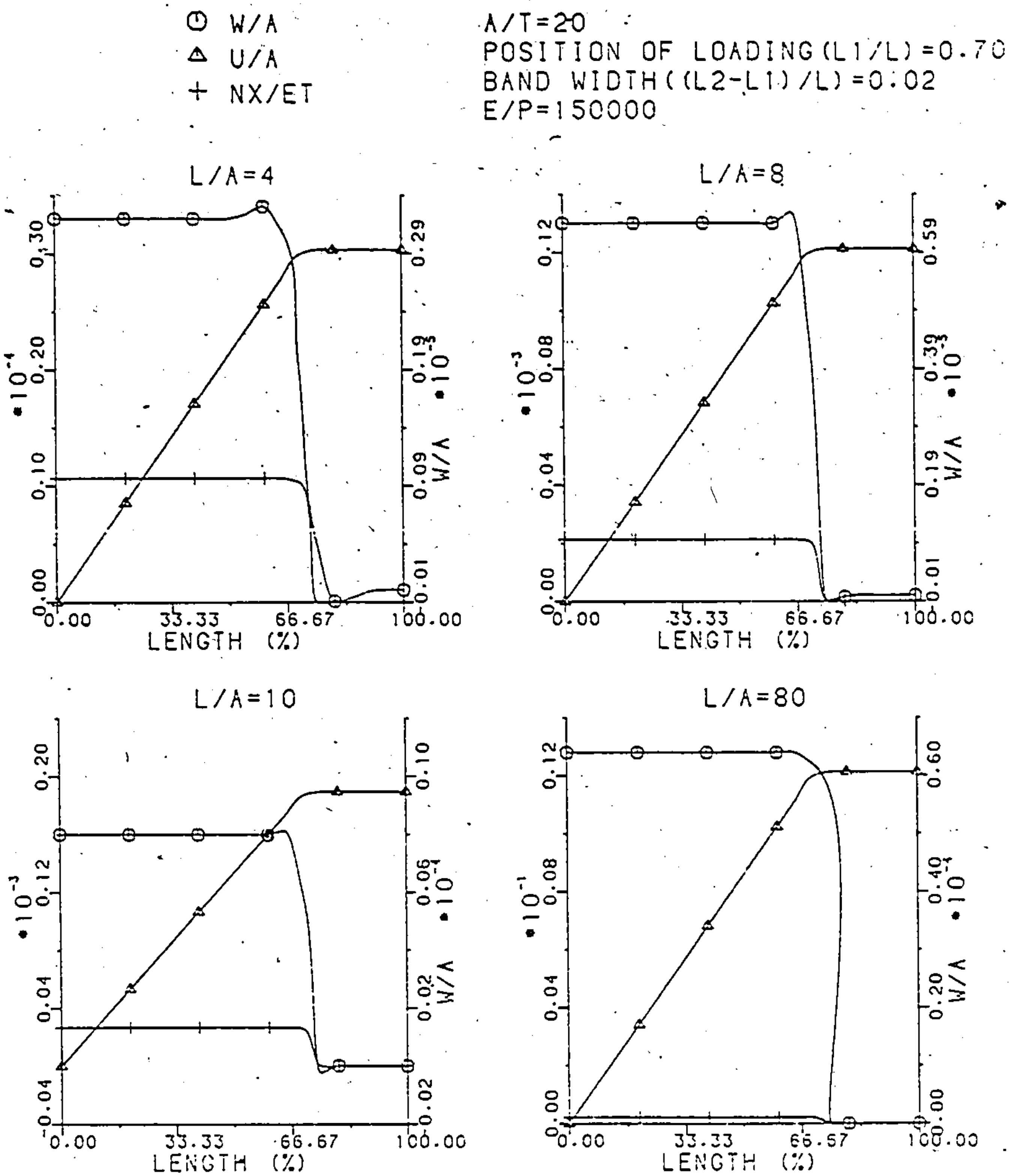

W/A
U/A
NX/ET
A/T=20
POSITION OF LOADING(L1/L)=0.70
BAND WIDTH((L2-L1)/L)=0.02
E/P=150000
L/A=4
L/A=8
L/A=10
L/A=80
LENGTH (%)
0.00
33.33
66.67
100.00
W/A

○ W/A
△ U/A
+ NX/ET

A/T=40
POSITION OF LOADING(L1/L)=0.70
BAND WIDTH((L2-L1)/L)=0.02
E/P=150000

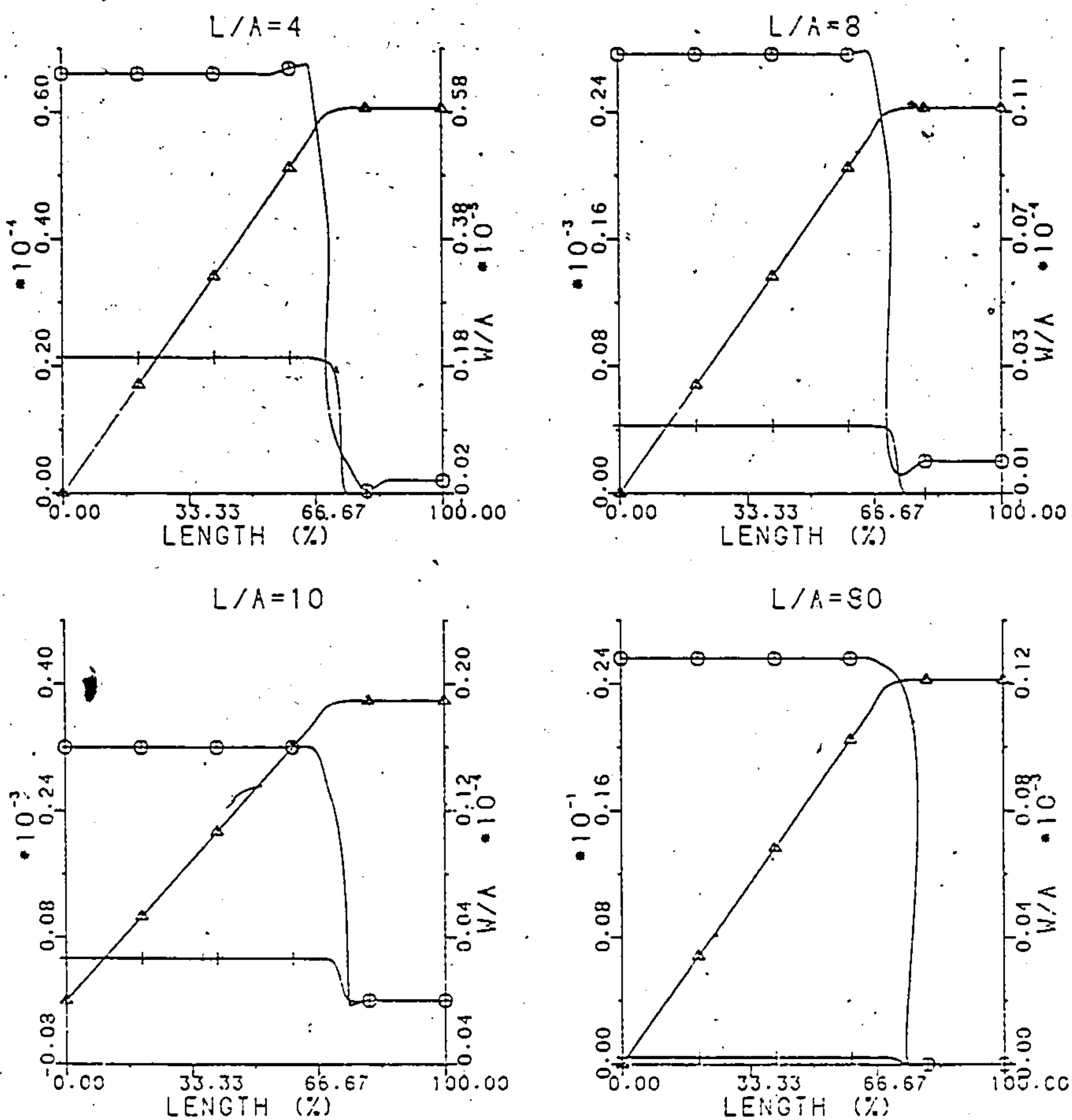

○ W/A
△ U/A
+ NX/ET

A/T=80
POSITION OF LOADING(L1/L)=0.70
BAND WIDTH((L2-L1)/L)=0.02
E/P=150000

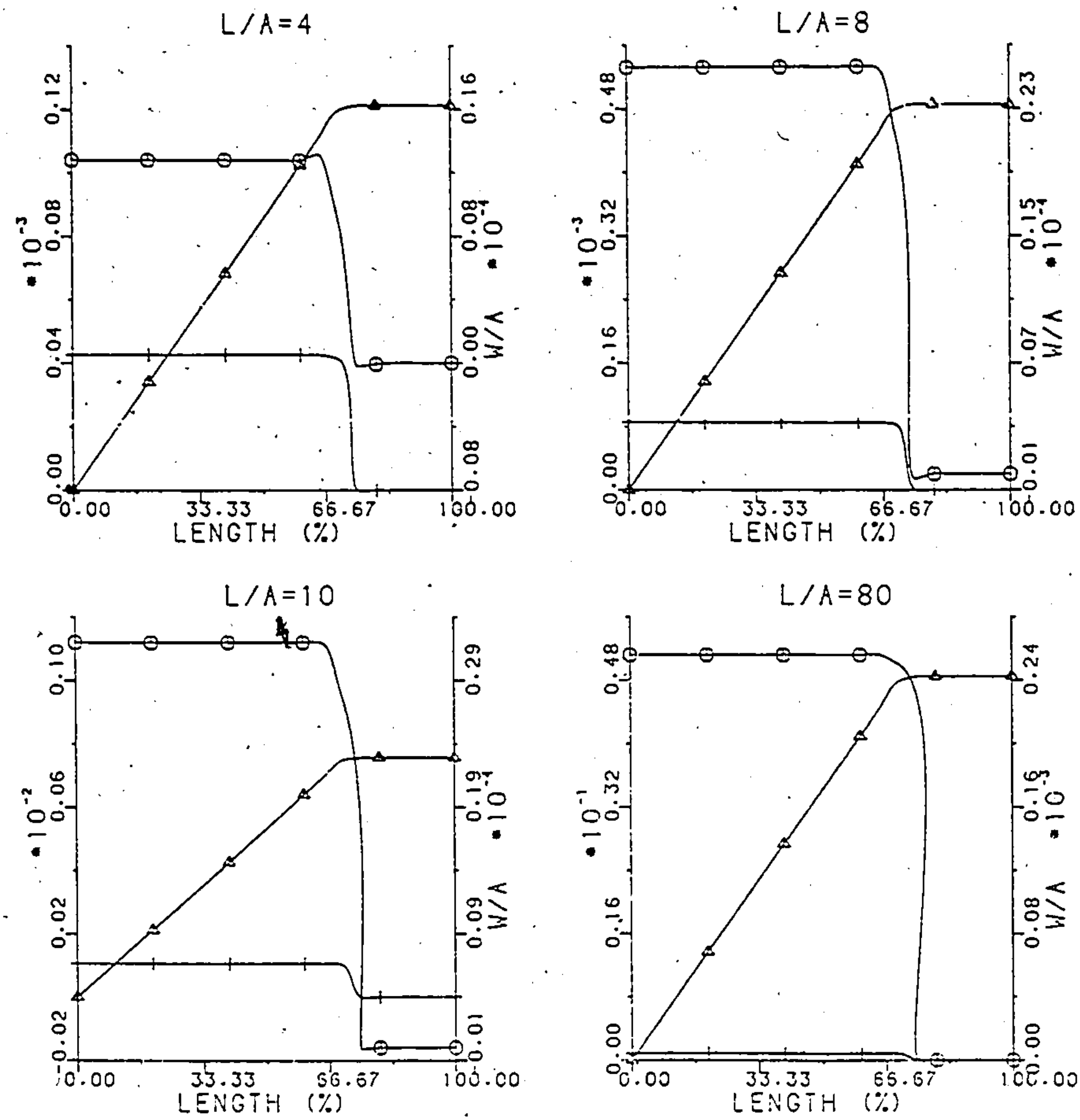

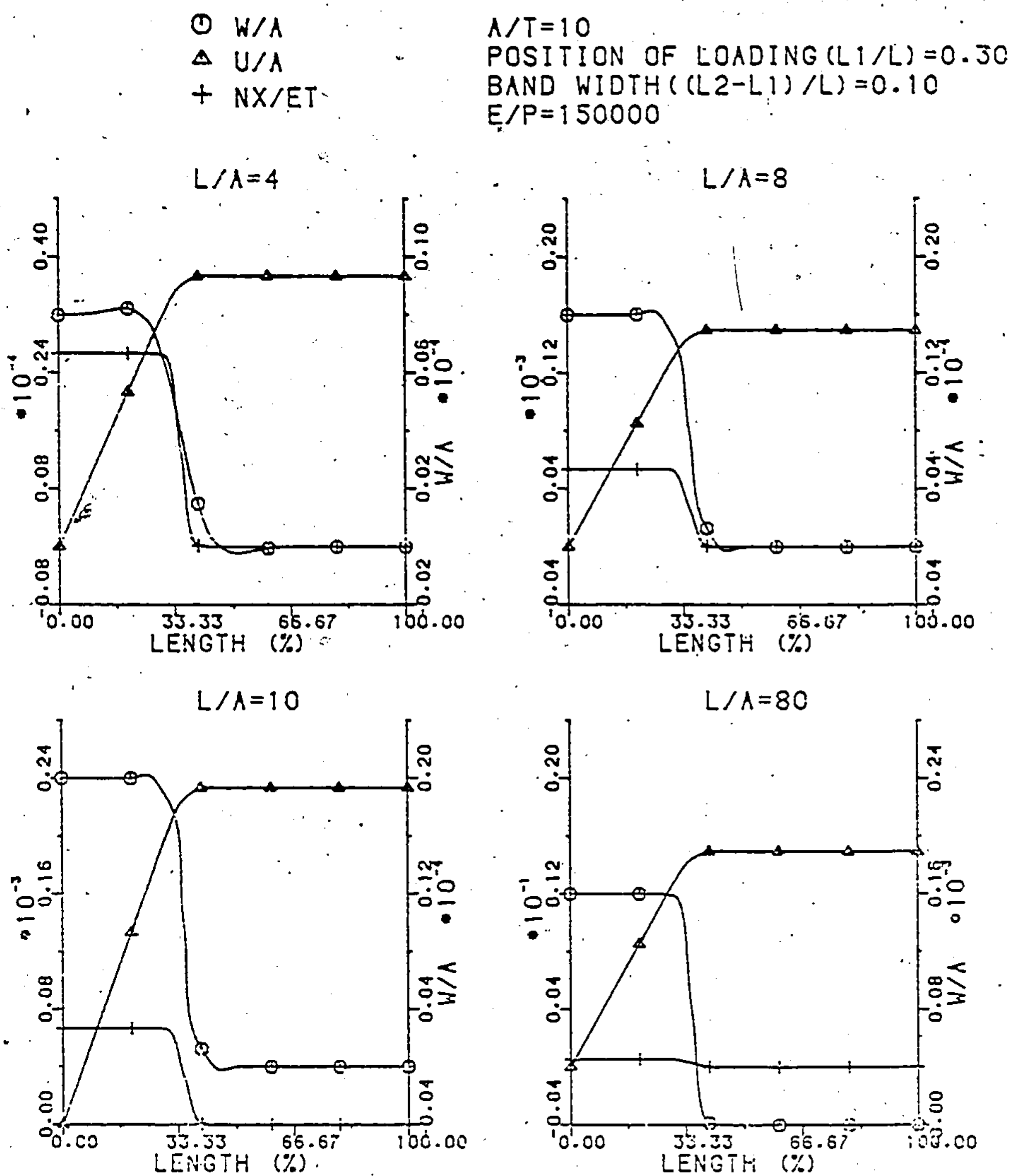
W/Λ
U/Λ
NX/ET
Λ/T=10
POSITION OF LOADING(L1/L)=0.30
BAND WIDTH((L2-L1)/L)=0.10
E/P=150000
L/Λ=4
L/Λ=8
L/Λ=10
L/Λ=80
LENGTH (%)
W/Λ

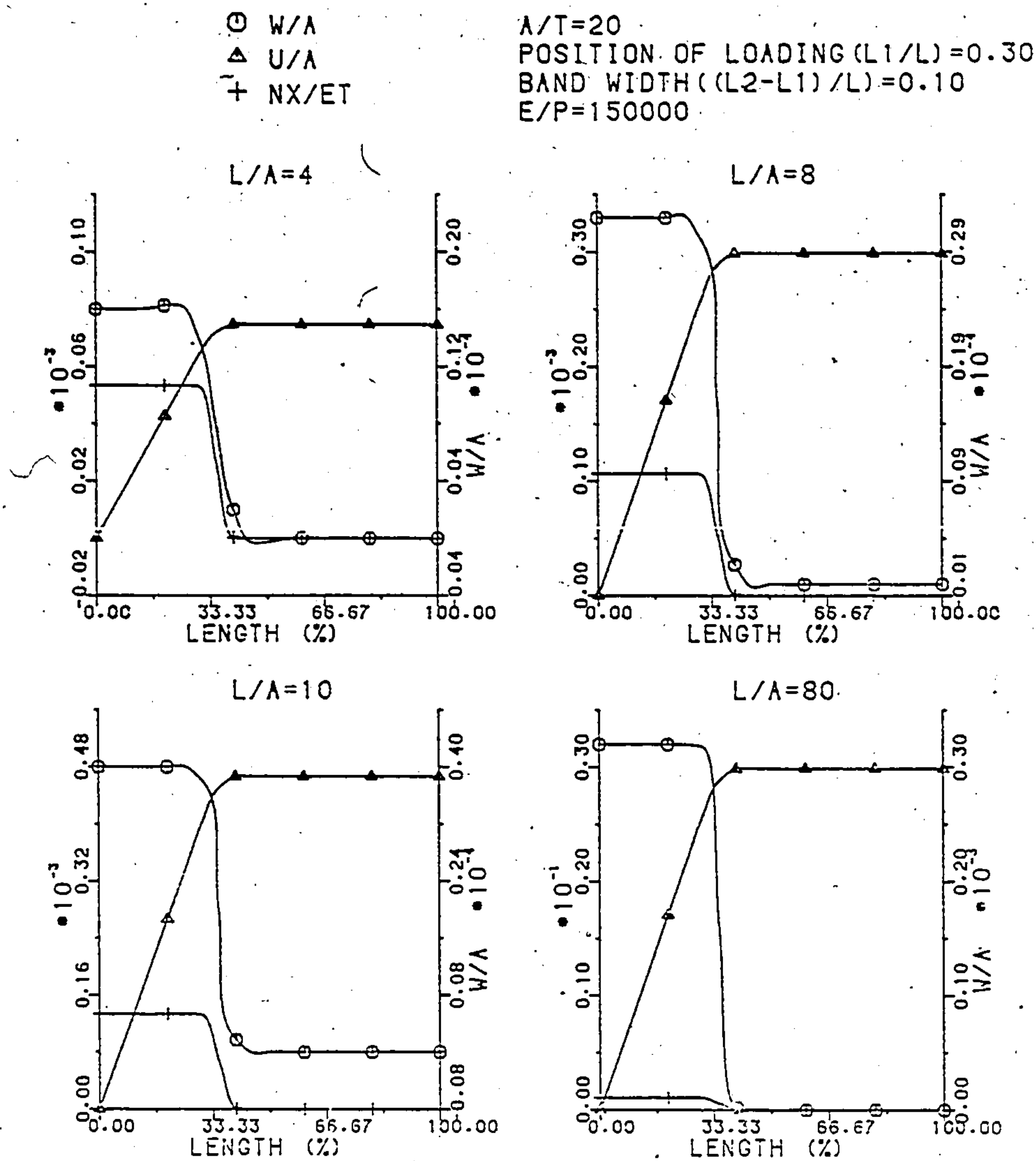

W/Λ
U/Λ
NX/ET
Λ/T=20
POSITION OF LOADING (L1/L)=0.30
BAND WIDTH ((L2-L1)/L)=0.10
E/P=150000
L/Λ=4
L/Λ=8
L/Λ=10
L/Λ=80
LENGTH (%)
W/Λ

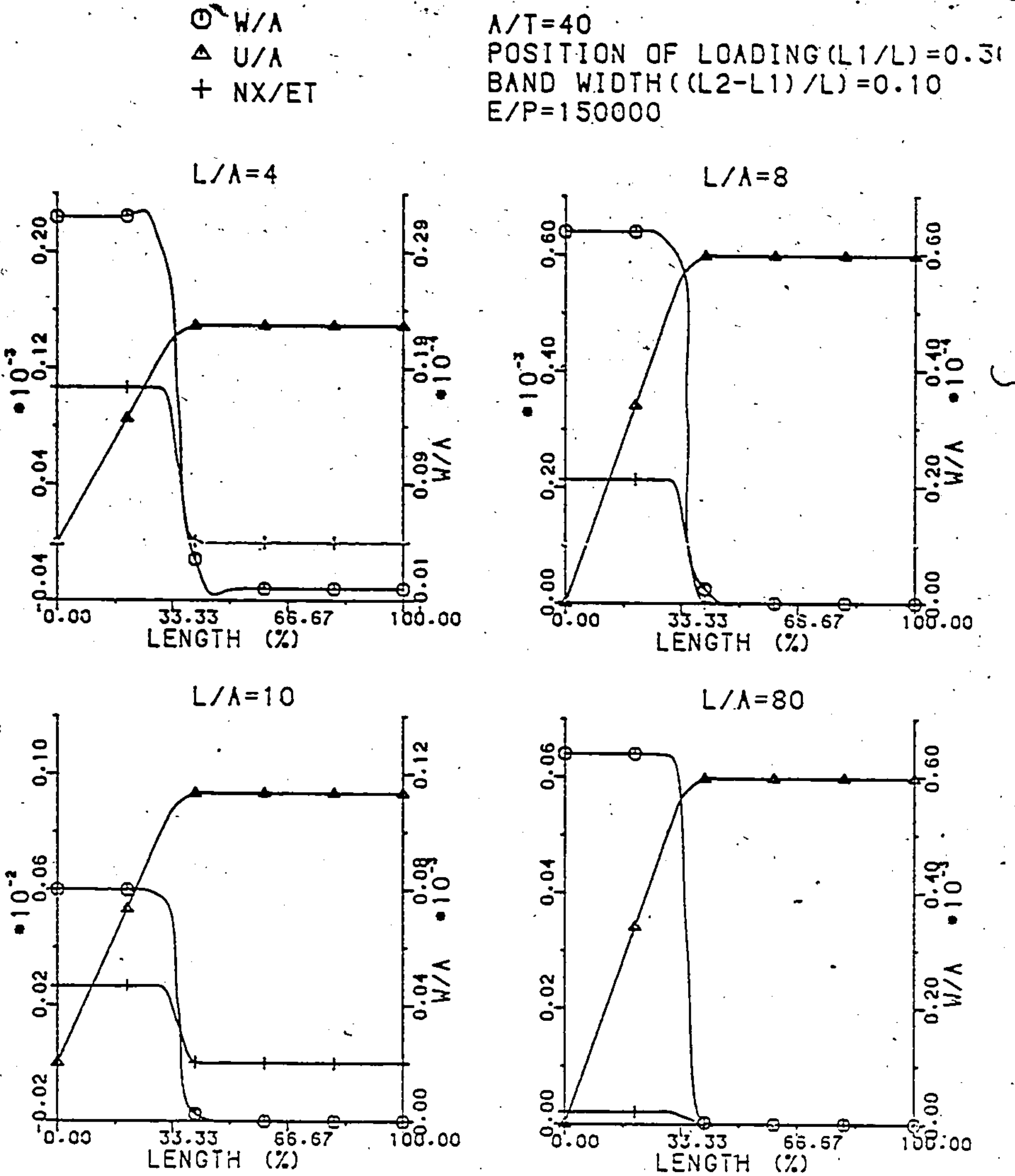
W/A
U/A
NX/ET
A/T=40
POSITION OF LOADING(L1/L)=0.3
BAND WIDTH((L2-L1)/L)=0.10
E/P=150000
L/A=4
L/A=8
L/A=10
L/A=80
LENGTH (%)
0.00
33.33
66.67
100.00
W/A

BIBLIOGRAPHY

1. American Society of Mechanical Engineers, ASME Boiler and Pressure Vessel Code, Section VIII, New York, 1980.

2. Bijlaard, P.P., Stresses from Radial Loads in Cylindrical Pressure Vessels, The Welding Journal, Research Supplement, 33, 1954, p.615s.

3. Bijlaard, P.P., Stresses from Radial Loads and External Moments in Cylindrical Pressure Vessels, The Welding Journal, Research Supplement, 34, 1955, p. 608s.

4. Bijlaard, P.P., Stresses from Local Loadings in Cylindrical Pressure Vessels, Trans. ASME, 77(6), 1955, p. 805-818.

5. Bijlaard, P.P., Additional Data on Stresses in Cylindrical Shells Under Local Loading, WRC-50, 1959.

6. Bijlaard, P.P. and Cranch, E.T., Interpretive Commentary on the Application of Theory to Experimental Results for Stresses and Deflections, due to Local Loads on Cylindrical Shell, WRC-60, 1960.

7. Cheung, Y.K. and Yeo, M.F., A Practical Introduction to Finite Element Analysis, A Pitman International Text, London, England, 1979.

8. Dodge, W.G., Secondary Stress Indices for Integral Structural Attachments to Straight Pipe, WRC-198, 1974.

9. Flügge, W., Stresses in Shells, New York, NY, Springer Verlay, 1962.

10. Hoff, N.J., Kempner, J., and Pohle, F.V., Line Load Applied Along Generators of Thin Walled Circular Cylindrical Shells of Finite Length, Quarterly of Applied Mathematics, Vol. 11-12, 1953-55, p. 411.

11. Huebner, K.H., The Finite Element for Engineers, John Wiley and Sons, N.Y., 1975.

12. Irons, B.M., A Frontal Solution Program for FEM, International Journal for Numerical Methods in Engineering, Vol. 2, NO. 1, 1970, p. 5-32.

13. Kempner,J., Sheng,J., and Pohle,F.V., Tables and Curves for Deformations and Stresses in Circular Cylindrical Shells Under Localized Loadings, Journal of the Aeronautical Sciences, February 1957, p. 119.

14. Nash,A.W. and Bridgland,T.F., Line Loadings on Finite Length Cylindrical Shells-Solution by the Finite Fourier Transform, Quart. Journ. Mech. and Apply. Math., Vol. 14, 1961, p. 129.

15. Natarajan,R., Personal Communication.

16. Rodabaugh,E.C.,Dodge,W.G. and Moore,S.E., Stress Indices at Lug Supports on Piping Systems, WRC-198, 1974.

17. Timoshenko,S.P., Theory of Plates and Shells, New York,McGraw Hill,1959.

18. Timoshenko,S.P. and Goodier,J.N., Theory of Elasticity, New York, NY, McGraw Hill, 1970.

19. Wichman,K.R.,Hopper,A.G. and Mershon,J.L., Local Stresses in Spherical and Cylindrical Shells due to External Loadings, WRC-107, 1965.

20. Widera,G.E.O.,Kitz,G.T.,Verma,V.K. and Lan,J.S., Piping Shear Lug Stress Analysis, Trans. of the Int. Conf. on Structure Mech. in React. Technol. 4th, Vol. F, Struct. Anal. of React. and Coolant Circuit Struct., San Fransisco, Calif., Aug. 15-19, 1977 Publ. by Commission of the European Communities, Luxemb., Pap F 2/9, p. 9.

21. Yuan,S.W., Thin Cylindrical Shells Subjected to Concentated Loads, Quarterly of Applied Mathematics,Vol. 3-4, 1945-47, p. 13-26.

22. Yuan,S.W. and Ting,L., On Radial Deflections of a Cylinder Subjected To Equal and Opposite Concentrated Radial Loads, Journal of Applied Mechanics, Trans. ASME, Vol. 23-24, 1956-1957, p. 278.

23. Zienkiewicz,O.C., The Finite Element Method in Engineering Science, McGraw Hill, London, England, 1977.